From microstructures to macroscale carbon export — influences of marine snow composition on settling velocity and microbial colonization

Dissertation

zur Erlangung des akademischen Grades eines Doktors der Naturwissenschaften

-Dr. rer. nat.-

im Fachbereich Geowissenschaften der Universität Bremen

Clara Maria Flintrop

Bremen, Juni 2019

Die vorliegende Arbeit wurde in der Zeit von Mai 2016 bis Juni 2019 an der Universität Bremen durchgeführt. Die Ergebnisse der Arbeit wurden am MARUM Zentrum für marine Umweltwissenschaften und am Alfred-Wegener-Institut Helmholtz-Zentrum für Polar- und Meeresforschung erarbeitet und im Rahmen des Programms “The International Max Planck Research School of Marine Microbiology” (MarMic) angefertigt.

Erstgutachter: **Prof. Dr. Morten Hvitfeldt Iversen**
Zweitgutachterin: **Prof. Dr. Helle Ploug**

Datum des Promotionskolloquiums: **2. August 2019**

SUMMARY

Sinking marine aggregates are a major component of the biological carbon pump. Together with zooplankton fecal pellets, they are responsible for the majority of organic carbon drawdown from the sea surface into the ocean interior, where carbon can be stored over geological time scales. Yet, only a very small fraction of aggregates makes it out of the upper 200 meters at all, as they are gazed on and colonized by zooplankton and bacteria in the water column. Organic matter transformations involved in the degradation of marine aggregates play a key role in the fate of organic carbon in the oceans. Yet, comparatively little is known about aggregate microstructures at the single- and sub-aggregate level because aggregates are exceedingly fragile particles that are easily destroyed.

Therefore, in **Paper I** we developed embedding and thin-sectioning of structurally preserved marine snow for structural analysis of the aggregate matrix and taxonomic identification of aggregate colonizers. We used a variety of stains for semi-quantitative measurements of aggregate porosity, and tested methods for taxonomic investigation of aggregate colonizers. Preserving the spatial structure of marine snow offers new possibilities to study the microstructure of marine aggregates in relation to aggregate colonizers. Cutting thin-sections between 5 to 100 µm enables examination of marine snow constituents and colonizers of varying sizes from bacteria over protozoans to phytoplankton. Coupled with taxonomic staining, embedding and thin-sectioning of marine snow can improve our knowledge of small-scale physical and biological processes associated with the biological carbon pump.

In **Paper II,** we developed hard resin-embedding and thin-sectioning of structurally preserved aggregates in addition to the soft-embedding method developed in Paper I. We again used Alcian Blue and Coomassie Blue to visualize the aggregate matrix and used DNA stains to-localize aggregate colonizers within the matrix. Furthermore, we developed a protocol for NanoSIMS analsysis of aggregate thin-sections for the investigation of isotope and element distributions. The slicing-

thickness of 2 µm of methacrylate-embedded samples enable very high resolution investigations of the aggregate matrix, including sub-cellular structures of aggregate colonizers. NanoSIMS analysis facilitates the investigation of niche partitioning of microbial consortia within aggregates, and potentially enables the detection of anaerobic metabolic processes in marine snow, for example sulfate reduction. This method can improve our view of element cycling within particle-associated microenvironments, and their biogeochemical implications.

The settling velocity of aggregates is one of the key determinants of carbon export efficiency as it controls how much carbon can be degraded per meter settled. Because of their high heterogeneity, the settling behavior of in situ aggregates is highly variable and the factors controlling settling velocity need further elucidation.

In **Paper III** we used Particle Image Velocimetry to visualize the flow field around in situ collected, natural marine aggregates to gain a better understanding of their settling behavior. We used this data to derive the drag coefficient of each aggregate using a mathematical model. We did microscopic imaging and measured independent parameters including aggregate size, settling velocity, solid hydrated density, and different shape factors for a comprehensive aggregate characterization. We found that the flow fields around natural marine snow strongly resembled those of impermeable, perfect agar spheres of comparable size and settling velocity. This implies that aggregate composition, porosity, and microstructures on the aggregate surface have little to no influence on overall settling behavior. Furthermore, it strongly suggests that the permeability of the aggregates collected in this study (which are representative of a large fraction of marine aggregates), is negligible, and that diffusion governs transport and mass exchange of gases and solutes into and out of aggregates, which has important consequences for the microbial colonization of settling aggregates.

In **Paper IV,** we incubated the diatom *Skeletonema marinoi* with different concentrations of plastic microfibers in roller tanks to examine the impact from microfibers on aggregate formation, size-distribution, settling velocity, and carbon content over time. The measurements of particle volume, settling velocity, and carbon

content in each treatment allowed us to estimate the impact from microfibers on the in potential export flux. Incorporation of microfibers into the aggregates reduced their size, size-specific settling velocities, and carbon content. During the initial phase of the study we even observed positively buoyant diatom aggregates when microfibers were incorporated. Together this resulted in a significant lower potential particulate organic carbon flux when comparing to the treatment without addition of microfibers. Since most major ocean basins are currently contaminated by microplastic, it is likely that the biological carbon pump is already compromised by the presence of microplastic.

ZUSAMMENFASSUNG

Sinkende organische Aggregate sind ein Hauptbestandteil der biologischen Kohlenstoffpumpe. Marine Aggregate sind zusammen mit Kotballen für den Großteil des organischen Kohlenstoffexports von der Meeresoberfläche in das Meeresinnere verantwortlich, wo Kohlenstoff über geologische Zeiträume gespeichert werden kann. Jedoch sinkt nur ein sehr geringer Anteil an Aggregaten überhaupt aus den oberen 200 Metern der Wassersäule aus, da sie vorher von Zooplankton und Bakterien in der Wassersäule gegrast und besiedelt werden. Umwandlungen organischer Stoffe durch mikrobiellen Abbau spielen eine Schlüsselrolle für das Schicksal organischen Kohlenstoffs in den Ozeanen. Über die Mikrostrukturen auf Einzel- und Subaggregatebene ist jedoch vergleichsweise wenig bekannt, da es sich bei Aggregaten um äußerst zerbrechliche Partikel handelt, die leicht zerstört werden können.

Paper I beschreibt die von uns weiterentwickelte Methode, marine Aggregate ohne Verlust der 3-dimensionalen Struktur in ein viskoses Kryogel einzubetten, einzufrieren, und dann wie einen Laib Brot (nur sehr viel dünner) zu schneiden. Dies ermöglicht eine räumlich aufgelöste Untersuchung der Aggregatmatrix und die Einfärbung ausgewählter taxonomischer Gruppen von Bakterien, die das Aggregat besiedeln. Der Erhalt der räumlichen Struktur bietet neue Möglichkeiten, die Mikrostruktur im Verhältnis zu mikrobiellen Besiedlern zu untersuchen. Dünnschnitte zwischen 5 und 100 µm ermöglichen die Untersuchung von Aggregatbestandteilen und Besiedlern unterschiedlicher Größe, von Bakterien über Protozoen bis hin zu Phytoplankton. In Verbindung mit taxonomischen Färbungen kann das Einbetten und Dünnschneiden von marinen Aggregaten unser Wissen über kleinräumige physikalische und biologische Prozesse verbessern, die mit der biologischen Kohlenstoffpumpe verbunden sind.

In **Paper II** haben wir, zusätzlich zu der in Paper I entwickelten Methode, das Einbetten und Schneiden von Aggregaten in Harzen entwickelt. Auch diese Methode ist mit der gleichzeitigen Abbildung der Aggregatmatrix und von Besiedlern der Matrix

kompatibel. Darüber hinaus ermöglicht sie die Untersuchung von Isotopen- und Elementverteilungen in Dünnschnitten mittels NanoSIMS-Analyse. Die Schnittdicke von 2 µm ermöglicht hochauflösende Untersuchungen der Matrix, einschließlich subzellulärer Strukturen von Besiedlern. Die NanoSIMS-Analyse erleichtert die Untersuchung der Nischenverteilung von mikrobiellen Konsortien innerhalb von Aggregaten und ermöglicht theoretisch den Nachweis von anaeroben Stoffwechselprozessen in marinen Aggregate, z. B. Sulfatreduktion. Diese Methode hat das Potential, unser Verständnis der Elementkreisläufe in Aggregat-assoziierten Mikroumgebungen und ihrer biogeochemischen Auswirkungen zu verbessern.

Die Sinkgeschwindigkeit von Aggregaten ist einer der Schlüsselfaktoren für die Effizienz des Kohlenstoffexports, da sie steuert, wieviel Kohlenstoff pro gesunkenem Meter abgebaut werden kann. Aufgrund ihrer hohen Heterogenität ist das Sinkverhalten von natürlich Aggregaten äußerst variabel, und die Faktoren, die die Sinkgeschwindigkeit steuern, bedürfen genauerer Untersuchungen.

In **Paper III** visualisieren wir das Strömungsfeld natürlicher Aggregate mit „Particle Image Velocimetry“, um so ein besseres Verständnis für das Sinkverhalten mariner Aggregate zu erlangen. Dank dieser Aufnahmen konnten wir den Strömmungswiderstandskoeffizienten aller beprobten Aggregate mithilfe eines mathematischen Modells ableiten. Mikroskopische Aufnahmen jedes Aggregates sowie die Messung unabhängiger Parametern wie Aggregatgröße, Sinkgeschwindigkeit, Dichte der festen Bestandteile und verschiedener Formfaktoren, ermöglichten eine umfassende Charakterisierung von in situ beprobten Aggregaten. Unsere Ergebnisse zeigten, dass die Strömungsfelder um natürliche Aggregate sehr stark denen von undurchlässigen, perfekt sphärischen Agarkugeln vergleichbarer Größe und Sinkgeschwindigkeit ähnelten. Dies impliziert, dass die Aggregatzusammensetzung, Porosität, und Mikrostrukturen auf der Aggregatoberfläche Alles in Allem einen verschwindend geringen Einfluss auf das Sinkverhalten haben. Dies deutet sehr stark darauf hin, dass die Permeabilität der in dieser Studie gesammelten Aggregate vernachlässigbar ist, und stattdessen Diffusion den Transport und Massenaustausch

von Gasen und gelösten Stoffen in und aus Aggregaten kontrolliert. Dies hat wichtige Konsequenzen für die mikrobielle Besiedlung sinkender Aggregate.

In **Paper IV** haben wir die Kieselalge *Skeletonema marinoi* mit unterschiedlichen Konzentrationen von Kunstoffmikrofasern in Rolltanks inkubiert, um den Einfluss von Mikrofasern auf Aggregatbildung, Größenverteilung, Sinkgeschwindigkeit und Kohlenstoffgehalt über Zeit zu untersuchen. Die Messungen des Partikelvolumens, der Sinkgeschwindigkeit und des Kohlenstoffgehalts in jeder Behandlung ermöglichten es uns, den Einfluss von Mikrofasern auf den möglichen Exportfluss abzuschätzen. Einarbeitung von Mikrofasern in Aggregate reduzierte deren Größe, größenspezifische Sinkgeschwindigkeiten, und deren Kohlenstoffgehalt. In der Anfangsphase der Inkubation beobachteten wir sogar auftreibende Diatomeenaggregate, in Rolltanks mit Mikrofasern. Zusammen führte dies im Vergleich zur Behandlung ohne Zugabe von Mikrofasern zu einem signifikant niedrigeren potenziellen Kohlenstofffluss. Da die meisten großen Meeresbecken derzeit durch Mikroplastik kontaminiert sind, ist es sehr wahrscheinlich, dass die biologische Kohlenstoffpumpe bereits durch Mikroplastik beeinflusst ist.

ACKNOWLEDGMENTS

Above all, I thank my supervisor Morten Iversen for the last three years and beyond. Thank you for taking me places, for mentoring me and for giving me the space and the inspiration to SCIENCE [sic]. Sincere thanks also to my 2nd reviewer Helle Ploug for taking the time to evaluate my thesis.

This work is very much the product of great collaborations. I thank Soeren Ahmerkamp, Andreas Rogge, Benedikt Geier, Cordelia Roberts, all co-authors, students, and many others who have helped me with my work and have given me advice. I also thank the captain, crew, and fellow scientists of FS Poseidon, FS Polarstern, RV Discovery and B/O Sarmiento de Gamboa for enabling me to do the work presented in this thesis.

I am indebted to all my current and former colleagues in the SeaPump group. I want to express special thanks to Helga van der Jagt and Christian Konrad, who helped me find my footing when I first arrived and have been there for me from day one. I am also grateful to my office buddies for the good atmosphere and for putting up with my shenanigans.

Another source of support, comfort and joy are my fantastic friends. Special thanks go out to my fellow MarMic survivors Andreas Sichert, Greta Giljan, Dolma Michellod and Candice Thorstenson. I am really lucky to have you. I also want to acknowledge those who have inspired me to pursue a PhD: Maria and David Chamberlain, and Isla Myers- Smith.

This thesis would have been a lot harder to write without great coffee and someone who kept me sane and had my back. Thank you, Christoph! Lastly, I thank my family, especially my mother Maria, who has always supported me unconditionally and encourages me to choose adventure.

TABLE OF CONTENTS

INTRODUCTION

1. Biological carbon sequestration in the ocean

Life on our planet is carbon-based.

There is a total of 550 gigatonnes of carbon distributed among all the kingdoms of life (Bar-On et al., 2018), which is equivalent to a cargo train filled with coal long enough to embrace the earth at the equator 3,430 times. This biomass is distributed among reservoirs that have the capacity to both store and release carbon ("carbon pools"), and is moved by processes that can transfer carbon between pools ("fluxes"). The ocean constitutes the largest of the five broad carbon pools (the others being the atmosphere, terrestrial vegetation, soils, and fossil fuels) (Lal, 2008).

The oceans' capacity to sequester atmospheric carbon dioxide over decadal to millennial time scale makes them an important carbon sink, both for naturally emitted and anthropogenic CO_2 (Quéré et al., 2018; Ciais et al., 2014; Passow and Carlson, 2012). Ocean carbon sequestration is mediated via physical and biological pumps which transport carbon that is dissolved in the ocean surface to the deep ocean, thereby causing a gradient of dissolved inorganic carbon that is increasing with depth (Gruber and Sarmiento, 2002; Volk and Hoffert, 1985). The removal of dissolved inorganic carbon (DIC) from the ocean surface to the deep sea lowers surface DIC concentrations, which in turn enables re-uptake of atmospheric carbon via air-sea gas exchange in equilibrium with atmospheric CO_2 concentrations.

In an abiotic ("Strangelove") ocean, carbon sequestration is induced by the temperature-dependent solubility of DIC. This results in carbon sequestration driven by the formation of DIC-rich deep water at high latitudes which becomes physically separated from the atmosphere by warmer, DIC-deplete water masses as it moves along the ocean conveyor belt. This mechanism of C sequestration is known as the "solubility pump" (Volk and Hoffert, 1985).

In a living ocean, marine biota create additional carbon pumps: Shell-forming organisms such as coccolithophorids, foraminifera, pteropods, and some calcareous

dinoflagellates use soluble hydrogencarbonate (HCO_3^-; one of three marine carbonate species) to form insoluble calcite or aragonite minerals in their shells. On short time-scales, this reduces net uptake of DIC due to a shift in the equilibrium of carbonate species, leading to the release of 0.6 mol CO_2 per 1 mol HCO_3^- (Frankignoulle et al., 1994). On geological time scales, sinking and sedimentation of calcareous organisms ("carbonate pump") lead to the formation of carbonate rocks which are some of the largest carbon reservoirs on earth (IPCC 2013).

The most important process for ocean carbon sequestration is the "biological carbon pump" (fig. 1). The biological carbon pump is built on the assimilation of DIC into particulate organic carbon (POC) through photosynthesis. Marine phytoplankton fix 50 PgC yr^{-1}, making up half of the annual global primary production (Field et al., 1998). When single cells collide and stick together, they form aggregates that sink out of the euphotic zone towards the deep ocean, thereby removing the assimilated carbon from the ocean surface and transporting it into the ocean interior (Alldredge and Silver, 1988; Alldredge and Gotschalk, 1988). By definition, aggregates exceeding a diameter of 0.5 mm are referred to as "marine snow" (Shanks and Trent, 1980). Together with fecal pellets egested by phytoplankton-grazing organisms, settling marine aggregates drive the biological carbon pump (Volk and Hoffert, 1985). Of the three pumps described, the biological carbon has by far the largest impact on oceanic carbon sequestration, accounting for 70% of the surface-to-deep gradient (Gruber and Sarmiento, 2002; Passow and Carlson, 2012).

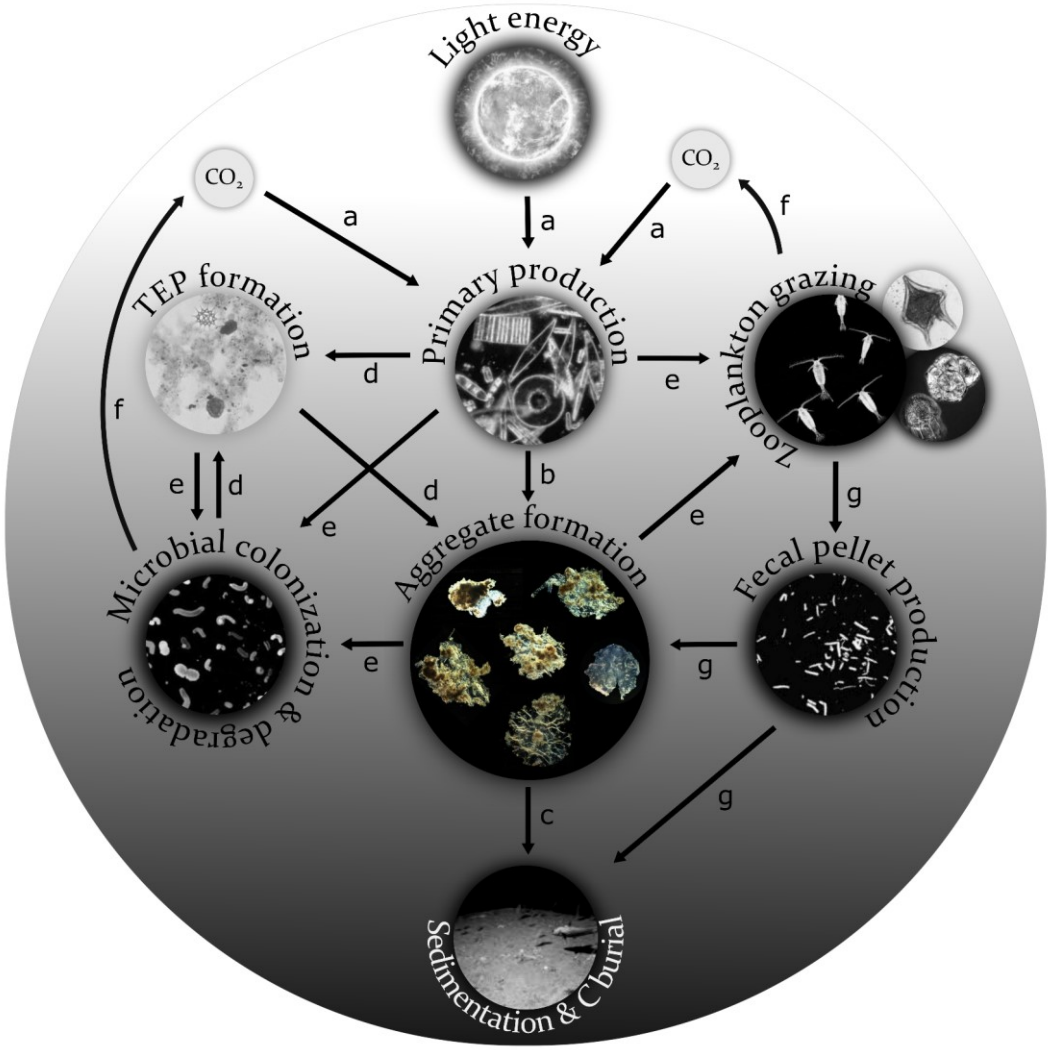

Figure 1. Schematic of the biological carbon pump and the biotic processes driving it (please refer to the main text for references): (a) Light energy drives the assimilation of particulate organic carbon by primary producers in the ocean surface; (b) Coagulation of phytoplankton leads to the formation of aggregates; (c) Settling aggregates export carbon out of the surface into the ocean interior, were carbon can be sequestered on long time scales. The magnitude of C export via the biological pump is controlled by biotically driven processes in the water column, which include (d) formation of TEP, which can be enhanced by phytoplankton-bacteria interactions and stimulates aggregate formation; (e) Zooplankton grazing and microbial degradation of phytoplankton cells and marine aggregates, which leads to (f) remineralization of POC back to CO_2, and also (g) the production of zooplankton fecal pellets, which can either settle out directly or be incorporated in aggregates. Image credits: Deep East 2001, NOAA/OER; E. DeLong, D. Karl, N. Hulbrit; Warren Photographic; 2013 All Enthusiast, Inc; Thuy et al. (2017); Dagg et al. (2014)

The conventional way of assessing the strength of the biological carbon pump assumes a process driven near-exclusively by gravitational settling of aggregates out of the ocean surface (e.g., Buesseler and Boyd, 2009). This simplistic concept underestimates the impact of physical mixing processes (Stukel et al., 2018), vertical migration of marine biota (Packard and Gómez, 2013; Hernández-León et al., 2001; Vinogradov, 1997), and the role of suspended organic matter (Riley et al., 2012). These processes can be unified in a conceptualization of the biological carbon pump that differentiates between a purely gravity-driven pump and "particle-injection pumps" (PIPs; Boyd et al., 2019) (fig. 2).

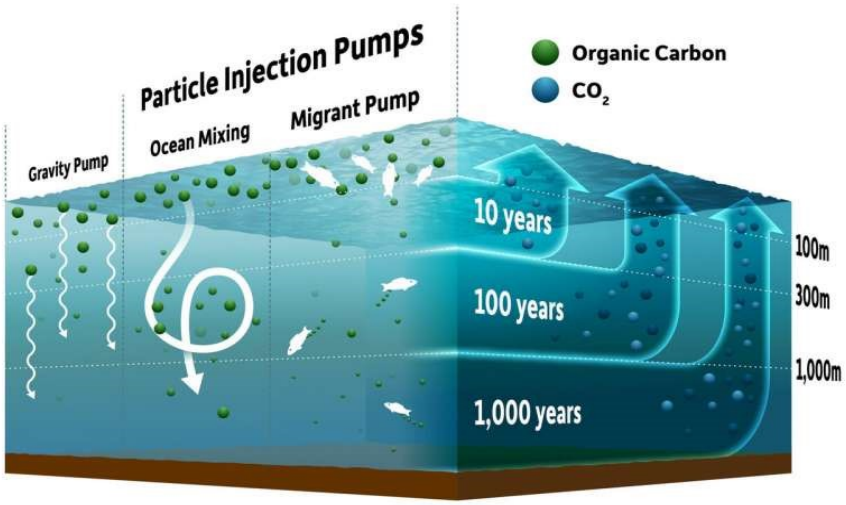

Figure 2. Simplified depiction of selected particle injection pumps in their role in biological carbon sequestration. Image credit: University of Rochester illustration/ Michael Osadciw

PIPs cut short the distance that organic matter needs to bridge to reach depths where it can be sequestered long-term by injecting particles deeper into the water column. Some PIPs are driven by physical mixing processes, for example by vertical circulation associated with fronts and eddies ("eddy-subduction pump"), or dynamic shallowing and deepening of the mixed layer ("mixed-layer pump"), while other PIPs are driven by biology such as zooplankton diel migration ("mesopelagic-migrant pump") or lipid catabolism at hibernation depth ("seasonal lipid pump"). Different PIPs act on very different time scales (from days to centuries), and vary in strength and relative importance depending on season,

region, and depth. The important commonality between PIPs is that they can act on suspended as well as settling particles and inclusion of mechanisms other than gravitational settling can help to resolve mismatches between the carbon demand of pelagic biota and the carbon supplied by considering C export by gravitational settling out of the sea surface alone (Boyd et al., 2019).

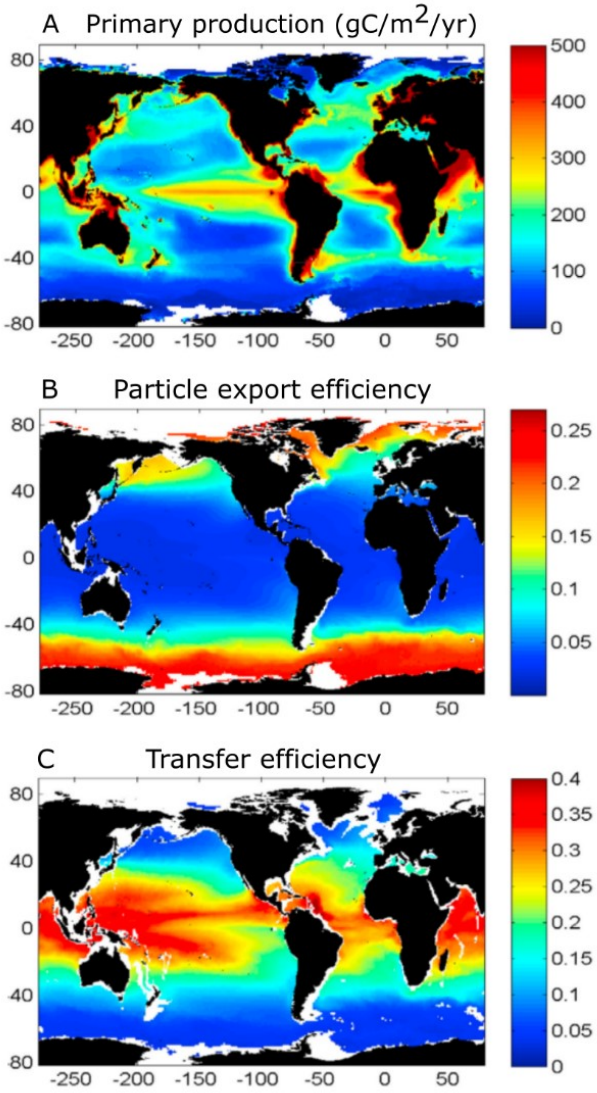

Figure 3. Comparison of a) global primary production, b) particle export efficiency, and c) transfer efficiency. Figure modified from Henson et al. (2012).

Overall, the biological carbon pump is relatively inefficient. Of the 50 PgC that are fixed photosynthetically every year, only about 10% make it out of the euphotic zone

(Martin et al., 1987), and about 2% of make it past 2000 m where carbon can be sequestered over long time scales (Tréguer et al., 2003). Particle export is defined as the amount of POC at 100 m water depth as a function of primary production, while transfer efficiency is the amount of POC that makes it from 100 m to 2000 m depth (fig. 3, Henson et al., 2012). Both particle export and transfer efficiency have large regional, seasonal, and temporal variations, which are caused to some extent by the composition and settling velocity of marine aggregates as well as the amount of grazing and microbial degradation. In the following, these aspects will be illuminated separately.

2. Physical formation and composition of marine aggregates

The transformation of small suspended particles into large, fast-sinking marine snow proceeds via three coupled mechanisms (McCave, 1984): (i) Brownian motion, i.e., the random movement of particles resulting from collisions with atoms in the ambient fluid, (ii) differential settling, i.e., scavenging of slow-sinking particles by fast particles, and (iii) turbulence, i.e., physical mixing of water masses resulting in particle collision. The composition and diversity of the particle standing stock in the surface ocean directly influences the amount of aggregation and the composition of the resulting aggregates, with immediate consequences for the magnitude of the export flux (Alldredge and Gotschalk, 1989; Riebesell, 1993; Bach et al., 2016). The diversity and heterogeneity of aggregates over depth and season is indicative of the complex processes leading to their formation and export (fig. 4).

Seasonal phytoplankton blooms commonly result in the formation of diatom aggregates (Kranck and Milligan, 1988; Alldredge and Gotschalk, 1989; Riebesell, 1991). Aggregation efficiency and export flux is strongly influenced by the composition of the bloom (Henson et al., 2012). Aggregation and mass sedimentation has even been found to be a potential bloom-terminating process (Kiørboe et al., 1994). Zooplankton grazing and egestion leads to frequent incorporation of fecal pellets (or pellet fragments) into marine aggregates (Alldregde and Silver, 1988). In areas with high dust input, lithogenic ballasting minerals are also frequently incorporated (Jagt et al., 2018; Passow and Rocha, 2006).

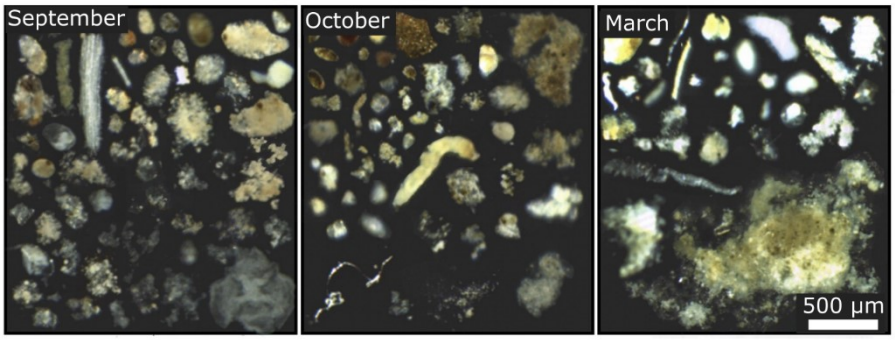

Figure 4. Sediment trap samples showing the diversity of settling marine aggregates. Modified from Durkin et al. (2015).

Marine snow is also formed by flux-feeding zooplankton (Alldredge and Silver, 1988). Organisms such as pteropods and appendicularians use specialized mucilaginous feeding structures to filter food particles out of the sinking carbon flux (Lalli and Gilmer, 1989; Gilmer and Harbison, 1986). They then consume and egest these webs, or discard and replace them if clogged. In the case of appendicularians, this process can be repeated up to 26 times a day (Sato et al., 2001). The discarded webs and houses, which are full of particulate organic matter, settle out towards the deep ocean, and contribute to the vertical carbon flux (Jackson, 1993).

Aggregate formation is heavily dependent on the probability of particles sticking together upon collision, which can be expressed as the "stickiness" of a particle. Of any of the commonly found particles in marine snow, diatoms have the highest stickiness (Alldredge and McGillivary, 1991), although stickiness can vary between species by orders of magnitude (Hansen et al., 1995; Kiørboe and Hansen, 1993). A strong contributor to stickiness is the formation of transparent exopolymer particles (TEP) (Alldredge et al., 1998; Engel, 2000; Passow, 2002), which are at least partly formed through phytoplankton-bacteria interactions (Grossart et al., 2006a; Grossart et al., 2006b; Gärdes et al., 2011). TEP is a complex mixture of organic molecules that is defined as being stainable with Alcian Blue and belongs to a larger group of high-molecular weight polymers termed exopolymeric substances (EPS) (Alldredge et al., 1993; Passow and Alldredge, 1995). Marine snow contains high amounts of TEP that act like a glue holding the matrix together and directly affect

aggregation efficiency and settling velocity (Alldredge et al., 1993; Engel, 2000; Engel and Schartau, 1999; Passow, 2002; Long and Azam, 1996; Arrigo, 2007).

Marine aggregates have highly variable structural properties, which depend heavily on the primary particles they are formed from (Alldredge and Silver, 1988; Iversen and Ploug 2010). The excess density of marine snow, i.e., the difference in aggregate density compared to the density of the ambient fluid depends on the density of the primary particles. However, the compactness of the aggregates, i.e., how much space there is between primary particle inside the aggregate, seems to be more important in determining the excess density (Iversen and Ploug; 2010). Ballasted aggregates often have high excess density compared to non-ballasted aggregates, which holds true for both lithogenic (Iversen and Robert, 2015) and biogenic ballasting (Iversen and Ploug, 2010). Aggregates with high TEP:solid particle fractions on the other hand have very low excess densities (Mari et al., 2005, 2017).

The composition of primary particles also affects the porosity of aggregates. For example, aggregates formed from mucilage have exceedingly high porosities greater than 99.9% (Alldredge and Crocker, 1995), followed by phytoplankton aggregates with porosities between 95-99% (Alldredge and Gotschalk, 1988; Ploug et al., 2008). Fecal pellets on the other hand are very tightly packed and have comparatively low porosities of 40-60% (Ploug et al., 2008). A long-standing question is if these pores allow advective flow, i.e., if aggregates are permeable. Evidence of this is conflicted and sparse, and it has been hypothesized that aggregates are impermeable due to clogging of pore space by TEP (Ploug and Passow, 2007).

3. Settling of marine aggregates

The magnitude of carbon export is closely linked to the settling velocity of aggregates, because the settling velocity plays an important part in the amount of carbon that can be degraded per meter settled (termed the “remineralization length scale”; Iversen and Ploug, 2010). Marine aggregates have settling velocities ranging from just two to several thousand

meters per day (Alldredge and Gotschalk, 1988; Laurenceau-Cornec et al., 2015 and references therein) (fig. 5).

The structural and physical properties defined by the composition of marine aggregates directly influence their settling velocities (Iversen and Ploug 2010, Bach et al., 2016). Aggregates that are high in dense materials have high excess densities which results in an increase in size-specific settling velocities: Zooplankton fecal pellets for example consist largely of indigestible phytoplankton frustules and settle between 5 and 2700 m/day (Turner et al., 2000, and references therein). Marine snow with incorporated lithogenic (dust, clay, silt) or biogenic ($CaCO_3$, silicate) ballasting minerals also have high size-specific settling velocities compared to non-ballasted aggregates (Iversen and Ploug, 2010; Ploug et al., 2008; Lombard et al., 2013a; Iversen and Robert, 2015; Jagt et al., 2018).

Other aggregate components can have the opposite effect. TEP, for instance, can reduce aggregate settling velocity because they are positively buoyant (Mari et al., 2017; Azetsu-Scott and Passow, 2004). Despite the important role of TEP in aggregate formation, marine aggregates only sink when the fraction of high-density particles is high enough to compensate the positive buoyancy of TEP (fig. 3 in Azetsu-Scott and Passow [2004]). A large fraction of dense particles compared to TEP will lead to immediate downward export, whereas a small fraction of dense particles compared to TEP will lead to prolonged retention in the euphotic zone and a spatial decoupling of aggregate formation and export (Mari et al., 2017).

Aggregate porosity also heavily influences the settling velocity of marine snow: pore water that is entrained in the aggregate pore space is continually exchanged via diffusion as aggregates settle. When an aggregate crosses a pycnocline, it can be retained at the density interface until the pore water is fully exchanged, which increases retention time and biotic remineralization in the surface ocean (Prairie et al., 2013; MacIntyre et al., 1995).

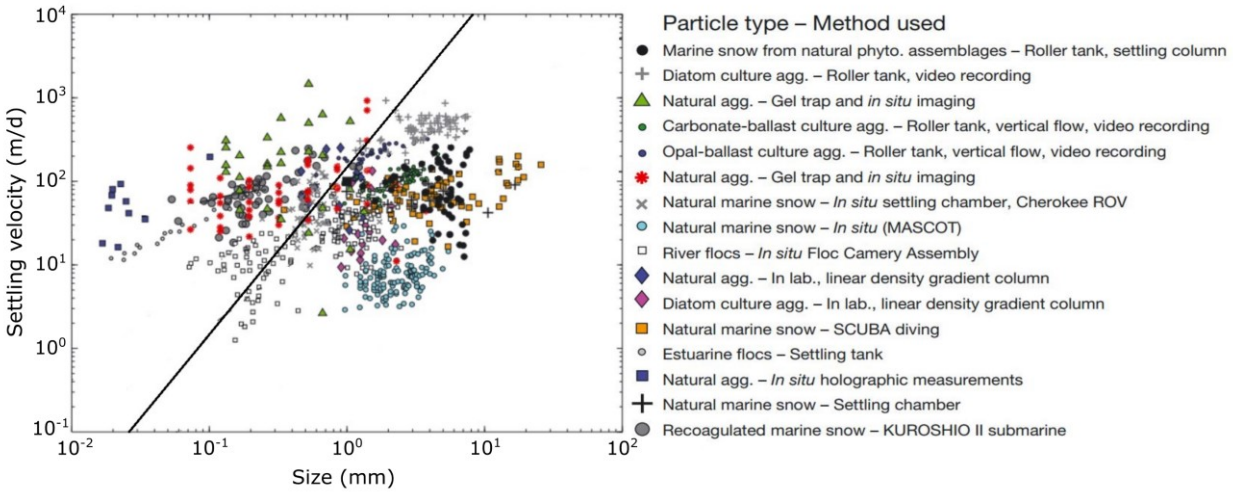

Figure 5. Range of size and settling velocities for natural and laboratory formed aggregates. Modified from Laurenceau-Cornec et al. (2015). The solid black line depicts the size-to-settling relationship of aggregates whose settling velocities were calculated using Stokes' law.

As aggregates settle through the water column, they are acted upon by forces that control their settling and govern solute and mass exchange with the ambient fluid. These forces act the same regardless of whether the aggregate is moving through a stagnant fluid, or the aggregate is stationary with water flow moving around it. For simplicity, I will describe them using an aggregate moving down the water column.

All settling aggregates experience fluid resistance, also called drag force, which is acting opposite to the settling direction. The drag force is directly dependent on the velocity of the aggregate and decreases the fluid velocity in its path relative to the aggregate (Stokes 1851). A settling aggregate will accelerate until the drag force is equal to the downward force of gravity. When these two forces are in balance, an aggregate has reached its terminal settling velocity (Stokes, 1851). The dimensionless drag coefficient can be calculated to quantitatively describe the drag experienced by aggregates, and is commonly determined based on the Reynolds number (*Re*; White, 1974).

The Reynolds number describes the relative importance of inertial forces to viscous forces acting on a settling aggregate and is dependent on its size, settling velocity, and the kinematic viscosity of the surrounding fluid. The Reynolds number is also used to predict flow patterns around moving objects (fig. 6). At low *Re*, fluid flow is laminar, which means

that layers of fluid are smoothly moving around a settling aggregate without lateral mixing. At higher *Re*, differences in the fluid speed and direction result in the formation of vortices or turbulence (fig. 6). Reynolds numbers of marine aggregates range from 0.2 to 32 (Alldredge and Gotschalk, 1988; Ploug et al., 2008; Iversen and Ploug, 2013), which suggests that flow around them is predominantly laminar, with the possibility of vortices forming at the back of the settling aggregate at higher *Re* (fig. 6). The *Re* regime of an aggregate further affects the appearance and the thickness of the fluid boundary layer, i.e., the layer of fluid around the settling aggregate where the effects of viscosity play a role. The thickness of the boundary is defined as the distance from the aggregate surface to the point where flow velocity is reduced to a certain percentage of the maximum flow velocity, usually 99% (e.g., Datta and Mishra, 1982).

An important descriptor of settling behavior that is closely linked to the Reynolds number is the flow field around aggregates, which is the visual representation of the magnitude and direction of the flow at every point around an aggregate. At low *Re*, aggregates have very symmetric flow fields with thick size-specific boundary layer and shallow velocity gradients within the boundary layer. With increasing *Re*, the flow field becomes increasingly asymmetric, with a thinning boundary layer at the equator and a longer “tail”, and the velocity gradients in the boundary layer become increasingly steep (fig.1 in Kiørboe et al., 2003).

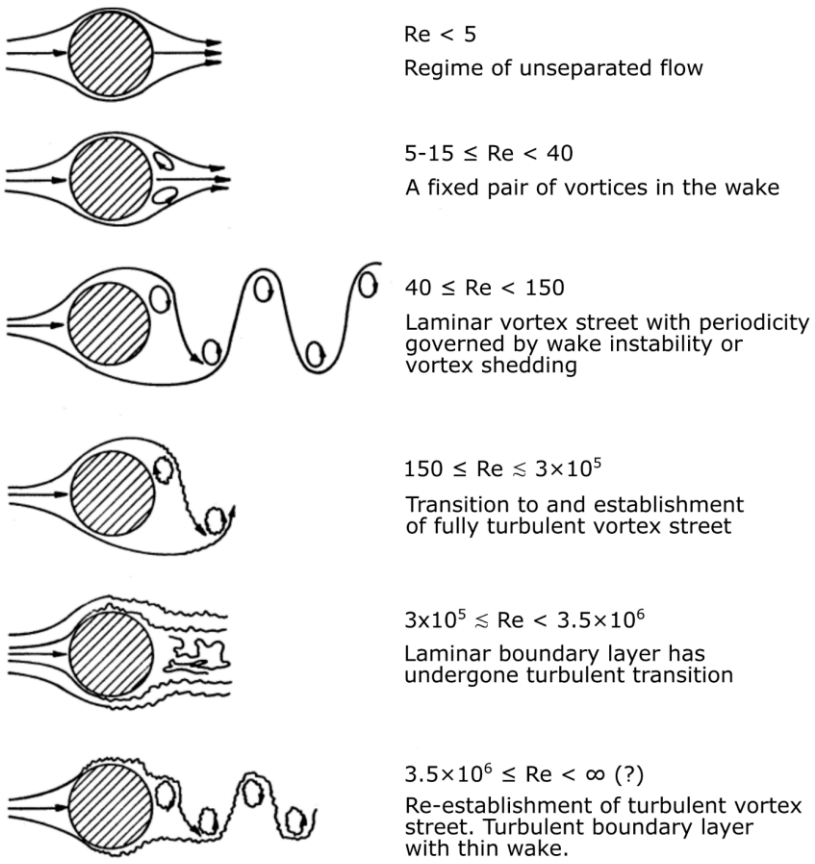

Figure 6. Streamlines across a cylinder at increasing Reynolds number. Modified from Lienhard (1966).

Wherever settling velocity of aggregates cannot be measured directly, it is possible to theoretically derive the settling velocity of aggregates using Stokes' law (Stokes, 1851). Stokes' law poses that settling velocity is a function of the squared aggregate diameter and the density of an aggregate—under the assumptions that flow around the aggregate is laminar, the aggregate is perfectly spherical, composed of homogeneous material, has a smooth surface, and is impermeable (Stokes, 1851). As discussed in previous chapters, marine snow does not comply with these assumptions, which can result in the deviations between measured and calculated settling velocities that are frequently observed (fig. 5; (Stemmann et al., 2004; Laurenceau-Cornec et al., 2015).

4. The role of zooplankton and bacteria in carbon flux attenuation

Carbon flux attenuation is controlled by heterotrophic degradation of settling aggregates. Grazing zooplankton and colonizing bacteria re-mineralize POC back to CO_2 (Simon et al., 2002; Iversen et al., 2010; Stemmann et al., 2004). The remineralization rate largely depends on aggregate settling velocity and the lability of the organic matter within (e.g., Grossart and Ploug, 2001). High extracellular enzymatic activities effect the release of dissolved organic matter (DOM) which can act as chemical attractants (fig. 7; Karner and Herndl, 1992; Arnosti, 2003). Therefore, aggregates are considered nutrient hotspots in the ocean (Azam and Long, 2001).

Along the water column, zooplankton seem to control the upper ocean carbon flux attenuation (Iversen et al., 2016; Iversen et al., 2010; Jackson and Checkley, 2011), while deep flux attenuation is seemingly dominated by microbial degradation (Stemmann et al., 2004). However, the relative contribution of zooplankton and bacteria to flux attenuation also depends on geographical region. Some regions are dominated by zooplankton control (Iversen et al., 2010, 2016; Jackson and Checkley, 2011), whereas others are dominated by bacteria (Giering et al., 2014) and protozoans, e.g., dinoflagellates (Poulsen and Iversen, 2008; Poulsen et al., 2011).

Zooplankton and bacteria have fundamentally different strategies to detect and feed on particles, which is due to them differing in size on an order of magnitude. Both zooplankton and bacteria can sense chemical cues. Swimming of certain copepod species is designed to maximize search space (Kiørboe, 2011; Olsen et al., 2000). When they encounter the solute plume of a settling aggregate, they can follow the plume to find and graze on the aggregate (Kiørboe and Thygesen, 2001; Lombard et al., 2013b). Chemotactic bacteria can sense chemical gradients followed by a run-and-tumble behavior that directs them to solute concentration maxima. For this reason, bacteria concentrate in the plumes of settling particles until the plume dissipates (Stocker et al., 2008). This mechanism does not allow chemotactic bacteria to follow the plume of aggregates as zooplankton does (Roman Stocker, pers. comm.). In laboratory systems with model particles, chemotactic bacteria can colonize and rapidly degrade particles (Datta et al., 2016; Enke et al., 2018;

Stocker and Seymour, 2012; Grossart et al., 2003; Kiørboe et al., 2003, 2002). However, assembly of the microbial community and colonization of natural settling aggregates is poorly studied.

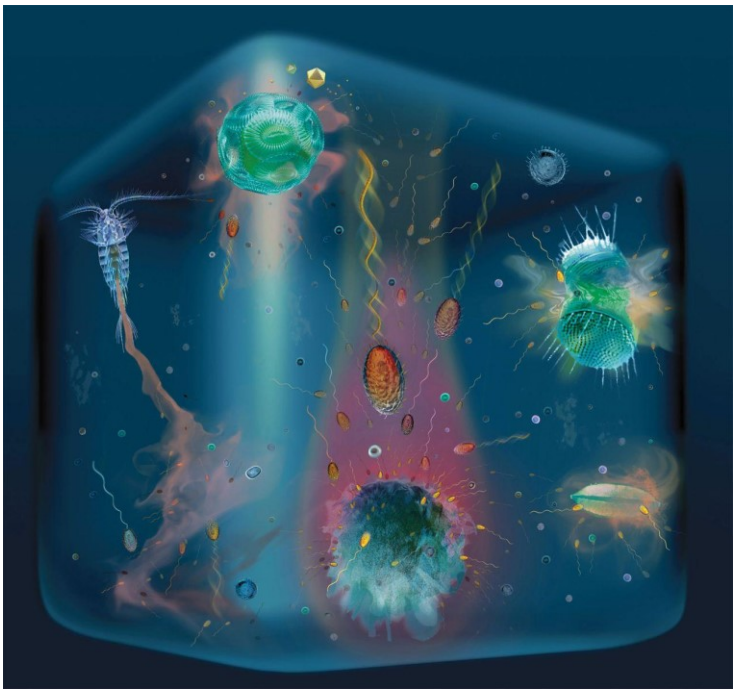

Figure 7. Artistic impression of gradients and hotspots encountered by bacteria in the water column. Reproduced from Stocker (2002). Image credits: R. Stocker, J. R. Seymour, G. Gorick

It was previously believed that bacteria would only remain on a settling aggregate for minutes to hours (Kiørboe et al., 2002) suggesting a constant exchange of bacteria between the ambient water column and the aggregate during settling. Yet, recent studies using both size fractionation and in situ collected aggregates have found little connection between bacteria in the water column and those associated with aggregates at depth (Bachmann et al., 2018; Fadeev et al., 2018; Mestre et al., 2017; Thiele et al., 2014). Instead, it is suggested that aggregates are colonized in the surface ocean during formation, and that changes in bacterial communities of aggregates with increasing depth are caused by successional dynamics of the resident bacterial assemblage rather than new colonization from the water column (Pelve et al., 2017; Thiele et al., 2014).

In addition to chemical cues, zooplankton can use hydrodynamic cues to detect food particles, including settling aggregates (Sanne and Kiørboe, 2012; Kiørboe and Thygesen, 2001; Visser, 2001). No such behavior is known from bacteria, possibly because their small size prevents them from sensing and reacting to velocity gradients the way zooplankton does. However, motile bacteria can benefit from hydrodynamics-mediated trapping, which enables passive capture of approaching microorganims onto a settling aggregate (Desai et al., 2019). Processes like this create an intimate connection between the settling behavior of aggregates and microbial colonization, yet their interactions are not well understood.

5. The biological carbon pump in the anthropocene

The biological pump is intimately connected to environmental changes induced in the anthropocene (Riebesell et al., 2009). Between 1870 and 2017, the oceans have taken up about 25% of total anthropogenic CO_2 emissions (Quéré et al., 2018). Because of air-sea equilibrium, rising CO_2 concentrations go hand in hand with increasing concentrations of sea surface DIC (Caldeira and Wickett, 2003; McNeil and Matear, 2006) leading to "ocean carbonation" (Riebesell et al., 2009).

There are two contrasting scenarios of how ocean carbonation can affect the efficiency of the biological pump: Increased DIC concentrations lower ocean pH (an effect known as "ocean acidification"; Caldeira and Wickett, 2003) which, among other things, reduces the availability of carbonate ions for calcium-carbonate shell forming organisms (Orr et al., 2005). This can reduce the settling velocity of these organisms and lead to a decrease in C export (Biermann and Engel, 2010). At the same time, an increase of surface DIC concentrations can lead to an increase in primary production (Hein and Sand-Jensen, 1997), POC formation (Engel et al., 2013) and TEP production (Engel, 2002), all of which can increase potential C export. However, TEP formation, aggregation and export dynamics can vary strongly depending on the synergies among multiple stress effects, suggesting a complex response to climate change (Mari et al., 2017; Cisternas-Novoa et al., 2019).

Rising atmospheric CO_2 concentrations have led to an increase in average global temperatures of approximately 0.2°C per 10 years (Vinnikov and Grody, 2003; Kerr, 1995).

This has increased mean sea surface temperatures by 0.18°C (Levitus et al., 2000; Levitus et al., 2012) and is melting Arctic sea ice (Notz and Stroeve, 2016; Johannessen, 2008) as well as changing global precipitation regimes (Pendergrass and Hartmann, 2014). Changes in water density, caused by decreasing salinity from meltwater discharge or increasing water temperature, affect surface mixed layer depth and lead to a decrease in vertical mixing ("stratification"). Stratification reduces the mixing and exchange of gases and nutrients in the water column. At low latitudes where the mixed layer is relatively shallow and surface nutrient concentration are low, primary producers rely on upward nutrient supply and stratification can be expected to reduce C export. At higher latitudes where the mixed layer is deep, the main limitation is light availability. Here, stratification leads to a shallowing of the mixed layer and an increase in POC production and potential export (Riebesell et al., 2009), although a countering effect of changes in the community composition on C export must not be ignored (Arrigo et al., 1999).

The reduced mixing of oxygen can intensify and expand oxygen minimum zones (OMZs), which does not directly affect primary production and POC formation, but affects grazing and carbon remineralization (Cavan et al., 2017). Because of oxygen limitation, OMZs are only sparsely populated by zooplankton (Wishner et al., 2013), and limited zooplankton grazing is confined to the surface (Williams et al., 2014) which is why most of the C remineralization in OMZs is microbial (Cavan et al., 2017). This reduced remineralization in OMZs can increase C export efficiency (Cavan et al., 2017), but it is uncertain if OMZ expansion will persist in the long-term (Resplandy, 2018).

Changes in environmental conditions caused by anthropogenic climate change also induce shifts in zooplankton community composition: In the Southern Ocean, increasing water temperatures have led to the range expansion of the tunicate *Salpa thompsoni* intruding into regions previously dominated exclusively by the Antarctic krill *Euphausia superba* (Atkinson et al., 2004; Pakhomov et al., 2002). Despite the high settling velocities measured for fresh, intact fecal pellets of *S. thompsoni*, they are recycled quickly in the upper water column, leading to an overall decrease in C export compared to krill (Iversen et al., 2016). Furthermore, a shift from the discriminate, size-selective grazing behavior of krill to indiscriminate grazing by salps can change particle-size spectra across the water

column, which can affect particle aggregation efficiency and aggregate formation (Burd, 2013; Jackson, 1995).

In addition to rising atmospheric CO_2 concentrations, other human activities such as overfishing, eutrophication and pollution also exert strong influences on marine ecosystem functioning (e.g., Daskalov et al., 2007; Diaz and Rosenberg, 2008; Derraik, 2002). Of special concern is the increase in microplastic pollution and the pervasiveness of microplastics in marine food webs (Galloway et al., 2017; Geyer et al., 2017). The occurrence of high concentrations of microfibers in deep-sea sediments has been attributed to incorporation of microplastics into settling aggregates including fecal pellets and marine snow (Van Cauwenberghe et al., 2013; Woodall et al., 2014). Aggregates readily incorporate microplastics and can export them to depth (Porter et al., 2018; Long et al., 2015). However, the effects of microplastic incorporation on the structure and settling behavior of marine aggregates, and concurrently on carbon export efficiency, are relatively unexplored.

6. Aims and objectives

The diversity of aggregates and their heterogeneous composition reflect the high spatio-temporal variability of the environment in which they are formed and through which they settle. The effect of structural heterogeneity on aggregate settling and degradation are difficult to study as this variability cannot be fully recreated in a controlled laboratory setting. Instead, techniques are needed to relate colonization and degradation of individual, in situ formed aggregates to their structural and physical properties using non-destructive sampling and imaging techniques. In this thesis, I develop methods to investigate the microstructure, microbial colonization, and settling behavior of in situ collected marine snow at the single-aggregate level. I also investigate the effect of changes in microstructure on aggregation and settling of laboratory-formed aggregates to gain a better mechanistic understanding of these processes. These are the specific objectives of my thesis:

I. Image the microstructure and selected microbial colonizers of in situ collected aggregates at the sub-aggregate level

II. Image the microstructure and single-cell element uptake of aggregates at the sub-aggregate level

III. Image the flow field around in situ collected aggregates to characterize their settling behavior at the single-aggregate level

IV. Investigate the influence of microfiber incorporation on aggregation dynamics and settling velocity of laboratory-formed marine snow at the single-aggregate level

References

Alldredge, A. 1998. The carbon, nitrogen and mass content of marine snow as a function of aggregate size, *Deep Sea Research Part I: Oceanographic Research Papers*, vol. 45, no. 4–5, pp. 529–541. DOI: 10.1016/S0967-0637(97)00048-4.

Alldredge, A. L. and Crocker, K. M. 1995. Why do sinking mucilage aggregates accumulate in the water column?, *Science of The Total Environment*, Marine Mucilages, vol. 165, no. 1, pp. 15–22. DOI: 10.1016/0048-9697(95)04539-D.

Alldredge, A. L. and Gotschalk, C. 1988. In situ settling behavior of marine snow, *Limnology and Oceanography*, vol. 33, no. 3, pp. 339–351. DOI: 10.4319/lo.1988.33.3.0339.

Alldredge, A. L. and McGillivary, P. 1991. The attachment probabilities of marine snow and their implications for particle coagulation in the ocean, *Deep Sea Research A*, vol. 38, pp. 431–443. DOI: 10.1016/0198-0149(91)90045-H.

Alldredge, A. L., Passow, U. and Logan, B. E. 1993. The abundance and significance of a class of large, transparent organic particles in the ocean, *Deep Sea Research Part I: Oceanographic Research Papers*, vol. 40, no. 6, pp. 1131–1140. DOI: 10.1016/0967-0637(93)90129-Q.

Alldredge, A. L. and Silver, M. W. 1988. Characteristics, dynamics and significance of marine snow, *Progress in Oceanography*, vol. 20, no. 1, pp. 41–82. DOI: 10.1016/0079-6611(88)90053-5.

Arnosti, C. 2003. 13 - Microbial Extracellular Enzymes and their Role in Dissolved Organic Matter Cycling, in Findlay, S. E. G. and Sinsabaugh, R. L. (eds), *Aquatic Ecosystems*, Aquatic Ecology, Burlington, Academic Press, pp. 315–342. DOI: 10.1016/B978-012256371-3/50014-7.

Arrigo, K. R. 2007. Carbon cycle: marine manipulations, *Nature*, vol. 450, no. 7169, pp. 491–492. DOI: 10.1038/450491a.

Arrigo, K. R., Robinson, D. H., Worthen, D. L., Dunbar, R. B., DiTullio, G. R., VanWoert, M. and Lizotte, M. P. 1999. Phytoplankton Community Structure and the Drawdown of Nutrients and CO_2 in the Southern Ocean, *Science*, vol. 283, no. 5400, pp. 365–367. DOI: 10.1126/science.283.5400.365.

Atkinson, A., Siegel, V., Pakhomov, E. and Rothery, P. 2004. Long-term decline in krill stock and increase in salps within the Southern Ocean, *Nature*, vol. 432, no. 7013, pp. 100–103. DOI: 10.1038/nature02996.

Azam, F. and Long, R. A. 2001. Sea snow microcosms, *Nature*, vol. 414, no. 6863, p. 495. DOI: 10.1038/35107174.

Azetsu-Scott, K. and Passow, U. 2004. Ascending marine particles: Significance of transparent exopolymer particles (TEP) in the upper ocean, *Limnology and Oceanography*, vol. 49, no. 3, pp. 741–748. DOI: 10.4319/lo.2004.49.3.0741.

Bach, L. T., Boxhammer, T., Larsen, A., Hildebrandt, N., Schulz, K. G. and Riebesell, U. 2016. Influence of plankton community structure on the sinking velocity of marine aggregates, *Global Biogeochemical Cycles*, vol. 30, no. 8, p. 2016GB005372. DOI: 10.1002/2016GB005372.

Bachmann, J., Heimbach, T., Hassenrück, C., Kopprio, G. A., Iversen, M. H., Grossart, H. P. and Gärdes, A. 2018. Environmental Drivers of Free-Living vs. Particle-Attached Bacterial Community Composition in the Mauritania Upwelling System, *Frontiers in Microbiology*, vol. 9. DOI: 10.3389/fmicb.2018.02836.

Bar-On, Y. M., Phillips, R. and Milo, R. 2018. The biomass distribution on Earth, *Proceedings of the National Academy of Sciences*, vol. 115, no. 25, pp. 6506–6511. DOI: 10.1073/pnas.1711842115.

Biermann, A. and Engel, A. 2010. Effect of CO_2 on the properties and sinking velocity of aggregates of the coccolithophore Emiliania huxleyi, *Biogeosciences (BG)*, vol. 7, pp. 1017–1029. DOI: 10.5194/bg-7-1017-2010.

Boyd, P. W., Claustre, H., Levy, M., Siegel, D. A. and Weber, T. 2019. Multi-faceted particle pumps drive carbon sequestration in the ocean, *Nature*, vol. 568, no. 7752, p. 327. DOI: 10.1038/s41586-019-1098-2.

Buesseler, K. O. and Boyd, P. W. 2009. Shedding light on processes that control particle export and flux attenuation in the twilight zone of the open ocean, *Limnology and Oceanography*, vol. 54, no. 4, pp. 1210–1232. DOI: 10.4319/lo.2009.54.4.1210.

Burd, A. B. 2013. Modeling particle aggregation using size class and size spectrum approaches, *Journal of Geophysical Research: Oceans*, vol. 118, no. 7, pp. 3431–3443. DOI: 10.1002/jgrc.20255.

Caldeira, K. and Wickett, M. E. 2003. Anthropogenic carbon and ocean pH, *Nature*, vol. 425, no. 6956, p. 365. DOI: 10.1038/425365a.

Cavan, E. L., Trimmer, M., Shelley, F. and Sanders, R. 2017. Remineralization of particulate organic carbon in an ocean oxygen minimum zone, *Nature Communications*, vol. 8, p. 14847. DOI: 10.1038/ncomms14847.

Ciais, P., Dolman, A. J., Bombelli, A., Duren, R., Peregon, A., Rayner, P. J., Miller, C., Gobron, N., Zehner, C., et al. 2014. Current systematic carbon-cycle observations and the need for implementing a policy-relevant carbon observing system, *Biogeosciences*, vol. 11, pp. 3547–3602. DOI: 10.5194/bg-11-3547-2014.

Cisternas-Novoa, C., Lee, C., Tang, T., de Jesus, R. and Engel, A. 2019. Effects of Higher CO_2 and Temperature on Exopolymer Particle Content and Physical Properties of Marine Aggregates, *Frontiers in Marine Science*, vol. 5. DOI: 10.3389/fmars.2018.00500.

Dagg, M. J., Jackson, G. A. and Checkley, D. M. 2014. The distribution and vertical flux of fecal pellets from large zooplankton in Monterey bay and coastal California, *Deep Sea Research Part I: Oceanographic Research Papers*, vol. 94, no. Supplement C, pp. 72–86. DOI: 10.1016/j.dsr.2014.09.001.

Daskalov, G. M., Grishin, A. N., Rodionov, S. and Mihneva, V. 2007. Trophic cascades triggered by overfishing reveal possible mechanisms of ecosystem regime shifts, *Proceedings of the National Academy of Sciences*, vol. 104, no. 25, pp. 10518–10523. DOI: 10.1073/pnas.0701100104.

Datta, M. S., Sliwerska, E., Gore, J., Polz, M. F. and Cordero, O. X. 2016. Microbial interactions lead to rapid micro-scale successions on model marine particles, *Nature Communications*, vol. 7, p. 11965. DOI: 10.1038/ncomms11965.

Datta, N. and Mishra, S. K. 1982. Boundary layer flow of a dusty fluid over a semi-infinite flat plate, *Acta Mechanica*, vol. 42, no. 1, pp. 71–83. DOI: 10.1007/BF01176514.

Derraik, J. G. B. 2002. The pollution of the marine environment by plastic debris: a review, *Marine Pollution Bulletin*, vol. 44, no. 9, pp. 842–852. DOI: 10.1016/S0025-326X(02)00220-5.

Desai, N., Shaik, V. A. and Ardekani, A. M. 2019. Hydrodynamic Interaction Enhances Colonization of Sinking Nutrient Sources by Motile Microorganisms, *Frontiers in Microbiology*, vol. 10. DOI: 10.3389/fmicb.2019.00289.

Diaz, R. J. and Rosenberg, R. 2008. Spreading Dead Zones and Consequences for Marine Ecosystems, *Science*, vol. 321, no. 5891, pp. 926–929. DOI: 10.1126/science.1156401.

Durkin, C. A., Estapa, M. L. and Buesseler, K. O. 2015. Observations of carbon export by small sinking particles in the upper mesopelagic, *Marine Chemistry*, Particles in aquatic environments: from invisible exopolymers to sinking aggregates, vol. 175, pp. 72–81. DOI: 10.1016/j.marchem.2015.02.011.

Engel, A. 2000. The role of transparent exopolymer particles (TEP) in the increase in apparent particle stickiness (α) during the decline of a diatom bloom, *Journal of Plankton Research*, vol. 22, no. 3, pp. 485–497. DOI: 10.1093/plankt/22.3.485.

Engel, A. 2002. Direct relationship between CO_2 uptake and transparent exopolymer particles production in natural phytoplankton, *Journal of Plankton Research*, vol. 24, no. 1, pp. 49–53. DOI: 10.1093/plankt/24.1.49.

Engel, A., Borchard, C., Piontek, J., Schulz, K. G., Riebesell, U. and Bellerby, R. 2013. CO_2 increases ^{14}C primary production in an Arctic plankton community, *Biogeosciences*, vol. 10, no. 3, pp. 1291–1308. DOI: https://doi.org/10.5194/bg-10-1291-2013.

Engel, A. and Schartau, M. 1999. Influence of transparent expolymer particles (TEP) on sinking velocity of Nitzschia closterum aggregates, *Marine Ecology Progress Series*, no. 182, pp. 69–76. DOI:10.3354/meps182069

Enke, T. N., Leventhal, G. E., Metzger, M., Saavedra, J. T. and Cordero, O. X. 2018. Microscale ecology regulates particulate organic matter turnover in model marine microbial communities, *Nature Communications*, vol. 9, no. 1, p. 2743. DOI: 10.1038/s41467-018-05159-8.

Fadeev, E., Salter, I., Schourup-Kristensen, V., Nöthig, E.-M., Metfies, K., Engel, A., Piontek, J., Boetius, A. and Bienhold, C. 2018. Microbial Communities in the East and West Fram Strait During Sea Ice Melting Season, *Frontiers in Marine Science*, vol. 5. DOI: 10.3389/fmars.2018.00429.

Field, C. B., Behrenfeld, M. J., Randerson, J. T. and Falkowski, P. 1998. Primary Production of the Biosphere: Integrating Terrestrial and Oceanic Components, *Science*, vol. 281, no. 5374, pp. 237–240. DOI: 10.1126/science.281.5374.237.

Frankignoulle, M., Canon, C. and Gattuso, J.-P. 1994. Marine calcification as a source of carbon dioxide: Positive feedback of increasing atmospheric CO_2, *Limnology and Oceanography*, vol. 39, no. 2, pp. 458–462. DOI: 10.4319/lo.1994.39.2.0458.

Galloway, T. S., Cole, M. and Lewis, C. 2017. Interactions of microplastic debris throughout the marine ecosystem, *Nature Ecology & Evolution*, vol. 1, no. 5, p. 0116. DOI: 10.1038/s41559-017-0116.

Gärdes, A., Iversen, M. H., Grossart, H.-P., Passow, U. and Ullrich, M. S. 2011. Diatom-associated bacteria are required for aggregation of Thalassiosira weissflogii, *The ISME Journal*, vol. 5, no. 3, pp. 436–445. DOI: 10.1038/ismej.2010.145.

Geyer, R., Jambeck, J. R. and Law, K. L. 2017. Production, use, and fate of all plastics ever made, *Science Advances*, vol. 3, no. 7, p. e1700782. DOI: 10.1126/sciadv.1700782.

Giering, S. L. C., Sanders, R., Lampitt, R. S., Anderson, T. R., Tamburini, C., Boutrif, M., Zubkov, M. V., Marsay, C. M., Henson, S. A., Saw, K., Cook, K. and Mayor, D. J. 2014. Reconciliation of the carbon budget in the ocean's twilight zone, *Nature*, vol. 507, no. 7493, pp. 480–483. DOI: 10.1038/nature13123.

Gilmer, R. W. and Harbison, G. R. 1986. Morphology and field behavior of pteropod molluscs: feeding methods in the families Cavoliniidae, Limacinidae and Peraclididae (Gastropoda: Thecosomata), *Marine Biology*, vol. 91, no. 1, pp. 47–57. DOI: 10.1007/BF00397570.

Grossart, H. P., Kirboe, T., Tang, K. W., Allgaier, M., Yam, E. M. and Ploug, H. 2006. Interactions between marine snow and heterotrophic bacteria: aggregate formation and

microbial dynamics, *Aquatic Microbial Ecology*, vol. 42, no. 1, pp. 19–26. DOI: 10.3354/ame042019.

Grossart, H.-P., Czub, G. and Simon, M. 2006. Algae-bacteria interactions and their effects on aggregation and organic matter flux in the sea, *Environmental Microbiology*, vol. 8, no. 6, pp. 1074–1084. DOI: 10.1111/j.1462-2920.2006.00999.x.

Grossart, H.-P., Kiørboe, T., Tang, K. and Ploug, H. 2003. Bacterial Colonization of Particles: Growth and Interactions, *Applied and Environmental Microbiology*, vol. 69, no. 6, pp. 3500–3509. DOI: 10.1128/AEM.69.6.3500-3509.2003.

Grossart, H.-P. and Ploug, H. 2001. Microbial degradation of organic carbon and nitrogen on diatom aggregates, *Limnology and Oceanography*, vol. 46, no. 2, pp. 267–277. DOI: 10.4319/lo.2001.46.2.0267.

Gruber, N. and Sarmiento, J. L. 2002. Large-scale biogeochemicalphysical interactions in elemental cycles, in John Wiley & Sons, Inc., New York, vol. Volume 12, pp. 337–399.

Hansen, J. L. S., Timm, U. and Kiørboe, T. 1995. Adaptive significance of phytoplankton stickiness with emphasis on the diatom Skeletonema costatum, *Marine Biology*, vol. 123, no. 4, pp. 667–676. DOI: 10.1007/BF00349109.

Hein, M. and Sand-Jensen, K. 1997. CO_2 increases oceanic primary production, *Nature*, vol. 388, no. 6642, pp. 526–527. DOI: 10.1038/41457.

Henson, S. A., Sanders, R. and Madsen, E. 2012. Global patterns in efficiency of particulate organic carbon export and transfer to the deep ocean, *Global Biogeochemical Cycles*, vol. 26, no. 1, p. GB1028. DOI: 10.1029/2011GB004099.

Hernández-León, S., Almeida, C., Yebra, L., Arístegui, J., Puelles, M. L. F. de and García-Braun, J. 2001. Zooplankton abundance in subtropical waters: is there a lunar cycle?, *Scientia Marina*, vol. 65, no. S1, pp. 59–64. DOI: 10.3989/scimar.2001.65s159.

IPCC, 2013*:* Climate Change 2013: The Physical Science Basis. Contribution of Working Group I to the Fifth Assessment Report of the Intergovernmental Panel on Climate Change [Stocker, T.F., D. Qin, G.-K. Plattner, M. Tignor, S.K. Allen, J. Boschung, A. Nauels, Y. Xia, V. Bex and P.M. Midgley (eds.)]. *Cambridge University Press, Cambridge, United Kingdom and New York, NY, USA,* 1535 pp, DOI:10.1017/CBO9781107415324

Iversen, M. H., Nowald, N., Ploug, H., Jackson, G. A. and Fischer, G. 2010. High resolution profiles of vertical particulate organic matter export off Cape Blanc, Mauritania: Degradation processes and ballasting effects, *Deep-Sea Research Part I-Oceanographic Research Papers*, vol. 57, no. 6, pp. 771–784. DOI: 10.1016/j.dsr.2010.03.007.

Iversen, M. H. and Ploug, H. 2010. Ballast minerals and the sinking carbon flux in the ocean: carbon-specific respiration rates and sinking velocity of marine snow aggregates, *Biogeosciences*, vol. 7, no. 9, pp. 2613–2624. DOI: 10.5194/bg-7-2613-2010.

Iversen, M. H. and Ploug, H. 2013. Temperature effects on carbon-specific respiration rate and sinking velocity of diatom aggregates – potential implications for deep ocean export processes, *Biogeosciences*, vol. 10, no. 6, pp. 4073–4085. DOI: 10.5194/bg-10-4073-2013.

Iversen, M. H. and Robert, M. L. 2015. Ballasting effects of smectite on aggregate formation and export from a natural plankton community, *Marine Chemistry*, Particles in aquatic environments: from invisible exopolymers to sinking aggregates, vol. 175, pp. 18–27. DOI: 10.1016/j.marchem.2015.04.009.

Iversen, M., Pakhomov, E., Hunt, B., van der Jagt, H., Wolf-Gladrow, D. and Klaas, C. 2016. Sinkers or floaters? Contribution from salp pellets to the export flux during a large bloom event in the Southern Ocean, *Deep Sea Research Part II: Topical Studies in Oceanography*, vol. 138. DOI: 10.1016/j.dsr2.2016.12.004.

Jackson, G. A. 1993. Flux feeding as a mechanism for zooplankton grazing and its implications for vertical particulate flux 1, *Limnology and Oceanography*, vol. 38, no. 6, pp. 1328–1331. DOI: 10.4319/lo.1993.38.6.1328.

Jackson, G. A. 1995. Comparing observed changes in particle size spectra with those predicted using coagulation theory, *Deep Sea Research Part II: Topical Studies in Oceanography*, vol. 42, no. 1, pp. 159–184. DOI: 10.1016/0967-0645(95)00010-N.

Jackson, G. A. and Checkley, D. M. 2011. Particle size distributions in the upper 100m water column and their implications for animal feeding in the plankton, *Deep Sea Research Part I: Oceanographic Research Papers*, vol. 58, no. 3, pp. 283–297. DOI: 10.1016/j.dsr.2010.12.008.

Jagt, H. van der, Friese, C., Stuut, J.-B. W., Fischer, G. and Iversen, M. H. 2018. The ballasting effect of Saharan dust deposition on aggregate dynamics and carbon export: Aggregation, settling, and scavenging potential of marine snow, *Limnology and Oceanography*, vol. 63, no. 3, pp. 1386–1394. DOI: 10.1002/lno.10779.

Johannessen, O. M. 2008. Decreasing Arctic Sea Ice Mirrors Increasing CO_2 on Decadal Time Scale, *Atmospheric and Oceanic Science Letters*, vol. 1, no. 1, pp. 51–56. DOI: 10.1080/16742834.2008.11446766.

Karner, M. and Herndl, G. J. 1992. Extracellular enzymatic activity and secondary production in free-living and marine-snow-associated bacteria, *Marine Biology*, vol. 113, no. 2, pp. 341–347. DOI: 10.1007/BF03347289.

Kerr, R. A. 1995. Scientists see greenhouse, semiofficially, *Science (New York, N.Y.)*, vol. 269, no. 5231, p. 1667. DOI: 10.1126/science.269.5231.1667.

Kiørboe, T. 2008. *A Mechanistic Approach to Plankton Ecology*, Princeton University Press.

Kiørboe, T. 2011. What makes pelagic copepods so successful?, *Journal of Plankton Research*, vol. 33, no. 5, pp. 677–685. DOI: 10.1093/plankt/fbq159.

Kiørboe, T., Grossart, H.-P., Ploug, H. and Tang, K. 2002. Mechanisms and Rates of Bacterial Colonization of Sinking Aggregates, *Applied and Environmental Microbiology*, vol. 68, no. 8, pp. 3996–4006. DOI: 10.1128/AEM.68.8.3996-4006.2002.

Kiørboe, T. and Hansen, J. L. S. 1993. Phytoplankton aggregate formation: observations of patterns and mechanisms of cell sticking and the significance of exopolymeric material, *Journal of Plankton Research*, vol. 15, no. 9, pp. 993–1018. DOI: 10.1093/plankt/15.9.993.

Kiørboe, T., Lundsgaard, C., Olesen, M. and Hansen, J. L. S. (1994) *Aggregation and sedimentation processes during a spring phytoplankton bloom: A field experiment to test coagulation theory* DOI: info:doi/10.1357/0022240943077145.

Kiørboe, T., Tang, K. W., Grossart, H. P. and Ploug, H. 2003. Dynamics of microbial communities on marine snow aggregates : Colonization, growth, detachment, and grazing mortality of attached bacteria, *Applied and Environmental Microbiology*, vol. 69, no. 6, pp. 3036–3047.

Kiørboe, T. and Thygesen, U. H. 2001. Fluid motion and solute distribution around sinking aggregates II : Implications for remote detection by colonizing zooplankters, *Marine Ecology - Progress Series*, vol. 211, pp. 15–25. DOI: 10.3354/meps211015.

Kjellerup, S. and Kiørboe, T. 2012. Prey detection in a cruising copepod, *Biology Letters*, vol. 8, no. 3, pp. 438–441. DOI: 10.1098/rsbl.2011.1073.

Kranck, K. and Milligan, T. G. 1988. Macroflocs from diatoms: in situ photography of particles in Bedford Basin, Nova Scotia, *Marine Ecology Progress Series*, vol. 44, no. 2, pp. 183–189.

Lal, R. 2008. Sequestration of atmospheric CO_2 in global carbon pools, *Energy & Environmental Science*, vol. 1, no. 1, pp. 86–100. DOI: 10.1039/B809492F.

Lalli, C. M. and Gilmer, R. W. 1989. *Pelagic Snails: The Biology of Holoplanktonic Gastropod Mollusks*, Stanford University Press.

Laurenceau-Cornec, E. C., Trull, T. W., Davies, D. M., Bray, S. G., Doran, J., Planchon, F., Carlotti, F., Jouandet, M.-P., Cavagna, A.-J., Waite, A. M. and Blain, S. 2015. The relative importance of phytoplankton aggregates and zooplankton fecal pellets to carbon export: insights from free-drifting sediment trap deployments in naturally iron-fertilised waters near the Kerguelen Plateau, *Biogeosciences*, vol. 12, no. 4, pp. 1007–1027. DOI: 10.5194/bg-12-1007-2015.

Levitus, S., Antonov, J. I., Boyer, T. P., Baranova, O. K., Garcia, H. E., Locarnini, R. A., Mishonov, A. V., Reagan, J. R., Seidov, D., Yarosh, E. S. and Zweng, M. M. 2012. World ocean heat content and thermosteric sea level change (0–2000 m), 1955–2010, *Geophysical Research Letters*, vol. 39, no. 10. DOI: 10.1029/2012GL051106.

Levitus, S., Antonov, J. I., Boyer, T. P. and Stephens, C. 2000. Warming of the World Ocean, *Science*, vol. 287, no. 5461, pp. 2225–2229. DOI: 10.1126/science.287.5461.2225.

Lombard, F., Guidi, L. and Kiørboe, T. 2013. Effect of Type and Concentration of Ballasting Particles on Sinking Rate of Marine Snow Produced by the Appendicularian Oikopleura dioica, *PLoS ONE*, vol. 8, no. 9. DOI: 10.1371/journal.pone.0075676.

Lombard, F., Koski, M. and Kiørboe, T. 2013. Copepods use chemical trails to find sinking marine snow aggregates, *Limnology and Oceanography*, vol. 58, no. 1, pp. 185–192. DOI: 10.4319/lo.2013.58.1.0185.

Long, M., Moriceau, B., Gallinari, M., Lambert, C., Huvet, A., Raffray, J. and Soudant, P. 2015. Interactions between microplastics and phytoplankton aggregates: Impact on their respective fates, *Marine Chemistry*, Particles in aquatic environments: from invisible exopolymers to sinking aggregates, vol. 175, pp. 39–46. DOI: 10.1016/j.marchem.2015.04.003.

Long, R. and Azam, F. 1996. Abundant protein-containing particles in the sea, *Aquatic Microbial Ecology*, vol. 10, pp. 213–221.

MacIntyre, S., Alldredge, A. L. and Gotschalk, C. C. 1995. Accumulation of marines now at density discontinuities in the water column, *Limnology and Oceanography*, vol. 40, no. 3, pp. 449–468. DOI: 10.4319/lo.1995.40.3.0449.

Marcos, Fu, H. C., Powers, T. R. and Stocker, R. 2012. Bacterial rheotaxis, *Proceedings of the National Academy of Sciences*, vol. 109, no. 13, pp. 4780–4785. DOI: 10.1073/pnas.1120955109.

Mari, X., Passow, U., Migon, C., Burd, A. B. and Legendre, L. 2017. Transparent exopolymer particles: Effects on carbon cycling in the ocean, *Progress in Oceanography*, vol. 151, pp. 13–37. DOI: 10.1016/j.pocean.2016.11.002.

Mari, X., Rassoulzadegan, F., Brussaard, C. P. D. and Wassmann, P. 2005. Dynamics of transparent exopolymeric particles (TEP) production by Phaeocystis globosa under N- or P-limitation: a controlling factor of the retention/export balance, *Harmful Algae*, Bloom Dynamics and Biological Control of Phaeocystis: a HAB Species in European Coastal Waters, vol. 4, no. 5, pp. 895–914. DOI: 10.1016/j.hal.2004.12.014.

McCave, I. N. 1984. Size spectra and aggregation of suspended particles in the deep ocean, *Deep Sea Research Part A. Oceanographic Research Papers*, vol. 31, no. 4, pp. 329–352. DOI: 10.1016/0198-0149(84)90088-8.

McNeil, B. I. and Matear, R. J. 2006. Projected climate change impact on oceanic acidification, *Carbon Balance and Management*, vol. 1, p. 2. DOI: 10.1186/1750-0680-1-2.

Mestre, M., Borrull, E., Sala, Mm. and Gasol, J. M. 2017. Patterns of bacterial diversity in the marine planktonic particulate matter continuum, *The ISME Journal*. DOI: 10.1038/ismej.2016.166.

Notz, D. and Stroeve, J. 2016. Observed Arctic sea-ice loss directly follows anthropogenic CO_2 emission, *Science*, vol. 354, no. 6313, pp. 747–750. DOI: 10.1126/science.aag2345.

Olsen, E. M., Jørstad, T. and Kaartvedt, S. 2000. The feeding strategies of two large marine copepods, *Journal of Plankton Research*, vol. 22, no. 8, pp. 1513–1528. DOI: 10.1093/plankt/22.8.1513.

Orr, J. C., Fabry, V. J., Aumont, O., Bopp, L., Doney, S. C., Feely, R. A., Gnanadesikan, A., et al. 2005. Anthropogenic ocean acidification over the twenty-first century and its impact on calcifying organisms, *Nature*, vol. 437, no. 7059, p. 681. DOI: 10.1038/nature04095.

Packard, T. T. and Gómez, M. 2013. Modeling vertical carbon flux from zooplankton respiration, *Progress in Oceanography*, vol. 110, pp. 59–68. DOI: 10.1016/j.pocean.2013.01.003.

Pakhomov, E. A., Froneman, P. W. and Perissinotto, R. 2002. Salp/krill interactions in the Southern Ocean: spatial segregation and implications for the carbon flux, *Deep Sea Research Part II: Topical Studies in Oceanography*, The Southern Ocean I: Climatic Changes in the Cycle of Carbon in the Southern Ocean, vol. 49, no. 9, pp. 1881–1907. DOI: 10.1016/S0967-0645(02)00017-6.

Passow, U. 2002. Production of transparent exopolymer particles (TEP) by phyto- and bacterioplankton, *Marine ecology-progress series*, vol. 236, pp. 1–12.

Passow, U. and Alldredge, A. L. 1995. A dye-binding assay for the spectrophotometric measurement of transparent exopolymer particles (TEP), *Limnology and Oceanography*, vol. 40, no. 7, pp. 1326–1335. DOI: 10.4319/lo.1995.40.7.1326.

Passow, U. and Carlson, C. A. 2012. The biological carbon pump in a high CO_2 world, *Marine Ecology Progress Series*, vol. 470, pp. 249–271. DOI: 10.3354/meps09985.

Passow, U. and Rocha, C. L. D. L. 2006. Accumulation of mineral ballast on organic aggregates, *Global Biogeochemical Cycles*, vol. 20, no. 1. DOI: 10.1029/2005GB002579.

Pelve, E. A., Fontanez, K. M. and DeLong, E. F. 2017. Bacterial Succession on Sinking Particles in the Ocean's Interior, *Frontiers in Microbiology*, vol. 8. DOI: 10.3389/fmicb.2017.02269.

Pendergrass, A. G. and Hartmann, D. L. 2014. Changes in the Distribution of Rain Frequency and Intensity in Response to Global Warming, *Journal of Climate*, vol. 27, no. 22, pp. 8372–8383. DOI: 10.1175/JCLI-D-14-00183.1.

Ploug, H., Iversen, M. H. and Fischer, G. 2008. Ballast, sinking velocity, and apparent diffusivity within marine snow and zooplankton fecal pellets: Implications for substrate turnover by attached bacteria, *Limnology and Oceanography*, vol. 53, no. 5, pp. 1878–1886. DOI: 10.4319/lo.2008.53.5.1878.

Ploug, H. and Passow, U. 2007. Direct measurement of diffusivity within diatom aggregates containing transparent exopolymer particles, *Limnology and Oceanography*, vol. 52, no. 1, pp. 1–6. DOI: 10.4319/lo.2007.52.1.0001.

Porter, A., Lyons, B. P., Galloway, T. S. and Lewis, C. 2018. Role of Marine Snows in Microplastic Fate and Bioavailability, *Environmental Science & Technology*, vol. 52, no. 12, pp. 7111–7119. DOI: 10.1021/acs.est.8b01000.

Poulsen, L. K. and Iversen, M. H. 2008. Degradation of copepod fecal pellets: key role of protozooplankton, *Marine Ecology Progress Series*, vol. 367, pp. 1–13. DOI: 10.3354/meps07611.

Poulsen, L. K., Moldrup, M., Berge, T. and Hansen, P. J. 2011. Feeding on copepod fecal pellets: a new trophic role of dinoflagellates as detritivores, *Marine Ecology Progress Series*, vol. 441, pp. 65–78. DOI: 10.3354/meps09357.

Prairie, J. C., Ziervogel, K., Arnosti, C., Camassa, R., Falcon, C., Khatri, S., McLaughlin, R. M., White, B. L. and Yu, S. 2013. Delayed settling of marine snow at sharp density transitions driven by fluid entrainment and diffusion-limited retention, *Marine Ecology Progress Series*, vol. 487, pp. 185–200. DOI: 10.3354/meps10387.

Quéré, C. L., Andrew, R. M., Friedlingstein, P., Sitch, S., Hauck, J., Pongratz, J., Pickers, P. A., Korsbakken, J. I., Zheng, B., et al. 2018. Global Carbon Budget 2018, *Earth System Science Data*, vol. 10, no. 4, pp. 2141–2194. DOI: https://doi.org/10.5194/essd-10-2141-2018.

Resplandy, L. 2018. Will ocean zones with low oxygen levels expand or shrink?, *Nature*, vol. 557, no. 7705, p. 314. DOI: 10.1038/d41586-018-05034-y.

Riebesell, U. 1991. Particle aggregation during a diatom bloom. II. Biological aspects, *Marine Ecology Progress Series*, vol. 69, pp. 281–291. DOI: 10.3354/meps069281.

Riebesell, U. 1993. Aggregation of Phaeocystis during phytoplankton spring blooms in the southern North Sea, *Marine Ecology-progress Series - MAR ECOL-PROGR SER*, vol. 96, pp. 281–289. DOI: 10.3354/meps096281.

Riebesell, U., Körtzinger, A. and Oschlies, A. 2009. Sensitivities of marine carbon fluxes to ocean change, *Proceedings of the National Academy of Sciences*, vol. 106, no. 49, pp. 20602–20609. DOI: 10.1073/pnas.0813291106.

Riley, J. S., Sanders, R., Marsay, C., Le Moigne, F. a. C., Achterberg, E. P. and Poulton, A. J. 2012. The relative contribution of fast and slow sinking particles to ocean carbon export, *Global Biogeochemical Cycles*, vol. 26, no. 1, p. GB1026. DOI: 10.1029/2011GB004085.

Sato, R., Tanaka, Y. and Ishimaru, T. 2001. House Production by Oikopleura dioica (Tunicata, Appendicularia) Under Laboratory Conditions, *Journal of Plankton Research*, vol. 23, no. 4, pp. 415–423. DOI: 10.1093/plankt/23.4.415.

Shanks, A. L. and Trent, J. D. 1980. Marine snow: sinking rates and potential role in vertical flux, *Deep Sea Research Part A. Oceanographic Research Papers*, vol. 27, no. 2, pp. 137–143. DOI: 10.1016/0198-0149(80)90092-8.

Simon, M., Grossart, H. P., Schweitzer, B. and Ploug, H. 2002. Microbial Ecology of Organic Aggregates in Aquatic Ecosystems., *Aquatic microbial ecology*, vol. 28, no. 2, pp. 175–211.

Stemmann, L., Jackson, G. A. and Ianson, D. 2004. A vertical model of particle size distributions and fluxes in the midwater column that includes biological and physical processes—Part I: model formulation, *Deep Sea Research Part I: Oceanographic Research Papers*, vol. 51, no. 7, pp. 865–884. DOI: 10.1016/j.dsr.2004.03.001.

Stocker, R. and Seymour, J. R. 2012. Ecology and physics of bacterial chemotaxis in the ocean, *Microbiology and molecular biology reviews: MMBR*, vol. 76, no. 4, pp. 792–812. DOI: 10.1128/MMBR.00029-12.

Stocker, R., Seymour, J. R., Samadani, A., Hunt, D. E. and Polz, M. F. 2008. Rapid chemotactic response enables marine bacteria to exploit ephemeral microscale nutrient patches, *Proceedings of the National Academy of Sciences*, vol. 105, no. 11, pp. 4209–4214. DOI: 10.1073/pnas.0709765105.

Stokes, G. G. 1851. On the Effect of the Internal Friction of Fluids on the Motion of Pendulums, *Transactions of the Cambridge Philosophical Society*, vol. 9, p. 8.

Stukel, M. R., Song, H., Goericke, R. and Miller, A. J. 2018. The role of subduction and gravitational sinking in particle export, carbon sequestration, and the remineralization length scale in the California Current Ecosystem, *Limnology and Oceanography*, vol. 63, no. 1, pp. 363–383. DOI: 10.1002/lno.10636.

Thiele, S., Fuchs, B. M., Amann, R. and Iversen, M. H. 2014. Colonization in the photic zone and subsequent changes during sinking determines bacterial community composition in marine snow, *Applied and Environmental Microbiology*, p. AEM.02570-14. DOI: 10.1128/AEM.02570-14.

Thuy, N. T., Huang, C.-P. and Lin, J.-L. 2017. Visualization and quantification of transparent exopolymer particles (TEP) in freshwater using an auto-imaging approach, *Environmental Science and Pollution Research*, vol. 24, no. 21, pp. 17358–17372. DOI: 10.1007/s11356-017-9292-y.

Tréguer, P., Légendre, L., Rivkin, R. T., Ragnueneau, O. and Dittert, N. 2003. Water column biogeochemstry below the euphotic zone, in Michael J. R. Fasham (ed), *Ocean Biogeochemistry: The Role of the Ocean Carbon Cycle in Global Change*, Springer-Verlag Berlin Heidelberg New York.

Van Cauwenberghe, L., Vanreusel, A., Mees, J. and Janssen, C. R. 2013. Microplastic pollution in deep-sea sediments, *Environmental Pollution*, vol. 182, pp. 495–499. DOI: 10.1016/j.envpol.2013.08.013.

Vinnikov, K. Y. and Grody, N. C. 2003. Global Warming Trend of Mean Tropospheric Temperature Observed by Satellites, *Science*, vol. 302, no. 5643, pp. 269–272. DOI: 10.1126/science.1087910.

Vinogradov, M. E. 1997. Some Problems of Vertical Distribution of Meso- and Macroplankton in the Ocean, in Blaxter, J. H. S., Southward, A. J., Gebruk, A. V., Southward, E. C., and Tyler, P. A. (eds), *Advances in Marine Biology*, The Biogeography of the Oceans, Academic Press, vol. 32, pp. 1–92. DOI: 10.1016/S0065-2881(08)60015-2.

Visser, A. W. 2001. Hydromechanical signals in the plankton, *Marine Ecology Progress Series*, vol. 222, pp. 1–24. DOI: 10.3354/meps222001.

Volk, T. and Hoffert, M. I. 1985. Ocean Carbon Pumps: Analysis of Relative Strengths and Efficiencies in Ocean-Driven Atmospheric CO_2 Changes, in Sundquist, E. T. and Broecker, W. S. (eds), *The Carbon Cycle and Atmospheric CO_2: Natural Variations Archean to Present*, American Geophysical Union, pp. 99–110. Available at http://onlinelibrary.wiley.com/doi/10.1029/GM032p0099/summary.

White, F. M. 1974. *Viscous fluid flow*, McGraw-Hill.

Williams, R. L., Wakeham, S., McKinney, R. and Wishner, K. F. 2014. Trophic ecology and vertical patterns of carbon and nitrogen stable isotopes in zooplankton from oxygen minimum zone regions, *Deep Sea Research Part I: Oceanographic Research*, vol. 90, pp. 36–47. DOI: 10.1016/j.dsr.2014.04.008.

Woodall, Lucy C., Sanchez-Vidal, Anna, Canals, Miquel, Paterson, Gordon L.J., Coppock, Rachel, Sleight, Victoria, Calafat, Antonio, Rogers, Alex D., Narayanaswamy, Bhavani E. and Thompson, Richard C. 2014. The deep sea is a major sink for microplastic debris, *Royal Society Open Science*, vol. 1, no. 4, p. 140317. DOI: 10.1098/rsos.140317.

PAPER I

Embedding and slicing of intact in situ collected marine snow

Clara M. Flintrop, Andreas Rogge, Sebastian Miksch, Stefan Thiele, Anya M. Waite, Morten H. Iversen

Limnol. Oceanogr. Methods 16: 339-355. DOI:10.1002/lom3.10251

LIMNOLOGY and OCEANOGRAPHY: METHODS

ASLO

Limnol. Oceanogr.: Methods 00, 2018, 00–00

doi: 10.1002/lom3.10251

Embedding and slicing of intact in situ collected marine snow

Clara M. Flintrop [1,2*] **Andreas Rogge** [1] **Sebastian Miksch,** [3] **Stefan Thiele,** [4] **Anya M. Waite** [1,5] **Morten H. Iversen** [1,2*]

[1]Alfred Wegener Institute for Polar and Marine Research, Bremerhaven, Germany
[2]MARUM and University of Bremen, Bremen, Germany
[3]Max-Planck-Institute for Marine Microbiology, Bremen, Germany
[4]Institute for Inorganic and Analytical Chemistry, Friedrich Schiller University, Jena, Germany
[5]FB2 Chemistry/Biology, University of Bremen, Bremen, Germany

Abstract

The biological carbon pump is largely driven by the formation and sinking of marine snow. Because of their high organic matter content, marine snow aggregates are hotspots for microbial activity, and microbial organic matter degradation plays an important role in the attenuation of carbon fluxes to the deep sea. Our inability to examine and characterize microscale distributions of compounds making up the aggregate matrix, and of possible niches inside marine snow, has hindered our understanding of the basic processes governing marine carbon export and sequestration. To address this issue, we have adapted soft-embedding and sectioning to study the spatial structure and components of marine aggregates at high resolution. Soft-embedding enables rapid quantitative sampling of undisturbed marine aggregates from the water column and from sediment traps, followed by spatially resolved staining and characterization of substrates of the aggregate matrix and the microorganisms attached to it. Particular strengths of the method include in situ embedding in sediment traps and successful fluorescence in situ hybridization (FISH)-probe labeling, supporting studies of microbial diversity and ecology. The high spatial resolution achieved by thin-sectioning of soft-embedded aggregates offers the possibility for improved understanding of the composition and structure of marine snow, which directly influence settling velocity, microbial colonization and diversity, degradation rates, and carbon content. Our method will help to elucidate the small-scale processes underlying large-scale carbon cycling in the marine environment, which is especially relevant in the context of rising anthropogenic CO_2 emissions and global change.

The world's oceans play a key role in the global carbon cycle because of their capacity to act as active carbon sinks (Passow and Carlson 2012; Ciais et al. 2014). There is an annual flux of 80 Pg C from the atmosphere to the ocean, of which 0.1 Pg C are exported to the deep sea where carbon is sequestered over timescales of $\geq 10^3$ yr (IPCC 2013). A central mechanism modulating marine carbon sequestration is the large-scale export of organic matter to the dark ocean via the Biological Carbon Pump: phytoplankton fix dissolved inorganic carbon through photosynthesis and, upon sinking, remove carbon from the euphotic zone in the form of particulate organic carbon (POC). Vertical carbon flux is dominated by zooplankton fecal pellets and aggregated organic matter, which together result in an estimated flux of ~ 0.04 Pmol C yr^{-1} (Honjo et al. 2008). Once aggregates are larger than 500 μm in diameter they are collectively called "marine snow" (Alldredge and Silver 1988). Zooplankton grazing and microbial degradation of marine snow are largely responsible for the attenuation of carbon flux to the deep sea, respiring and consuming $\geq 97\%$ of carbon fixed in the surface ocean (Turner 2015).

Despite the important role of marine snow in the marine carbon cycle, the in situ processes and mechanisms underlying colonization and degradation by heterotrophic microorganisms on a sub-aggregate level are relatively unexplored. There are two main reasons for this: (1) the difficulty of sampling undisturbed particles in situ, particularly at depths in the water column where aggregate collection by scuba diving is not possible, and (2) their intricate three-dimensional (3D) structure and composition, which create a heterogeneous habitat with several micro-niches. As a result, microbial colonization and degradation vary in space and intensity both

*Correspondence: clara.flintrop@awi.de; morten.iversen@awi.de

Additional Supporting Information may be found in the online version of this article.

Table 1. Oligonucleotide probes used in this study with specified target organism, oligonucleotide sequence, formamide (FA) concentration in hybridization buffer, and FISH method(s) the probe was used with (mono-FISH, CARD-FISH and/or Mil-FISH).

Probe	Target	Sequence (5′–3′)	FA (%)	FISH method
EUB338	Most bacteria	GCTGCCTCCCGTAGGAGT	35	mono, CARD, MiL
EUB II	Planctomycetes	GCAGCCACCCGTAGGTGT	35	mono, CARD, MiL
EUB III	Verrucomicrobiales	GCTGCCACCCGTAGGTGT	35	mono, CARD, MiL
CF319a	Bacteroidetes	TGGTCCGTGTCTCAGTAC	35	CARD
ALT1413	Alteromonas/Colwellia	TTTGCATCCCACTCCCAT	40	CARD
SYN405	Synechococcus	AGAGGCCTTCATCCCTCA	30	CARD
NON338	Control	ACTCCTACGGGAGGCAGC	35	mono, CARD, MiL

between and within aggregates, and information about biogeochemical processes and microbial interactions is lost without the means to study marine snow at sub-aggregate resolution. Solid, dense material regularly makes up less than 1% of the aggregate volume (Ploug et al. 2008) and consists of a variety of organic and inorganic matter including phytoplankton, fecal pellets, phyto- and zoo-detritus, and ballasting minerals like airborne dust, biominerals, and silt from glaciers (Alldredge and Silver 1988; Ransom et al. 1998; Van der Jagt et al. 2018). How tightly these solids are packed affects the porosity of marine snow, which in turn affects settling behavior and carbon remineralization (Ploug et al. 2008; Iversen and Ploug 2010). In addition to the solid fraction, marine aggregates contain high amounts of extracellular polymeric substances (EPS) including transparent exopolymer particles (TEP). TEP are defined as discrete particles that consist predominantly of surface-active acidic polysaccharides and are stained by Alcian Blue (Alldredge et al. 1993). They can exert significant control over carbon export due to their sticky nature and molecular composition, which influence aggregation dynamics and aggregate buoyancy (Mari et al. 2017). TEP have also been proposed to render aggregates impermeable due to clogging of aggregate pore space (Ploug and Passow 2007). While there is a widely used method to quantify TEP spectrophotometrically (Passow and Alldredge 1995), no method currently exists to assess the spatial distribution and extent of pore space reduction and clogging caused by different fractions of EPS.

Organic matter distribution and quality are tightly interlinked with microbial colonization of aggregates. Bacterial abundance, diversity, enzymatic activity, and carbon respiration per volume aggregate are higher than in the surrounding water column due to increased substrate availability (Alldredge and Gotschalk 1990; DeLong et al. 1993; Smith et al. 1992; Ploug and Grossart 2000; D'Ambrosio et al. 2014). Krupke et al. (2016) showed how quorum sensing can regulate enzymatic activity and POC degradation in sinking aggregates, suggesting that the positioning and connectivity of microbial clusters within aggregates is an important determinant of microbial activity. This further corroborates the importance of studying the spatial distribution of solid material and EPS/TEP, especially in relation to the localization of heterotrophic microorganisms, to better understand the microbial ecology and small-scale degradation dynamics of marine snow. Advances in the in situ collection of marine snow, e.g., by using a Marine Snow Catcher (MSC; Riley et al. 2012) or sediment traps containing gel-filled collection cups (first proposed by Lundsgaard 1995), have made it possible to non-destructively sample individual aggregates, but the spatial distribution of matter and cells inside aggregates remains obscure without the means to preserve their 3D structure during staining and microscopy.

Published works exploring aggregates that were structurally preserved include studies of the structure and colonization of resin-embedded, microtome-sectioned marine aggregates using Transmission Electron Microscopy (Heissenberger et al. 1996; Leppard et al. 1996), confocal laser scanning microscopy (CLSM) of whole marine aggregates (Holloway and Cowen 1997; Waite et al. 2000), riverine aggregates (Neu 2000; Böckelmann et al. 2002) and microtome-sectioned sludge aggregates (Chu et al. 2004), and cryosectioning of riverine aggregates (Luef et al. 2009a,2009b). To study the 3D structure of marine snow with special regard to the localization of matrix components and microbial colonizers, we have developed cryosectioning of gel-embedded, in situ collected marine snow. This approach is suited for rapid subsampling of aggregates collected in situ using sediment trap gels, and for probing of aggregates with bioactive markers such as FISH. We present a modular workflow that enables spatially resolved visualization of individual aggregates and their components, and will advance the study of small-scale processes governing microbial assemblages in marine snow and their connection to carbon cycling in the marine environment.

Materials and procedures

The workflow is divided into (1) aggregate collection, (2) aggregate embedding and sectioning, (3) visualization and imaging of the aggregate matrix, including staining of EPS, 3D-reconstruction, and assessment of aggregate porosity, and (4) visualization of aggregate colonizers, including nucleic

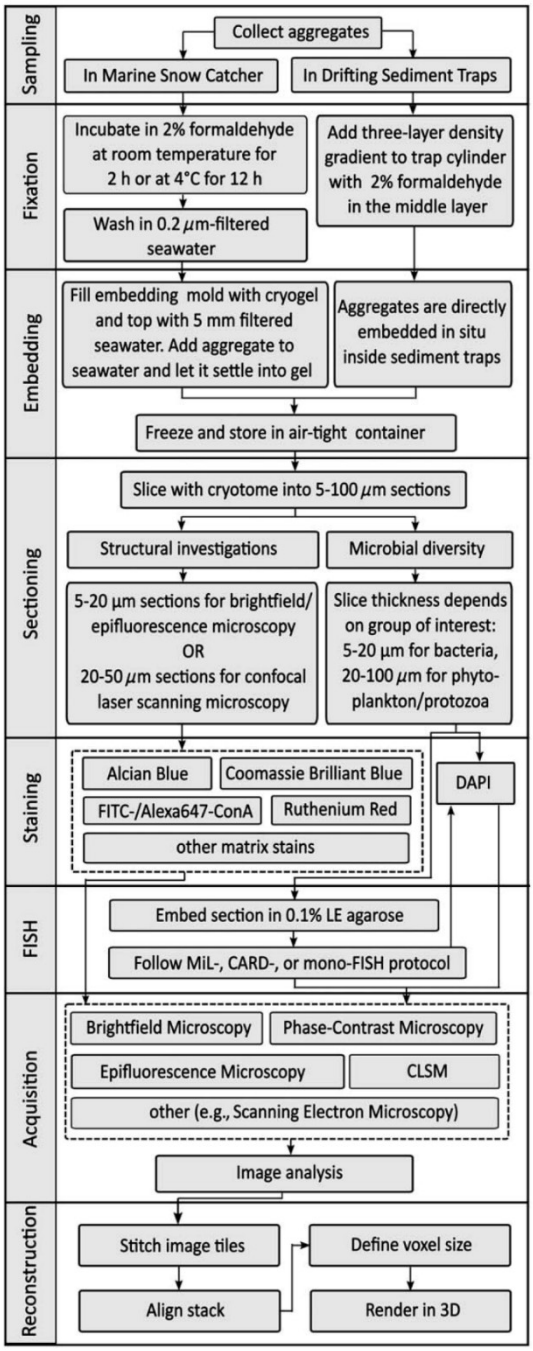

Fig. 1. Work flow of soft-embedding method. Boxes framed by dashed lines denote a "mix-and-match" process depending on the targeted substrate and the required imaging technique. The order in which staining and FISH are carried out depends on the FISH method used. Please refer to "Materials and procedures" section for details.

acid (DAPI) staining and probing of selected bacterial clades using FISH. Please refer to the accompanying flow chart (Fig. 1) for a step-by-step breakdown of the procedures involved.

Sample collection

Samples were collected during the research cruises POS495 and POS508 (RV *Poseidon*) to Cape Blanc, Mauretania in 2016/2017, and DY050 (RRS Discovery) to the Porcupine Abyssal Plain observatory in 2016, using a Marine Snow Catcher and free-drifting sediment traps containing gel-filled collection cups. The MSC was lowered to a chosen depth and closed using a drop weight. Back on deck, aggregates contained in the 100 L volume of seawater were left to settle for any desired amount of time ($\leq$ 2 h for fast-settling particles, longer for a broader range of particles). Hereafter, the water in the top part of the MSC was gently drained and the base of the MSC containing the sedimented aggregates was removed.

For passive handling and to collect samples over depth and time, drifting sediment traps containing gel-filled collection cups were deployed (Fig. 2a). Prior to deployment, one 1 m-long trap cylinder per depth was fitted with a collection cup containing 200 ml of frozen Tissue-Tek® O.C.T.™ Compound (Sakura FineTek; from here on referred to as "Tissue-Tek" or "cryogel") (Wiedmann et al. 2014; Thiele et al. 2015). Tissue-Tek is a viscous transparent cryogel and was selected as the embedding medium to allow a slow diffusive exchange of pore water with the cryogel during settling. To allow for analysis of the microbial community with FISH, a three-layer salinity gradient containing 2% v/v formaldehyde solution (diluted from 37% formaldehyde solution with filtered seawater) in the middle layer was added to each tube by dissolving different concentrations of sodium chloride (2‰, 4‰, or 6‰) in GF/F filtered seawater (*see* Thiele et al. 2015 for a detailed description of the in situ fixation method). The cylinders were suspended gyroscopically at depths of 100 m, 200 m, and 400 m, and any aggregates settling directly into the trap cylinders were first fixed with 2% formaldehyde, then washed in the lower and densest water layer before they settled into the gel, where they were recovered after 24 h (Fig. 2b). Prior to removing the gel cup, aggregates contained in the trap cylinder were left to settle for 6–12 h (depending on the height of the trap tube) to ensure that slow-settling particles would also be embedded in the gel. Gel cups were photographed at high magnification (Fig. 2c,d) and stored at −20°C until further processing.

Embedding and slicing

Aggregates picked from the detached base of the MSC were transferred to a disposable embedding mold (22 × 22 × 20 mm) containing Tissue-Tek with a wide-bore pipette. To maximize structural preservation, aggregates were not added directly to the gel, but to an approximately 5 mm thick layer of filtered seawater added on top, and left to settle into the

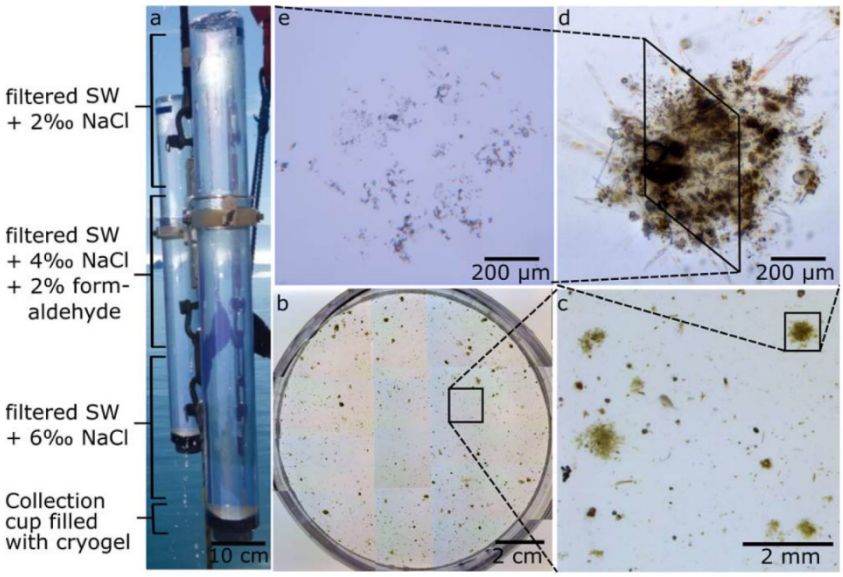

Fig. 2. Collecting and embedding marine snow in situ (counter-clockwise). (**a**) annotated sediment trap cylinder (SW = seawater; NaCl = sodium chloride); (**b**) top view of gel collection cup with in situ embedded aggregates; (**c**) close-up of the gel cup; (**d**) microscopic image of gel-embedded aggregate; (**e**) 10 μm thin-section of in situ embedded aggregate.

gel. Prior to freezing, the position of the aggregate was marked to facilitate the localization of the sample when mounted on the cryotome.

Aggregates embedded in situ in the drifting traps were cut out directly from the frozen collection cup using a small corer. The frozen embedded samples were mounted on a CM-3050S cryostat (Leica Biosystems). Knowing the position of the embedded aggregate, the block containing the sample was cut to size with a razor blade for better handling. Using an object temperature of −30°C and a chamber temperature of −35°C, samples were cut into sections ranging from 5 μm to 100 μm (Fig. 2e). Immediately after cutting, sections were mounted on Superfrost™ Plus slides (ThermoFisher Scientific) and stored at 4°C for short-term processing (within weeks) or at −20°C for longer-term storage (months to years). For microscopic examination, sections were embedded in mounting medium made up of 80% (v/v) Citifluor AF1 (Electron Microscopy Sciences) and 20% (v/v) Vectashield (Vector Laboratories) and covered with a cover slip (ThermoFisher Scientific). The cover slip was sealed with nail polish to avoid smearing the underlying sample.

Visualization and imaging of the aggregate matrix

Staining of EPS

To visualize the EPS matrix, we stained aggregate sections with dyes commonly used for marine snow such as Alcian Blue and Coomassie Brilliant Blue and tested dyes targeting different EPS fractions, including Ruthenium Red, Periodic Acid Schiff-base stain, and the fluorophore-conjugated lectin stain Concanavalin A. Acidic polysaccharides were stained with 0.2 μm-filtered 0.02% Alcian Blue (Sigma-Aldrich) dissolved in 0.06% (v/v) acetic acid (pH 2.5) for 5 s and washed with ultrapure water (UPW; Passow and Alldredge 1995; Long and Azam 1996). A-mannopyranosyl- and α-glucopyranosyl residues of other EPS fractions were targeted with Concanavalin A conjugated with FITC (FITC-ConA; Sigma-Aldrich) or Alexa647 (Alexa647-ConA; Life Technologies) dissolved in 0.3% NaCl was tested at concentrations ranging from 100 μg/mL to 1000 μg/mL (after Uthicke et al. 2009). Proteinaceous particles were stained with Coomassie Brilliant Blue (Sigma-Aldrich). Proteins were stained with 0.2 μm-filtered 0.04% (w/v) Coomassie Brilliant Blue G-250 dissolved in UPW (pH 7.4) for 30 s and washed with UPW (Passow and Alldredge 1995; Long and Azam 1996). Glycosaminoglycans were stained with 0.05% (w/v) Ruthenium Red (Sigma-Aldrich) dissolved in UPW for 10 min followed by washing with UPW (Tiessen and Stewart 1988), and with a Periodic Acid-Schiff kit (Sigma-Aldrich) following the protocol enclosed. Briefly, sections were stained with Periodic Acid Solution for 5 min, with Schiff's reagent for 15 min and counterstained with Hematoxylin Solution, Gill No. 3, for 90 s including intermediate washing steps with UPW.

All stains were applied to untreated sections as well as to sections embedded in 25 μL 0.1% LE agarose prior to staining to test if agarose-embedding can minimize sample loss, as reported for filtered samples. (N.B. in this study, "agarose-embedding" refers to applying a drop of agarose to the sample, and must not to be confused with embedding of intact whole aggregates in agarose).

Aggregate porosity

For a direct, optical measure of porosity (from here on referred to as "optical porosity"), thin-sections were photographed at 200X magnification with phase-contrast microscopy. In addition to in situ collected marine snow, we also examined the optical porosity of marine snow formed in the laboratory from cultures of the diatom *Skeletonema marinoi* to compare porosity between structurally complex, in situ collected aggregates and homogeneous aggregates formed from a monoculture (*see* Iversen and Ploug 2013 for a detailed protocol of diatom culturing and marine snow formation). To assess the reduction of pore space caused by EPS, aggregates were stained with combinations of Alcian Blue, Ruthenium Red, and FITC-ConA/Alexa647-ConA (please refer to "Staining of EPS" for a detailed staining protocol). Alcian Blue and Ruthenium Red-stained sections were photographed at 200X magnification using a light microscope. FITC-ConA/Alexa647-ConA stained sections were imaged at 200X magnification with an epifluorescence microscope (FITC Ex/Em 490 nm/525 nm; Alexa647 Ex/Em 590 nm/617 nm).

All images where processed with the image processing software package FIJI/ImageJ (Schindelin et al. 2012, 2015; Schneider et al. 2012). Images of partial sections ("tiles") were stitched with the FIJI TrakEM2 plug-in (Saalfeld et al. 2010, 2012; Cardona et al. 2012). For processing, images were converted to 8-bit and a threshold value was chosen to separate the aggregate from the background. To measure optical porosity, the area of the solid or stained fraction was measured using the "Analyze Particles" function in ImageJ, divided by the total area of the section and the quotient subtracted from 1. Optical porosity was then compared (1) to the most commonly used method of calculating porosity, where porosity is indirectly inferred from aggregate volume, solid hydrated density, and dry weight (Alldredge and Gotschalk 1988); (2) between and across sections of the same aggregate to assess the distribution of pore space within individual aggregates; (3) between sections of stained and unstained aggregates to assess the respective contributions of selected EPS fractions to changes in porosity.

3D-reconstruction

Two fully sectioned aggregates were selected for 3D reconstruction: one Alcian Blue-stained aggregate sectioned into 50 slices of 10 μm thickness, of which 46 were successfully recovered for alignment; and one unstained aggregate that had been incubated with fluorescently labeled bacteria and was sectioned into 38 sections of 10 μm thickness, of which 35 were successfully recovered. Recovered sections were photographed at 200X magnification using light or epifluorescence microscopy. Image tiles were stitched using the FIJI TrakEM2 plug-in followed by alignment of stitched tiles of consecutive sections in the z-direction using the same plug-in. Sections were aligned based on the positioning of Alcian Blue-stained or green fluorescent material. The aligned sections were exported and rendered in 3D using the 3D viewer plug-in in ImageJ (Schmid et al. 2010).

Visualization of aggregate colonizers

DAPI staining

To visualize microbial cells, cryosections were stained with 1 μg/mL 4′,6-diamidino-2-phenylindole (DAPI) for 10 min at room temperature in the dark. After careful rinsing with UPW, sections were air-dried and embedded in mounting medium for microscopic identification. Alternatively, 1% (v/v) DAPI solution (100 μg/mL) was added directly to the embedding medium. DAPI-stained cells were imaged with epifluorescence or confocal laser scanning microscopy (DAPI Ex/Em 358 nm/461 nm).

Fluorescence in situ hybridization (FISH)

For a more targeted identification of different bacterial groups, we used existing protocols for mono-labeled fluorescence in situ hybridization (mono-FISH), catalyzed reporter deposition fluorescence in situ hybridization (CARD-FISH; Amann et al. 1990; Pernthaler et al. 2002) and multi-labeled fluorescence in situ hybridization (MiL-FISH; Schimak et al. 2015) for staining aggregate thin-sections on glass slides (see Table 1 for a list of organisms targeted in this study and their corresponding oligonucleotide probes). Prior to staining, sections were circled with a hydrophobic PAP pen (Sigma-Aldrich) to retain buffer solutions. Sections were embedded in 25 μL 0.1% low-melting point agarose to maximize structural preservation. For mono- and multi-labeled FISH, hybridization buffer (5M NaCl, 1M TrisHCl, 20% SDS, formamide) with 50 ng/μL probe at a ratio of 15 : 1 was applied followed by hybridization at 46°C for 2 h and subsequent washing at 48°C for 15 min with the adjusted washing buffer (5M NaCl, 1M Tris/HCl, 20% SDS, 0.5M EDTA). For CARD-FISH, thin-sections were treated with lysozyme (50 mg lysozyme dissolved in 500 μL 0.5M EDTA + 500 μL 1M Tris/HCl + 4 mL UPW) for 30–60 min at 37°C for cell wall permeabilization. Hybridization buffer (900 mM NaCl, 20 mM Tris-HCl (pH 7.5), 0.02% sodium dodecyl sulphate (SDS), 10% dextran sulphate (w/v) and 1% (w/v) Blocking Reagent) was mixed with the probe at a buffer : probe ratio of 300 : 1 and applied to the sample. Hybridization at 46°C for 3 h was followed by a subsequent 10 min wash step at 48°C with the adjusted washing buffer (14–900 mM NaCl, 20 mM Tris/HCl, pH 8, 5 mM EDTA, pH 8 and 0.01% SDS). Amplification buffer (×1 PBS [pH 7.3], 0.0015% [v/v] H_2O_2, 1% Alexa Fluor 488 or 594 dye ThermoFisher Scientific, Waltham, Massachusetts, U.S.A.) was prepared and slides incubated for 1 h at 46°C in a humid chamber until a final wash for 10 min in ×1 PBS. After washing, sections were incubated with a 1 μg/mL DAPI solution for 5–10 min at room temperature in the dark, washed with UPW, air-dried and embedded with 4 : 1 Citifluor/Vectashield mounting medium. Mounted samples were imaged with an epifluorescence microscope

(Ex/Em 490 nm/525 nm for FITC-labeled probes or tyramides, Ex/Em 358 nm/461 nm for CY3-labeled probes or tyramides).

Assessment

Embedding and slicing

We assessed the feasibility of aggregate embedding and thin-sectioning based on criteria relating to the direct ease of the procedure, the cost and time involved, and the quality of the sections obtained. Embedding of marine snow in Tissue-Tek was a fast and simple process. All aggregates collected from the MSC for this study were ballasted enough to sink into the cryogel within less than 1 h. Moreover, aggregates embedded in situ were spread evenly across the collection cup, enabling clear differentiation between aggregate types before slicing (Fig. 2b,c). Close examination showed very good structural preservation of gel-embedded aggregates with intact pigments and clearly identifiable components, e.g., diatoms protruding from the center of the aggregate (Fig. 2c,d). To avoid gradual dehydration of the Tissue-Tek during frozen storage, we recommend leaving a layer of 0.2 μm-filtered seawater on top of the gel and placing the frozen embedded samples in air-tight bags. During thawing, the relatively higher density of the cryogel prevents mixing with the water layer, which can be removed gently before the gel is re-frozen, mounted, and sectioned.

Tissue-Tek embedded marine snow was successfully sectioned with a mounting efficiency of 90% (± 10%). The material properties of Tissue-Tek permitted cutting sections between 5 μm and 100 μm in thickness, which enabled spatially resolved examination of organisms and structures spanning two orders of magnitude. Sections below 5 μm were prone to rupturing, probably because the supporting embedding matrix was not rigid enough to allow structurally preserved slicing of ultra-thin sections. Sections thicker than 100 μm on the other hand were prone to breaking during sectioning because of the rigidity of frozen cryogel. Thick sections (> 50 μm) yielded optimal results when studying the distribution of larger organisms such as phytoplankton cells or flagellates within an aggregate, or in conjunction with CLSM, where optical sectioning of nano- to micrometer-thick slices can be combined with cryotome-sectioning to reduce physical disturbance. However, Tissue-Tek is liquid (albeit highly viscous) at room temperature and in sections thicker than 50 μm the gel was observed to spill over the original boundaries of the section after thawing, resulting in flattening and possible distortion of the 3D structure. Therefore, we recommend a section thickness of 50–100 μm when studying larger organisms, and a section thickness of 5–50 μm for porosity measurements and reconstruction of the aggregate matrix.

Other possible artifacts introduced through slicing include smearing of the sample due to high amounts of silica and lithogenic material found in marine snow which can break along fault lines or be dragged across the section, resulting in the displacement and rupture of material. While this is a potentially strong contraindication against soft-embedding, we did not observe smearing in sections thicker than 5 μm and successfully reconstructed entire aggregates in three dimensions from thin-sections (*see* "3D-reconstruction" section). Optionally, cutting relatively thick sections (> 30 μm) combined with optical sectioning using CLSM can be used to obtain high depth resolution while avoiding smearing. The freezing process during soft-embedding has also been reported to cause damage, mainly through tissue rupturing due to ice crystal formation (Tokuyasu 1973). Ice crystal formation can be minimized through freezing at −80°C or snap-freezing in liquid nitrogen, although no freezing artifacts were observed in cryosections of marine snow frozen at −20°C, possibly due to loose connectivity of the solid fraction and thorough infiltration of pore space by the cryogel.

Soft-embedding and cryosectioning required low-cost consumables, and costs could be reduced further by using non-coated glass slides, applying a coating, or only mounting every n^{th} section of the aggregate, depending on the purpose of sectioning. We conclude that due to easy manipulation and mounting of frozen embedded samples and high recovery efficiency of sections, soft-embedding is a feasible tool for users with little to no previous experience with thin-sectioning.

Visualization and imaging of the aggregate matrix

Staining of the aggregate matrix was assessed based on the coverage and visibility of the stain, the compatibility with cell stains, the compatibility with soft-embedding, and the comparison to whole-aggregate staining. Generally, any stain applicable to aggregates filtered as a whole could also be used on aggregate sections. Concerning the brightness and visibility of any stain, the issue of strong autofluorescence of aggregate components applied here as much as it has been noted to be a problem for whole aggregate examination (Fig. 3; Woebken et al. 2007; Thiele et al. 2015).

When using fluorescent stains, we found that examining sections prior to staining helped with selecting a suitable stain with little overlap in the spectrum of autofluorescent material. We observed the highest amount of autofluorescence to be emitted in the green spectrum, while autofluorescence was weakest in the blue, red and deep red spectra. However, this may change according to aggregate composition and is highly dependent on organic matter quality, as e.g., chlorophyll *a* emits red fluorescence and was observed to have high fluorescent intensities in laboratory-formed aggregates containing healthy, active diatom cells, but not in in situ collected marine snow.

Staining of EPS

Alcian Blue successfully stained TEP of the aggregate matrix (Fig. 4a–c), as previously reported for whole, filtered

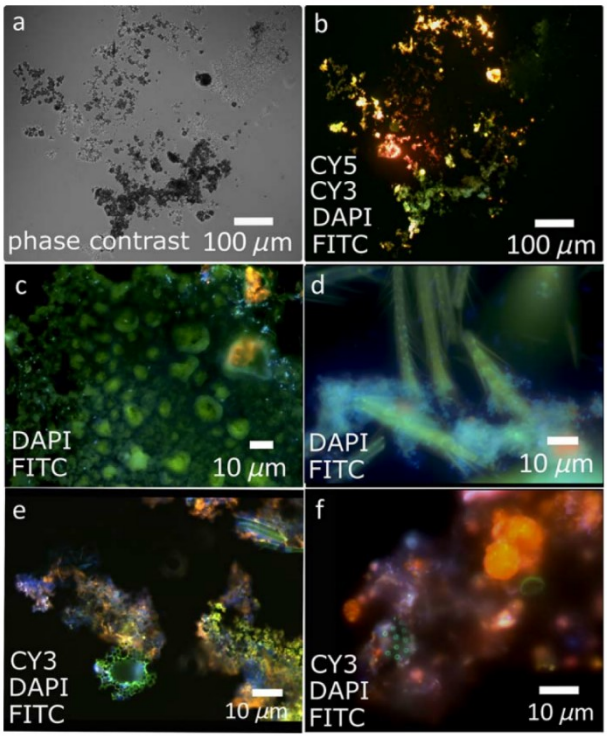

Fig. 3. Autofluorescent matrix components of unstained aggregate sections. (**a**) phase-contrast image of 10 μm-thick section; (**b**) the same section imaged with fluorescence microscopy; (**c**) unidentified structure with sparse bacterial attachment (DAPI-stained cells in blue); (**d**) heavy colonization of copepodide legs by DAPI-stained bacteria (blue); (**e**, **f**) unidentified structures.

marine snow (Passow and Alldredge 1995; Cisternas-Novoa et al. 2015). Coomassie Brilliant Blue staining yielded visible but weak signals of CSP and we observed CSP to be considerably less abundant than TEP, if not completely absent, which could be explained by the higher solubilization of proteins compared to polysaccharides in marine snow (Smith et al. 1992). FITC-ConA and Alexa647-ConA also successfully stained the aggregate matrix at concentrations as low as 100 μg/mL (Figs. 4d, 7), which was expected as lectin stains have been explored in considerable depth for staining EPS in biofilms (Neu et al. 2001; Strathmann et al. 2002), river snow (Neu 2000; Böckelmann et al. 2002), and sludge aggregates (McSwain et al. 2005; Weissbrodt et al. 2013). Compared to Alcian Blue, FITC-ConA/Alexa647-ConA covered similar areas of the aggregate matrix but stained slightly distinctive features. A similar observation was made for Ruthenium Red (Fig. 4). All three stains partially overlapped in their specificity for certain polysaccharides, but also bound to substrates not targeted by any of the other tested stains, highlighting the necessity to further explore polysaccharide diversity and their respective effects on particle aggregation (their "stickiness"), pore space reduction and degradation dynamics.

Special attention must be paid to avoid sample loss during rigorous staining or washing because of the solubility of cryogel in water. The SuperFrost Plus™ coating of the glass slides used in this study is designed to confer maximum samples adherence, but there is a risk of material being washed off, especially of thicker sections where material is not in direct contact with the adhesive coating of the slide. Decreased adhesion was seen in sections that had been stored for > 1 yr, meaning that swift processing of sections is advisable. We found that carefully applying the staining or washing solution with a pipette, removing the liquid with a pipette and lint-free wipes, and letting the sample dry face up (not tilted) caused negligible displacement or washing off of material, resulting in well preserved, distinctly stained sections. However, there was a limit of staining and washing steps before sample loss became difficult to avoid. For example, PAS staining successfully stained matrix components (Fig. 4g–i) but the intense staining and washing protocol led to visible disruption of section integrity (Fig. 4g). For staining procedures involving multiple staining and washing steps, agarose-embedding of sections added structural stability and improved section integrity and preservation. However, agarose-embedding is limited by non-specific binding to agarose by lectins (as observed in our study and reported by Bennke et al. 2013). Staining prior to embedding in cryogel may be considered to sidestep this problem, but limits the possibility of combining incompatible stains across consecutive slices and excludes aggregates embedded in situ.

Aggregate porosity

Optical porosity vs. calculated porosity Optical porosity of aggregate thin-sections ranged from 0.8 to 0.97 (void volume/total volume), and was found to be about 5–10% lower than calculated porosity (Alldredge and Gotschalk 1988). A possible cause was the integration of multiple layers of matter across the thickness of the section, leading to the omission of pore space and therefore underestimation of porosity. To minimize pore space omission, sections for measuring optical porosity should be cut as thinly as possible, i.e., 5–10 μm using our soft-embedding technique. Combining cryosectioning with optical sectioning (i.e., CLSM) improved resolution across depth, but was dependent on autofluorescence of solids or fluorescently stained substrates. Boundaries of aggregate thin-sections proved to be hard to determine due to loose connectivity and heterogeneous distribution of the solid fraction. We found that optical porosity varied by up to 50% depending on how the aggregate boundary was determined. This strongly suggested that a consistent approach for defining the section boundary was necessary. We compared various shapes for approximating the outer boundary of the sectioned aggregate (convex hull fittings, various ellipsoid fittings, polygons), and observed that the most robust approach for determining the outer boundary, and consequently to estimate the total area

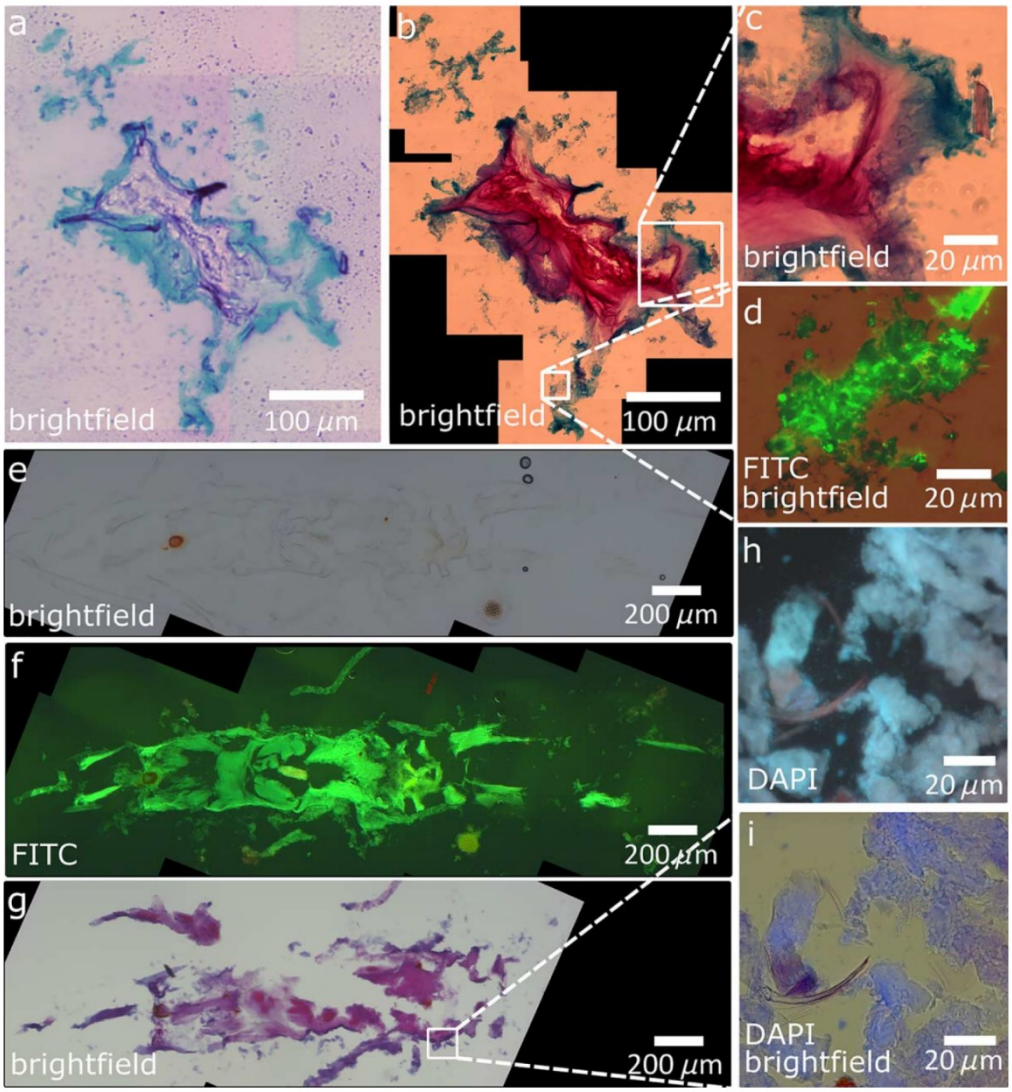

Fig. 4. Overview of matrix components in two separate thin-sections stained with selected dyes (section I **a**–**d**, section II **e**–**i**). (**a**) 10 μm-thick section I stained with Alcian Blue; (**b**) section I stained with Alcian Blue and Ruthenium Red; (**c**) close-up of section I stained with Alcian Blue and Ruthenium Red; (**d**) close-up of section I stained with Alcian Blue and FITC-ConA; (**e**) unstained 20 μm-thick section II imaged with brightfield microscopy; (**f**) section II imaged with fluorescence microscopy; (**g**) section II stained with PAS; (**h**) close-up of section II imaged with fluorescence microscopy; (**i**) close-up of section II imaged with fluorescence and brightfield microscopy.

of the section, was to fit an ellipse to the maximum aggregate width and height (Fig. 5). The same approach is used for measuring aggregate volume for porosity calculations (Alldredge and Gotschalk 1988) which is why this fitting resulted in the closest match to calculated porosity.

Pore size distribution between and across aggregate sections Optical porosity values were relatively constant across stacked aggregates sections, with mean values of 0.975 (SD ± 0.013) measured for the unstained aggregate. Porosity and pore size was much more variable across single sections where we generally observed regions with high porosity interspersed by regions of low porosity, with pore space being distributed more heterogeneously in aggregates collected in situ (Fig. 5a,b,d–f,h) compared with aggregates formed from diatom monocultures in the laboratory (Fig. 5c,g). Further, we observed large reductions in porosity down to 0.8454 (SD ± 0.040) in sections stained with Alcian Blue (Fig. 5g,h). Direct

assessment of thin-sections not only enabled the determination of porosity defined as the fraction of solid components to overall aggregate volume, but also of the effective porosity, i.e., porosity defined as the fraction of "non-void" components, including the EPS matrix, to aggregate volume. While Alcian Blue-staining reduced porosity by approximately 10%, we observed that Ruthenium Red reduced optical porosity by another 5–10%, but these observations can be expected to vary greatly depending on aggregate type and source. Thus, a combination of stains covering a broad range of polymers found in the marine snow matrix could potentially help to obtain more accurate estimates of effective aggregate porosity.

3D-reconstruction

3D reconstruction from cryosections highlighted the porous nature and heterogeneity of marine snow because of the possibility to examine aggregates from any chosen angle. The decrease in effective pore size by TEP became especially obvious when comparing the unstained with the Alcian Blue-stained reconstructed aggregate (Fig. 6). However, the patchy distribution of visible substrates and large amount of pore space complicated alignment of sections along the *z*-axis and stains with higher coverage (e.g., Alcian Blue) facilitated more precise alignment because of better cross-referencing between consecutive sections. To enable alignment independent of staining, we suggest introducing an external reference into the embedding matrix, which we so far have not achieved.

Visualization of aggregate colonizers

In addition to staining the aggregate matrix, we tested methods of staining bacteria in aggregate sections. Nucleic acid (DAPI) staining clearly visualized bacterial cells and their localization relative to autofluorescent and ConA-stained substrate, showing close bacteria-substrate associations (Figs. 3c,d, 7, 8).

Of the three FISH methods tested (mono-labeled FISH, multi-labeled FISH, and CARD-FISH), we determined multi-labeled FISH to be the most versatile method for staining selected clades of bacteria or archaea in soft-embedded sections: mono-labeled FISH (Fig. 8d) resulted in low fluorescent signal intensity and labeling success, possibly due to high autofluorescence of the samples (Fig. 3). CARD-FISH (Fig. 8c, e–g) yielded distinctive signals, but CARD-chemistry necessitates additional permeabilization and washing steps that can destabilize the integrity of the section and thus requires agarose-embedding of sections prior to CARD-FISH. Multi-labeled FISH combines the high signal intensity of CARD-FISH with the low amount of washing and sample handling of mono-labeled FISH (Fig. 8a,b). An additional advantage of multi-labeled FISH is the option of multiplexing several probes on the same section without the horseradish peroxidase inactivation necessary for CARD-FISH.

Following the FISH protocol without prior embedding of sections in 0.1% LE agarose led to some sections being lost in the process. Although not all sections were washed off, we observed that soft-embedding cannot provide sufficient structural support during FISH to guarantee sustained integrity of the sections, and recommend agarose-embedding before FISH.

Agarose-embedding has been found to limit the use of lectins in conjunction with CARD-FISH, as unspecific binding to agarose prohibits staining after CARD-FISH, but staining prior to embedding and CARD-FISH leads to severely reduced fluorescent signal intensity of the lectin stain. However, we did not observe any impact on the quality of the lectin stain following the mono- or multi-labeled FISH protocols. We attributed this to the lower number of washing steps compared to CARD-FISH which reduces loss of the label ligand as well as to the absence of protein-denaturing buffer solutions that are part of the CARD-FISH protocol. This endorses the use of multi-labeled FISH to be used in conjunction with EPS staining, as a protective agarose coating can be applied to the section after lectin staining but prior to multi-labeled FISH. Combining multi-labeled FISH and lectin staining in structurally preserved sections, we could see the accumulation of bacteria inside small channels in the polysaccharide matrix (Fig. 8a).

Discussion

In this study, we showed how combining soft-embedding with thin-sectioning of in situ collected aggregates provides insight into their physical structure and the distribution and diversity of microbial colonizers. A particular strength of this method lies in the minimal amount of active handling, particularly of aggregates embedded in situ in gel-filled collection cups. Without the possibility to analyze the composition and 3D structure of intact, non-embedded macro-aggregates, the degree of structural preservation during embedding and slicing cannot be assessed quantitatively. However, the consistent agreement of our findings regarding stainability, porosity, and composition to existing literature (as discussed in the "Assessment" section) strongly suggest minimal disturbance of aggregates during embedding and slicing. Good structural preservation during embedding is further supported by observations of natural aggregates collected with gel traps in previous studies (Ebersbach and Trull 2008; Laurenceau-Cornec et al. 2015; Wiedmann et al. 2016). Although some disturbance during sectioning and staining cannot be ruled out we have provided recommendations on how potential disturbances can be minimized (*see* "Assessment" for details). This is further supported by good alignment of consecutive sections enabling 3D reconstruction. The relative ease, lack of hazardous chemicals or specialized equipment, and low time expenditure for the embedding process make this method especially suited for ship- or field-based sampling. The compatibility with existing FISH protocols offers a previously unattainable spatial resolution of the distribution of microbial groups

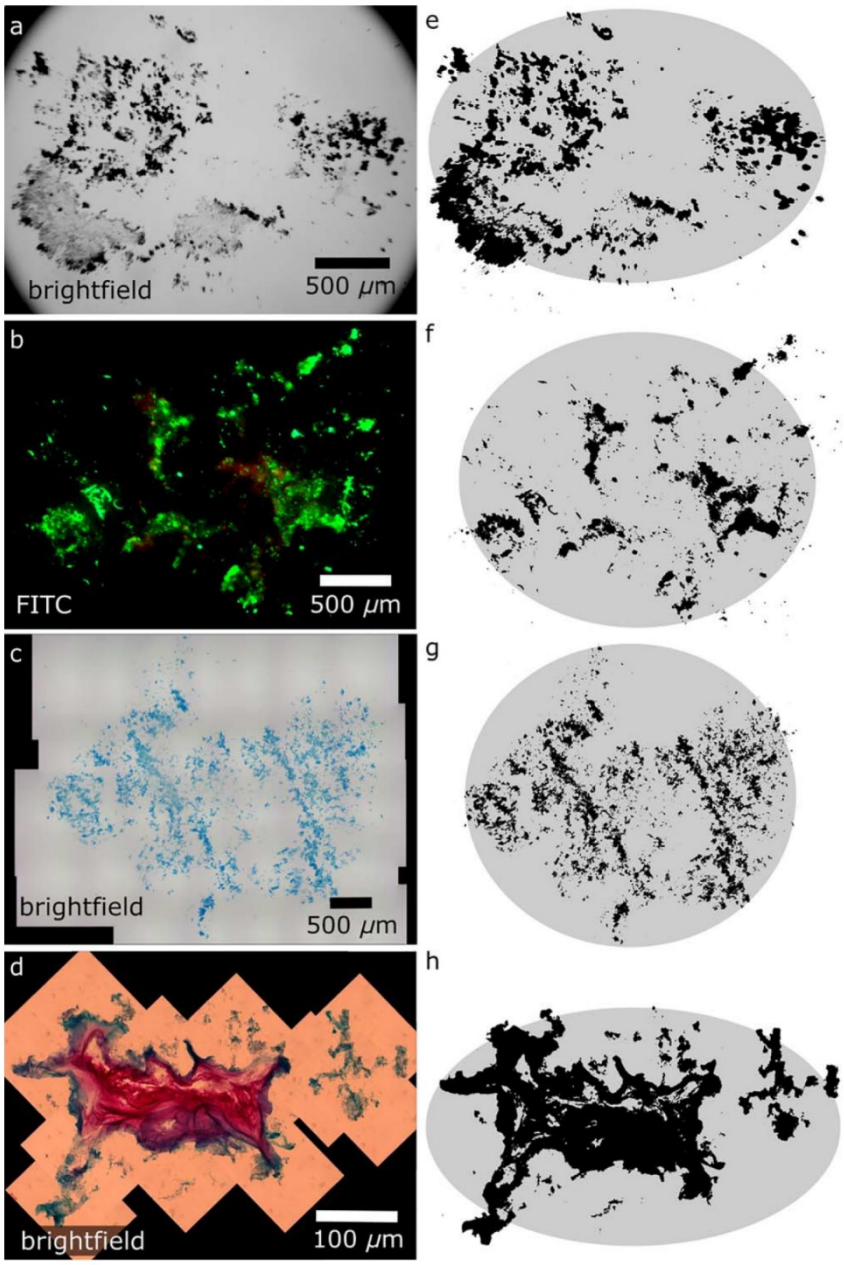

Fig. 5. Sections used to test optical porosity measurements. (**a**, **b**) Unstained 10 μm section of in situ collected aggregates; (**c**) Alcian Blue-stained 10 μm section of laboratory-formed *S. marinoi* aggregate; (**d**) Alcian Blue and Ruthenium Red-stained 10 μm section of in situ collected aggregate; (**e**–**h**) corresponding thresholded images used for measuring the area of solid or stained fractions (black) and ellipses fitted using the maximum width and height of the section to measure the total area of the section (overlay in gray).

within individual aggregates, with the added possibility of studying their co-localization with selected substrates of the aggregate matrix.

Preserving aggregate structure throughout staining and microscopy can shed light on attributes of marine snow that could so far not be examined because of disaggregation and

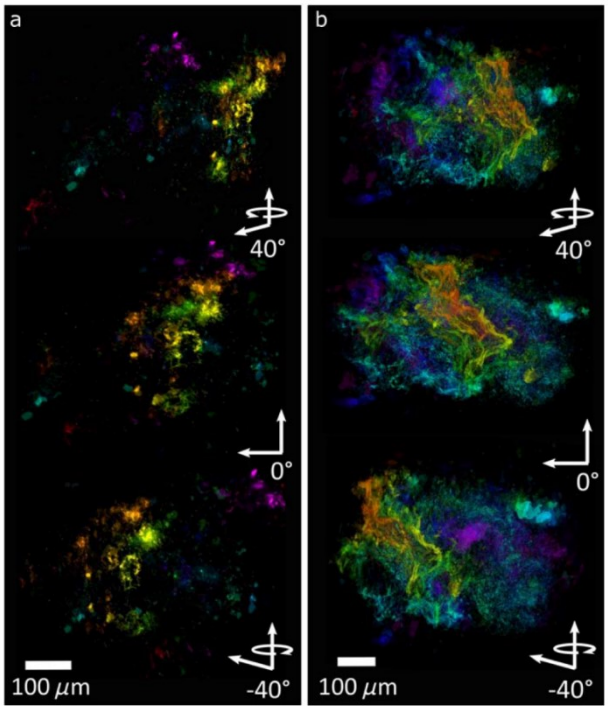

Fig. 6. 3D reconstruction of two 10 μm-sectioned aggregates based on (**a**) green autofluorescence and (**b**) Alcian Blue staining. Aggregates are pictured from three different angles, with a gradual change in color representing an increase in *z*-depth (frontback). Rotating video clips of both aggregates are available as Supporting Information.

structural disturbance during filtering. Several studies have explored the use of confocal laser scanning microscopy for the examination of structurally intact marine, riverine, and sludge aggregates (Thill et al. 1998; Neu 2000; Waite et al. 2000; Böckelmann et al. 2002). Compared to optical sectioning, embedding followed by physical sectioning can introduce sectioning artifacts (*see* "Assessment" section). However, optical sectioning also produces artifacts such as effects of self-shadowing, reduced fluorescent signal intensity with increasing scanning depth, bleaching of fluorescent signals, and limited working distance for larger samples (Dixon et al. 1991). Marine snow regularly reaches sizes of several millimeters, thereby limiting the resolution at which aggregates can be studied using Confocal Laser Scanning Microscopy alone. Embedding enables structurally preserved storage of samples, whereas optical sectioning requires immediate analysis as samples lack a supporting embedding matrix to retain structural integrity. Perhaps most importantly, we showed how physical sectioning offers the possibility of applying different stains to consecutive sections of the same aggregate to study the distribution of different matrix components across the aggregate (a form of pseudo-multiplexing), thus reducing limits imposed by overlapping color spectra of stains, fluorescent quenching, and stain incompatibility or interference. We do not consider optical section to be a feasible stand-alone method for analyzing in situ collected marine snow, but as we demonstrated in this study it can be a valuable complement to physical sectioning by increasing resolution across section depth, which is especially useful with respect to porosity measurements.

An alternative to the soft-embedding method presented here is embedding aggregates in hard resin (Leppard et al. 1996; Chu et al. 2004). Hard-embedding matrices support sectioning of ultra-thin slices (< 1 μm), which can be particularly useful for the investigation of sub-cellular structures and compartments (Heissenberger et al. 1996). Moreover, the resin matrix cannot be re-dissolved after polymerization, effecting high structural cohesion during washing and staining. Transport and long-term storage of hard-embedded samples is also more convenient, as it is not dependent on maintaining sub-zero temperatures. However, it is impossible

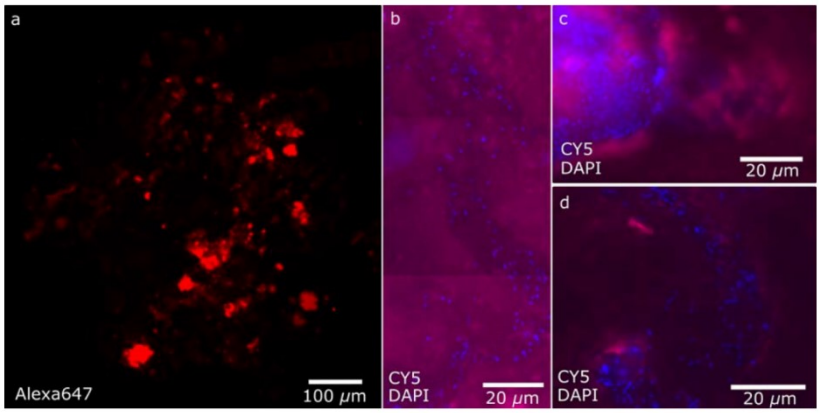

Fig. 7. (**a**) Section stained with Alexa647-ConA; (**b–d**) details showing ConA matrix (purple) with DAPI-stained bacteria embedded (blue).

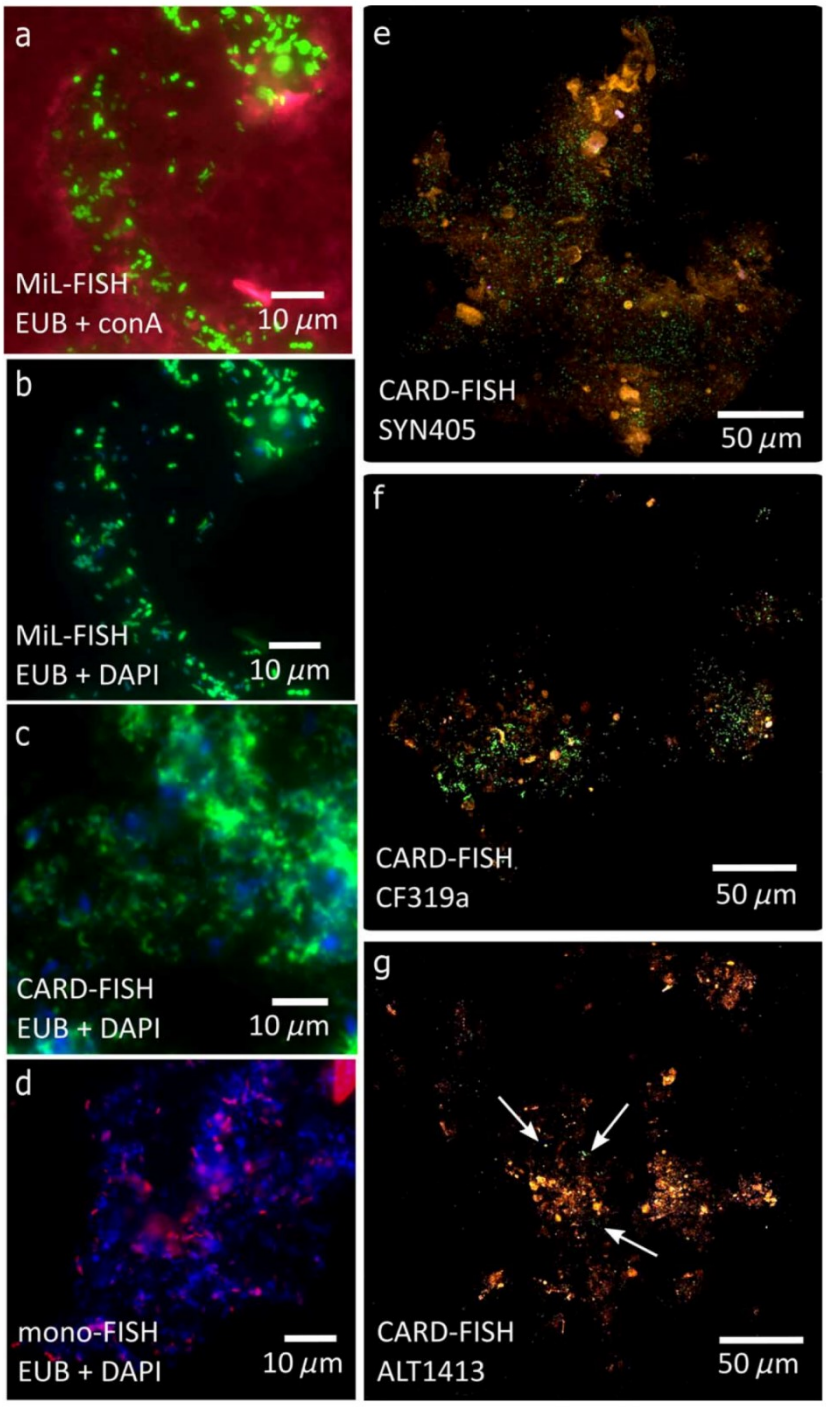

Fig. 8. FISH-probing of marine snow thin-sections. (**a**) EUB-labeled bacteria (green) embedded in channels inside the aggregate EPS matrix stained by conA (purple); (**b**–**d**) comparison of EUB labeling efficiency and fluorescent signal intensity for the three FISH methods used in this study: (**b**) MiL-FISH (green-fluorescent fluorophores); (**c**) CARD-FISH (green-fluorescent tyramides); (**d**) mono-FISH (red-fluorescent fluorophores); (**e**–**g**) thin-section from one in situ collected aggregate (phytoplankton autofluorescence shown in red) stained with probes for selected bacterial clades (green) using CARD-FISH: (**e**) *Synechococcus* spp.-specific probe; (**f**) *Bacteroidetes*-specific probe; (**g**) *Alteromonadales*-specific probe (arrows indicate localization of hardly visible FISH-stained bacteria). Rotating video clips of aggregate sections (**e**–**g**) are available as Supporting Information.

to equip sediment traps with hard resins to embed aggregates in situ. We consider direct fixation, washing, and embedding in situ to be one of the most substantial features of soft-embedding, as the absence of active handling prevents any risks of handling artifacts. The handling steps for soft-embedding of aggregates collected with a Marine Snow Catcher exclude the heating and complete dehydration that are needed for hard-embedding. The compatibility with FISH protocols furthermore enables taxonomic analysis of aggregate colonizers.

Practical applications of soft-embedding

Aggregate structure and porosity

By successfully staining the matrix of soft-embedded aggregate thin-sections using established staining protocols, we could visualize the spatial distribution of TEP and other EPS. By aligning consecutive sections along the *z*-axis we succeeded in rendering a 3D reconstruction of entire aggregates based on solid and Alcian Blue-stained fractions of the matrix. Aside from an increased appreciation of the aggregate-scale distribution of selected matrix fractions, 3D rendering enables clearer determination of aggregate boundaries in any direction than can be achieved by analyzing single sections. The current standard of quantifying TEP (and by extension EPS) developed by Passow and Alldredge (1995) involves filtering of organic material onto polycarbonate filters followed by staining and subsequent dissolution in sulfuric acid for spectrophotometric analysis, meaning no inferences can be made about the spatial distribution of TEP in aggregates.

In combination with spectrophotometric Alcian Blue assays (or lectin quantification assays as developed by Uthicke et al. 2009), and/or incubation experiments, examining the distribution and patchiness of EPS on a sub-aggregate level can advance our knowledge of what determines "stickiness" of aggregates and their components both during formation and disaggregation, and of the contribution by different EPS fractions to effective pore-space reduction. We also showed how applying several stains to cover a range of EPS could be used as a measure for "non-void," i.e., effective porosity, which can be used to approximate aggregate permeability. A separation into total and effective porosity can be useful to better understand mass transport of particulate and dissolved matter between aggregates and ambient water, as solid matter is restricted to being transported via actual pores, whereas fluids and gases can diffuse into and out of the aggregate matrix, which is of significance for colonization, nutrient release, oxygen supply, settling velocities, and mass fluxes.

Measuring the area of the solid or stainable fraction relative to the total area of thin-sections enabled us to estimate the optical porosity of sectioned aggregates and to give a spatially resolved structural description of intact marine snow. We do not suggest that the "optical porosity method" introduced here is superior to calculated porosity, as the inherent challenges (definition of the aggregate boundary, integration of matter across section depth) require further revision of this method. However, we regard it as a valuable complement to existing methods of calculating porosity, as direct visualization of matrix fractions and pore space can address questions that could so far not be resolved, including the effect of different solid and EPS fractions on porosity and pore distribution, and the variability of pore space across single sections. Furthermore, optical porosity can be estimated from singles aggregates, whereas calculating porosity according to Alldredge and Gotschalk (1988) requires averaging of values obtained from multiple aggregates due to methodological constraints. Analysis of pore distribution-connectivity across single sections together with alignment of consecutive sections and 3D reconstruction as demonstrated in this study, can enable detection of any channels through the aggregate matrix that could permit advective flow (i.e., channels that are connected to the outside of the aggregate and have a diameter greater than the Kolmogorov length scale of 5 μm, below which advection is drastically limited by viscosity). Exploring the presence and extent of advective flow remains a key goal, as advection has the potential to influence metabolic processes inside marine snow through influx of oxygenated water that reduces the occurrence or increases the patchiness of processes other than aerobic respiration (e.g., denitrification).

Microbial colonization and taxonomic diversity

Because of the preserved structure of embedded aggregates, we could spatially resolve the distribution of microbial colonizers inside individual aggregates. We consider this an important step toward exploring microbial colonization of marine snow in situ which can help resolve many outstanding questions about the colonization and succession dynamics on settling aggregates. Chemotactic, pelagic bacteria have been shown to be highly successful at seeking out small-scale nutrient patches like diatom cells or chains (Stocker et al. 2008; Smriga et al. 2016) and settling particles, which were newly colonized on scales of minutes to hours (Kiørboe et al. 2002, 2003; Grossart et al. 2003, 2006). Because of the dynamic aggregation and disaggregation of marine aggregates it is particularly hard to study in situ bacterial colonization and succession patterns. Often, such studies have been restricted to laboratory model systems (Datta et al. 2016) or inferences made from comparing community composition of free-living and particle-attached bacteria using filtered size-fractions (e.g., Mestre et al. 2017). Unfortunately, taxonomic composition of filter fractions has been shown to deviate notably from that of non-fractionated samples (Craig 1986; Padilla et al. 2015). In situ gel-embedding of marine aggregates sidesteps this issue as aggregates can be picked selectively from the gel to analyze their microbial composition, e.g., using FISH (Thiele et al. 2015). Thin-sectioning of embedded aggregates further allows high resolution studies of microbial colonization processes and dynamics in relation to small-scale aggregate structure and composition.

With preserved spatial structure, we showed the accumulation of bacteria inside small channels in the polysaccharide matrix. These channels could be formed through hydrolysis of the substrate by colonizing bacteria, or during aggregation and direct advective and diffusive flow of water carrying microorganisms through the aggregate matrix. Analyzing the localization of microbial groups or clusters inside aggregates over water depth and/or time could provide a way to study the respective importance or dominance of the bacterial community originally present during aggregate formation with that of bacteria attaching to (or being scavenged by) the aggregates during settling. Imaging of bacterial clades co-localized with substrates or degradation products also presents a way to directly visualize microbe–substrate interactions and complement current techniques used to infer microbial activity such as tracer addition to incubation experiments, transcriptomics, or single-cell uptake measurements.

Marine carbon fluxes and closing statement

Collecting and embedding aggregates in situ using drifting sediment traps not only minimizes active handling but presents a new and exciting possibility to study the micro-scale structure, composition and diversity of the aggregate matrix and aggregate colonizers in combination with particle characteristics, biogeochemical fluxes, and molecular methods applied to sediment trap material (e.g., DNA/RNA extraction). We consider this an important step toward understanding the ecology and connectivity of the pelagic zone with strong potential to open up new possibilities to research the microbial processes controlling the biological carbon pump and recycling of organic matter in the water column.

References

Alldredge, A. L., and C. Gotschalk. 1988. In situ settling behavior of marine snow. Limnol. Oceanogr. **33**: 339–351. doi:10.4319/lo.1988.33.3.0339

Alldredge, A. L., and M. W. Silver. 1988. Characteristics, dynamics and significance of marine snow. Prog. Oceanogr. **20**: 41–82. doi:10.1016/0079-6611(88)90053-5

Alldredge, A. L., and C. C. Gotschalk. 1990. The relative contribution of marine snow of different origins to biological processes in coastal waters. Cont. Shelf Res. **10**: 41–58. doi:10.1016/0278-4343(90)90034-J

Alldredge, A. L., U. Passow, and B. E. Logan. 1993. The abundance and significance of a class of large, transparent organic particles in the ocean. Deep-Sea Res. Part I **40**: 1131–1140. doi:10.1016/0967-0637(93)90129-Q

Amann, R. I., B. J. Binder, R. J. Olson, S. W. Chisholm, R. Devereux, and D. A. Stahl. 1990. Combination of 16S RRNA-targeted oligonucleotide probes with flow cytometry for analyzing mixed microbial populations. Appl. Environ. Microbiol. **56**: 1919–1925.

Bennke, C. M., T. R. Neu, B. M. Fuchs, and R. Amann. 2013. Mapping glycoconjugate-mediated interactions of marine bacteroidetes with diatoms. Syst. Appl. Microbiol. **36**: 417–425. doi:10.1016/j.syapm.2013.05.002

Böckelmann, U., W. Manz, T. R. Neu, and U. Szewzyk. 2002. Investigation of lotic microbial aggregates by a combined technique of fluorescent in situ hybridization and lectin-binding-analysis. J. Microbiol. Methods **49**: 75–87. doi:10.1016/S0167-7012(01)00354-2

Cardona, A., and others. 2012. TrakEM2 software for neural circuit reconstruction. PLoS One **7**: e38011. doi:10.1371/journal.pone.0038011

Chu, C. P., D. J. Lee, and X. F. Peng. 2004. Structure of conditioned sludge flocs. Water Res. **38**: 2125–2134. doi:10.1016/j.watres.2004.02.003

Ciais, P., and others. 2014. Current systematic carbon-cycle observations and the need for implementing a policy-relevant carbon observing system. Biogeosciences **11**: 3547–3602. doi:10.5194/bg-11-3547-2014

Cisternas-Novoa, C., C. Lee, and A. Engel. 2015. Transparent exopolymer particles (TEP) and Coomassie stainable particles (CSP): Differences between their origin and vertical distributions in the ocean. Mar. Chem. **175**: 56–71. doi:10.1016/j.marchem.2015.03.009 doi:10.1016/j.marchem.2015.03.009

D'Ambrosio, L., K. Ziervogel, B. MacGregor, A. Teske, and C. Arnosti. 2014. Composition and enzymatic function of particle-associated and free-living bacteria: A coastal/offshore comparison. ISME J. **8**: 2167–2179. doi:10.1038/ismej.2014.67

Datta, M. S., E. Sliwerska, J. Gore, M. F. Polz, and O. X. Cordero. 2016. Microbial interactions lead to rapid micro-scale successions on model marine particles. Nat. Commun. **7**: 11965. doi:10.1038/ncomms11965

DeLong, E. F., D. G. Franks, and A. L. Alldredge. 1993. Phylogenetic diversity of aggregate-attached vs. free-living marine bacterial assemblages. Limnol. Oceanogr. **38**: 924–934. doi:10.4319/lo.1993.38.5.0924

Dixon, A. E., S. Damaskinos, and M. R. Atkinson. 1991. A scanning confocal microscope for transmission and reflection imaging. Nature **351**: 551–553. doi:10.1038/351551a0

Ebersbach, F., and T. W. Trull. 2008. Sinking particle properties from polyacrylamide gels during the Kerguelen Ocean and Plateau compared Study (KEOPS): Zooplankton control of carbon export in an area of persistent natural iron inputs in the Southern Ocean. Limnol. Oceanogr. **53**: 212–224. doi:10.4319/lo.2008.53.1.0212

Grossart, H. P., T. Kiørboe, K. Tang, and H. Ploug. 2003. Bacterial colonization of particles: Growth and interactions. Appl. Environ. Microbiol. **69**: 3500–3509. doi:10.1128/AEM.69.6.3500-3509.2003

Grossart, H. P., T. Kirboe, K. W. Tang, M. Allgaier, E. M. Yam, and H. Ploug. 2006. Interactions between marine snow and heterotrophic bacteria: Aggregate formation and microbial dynamics. Aquat. Microb. Ecol. **42**: 19–26. doi:10.3354/ame042019

Heissenberger, A., G. G. Leppard, and G. J. Herndl. 1996. Ultrastructure of marine snow. II. Microbiological considerations. Mar. Ecol. Prog. Ser. **135**: 299–308. doi:10.3354/meps135299

Holloway, C. F., and J. P. Cowen. 1997. Development of a scanning confocal laser microscopic technique to examine the structure and composition of marine snow. Limnol. Oceanogr. **42**: 1340–1352. doi:10.4319/lo.1997.42.6.1340

Honjo, S., S. J. Manganini, R. A. Krishfield, and R. Francois. 2008. Particulate organic carbon fluxes to the ocean interior and factors controlling the biological pump: A synthesis of global sediment trap programs since 1983. Prog. Oceanogr. **76**: 217–285. doi:10.1016/j.pocean.2007.11.003

IPCC. 2013. Climate change 2013: The Physical Science Basis. 1535 pp. *In* T. F. Stocker, D. Qin, G.-K. Plattner, and others [eds.], Contribution of Working Group I to the Fifth Assessment Report of the Intergovernmental Panel on Climate Change. Cambridge University Press, Cambridge, United Kingdom and New York, NY, USA, doi:10.1017/CB09781107415324

Iversen, M. H., and H. Ploug. 2010. Ballast minerals and the sinking carbon flux in the ocean: Carbon-specific respiration rates and sinking velocity of marine snow aggregates. Biogeosciences **7**: 2613–2624. doi:10.5194/bg-7-2613-2010

Iversen, M. H., and H. Ploug. 2013. Temperature effects on carbon-specific respiration rate and sinking velocity of diatom aggregates – potential implications for deep ocean export processes. Biogeosciences **10**: 4073–4085. doi:10.5194/bg-10-4073-2013 doi:10.5194/bg-10-4073-2013

Kiørboe, T., H. P. Grossart, H. Ploug, and K. Tang. 2002. Mechanisms and rates of bacterial colonization of sinking aggregates. Appl. Environ. Microbiol. **68**: 3996–4006. doi:10.1128/AEM.68.8.3996-4006.2002

Kiørboe, T., K. W. Tang, H. P. Grossart, and H. Ploug. 2003. Dynamics of microbial communities on marine snow aggregates: Colonization, growth, detachment, and grazing mortality of attached bacteria. Appl. Environ. Microbiol. **69**: 3036–3047. doi:10.1128/AEM.69.6.3036-3047.2003

Krupke, A., L. R. Hmelo, J. E. Ossolinski, T. J. Mincer, and B. A. S. Van Mooy. 2016. Quorum sensing plays a complex role in regulating the enzyme hydrolysis activity of microbes associated with sinking particles in the ocean. Front. Mar. Sci. **3**: 55. doi:10.3389/fmars.2016.00055

Laurenceau-Cornec, E. C., and others. 2015. The relative importance of phytoplankton aggregates and zooplankton fecal pellets to carbon export: Insights from free-drifting sediment trap deployments in naturally iron-fertilised waters near the Kerguelen Plateau. Biogeosciences **12**: 1007–1027. doi:10.5194/bg-12-1007-2015

Leppard, G. G., A. Heissenberger, and G. J. Herndl. 1996. Ultrastructure of marine snow. I. Transmission electron microscopy methodology. Mar. Ecol. Prog. Ser. **135**: 289–298. doi:10.3354/meps135289

Long, R., and F. Azam. 1996. Abundant protein-containing particles in the sea. Aquat. Microb. Ecol. **10** (June): 213–221. doi:10.3354/ame010213

Luef, B., T. R. Neu, and P. Peduzzi. 2009*a*. Imaging and quantifying virus fluorescence signals on aquatic aggregates: A new method and its implication for aquatic microbial ecology. FEMS Microbiol. Ecol. **68**: 372–380. doi:10.1111/j.1574-6941.2009.00675.x

Luef, B., T. R. Neu, I. Zweimüller, and P. Peduzzi. 2009b. Structure and composition of aggregates in two large European rivers, based on confocal laser scanning microscopy and image and statistical analyses. Appl. Environ. Microbiol. **75**: 5952–5962. doi:10.1128/AEM.00186-09

Lundsgaard, C. 1995. Use of a high viscosity medium in studies of aggregates, p. 141–152. *In* S. Floderus, A.-S. Heisakanen, M. Oleson, and P. Wassman [eds.], Sediment trap studies in the Nordic countries 3. Proceedings of the Symposium on Seasonal Dynamics of Planktonic Ecosystems and Sedimentation in Coastal Nordic Waters.

Mari, X., U. Passow, C. Migon, A. B. Burd, and L. Legendre. 2017. Transparent exopolymer particles: Effects on carbon cycling in the ocean. Prog. Oceanogr. **151** (February): 13–37. doi:10.1016/j.pocean.2016.11.002

McSwain, B. S., R. L. Irvine, M. Hausner, and P. A. Wilderer. 2005. Composition and distribution of extracellular polymeric substances in aerobic flocs and granular sludge. Appl. Environ. Microbiol. **71**: 1051–1057. doi:10.1128/AEM.71.2.1051-1057.2005

Mestre, M., E. Borrull, M. Montserrat Sala, and J. M. Gasol. 2017. Patterns of bacterial diversity in the marine planktonic particulate matter continuum. ISME J. **11**: 999–1010. doi:10.1038/ismej.2016.166

Neu, T. R. 2000. In situ cell and glycoconjugate distribution in river snow studied by confocal laser scanning microscopy. Aquat. Microb. Ecol. **21**: 85–95. doi:10.3354/ame021085

Neu, T., G. D. Swerhone, and J. R. Lawrence. 2001. Assessment of lectin-binding analysis for in situ detection of glycoconjugates in biofilm systems. Microbiology **147** (Pt 2): 299–313. doi:10.1099/00221287-147-2-299

Padilla, C. C., S. Ganesh, S. Gantt, A. Huhman, D. J. Parris, N. Sarode, and F. J. Stewart. 2015. Standard filtration practices may significantly distort planktonic microbial diversity estimates. Front. Microbiol. **6**: 547. doi:10.3389/fmicb.2015.00547

Passow, U., and A. L. Alldredge. 1995. A dye-binding assay for the spectrophotometric measurement of transparent exopolymer particles (TEP). Limnol. Oceanogr. **40**: 1326–1335. doi:10.4319/lo.1995.40.7.1326

Passow, U., and C. A. Carlson. 2012. The biological carbon pump in a high CO2 world. Mar. Ecol. Prog. Ser. **470**: 249–271. doi:10.3354/meps09985

Pernthaler, A., J. Pernthaler, and R. Amann. 2002. Fluorescence in situ hybridization and catalyzed reporter

deposition for the identification of marine bacteria. Appl. Environ. Microbiol. **68**: 3094–3101. doi:10.1128/AEM.68.6.3094-3101.2002

Ploug, H., and H.-P. Grossart. 2000. Bacterial growth and grazing on diatom aggregates: Respiratory carbon turnover as a function of aggregate size and sinking velocity. Limnol. Oceanogr. **45**: 1467–1475. doi:10.4319/lo.2000.45.7.1467

Ploug, H., M. H. Iversen, and G. Fischer. 2008. Ballast, sinking velocity, and apparent diffusivity within marine snow and zooplankton fecal pellets: Implications for substrate turnover by attached bacteria. Limnol. Oceanogr. **53**: 1878–1886. doi:10.4319/lo.2008.53.5.1878

Ploug, H., and U. Passow. 2007. Direct measurement of diffusivity within diatom aggregates containing transparent exopolymer particles. Limnol. Oceanogr. **52**: 1–6. doi:10.4319/lo.2007.52.1.0001

Ransom, B., K. F. Shea, P. J. Burkett, R. H. Bennett, and R. Baerwald. 1998. Comparison of pelagic and nepheloid layer marine snow: Implications for carbon cycling. Mar. Geol. **150**: 39–50. doi:10.1016/S0025-3227(98)00052-8

Riley, J. S., R. Sanders, C. Marsay, F. A. C. Le Moigne, E. P. Achterberg, and A. J. Poulton. 2012. The relative contribution of fast and slow sinking particles to ocean carbon export. Global Biogeochem. Cycles **26**: GB1026. doi:10.1029/2011GB004085

Saalfeld, S., A. Cardona, V. Hartenstein, and P. Tomančák. 2010. As-rigid-as-possible mosaicking and serial section registration of large ssTEM datasets. Bioinformatics **26**: i57–i63. doi:10.1093/bioinformatics/btq219

Saalfeld, S., R. Fetter, A. Cardona, and P. Tomancak. 2012. Elastic volume reconstruction from series of ultra-thin microscopy sections. Nat. Methods **9**: 717–720. doi:10.1038/nmeth.2072

Schimak, M. P., M. Kleiner, S. Wetzel, M. Liebeke, N. Dubilier, and B. M. Fuchs. 2015. MiL-FISH: Multi-labelled oligonucleotides for fluorescence in situ hybridisation improve visualization of bacterial cells. Appl. Environ. Microbiol. **82**:62–70. doi:10.1128/AEM.02776-15

Schindelin, J., and others. 2012. Fiji: An open-source platform for biological-image analysis. Nat. Methods **9**: 676–682. doi:10.1038/nmeth.2019

Schindelin, J., C. T. Rueden, M. C. Hiner, and K. W. Eliceiri. 2015. The ImageJ ecosystem: An open platform for biomedical image analysis. Mol. Reprod. Dev. **82**: 518–529. doi:10.1002/mrd.22489

Schmid, B., J. Schindelin, A. Cardona, M. Longair, and M. Heisenberg. 2010. A high-level 3D visualization API for Java and ImageJ. BMC Bioinf. **11**: 274. doi:10.1186/1471-2105-11-274

Schneider, C. A., W. S. Rasband, and K. W. Eliceiri. 2012. NIH Image to ImageJ: 25 years of image analysis. Nat. Methods **9**: 671–675. doi:10.1038/nmeth.2089

Smith, D. C., M. Simon, A. L. Alldredge, and F. Azam. 1992. Intense hydrolytic enzyme activity on marine aggregates and implications for rapid particle dissolution. Nature **359**: 139–142. doi:10.1038/359139a0

Smriga, S., V. I. Fernandez, J. G. Mitchell, and R. Stocker. 2016. Chemotaxis toward phytoplankton drives organic matter partitioning among marine bacteria. Proc. Natl. Acad. Sci. USA **113**: 1576–1581. doi:10.1073/pnas.1512307113

Stocker, R., J. R. Seymour, A. Samadani, D. E. Hunt, and M. F. Polz. 2008. Rapid chemotactic response enables marine bacteria to exploit ephemeral microscale nutrient patches. Proc. Natl. Acad. Sci. USA **105**: 4209–4214. doi:10.1073/pnas.0709765105

Strathmann, M., J. Wingender, and H.-C. Flemming. 2002. Application of fluorescently labelled lectins for the visualization and biochemical characterization of polysaccharides in biofilms of Pseudomonas aeruginosa. J. Microbiol. Methods **50**: 237–248. doi:10.1016/S0167-7012(02)00032-5

Thiele, S., B. M. Fuchs, R. Amann, and M. H. Iversen. 2015. Colonization in the photic zone and subsequent changes during sinking determines bacterial community composition in marine snow. Appl. Environ. Microbiol. **81**: 1463–1471. doi:10.1128/AEM.02570-14

Thill, A., S. Veerapaneni, B. Simon, M. Wiesner, J. Y. Bottero, and D. Snidaro. 1998. Determination of structure of aggregates by confocal scanning laser microscopy. J. Colloid Interface Sci. **204**: 357–362. doi:10.1006/jcis.1998.5570

Tiessen, H., and J. W. B. Stewart. 1988. Light and electron microscopy of stained microaggregates: The role of organic matter and microbes in soil aggregation. Biogeochemistry **5**: 312–322. doi:10.1007/BF02180070

Tokuyasu, K. T. 1973. A technique for ultracryotomy of cell suspensions and tissues. J. Cell Biol. **57**: 551–565. doi:10.1083/jcb.57.2.551

Turner, J. T. 2015. Zooplankton fecal pellets, marine snow, phytodetritus and the ocean's biological pump. Prog. Oceanogr. **130**: 205–248. doi:10.1016/j.pocean.2014.08.005

Uthicke, S., L. Llewellyn, and F. Eder. 2009. Fluorescent lectin assay to quantify particulate marine polysaccharides on 96-well filtration plates. Limnol. Oceanogr.: Methods **7**: 449–458. doi:10.4319/lom.2009.7.449

Van der Jagt, H., C. Friese, J.-B. W. Stuut, G. Fischer, and M. H. Iversen. 2018. The ballasting effect of Saharan dust deposition on aggregate dynamics and carbon export: Aggregation, settling, and scavenging potential of marine snow. Limnol. Oceanogr. 9. doi:10.1002/lno.10779

Waite, A. M., R. J. Olson, H. G. Dam, and U. Passow. 1995. Sugar-containing compounds on the cell surfaces of marine diatoms measured using concanavalin a and flow cytometry. J. Phycol. **31**: 925–933. doi:10.1111/j.0022-3646.1995.00925.x

Waite, A. M., K. A. Safi, J. A. Hall, and S. D. Nodder. 2000. Mass sedimentation of picoplankton embedded in organic aggregates. Limnol. Oceanogr. **45**: 87–97. doi:10.4319/lo.2000.45.1.0087

Weissbrodt, D. G., T. R. Neu, U. Kuhlicke, Y. Rappaz, and C. Holliger. 2013. Assessment of bacterial and structural dynamics in aerobic granular biofilms. Front. Microbiol. **4**: 175. doi:10.3389/fmicb.2013.00175

Wiedmann, I., M. Reigstad, M. Marquardt, A. Vader, and T. M. Gabrielsen. 2016. Seasonality of vertical flux and sinking particle characteristics in an ice-free high arctic fjord—Different from subarctic fjords? J. Mar. Syst. **154(B)**: 192–205. doi:10.1016/j.jmarsys.2015.10.003

Wiedmann, I., M. Reigstad, A. Sundfjord, and S. Basedow. 2014. Potential drivers of sinking particle's size spectra and vertical flux of particulate organic carbon (POC): Turbulence, phytoplankton, and zooplankton. J. Geophys. Res. Oceans **119**: 6900–6917. doi:10.1002/2013JC009754

Woebken, D., B. M. Fuchs, M. M. M. Kuypers, and R. Amann. 2007. Potential interactions of particle-associated anammox bacteria with bacterial and archaeal partners in the Namibian upwelling system. Appl. Environ. Microbiol. **73**: 4648–4657. doi:10.1128/AEM.02774-06

Acknowledgments

We thank Bernhard Fuchs, Manuel Liebeke, Benedikt Geier, Mario Schimak, Jörg Wulf, and Andreas Ellrott for their support and advice developing the method presented in this paper. We appreciated the helpful comments provided by Helga van der Jagt and Allison Fong for editing this manuscript. This study was supported by the Helmholtz Association and the Alfred Wegener Institute for Polar and Marine Research (CMF, AR, AMW, MHI), the DFG-Research Center/Cluster of Excellence "The Ocean in the Earth System" (CMF, MHI), and the Max Planck Institute for Marine Microbiology (SM, ST). This publication is supported by the HGF Young Investigator Group SeaPump "Seasonal and regional food web interactions with the biological pump": VH-NG-1000.

Conflict of Interest

None declared.

Submitted 29 September 2017
Revised 01 February 2018; 13 March 2018
Accepted 16 March 2018

Associate editor: Gordon Taylor

PAPER II

Hard and soft plastic resin embedding for single-cell element uptake investigations of marine-snow-associated microorganisms using nano-scale secondary-ion mass spectrometry

Andreas Rogge, Clara M. Flintrop, Morten H. Iversen, Ian Salter, Allison A. Fong, Angela Vogts, Anya M. Waite

Limnol. Oceanogr. Methods 16: 484-503. DOI:10.1002/lom3.10261

LIMNOLOGY and OCEANOGRAPHY: METHODS

ASLO

Limnol. Oceanogr.: Methods 00, 2018, 00–00

doi: 10.1002/lom3.10261

Hard and soft plastic resin embedding for single-cell element uptake investigations of marine-snow-associated microorganisms using nano-scale secondary ion mass spectrometry

Andreas Rogge,*[1] **Clara M. Flintrop**,[1,2,3] **Morten H. Iversen**,[1,2] **Ian Salter**,[1,4] **Allison A. Fong**,[1] **Angela Vogts**,[5] **Anya M. Waite**[1,6]

[1]Alfred Wegener Institute Helmholtz Centre for Polar and Marine Research (AWI), Bremerhaven, Bremen, Germany
[2]Marum and University of Bremen, Bremen, Germany
[3]Max-Planck-Institute for Marine Microbiology, Bremen, Germany
[4]Faroe Marine Research Institute, Tórshavn, Faroe Islands
[5]Leibniz Institute for Baltic Sea Research Warnemünde (IOW), Rostock-Warnemünde, Mecklenburg-Vorpommern, Germany
[6]FB2 Biology/Chemistry, University of Bremen, Bremen, Germany

Abstract

Marine snow aggregates are microhabitats for diverse microbial communities with various active metabolic pathways. Rapid recycling and symbiotic transfer of nutrients within aggregates poses a significant challenge for accurately assessing aggregate-associated turnover rates. Although single-cell uptake measurements are well-established for free-living microorganisms, suitable methods for cells embedded in marine snow are currently lacking. Comparable cell-specific measurements within sinking pelagic aggregates would have the potential to address core questions regarding aggregate-associated fluxes. However, the capacity to perform microscale studies is limited by the difficulty of sampling and preserving the fragile aggregate structure. Furthermore, the application of nano-scale secondary ion mass spectrometry (NanoSIMS) to aggregates is complicated by technical requirements related to vacuum and ablation resistance. Here, we present a NanoSIMS-optimized method for fixation, embedding, and sectioning of marine snow. Stable isotope labeling of laboratory-generated aggregates enabled visualization of label incorporation into prokaryotic and eukaryotic cells embedded in the aggregate structure. The current method is also amenable to various staining procedures, including transparent exopolymer particles, Coomassie stainable particles, nucleic acids, and eukaryotic cytoplasm. We demonstrate the potential for using structural stains to generate three-dimensional (3D) models of marine snow and present a simplified calculation of porosity and fractal dimension. This multipurpose method enables combined investigations of 3D aggregate structure, spatial microbial distribution, and single-cell activity within individual aggregates and provides new possibilities for future studies on microbial interactions and elemental uptake within marine snow.

Marine aggregates play a crucial role in the sequestration of photosynthetically produced organic matter, moving carbon from the euphotic zone to the deep ocean, which has an important impact on the global carbon budget (Turner 2015). They range from small conglomerates of organisms to aggregates of several millimeters in diameter, which also includes marine snow (aggregates > 500 μm; Alldredge and Silver 1988). The primary components of marine snow are phytodetritus, discarded appendicularian houses, fecal pellets, and other detrital material which stick together due to a matrix of exuded polymeric substances, including transparent exopolymer particles (TEP) (Passow et al. 1994; Passow et al. 2001; Turner 2015). The latter are defined as discrete exopolymers that consist predominantly of surface-active acidic polysaccharides and that are stainable with Alcian Blue (Alldredge et al. 1993; Cisternas-Novoa et al. 2015). Early studies revealed the importance of non-TEP extracellular polymeric substances (Stoderegger and Herndl 1999; Waite et al. 2005), and proteinaceous Coomassie stainable particles (CSP) (Long and Azam 1996) for aggregate structure. The first marine snow microstructure investigations also confirmed

*Correspondence: andreas.rogge@awi.de

Additional Supporting Information may be found in the online version of this article.

these findings and provided insights into organism distribution (Heissenberger et al. 1996a; Leppard et al. 1996).

Microorganisms within organic aggregates benefit from highly concentrated substrate conditions (Shanks and Trent 1979; Lyons and Dobbs 2012) which characterize them as microscale nutrient patches in an otherwise homogeneous water column. Microbial abundances can be 10^3–10^5-fold higher than in the surrounding water column (Waite et al. 2000) and are typically associated with comparatively high-metabolic activity (Lyons and Dobbs 2012). Direct measurements of primary and bacterial production (Gotschalk and Alldredge 1989; Turley and Stutt 2000) and extracellular enzymatic activity (Karner and Herndl 1992; Zoppini et al. 2005) typically display enhanced values on aggregates relative to the water column.

Genomic profiling has also revealed that phylogenetic diversity of microbial assemblages associated with aggregates can differ from free-living communities (DeLong et al. 1993; Rath et al. 1998; Fontanez et al. 2015). Additionally, phylogenetic analyses revealed the presence of microbial communities capable of performing rare pelagic nutrient cycling processes such as ammonification (Shanks and Trent 1979), nitrification (Phillips et al. 1999), or methane production by archaea (Marty 1993; Maarel et al. 1999). Early studies suggested the potential existence of sub- or anoxic microzones within aggregates (Gowing and Silver 1983; Paerl and Pinckney 1996), and more recent work has demonstrated sub- and anoxic metabolic processes, such as anammox (Woebken et al. 2007), sulfate reduction (Vojvoda et al. 2014), or even chemolithoautotrophy (Swan et al. 2011) within aggregates from oxic or suboxic environments.

Based on a size-resolved particle model, Bianchi et al. (2018) estimated very recently that the anaerobic niche in the world oceans is expanded by particle-associated microenvironments which increases the rates of denitrification and sulfate reduction in the water column massively. Direct quantification of those and other nutrient turnover rates associated with marine snow, however, is difficult because numerous aggregates are required to generate results above measurable threshold values. This in turn necessitates bulk measurements which can be challenging to interpret due to the heterogeneous nature of aggregates. Furthermore, there is potential overlap of opposing metabolic pathways that can result in cryptic elemental cycling within single aggregates, as recently observed for the pelagic sulfur cycle in the Peruvian OMZ (Canfield et al. 2010). Emerging techniques such as single-cell measurements using nanoscale secondary ion mass spectrometry (NanoSIMS), or other modern technologies requiring vacuum conditions like electron dispersive X-ray, are powerful tools with the potential to yield insights into aggregate-associated nutrient fluxes. However, microzone investigations on marine aggregates that combine single-cell visualization, uptake measurements, and porosity measurements pose a significant challenge. Notable difficulties include (1) the preservation and handling of fragile marine snow to reduce material loss, (2) the possibility for specific structural staining processes with reduced sample loss and dye precipitation, (3) the preservation of the three-dimensional (3D) structure enabling structure reconstruction for calculations of porosity and 3D fractal dimension, (4) the suitability for stable isotope enrichment measurements using NanoSIMS analyses with minimal enrichment dilution, and finally (5) stable storage conditions to ensure effective analyses in the field and at shore-based laboratories.

Here, we present a multidisciplinary method synthesis to address the challenges stated above, resulting in a widely applicable approach for microscopic investigations of marine snow, uptake measurements employing NanoSIMS, and structure reconstruction to facilitate porosity calculations. The characteristics of the resulting specimen matrix, including vacuum stability and negligible nitrogen and sulfur content, provide great potential for NanoSIMS-based flux investigations of individual organisms within an aggregate. Moreover, a streamlined workflow for biological and structural fixation combined with stable storage enables effective analyses in the field or at shore-based laboratories. Our preliminary investigations, as well as the recent literature (McGlynn et al. 2015), indicate that the fixation and storage conditions optimized for NanoSIMS and structural staining are potentially compatible with taxonomic staining procedures, such as fluorescence in situ hybridization (FISH) or catalyzed reporter deposition in situ fluorescence hybridization (CARDFISH), but this aspect of the method requires further optimization beyond the scope of the present objectives (*see* Supporting Information Chapter 1). A complementary embedding approach based on cryogel embedding is described in the companion paper by Flintrop et al. (2018), which enables taxonomic identification using FISH. We provide direct comparison of the two approaches (*see* "Discussion" section).

Using the plastic resin embedding procedure and structural stains, we describe a simplified calculation to determine porosity and fractal dimension based on a 3D reconstruction model. We also provide an alternative embedding protocol for aggregates comprised of very dense and/or terrigenous material, which allows structure-preserving bright field investigations and NanoSIMS measurements. A detailed description of the current methods and proposed applications is provided, as well as a field test of the embedding and structural staining. Our preliminary application of this approach demonstrates its potential to address existing gaps in our knowledge concerning biogeochemical fluxes as anaerobic cycling and microbial ecology of marine snow.

Methods

The final method for embedding of marine snow into an acrylic or epoxy resin consists of eight major steps (see Flowchart in Fig. 1): (1) The inactivation of biological activity and aggregate fixation with formaldehyde solution with subsequent washing in sterile seawater. Fixed aggregates are

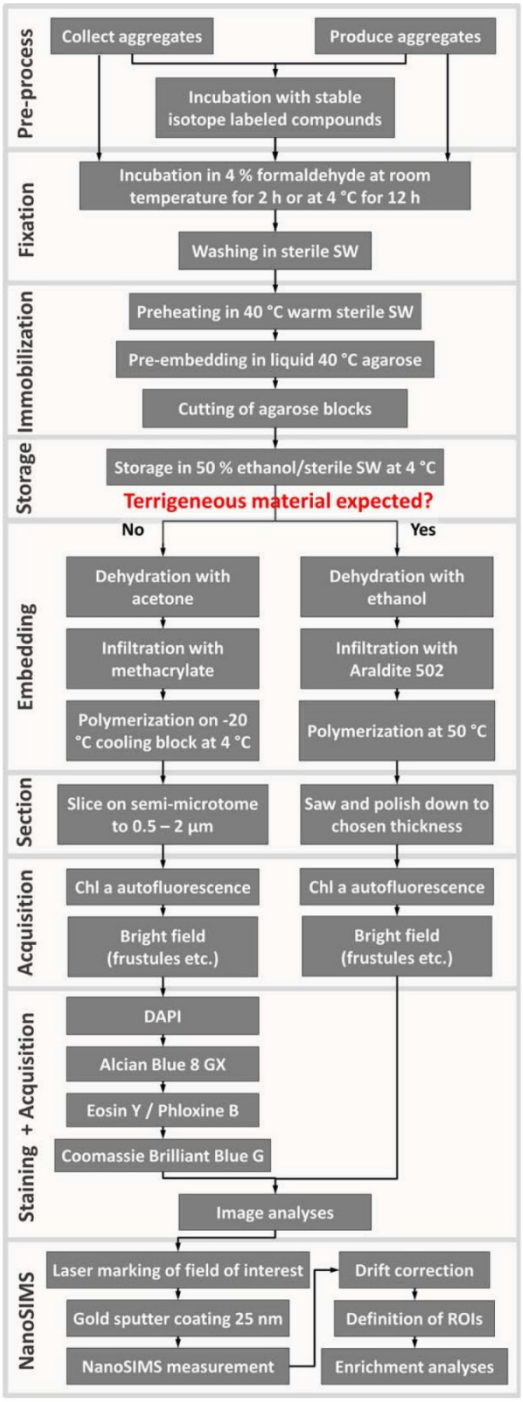

Fig. 1. Schematic outline of the presented method.

subsequently (2) immobilized and stabilized by pre-embedding in liquid agarose which can be followed by a storage step in ethanol solution. The stabilized aggregate is then (3) embedded in an acrylic or epoxy resin of choice, resulting in final structural and biological preservation, (4) sectioned and (5) stained using different structural, histological, and molecular dyes. Images of stained TEP, CSP, cytoplasm, and nucleic acid compounds as well as chlorophyll *a* (Chl *a*) auto-fluorescence are acquired and (6) structure is reconstructed in two or three dimensions, to allow porosity calculations. Finally, (7) embedded slices are prepared for NanoSIMS investigations, including laser-marking of the fields of interest, sputter coating, and fitting into the sample holder, followed by (8) NanoSIMS- and post-analysis.

In order to create a method suitable for structural staining and NanoSIMS analyses, we performed laboratory tests using a range of laboratory-generated aggregates, produced under controlled conditions (see details below). Mixed plankton communities were supplemented with natural marine bacterioplankton, and then incubated for 24 h with stable isotope-labeled glucose, nitrate, and sulfate (see below). We tested agarose as a pre-embedding matrix and the histological resin methacrylate as a final embedding medium. We applied several staining procedures, including Alcian Blue staining for TEP, Coomassie Blue staining for proteins, DAPI staining for nucleic acids, and eosin staining for eukaryotic cytoplasm proteins. The different structural signals were merged and a 3D model was created to illustrate the preserved structural features. NanoSIMS measurements were performed on one of the test aggregates to demonstrate the capacity to investigate single-cell element uptake employing the presented approach. To assess potential difficulties during the slicing process for aggregates with dense or terrigenous material, we also performed a test on dense aggregates, using agarose as a pre-embedding matrix and the resin Araldite 502 as a final embedding medium. This enables more precise sectioning for dense aggregates.

Generation of aggregates from laboratory phytoplankton cultures and surface water

Laboratory aggregates for methacrylate embeddings tests included a mixture of *Thalassiosira hyalina*, *T. marinoii*, *Emiliania huxleyi*, and *Micromonas pusilla* cultures in equal parts. This ensures applicability of the method for a diversity of aggregates by including soft as well as hard compounds, such as diatom frustules and coccoliths. Cultures were grown in F/2r medium (Guillard and Ryther 1962) with 12/12 h dark/light cycles for 7 d until the culture was opaque (cell numbers or growth phase not determined) before transfer of 1.8 L of culture mix into 2.1 L roller tanks. For bacterial colonization, 300 mL of 2 μm prefiltered North Seawater sampled in May off Bremerhaven (Germany) was added to the roller tanks (cell numbers not determined). The cultures were allowed to aggregate for 2 d at 2 rpm and 15°C in roller tanks in the dark.

In order to create very dense aggregates for alternative Araldite 502 embeddings, surface water sampled in March off Helgoland (Germany) was aggregated in roller tanks as described above for 4 weeks followed by direct fixation and embedding (*see* iii (b) "Methods" section) without prior incubation with stable isotope labeled compounds.

Stable isotope enrichment incubations

Aggregates containing stable-isotope-enriched organisms for NanoSIMS tests were formed by incubating laboratory generated aggregates in roller tanks with ^{13}C-labeled glucose, ^{15}N-labeled potassium nitrate, and ^{34}S-labeled sodium sulfate (see details below). Background concentrations of nitrate and sulfate in the sterile (0.2 μm filtered) North Seawater (sNSW) were measured prior to incubation using a QuAAtro39 Auto-Analyzer (Seal Analytical) to ensure correct labeling of ^{15}N and ^{34}S. All aggregate handlings and transfers were performed very gently, using either a bore pipette or a 1 mL pipette with cut pipette tips (*see* Table 1).

The lab aggregates were separated from free-living microorganisms by transferring each aggregate into a 50 mL centrifugation tube filled with sNSW. The aggregates were allowed to settle in the tube without reaching the bottom and then transferred into another tube with fresh sNSW, followed by transfer into a 50 mL roller tank. Triplicate 50 mL roller tanks, including 20–30 "washed" aggregates, were spiked with 10% $^{15}NO_3$ (Cambridge Isotope Laboratories, Cat.-No. NLM-765-PK) and 15% $^{34}SO_4$ (Sigma-Aldrich; Cat.-No. 718882) of the respective ambient concentration (12.47 μM NO_3, 25.44 mM SO_4), as well as 100 nM ^{13}C-glucose (D-glucose-$^{13}C_6$; Sigma-Aldrich; Cat.-No. 389374; background concentration not determined). Roller tanks were closed with a silicon stopper and rotated at 1.25 rpm and 15°C in the dark for 24 h before harvesting and embedding. To ascertain enrichment detection, triplicate controls were incubated with the same amount of unlabeled compounds and both groups analyzed to ensure an appropriate number of enriched aggregates for the analyses.

Aggregate embedding and analysis protocol

Biological fixation in formaldehyde solution and washing followed by immobilization in agarose is the first step in the procedure (Fig. 1). This step is the only step executed in the field. This prevents the risk of disaggregation during subsequent procedure and enables quick and easy sample handling during field campaigns as well as stable storage. The following dehydration, infiltration, and polymerization with resin enables thin sectioning of the aggregates in preparation for microscopy and SIMS analyses. A list of materials required is provided in Table 1.

i. Inactivation of biological activity and aggregate fixation

At the end of the 24 h aggregate incubation period, or immediately after aggregation in case of dense surface-water aggregates, aggregates were fixed in petri dishes filled with 0.2 μm-filtered 4% (v/v) formaldehyde/sNSW solution for 2 h at room temperature or at 4°C overnight (12 h). Stable isotope-labeled aggregates were subsequently washed in sNSW for 10 min and dense aggregates were washed for 30 min.

ii. Pre-embedding in liquid agarose and storage

Agarose solution was heated to boiling using a microwave. It was then kept at 40°C, along with the sNSW, in a hot water bath.

Following fixation, aggregates of both types were preheated by transferring them into 40°C warm sNSW for 10 min before transferring them into liquid, 40°C warm 6% (w/v) low-melting-point agarose (Omnipur® Agarose Low-Melting; EMD Chemicals) within silicon embedding molds. After cooling of the agarose at 4°C for 2 h, aggregates were cut out of the solid block using a sterile scalpel and forceps and transferred immediately into 2 mL centrifugation tubes filled with 0.2-μm-filtered 50% (v/v) ethanol/sNSW solution (molecular biology grade undenaturated absolute ethanol; Serva) to reduce biological degradation. Samples were stored at 4°C for 2 months.

iii. Embedding in acrylic resins

Final preservation was accomplished by embedding aggregates in an artificial resin resulting in solid, dehydrated, and sectionable blocks. Many resins for embedding were excluded prior to testing due to background fluorescence, polymerization temperatures above 60°C, or significant nitrogen and sulfur content rendering them unsuitable for potential rRNA-based hybridizations and NanoSIMS analyses, respectively. Moreover, hard materials such as sediments from terrigenous sources lead to rupture of the sections during the slicing process. Therefore, we tested the histology-originated methacrylate embedding medium for common "open ocean" aggregate samples which were sliced using a steel knife. We also tested the geology and soil sciences originated epoxy resin Araldite 502 which we sawed and polished to the desired thickness (40–140 μm).

(a) Methacrylate embedding for aggregates without terrigenous material

The methacrylate embedding protocol has been modified from the standard protocol (Velde et al. 1977). Dehydration was carried out in an increasing concentration series of acetone: Pre-embedded aggregates were transferred into snap cap vials and incubated twice with 50%, 70%, and 100% acetone on a tumbler for 1 h at room temperature. The methacrylate monomer was prepared by thoroughly mixing together 240 mL 2-hydroxyethyl methacrylate (Sigma Aldrich), 36 mL ethylene glycol butyl ether (Sigma Aldrich), and 0.81 g benzoyl peroxide (Luperox® A75; Sigma Aldrich). Infiltration started with a washing step with methacrylate monomer for 30 min followed by infiltration with monomer on a tumbler overnight at room temperature. Activator was

Table 1. List of required materials and instruments (n. d. = not determined).

Material	Company
Fixation	
Formaldehyde	Sigma Aldrich
sterile (0.2 μm filtered) seawater	n. d.
Petri dish	n. d.
Pre-embedding	
1 mL pipette	Eppendorf
Cut 1 mL pipette tips	Eppendorf
Bore pipette	n. d.
Agarose low-melting	Omnipur®; EMD chemicals
Sterile (0.2 μm filtered) seawater	n. d.
Embedding molds	n. d.
Microwave	Sharp
Water bath	Thermo Fisher Scientific
Scalpell	n. d.
Forceps	n. d.
50 mL centrifugation tubes	Sarstedt
Storage	
2 mL centrifuge tubes	Eppendorf
Ethanol (undenaturated for molecular biology)	Serva
Sterile (0.2 μm filtered) seawater	n. d.
Methacrylate embedding	
Forceps	n. d.
Scalpell	n. d.
Embedding molds	n. d.
Holder blocks	Custom made
Tumbler	Custom made
Refrigerator (4°C)	n. d.
Cooling blocks	n. d.
Snap cap vials	n. d.
Ultra-pure water	Millipore
Acetone	Sigma Aldrich
2-hydroxyethyl methacrylate	Sigma Aldrich
Ethylene glycol butyl ether	Sigma Aldrich
Benzoyl peroxide Luperox® A75	Sigma Aldrich
Polyethylene glycol 200	Sigma Aldrich
N,N-dimethylaniline	Sigma Aldrich
Methacrylate slicing	
Semi-automatic microtome	Leica
Humidity chamber	n. d.
Ultra-pure water	Millipore
Acetone	Sigma Aldrich
Biobond	EMS
Slides	Unimark
Heat plate	n. d.
Araldite 502 embedding	
Forceps	n. d.
Scalpell	n. d.
Embedding molds	n. d.
Tumbler	Custom made
Snap cap vials	n. d.
Oven	n. d.
Ultra-pure water	Millipore
Ethanol (undenaturated for molecular biology)	Serva
Propylene oxide	Sigma Aldrich
Araldite 502 kit including DDSA and DMP-30	Electron microscopy sciences
Araldite 502 sectioning	
Grinding wheel	Wirtz
Carbid powder	Theodor Ehrich
Tap water	n. d.
Ethanol	n. d.
Körapox 439	Sikora
Stone saw Woco 50	Conrad
Grinding machine MPS 2 120	G&N
Grinding machine MPS 2 R 300	G&N
Aluminium oxide powder	Bühler
DAPI counterstaining	
Cover slips	Thermo Fisher Scientific
Ethanol for cleaning	Merck
4′,6-diamidino-2-phenylindole	Sigma Aldrich
Citifluor	Electron microscopy sciences
Vectashield	Vector laboratories
Ultra-pure water	Millipore
Sodium dodecyl sulfate	Merck
Alcian Blue staining	
Alcian Blue 8GX	Sigma Aldrich
Ultra-pure water	Millipore
Acetic acid	Merck
Ethanol (undenaturated for molecular biology)	Serva
Eosin staining	
Alcoholic eosin Y/phloxine B solution	Merck
Ultra-pure water	Millipore
Acetic acid	Merck
Coomassie Brilliant Blue staining	
Coomassie Brilliant Blue G	Sigma Aldrich
Ultra-pure water	Millipore
Ethanol (undenaturated for molecular biology)	Serva
Acetic acid	Merck

prepared by mixing 2 mL polyethylene glycol 200 (Sigma Aldrich) and 0.2 mL N,N-dimethyl aniline (Sigma Aldrich). All the infiltrated agarose blocks were carefully placed into individual embedding molds before 2 mL activator was added to 92 mL methacrylate monomer. The activated resin was added quickly into the molds, a holder block was placed on top of the molds and the embedding form was carefully

placed on a −20°C precooled cooling block and transferred into a 4°C refrigerator to avoid high temperatures during the exothermic reaction. After polymerization, resin blocks were cleaned of nonpolymerized resin using paper towel and were allowed to dry for several days at room temperature to finalize the hardening.

(b) Alternative Araldite 502 embedding for aggregates containing hard or terrigenous material

In order to embed dense aggregates, we used the Araldite 502 Kit (Electron Microscopy Sciences; Cat.-No. 13900). Embedding medium, consisting of 100 mL Araldite 502 (Sigma-Aldrich), 110 mL dodecenyl succinic anhydride (DDSA), and 4 mL 2,4,6-Tris(dimethylaminomethyl)phenol (DMP-30) was mixed thoroughly and stored at 4°C in sealed syringes until further processing.

Agarose blocks were dehydrated in snap-cap-vials on a tumbler, using an increasing concentration series of ethanol (molecular biology grade undenaturated absolute ethanol; Serva): 70% ethanol for 10 min, followed by two times 100% ethanol for 10 min. Afterward, ethanol was replaced by propylene oxide by incubating the blocks twice for 10 min in 100% propylene oxide, which enhanced the following infiltration with monomer.

Dehydrated agarose blocks were incubated in snap-cap-vials on a specimen rotator in an increasing concentration series of embedding medium and propylene oxide: starting with 25%, 50%, and finally 75% Araldite embedding medium in propylene oxide for 1 h, respectively. At last, agarose blocks were incubated in 100% embedding medium overnight (12 h) before transferring them into embedding molds and removing air bubbles in a desiccator under vacuum. Afterward, polymerization was carried out at 60°C for a minimum of 12 h.

i. Sectioning

To study the microscale 3D structure in aggregates of different densities, embeddings were sectioned using different approaches. Methacrylate embeddings were sliced on a semi-automatic microtome using steel knives, similar to the preparation of biological tissue samples, while Araldite 502 embeddings were sectioned by sawing and polishing; similar to petrographic thin sections.

In order to reconstruct the aggregate structure in three dimensions, we sectioned a 142 μm thick portion of one of our methacrylate embedded laboratory aggregate. To demonstrate the possibility for porosity and 3D fractal dimension estimation, we used 23 of the resulting 71 planes for the structural model.

(a) Sectioning of methacrylate embeddings

Methacrylate resin blocks were sliced with a thickness of 2 μm on a semi-automatic microtome (Leica) using a steel knife. Prior to slicing, resin blocks were placed in a humidity chamber (wet paper towel in closed plastic box) for at least 30 min to soften them and ease the slicing process. Slices were placed on a drop of ultrapure water (UW; 18.2 Ω) on a clean glass slide (Unimark) followed by drying on a heat plate for 1 h (< 50°C).

(b) Sectioning of Araldite 502 embeddings

Alternative Araldite 502 embeddings were grinded and polished to different thicknesses down to 40 μm at the geology section of the University of Bremen. Samples were polished on a grinding wheel (Wirtz) using silicon carbid powder (Theodor Erich) and tap water until samples were level before they were cleaned with ethanol and adhered without air bubbles onto a transparent specimen holder using Körapox 439 resin (Sikora). Specimens were sawed using a Woco 50 stone saw (Conrad) to a thickness of 500–1000 μm before rough polishing down to the approximate thickness using a MPS 2 120 grinding machine (G&N). Finally, fine grinding to the final thickness of 40–140 μm and ultra-plane surface was done on a MPS 2 R 300 grinding machine (G&N) using aluminum oxide powder (Bühler).

ii. Structural and histological staining

To prevent overlapping of individual stains, staining and microscopy was performed in succession. After DAPI staining, DAPI signal and Chl *a* auto-fluorescence was acquired, followed by Alcian Blue staining and acquisition, eosin/phloxine staining and acquisition, and finally, Coomassie Blue staining and acquisition.

(a) DNA staining

Methacrylate slices were embedded with DAPI oil, consisting of 1% (v/v) 4′,6-diamidino-2-phenylindole (DAPI; Sigma-Aldrich) solution (100 μg mL^{-1}), 85% (v/v) Citifluor AF1 (Electron Microscopy Sciences) and 14% (v/v) Vectashield (Vector Laboratories), and closed with a cover slip (Thermo Fisher Scientific). After image acquisition (*see* vi in "Methods" section) of the DAPI and Chl *a* signal, the cover slip was removed very gently and DAPI-oil was washed off the specimen using 1% (v/v) sodium dodecyl sulfate solution for 15 min at room temperature followed by a washing step in UW for 10 min at room temperature and air drying.

(b) TEP staining

Alcian Blue, a polyvalent basic dye, was used to stain the TEP-fraction of aggregates. Alcian Blue stain solution consisted of 0.125% (w/v) Alcian Blue 8GX (Sigma Aldrich), 10% (v/v) acetic acid, 25% (v/v) ethanol, and 64.875% UW. Destain solution consisted of 25% ethanol, 10% acetic acid, and 65% UW. Sliced samples were incubated for 18 h in 0.2 μm filtered Alcian Blue stain solution at 4°C followed by a washing step in destain solution for 30 min to remove excess stain and to enhance contrast before 1 min of UW-washing and air drying.

(c) Cytoplasm staining

Cytoplasm structures, including proteins were stained with Eosin; a negatively charged acidic dye that stains basic and acidophilic structures. A mixture of eosin Y and phloxine B was used to enhance bright field signal intensity. Due

to the fluorescent properties of phloxine B, this combination of stains improved signal isolation during subsequent overlapping of images required for the structural model. Acetic acid was added to alcoholic eosin Y/phloxine B solution (Merck) to a final concentration of 0.25% (v/v). Samples were incubated at room temperature for 8 min in 0.2 μm filtered stain solution and subsequently washed in 0.25% (v/v) acetic acid in 90% ethanol/UW (v/v) for 30 min at room temperature to remove excess stain and to enhance contrast before 1 min of UW washing and air drying.

(d) Protein staining

Protein staining was accomplished by using the triphenylmethane dye Coomassie Brilliant Blue in an alcoholic and acetic solution. Coomassie Brilliant Blue solution consisted of 0.1% (w/v) Coomassie Brilliant Blue G 250 (Sigma Aldrich), 20% ethanol, and 3.75% acetic acid in UW. Slides were incubated in 0.2 μm filtered Coomassie Brilliant Blue solution for 1 h at 4°C, and washed for 30 min in 20% ethanol and 0.4% acetic acid at room temperature in UW to remove stain and enhance contrast. After a short washing step (1 min) in UW, the samples were air dried.

iii. Image acquisition, two-dimensional and three-dimensional reconstruction, and porosity calculation

Images were acquired on an Axioskop 2 plus epifluorescence microscope (Zeiss) equipped with a Ph1 Plan-Neofluar 10× objective and an Axiocam MRc5 camera (Zeiss) using Zeiss' Axiovision software. Alcian Blue, eosin Y/phloxine B, and Coomassie Blue images were acquired using bright field whereas DAPI, Chl *a* autofluorescence, and phloxine using the respective excitation and emission filter set. Using the software GIMP 2 (GNU Image Manipulation Program; Kimball et al. 1997–2017), images were contrast and brightness corrected. For overlap images, respective specific original channels (Coomassie and Alcian Blue, blue; DAPI, blue and cyan; Chl *a* autofluorescence as well as eosin/phloxine, red) were overlapped whereas residual channels were converted to the transparent alpha channel. For better visibility, colors were changed, i.e., when combining Alcian Blue and Coomassie Blue resulting in two blue channels (See figure descriptions). For the 3D model, aggregate positions of the individual planes were aligned manually (shift and rotation function) followed by aligning the dimensions (cut function). Construction of the 3D model was accomplished by importing all planes per channel as hyperstack into the Fiji-Bundle (Schindelin et al. 2012) of ImageJ (Schneider et al. 2012; Schindelin et al. 2015) using the importer of the Bioformats plugin (Linkert et al. 2010). The selected channel stacks were merged and the model calculated using the 3D-Viewer plugin (Schmid et al. 2010).

Porosity calculations were accomplished by merging all channels and thresholding the resulting stack with the optimal value to a binary stack. In every plane, the aggregate was defined manually by using the ROI-Manager tool (region of interest [ROI]) followed by interpolating those ROIs into three dimensions using the Interpolate ROIs tool of the ImageJ plugin BoneJ (Doube et al. 2010). Afterward, the percentage of pore volume to total aggregate volume inside the interpolated 3D-ROI was calculated using the surface mesh-based Volume Fraction function of BoneJ resulting in % of empty space or % porosity. The aggregate inside the interpolated 3D ROI (surface mesh) was visualized within the 3D-Viewer plugin of ImageJ.

Three-dimensional fractal dimension was calculated using the Fractal Dimension tool of BoneJ. The tool estimated the fractal dimension of the binary image stack by applying the box-counting algorithm as described for trabecular bone elsewhere (Fazzalari and Parkinson 1996). The program scanned boxes of diminishing size over the images and the number of boxes of each size containing foreground (aggregate) is counted. As the box size decreases, the proportion of boxes containing foreground increases in a fractal structure. The slope of the resulting linear function equals the fractal dimension.

iv. NanoSIMS preparations

Laser marking of spots of interest as well as bright field and DAPI image acquisition for later identification was carried out using a LMD7000 microscope (Leica) for labeled samples as well as controls. LMD-marked samples were cut to sample holder size using a glass cutter (Silberschnitt) and sputter coated with 25 nm gold using a 108 auto sputter coater (Cressington).

v. NanoSIMS measurements of single cells, image acquisition, and data processing

In order to measure single-cell uptake of stable-isotope-labeled glucose, nitrate, and sulfate, NanoSIMS imaging was performed using a NanoSIMS 50L instrument (Cameca, France) at the Leibniz-Institute for Baltic Sea Research Warnemünde (IOW). A $^{133}Cs^+$ primary ion beam was used to erode and ionize atoms of the sample surface. Six mass detectors equipped with electron multipliers (Hamamatsu) were used to record the received secondary ions $^{12}C^-$, $^{13}C^-$, $^{12}C^{14}N^-$, $^{12}C^{15}N^-$, $^{32}S^-$, and $^{34}S^-$ from the LMD-marked areas simultaneously. To suppress interferences, the mass resolving power was adjusted, allowing the separation of, e.g., $^{12}C^{15}N^-$ from interfering ions such as $^{13}C^{14}N^-$. Sample areas were sputtered for 1 min with 600 pA prior to analysis to reach the steady state of secondary ion formation. The primary ion beam current during the analysis was 2–3 pA; the scanning parameters were 512 × 512 px for areas of 20 × 20 μm to 60 × 60 μm, with a dwell time of 250 μs per pixel. Up to 120 planes were recorded.

The scans of each mass were accumulated and shift-corrected using the software Look@NanoSIMS (LANS; Polerecky et al. 2012). Cells were defined as ROI based on the $^{12}C^{14}N$ signal using the interactive threshold tool of the

same software. Isotope abundances for ^{13}C, ^{15}N, and ^{34}S were calculated and exported for each cell. Prokaryotic and algal cells were identified by shape using the DAPI, Chl *a*, and Bright Field image acquired prior to analysis.

Isotope abundances of individual ROIs of the labeled samples were corrected using the methacrylate resin as internal standard. The average stable isotope abundance of the resin of the unlabeled control measurements was subtracted from the stable isotope abundance of the resin of each measurement of each labeled sample. The resulting correction value was then added to each ROI of the respective measurement.

Enrichment threshold was defined for each type of heavy isotope as the maximum Poisson Error, calculated by LANS, of the unlabeled standard cells, respectively. Cells containing values greater than the threshold were defined as enriched. NanoSIMS images of the different isotope ratios were prepared as hue, saturation, and intensity (HSI) images using the software ImageJ and the plug-in OpenMIMS (Gormanns et al. 2012).

Field test using in situ collected marine snow

Aggregate samples were collected during the research cruise PS99 in July 2016 on board RV Polarstern west off Svalbard (78°58.85′N, 9°30.58′E) using a marine snow catcher (Osil, UK) with a volume of 100 L at 50 m depth. After recovery of the marine snow catcher, aggregates were allowed to settle down to the bottom chamber. The bottom chamber was then removed, and aggregates were harvested by hand using a 1 mL pipette with cut pipette tips. Fixation, storage, and methacrylate embedding as well as sectioning, DAPI, and TEP staining were performed as described in the main protocol above.

Assessment

The key challenges of microscale research on intact marine snow are (1) to reduce the loss of material, (2) ensure specific staining of structural compounds, (3) preserve the 3D structure to enable structure reconstruction for calculations of porosity and fractal dimension, (4) produce suitable samples for stable isotope enrichment measurements using nano-scale secondary ion mass spectrometer analyses with reduced enrichment dilution, and (5) to optimize the storage period to ensure effective analyses in the field and at shore-based laboratories. We tested how the method overcomes these challenges on laboratory-generated phytodetritus and also provide a (6) field test of the embedding principle by applying nucleic acid and TEP stain on methacrylate embedded marine snow sampled west off Svalbard.

Loss of material

While our method prevents loss of insoluble material during the washing and staining procedures that follow embedding, it is very difficult to estimate any loss of material during the embedding process itself. Appropriate approaches to address material loss during handling are currently lacking. Considering the limited physical interaction with the aggregate surface following pre-embedding, it is reasonable to assume that the risk of losing insoluble material is limited to the period prior to completion of pre-embedding. Until this point, however, aggregates should be handled very carefully to reduce material loss and retain structural integrity during transfer. In particular, it is important to minimize the volume of water surrounding the aggregate to < 200 μL when it is transferred into agarose. Otherwise, dilution effects can result in soft pre-embeddings that perturb structure. Following these careful handling techniques, TEP structures and proteins remain undisturbed and are clearly arranged around algal cells (Fig. 2A,C, Supporting Information Fig. S1), demonstrating the procedure is capable of preserving aggregate structure.

It is also difficult to fully account for the loss of soluble material in water and the organic solvents (acetone or ethanol) used during resin embedding and the staining process. Nevertheless, we could clearly observe visible pigments in the chlorophyll auto-fluorescence signal (Fig. 2B), suggesting that pigments remain intact and can be used to visualize chloroplasts.

One possible limitation of our method is that the presence of very hard compounds, such as terrigenous material and diatom frustules, may lead to rupture of the specimen during the slicing process. We found that ensuring the use of newly sharpened knives on the microtome was able to prevent sample rupture in the presence of numerous diatom frustules. However, this is more problematic in the case of terrigenous material since the risk of damaging the microtome knife is very high. For aggregates of this nature, we recommend Araldite 502, instead of methacrylate, which is a more appropriate resin for hard embeddings (Fig. 3). Araldite 502 can be sawed and polished down to different section thicknesses. The equipment we had available when applying the Araldite 502 embedding procedure produced relatively thick sections (> 40 μm) that showed optimal characteristics for NanoSIMS as reported elsewhere (Herrmann et al. 2007; Mueller et al. 2012; Kaiser et al. 2015). However, structural staining was not applicable to Araldite 502 slices > 40 μm and it was only possible to prepare one slice per aggregate.

During the staining of methacrylate resin slices, detachment of the slice from the microscope slide may lead to the establishment of folds and sample loss. In order to address this limitation, we experimented with the use of adhesive coated slides (Biobond; Electron Microscopy Sciences), which proved successful for structural staining. However, also other adhesives, such as poly-L-lysine are widely used for this purpose (Huang et al. 1983; McGlynn et al. 2015). In our tests, also the use of a mixture of 2–10% acetone in UW as bedding between the slide and slice resulted in improved bonding characteristics that eliminated folding artifacts.

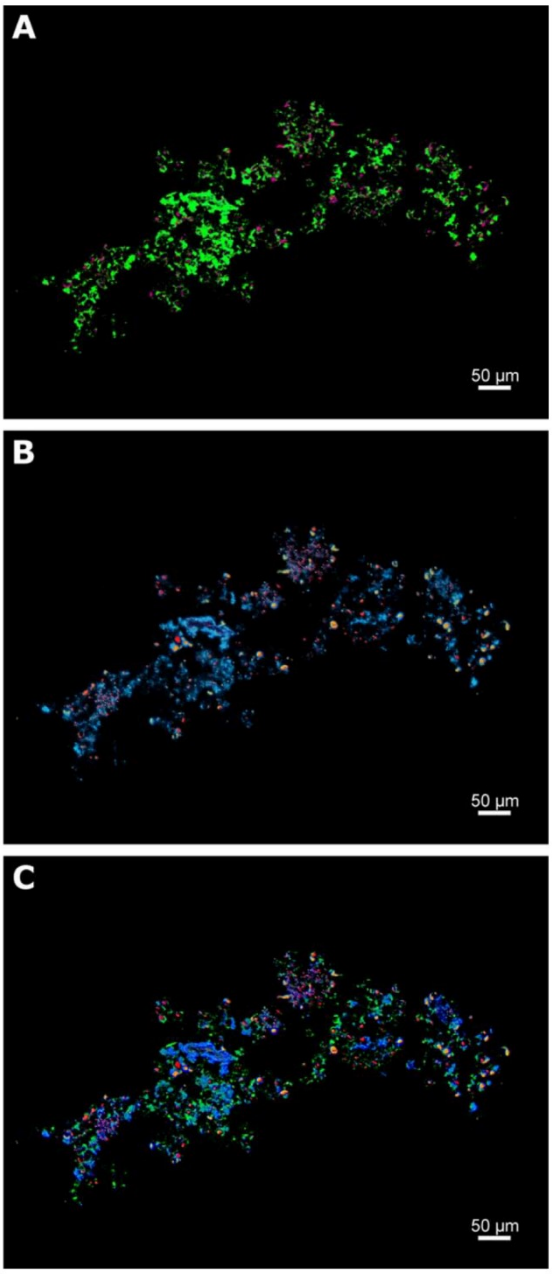

Fig. 2. Image overlap of the staining approaches. (**A**) Structural compounds TEP (green) and Coomassie stained proteins (magenta). (**B**) Distribution of nucleic acids stained with DAPI (blue), chlorophyll (red), and eukaryotic cytoplasm stained with eosin Y/phloxine B (yellow). (**C**) Overlap of all compounds mentioned above. Note that nucleic acid-rich areas without chlorophyll represent prokaryotes. Prokaryotes are distributed around algal cells and within a TEP matrix. Original images of each channel are provided in the Supporting Information Figs. S2–S7.

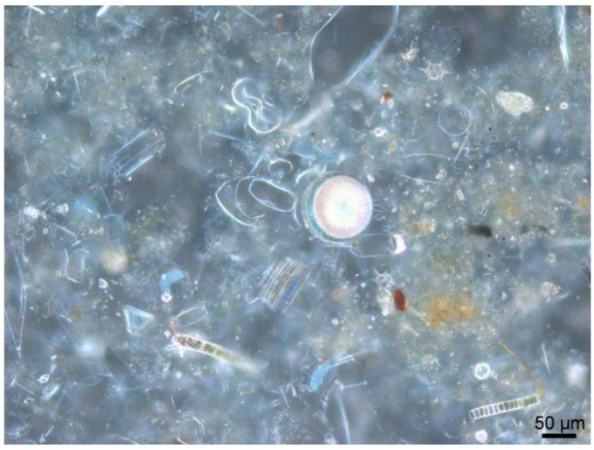

Fig. 3. Bright-field micrograph of an 80 μm thick slice through an Araldite 502 embedded aggregate formed from surface water off Helgoland, Germany. The resin did not allow structural staining, but valves and pigments are clearly visible. Araldite 502 sections are also amenable to NanoSIMS.

Stainability

The result of the different staining approaches for polysaccharides, proteins, cytoplasm, and nucleic acids are summarized in Fig. 2. Figure 2A exemplifies structural TEP and CSP staining, Fig. 2B shows organism distribution by visualizing nucleic acids, chlorophyll, and eosin, and Fig. 2C is an overlap of all channels. Examples for original images are provided in the Supporting Information Figs. S2–S7.

DAPI staining showed clear results that were distinguishable from background values, especially under higher magnification (Fig. 4). Prokaryotic cells were densely distributed around algal cells embedded within TEP-structures (Fig. 2B and Supporting Information Fig. S2). While the use of DAPI-oil is fast and convenient, we observed that even with anti-fading solution (Vectashield) bleaching of the dye occurred relatively quickly, by observation with UV-light ($\sim$ 5 min). An aqueous staining approach followed by embedding in anti-fading solution as reported for methacrylate embedded tissue might provide better results in cases where longer observation times are required (Bako et al. 2015).

Staining with Alcian Blue is a well-established method, which enables the visualization of negatively charged, sulfated, and carboxylated polysaccharides (Decho 1990) and was first reported for transparent exopolymeric particles by Alldredge et al. (1993). There are no reports of Alcian Blue staining of TEP-compounds with methacrylate embedded samples; however, we were able to achieve successful staining when applied in an ethanol solution. The stain is distinctly visible and the localization of TEP around algal cells follows the expectation that phytoplankton exudates would be present in aggregates (Fig. 2A, Supporting Information

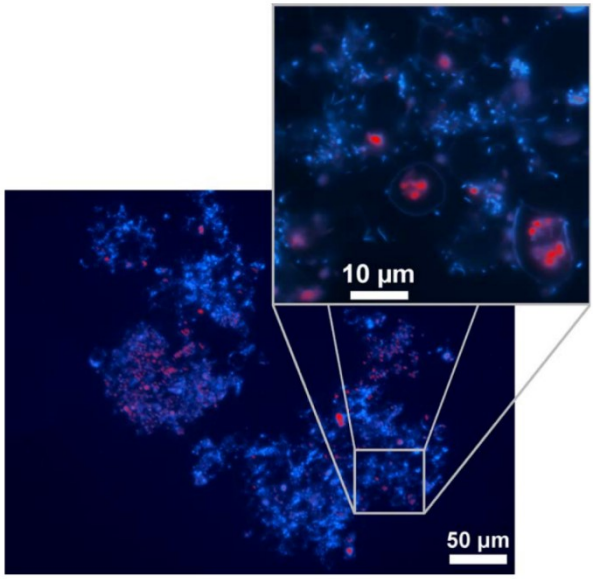

Fig. 4. Two micrometer thick slice of the methacrylate embedded aggregate used for NanoSIMS: The overlap of the DAPI stained nucleic acid channel in blue and the red Chl *a* autofluorescence channel enables the identification and distribution of prokaryotes and algae. Bigger cells with red compartments are chloroplast containing algae which are mostly surrounded by small prokaryotes without chlorophyll. The inset area represents area analyzed by NanoSIMS (*see* "Utility for stable isotope enrichment measurements" section). Note that cells and compartments that are not in focus are located in deeper slice layers and might not appear in the surface based NanoSIMS image.

Fig. S1). Importantly, dye coagulation or interference with salts which lead to overestimations of TEP signals as reported for staining in situ or on filters (Passow and Alldredge 1995; Cisternas-Novoa et al. 2015), can be excluded here. Since aggregate sections are still embedded within the resin during the staining process, it is possible to remove Alcian Blue particles by intense washing without risking sample loss.

Eosin, a halogenated derivative of fluorescein, binds to basic poly-amino acids, such as histidine, arginine, lysine, and tryptophan under acidic conditions (Waheed et al. 2000). It is a well-established and commonly used method to stain eukaryotic cytoplasm in histology (e.g., Veta et al. 2014), whereas mainly negatively charged bacterial cytoplasm may be stained with other dyes instead (Becerra et al. 2016). In combination with phloxine B, a chemically related compound to eosin Y, it is possible to increase bright-field intensity and enhance fluorescence signals (Carvalho and Taboga 1996; Aylon et al. 2016) (Fig. 2B, Supporting Information Figs. S5, S6). In our laboratory aggregates, the signal of eosin Y/phloxine B overlapped with chlorophyll, which is expected since eukaryotic organisms were the only cytoplasm containing cells stainable with eosin. This results in a combined approach necessary for total cytoplasm visualization in future studies.

Coomassie Brilliant Blue, originally used to stain proteins in polyacrylamide gels (Fazekas et al. 1963), is a common dye for proteinaceous particles in the water column (Long and Azam 1996). We show that when applied in an alcoholic and acidified solution, it is also possible to stain methacrylate sections (Supporting Information Fig. S7). However, we only detected distinct CSP signals within internal algae structures (Fig. 2A), i.e., no external signals were visible. It is possible that since Coomassie Brilliant Blue staining was done after TEP staining the stains overlapped precluding the identification of CSP structures within the aggregate. Alternatively, the lack of areas with exclusive extracellular CSP labeling might also be explained by aggregate composition. Differences would be expected in aggregates with TEP-producing eukaryotic algae and microbes only, compared to different types of particles (CSP) produced by different species such as cyanobacteria at different growth phases (Cisternas-Novoa et al. 2015). However, due to the observation of stained protein-containing algal structures, CSP remains a possibility for staining in future studies. As reported for Alcian Blue staining above, an overestimation of CSP by dye precipitation can be excluded by intense washing of the specimen without sample loss.

Alternative Araldite 502 embeddings for dense aggregates were not stainable with any of the dyes tested above. However, observation of nontransparent compounds, such as frustules and pigments was possible (Fig. 3).

Three-dimensional aggregate structure

Two-dimensional visualizations enable investigations on organism distributions, including algae-bacteria associations or inter-cellular material distributions such as TEP or CSP (*see* Fig. 5C). However, structural investigations on porosity or fractal dimension require the implementation of the third dimension. Therefore, we demonstrate the reconstruction of a 3D structure using 23 of 71 planes of a 142 μm thick segment of a laboratory-generated aggregate (Fig. 5).

Using the plugin BoneJ, we calculated the number of voxels (volumetric pixels) filled by particulate material (merged channels of TEP, CSP, nucleic acid chlorophyll, and cytoplasm) and the total number of voxels. Definition of the aggregate boundary is difficult and controversial, and currently beyond the scope of this study. To illustrate the possibility of porosity calculation, using our embedding method, we defined the boundary manually as close as possible to the particulate material while including pores (*see* Fig. 5C). For future investigations, we recommend a standardized approach to define the boundary, such as by applying a modified script of the automatic ROI definition tool in ImageJ or elliptical approximations of the boundary using the estimated cross-sectional area as reported elsewhere (Dörgens et al. 2015; Flintrop et al. 2018). In this

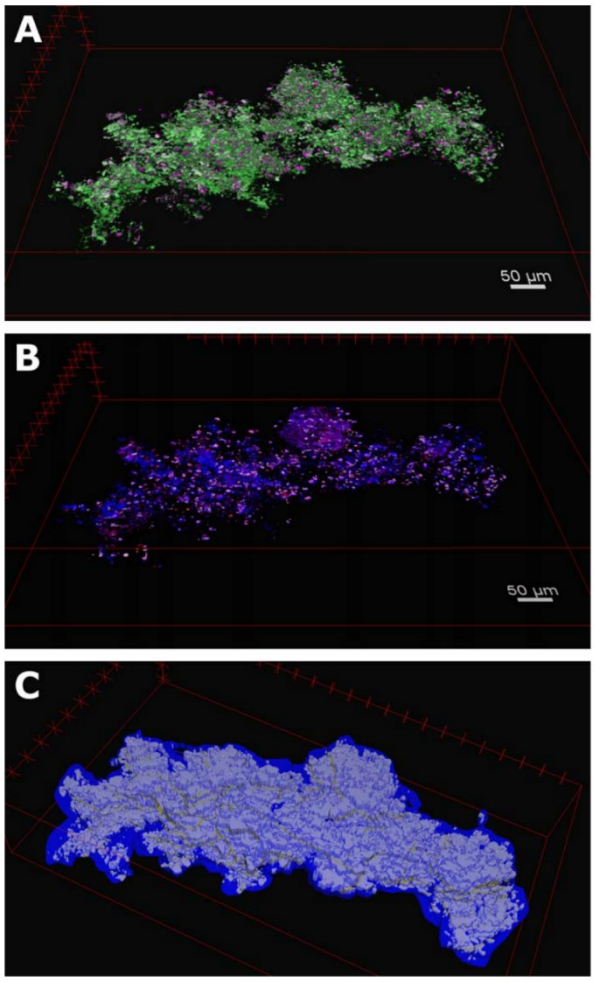

Fig. 5. Three-dimensional reconstruction of an aggregate segment. (**A**) Structural compounds TEP (green) and Coomassie Brilliant Blue stained proteins (magenta). (**B**) Nucleic acids (blue) and chlorophyll (red) as well as eukaryotic cytoplasm (yellow). (**C**) Visualization of the porosity calculation using BoneJ. All channels were merged and converted to a binary stack, whereas a 3D ROI (blue) defined the boundary of the aggregate.

demonstration, we used 23 of 71 planes, but we recommend using as many planes as possible to increase precision. We estimated a porosity of 66.5% in our test aggregate compartment. This is somewhat low compared to other calculations of phytodetritus aggregates (97–99.9%; Alldredge and Gotschalk 1988) and is closer to values reported for copepod fecal pellets (Ploug et al. 2008). Previous estimates of marine aggregate porosity are based on volume to dry weight ratios (Alldredge and Gotschalk 1988; Ploug et al. 2008). The approach employed here was based exclusively on volumetric ratios, i.e., the ratio of stained hydrated compounds to total aggregate volume. Water-containing compounds in bacteria or algae, as well as TEP or CSP may have higher volumes when hydrated leading to lower porosity estimates in our approach. This is of course a matter of definition, but when considering, that these values may be used in hydrodynamic models for aggregate and particle settling behavior, our approach might provide realistic results because water does not flow through enclosed water intrusions such as organisms, or hydrated matter as TEP or CSP. For the same aggregate portion, we also calculated a 3D fractal dimension of 2.13. Natural aggregates are characterized by fractal dimensions between 1 (tenuous and stringy) and 3 (dense and opaque) (Kranenburg 1994). The fractal dimension calculated in this approach is comparable to aggregates sampled at depths > 400 m (Risović 1998), when considering the likely differences that exists between laboratory-generated and natural aggregates.

Utility for stable isotope enrichment measurements

Methacrylate embedded samples investigated via NanoSIMS were characterized by a plane surface and a stabilized structure under ultra-high vacuum conditions with no outgassing observed. This is also evident from comparisons of epifluorescence (Fig. 4) and secondary electron images of the same region (Fig. 6). The airlock reached full vacuum (3.7–8 mbar) in 60 h after loading three 2 μm thick methacrylate samples into the chamber. When the samples were loaded into the NanoSIMS analysis chamber, normal operation vacuum (2.5–10 mbar) was reached within 15 min. This behavior indicates negligible outgassing of methacrylate when applying a slice thickness of 2 μm. Several failures on the surface, such as scratches and holes could be observed in the secondary electron image (Fig. 6), which was likely due to slightly rough handling while placing the sample into the holder. Negative effects, such as ablation, however, were not observed.

Element uptake into single cells was successfully visualized and calculated based on NanoSIMS measurements of methacrylate embedded aggregates. We observed one ^{15}N and several ^{34}S enriched organisms in laboratory generated aggregates incubated with stable isotope tracer compounds occurring predominantly in prokaryotic cells (Figs. 7 and 8). The low number of ^{15}N enriched cells may, next to inactive cells, be explained by the use of alternative nitrogen sources such as ammonia. Moreover, the location of enzymes involved in prokaryotic nitrate reduction may prevent uptake: only assimilatory reductase enzymes (Nas) are located within the cytoplasm, whereas respiratory (Nar), and dissimilatory nitrate reductase (Nap) enzymes are membrane-bound or located in the periplasm, respectively (Moreno-Vivián et al. 1999). The latter enzyme leads to direct export of nitrate reduction products out of the cell after uptake inside the periplasm.

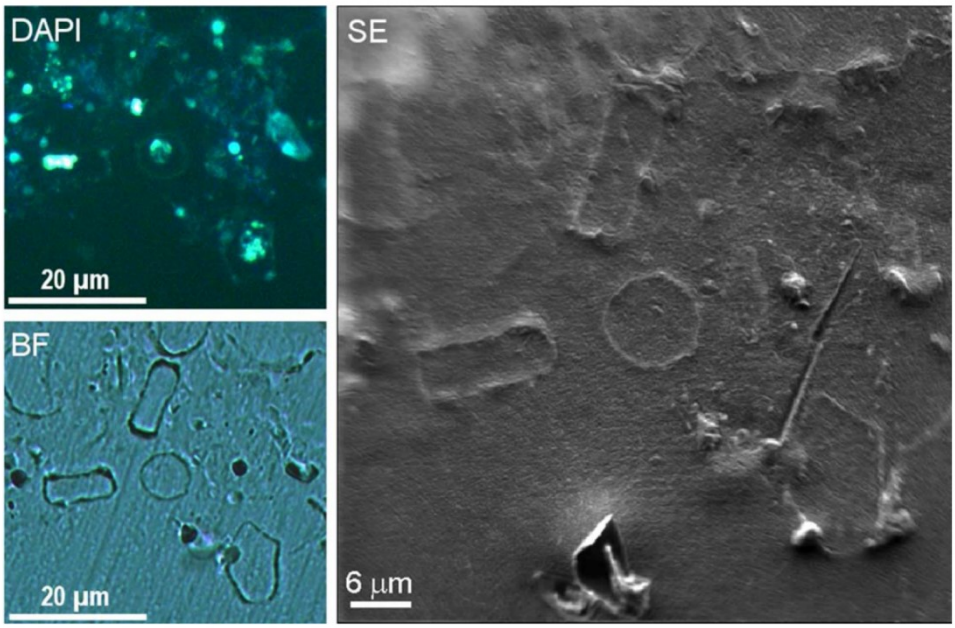

Fig. 6. Structural characteristics of methacrylate embeddings during the NanoSIMS measuring process: DAPI and bright field (BF) images were taken on a Laser Micro Dissection microscope (LMD7000, Leica) and the secondary electron image was acquired in the NanoSIMS 50L (Cameca). Structural differences caused by ultra-high vacuum as inflation, contraction, or detachment could not be observed compared to the sample structure at atmospheric pressure. Visible effects as the hole on the bottom or the scratch in the right middle were caused by sample treatment using forceps. Note that fluorescence differences to Fig. 4 are caused by removed DAPI stain and immersion oil prior to Laser marking.

Original abundance values of cells from ^{13}C incubations have on average an approximately 1‰ lower ^{13}C abundance compared to control incubations (Supporting Information Fig. S16). Higher Poisson errors associated with these cells indicate internal measurement effects as a likely explanation for this difference. These may include a different angle of the primary ion beam or slightly shifted detector positions on the mass peak of the respective isotopes due to the separation of measurements by several days. Based on the fact that all our methacrylate samples were embedded using the same batch of resin mixture at the same time, we were able to use an abundance correction approach based on resin abundances serving as internal standard. This calculation eliminates the internal measurement effects and enables correct result interpretation (Fig. 8 vs. Supporting Information Fig. S16). Taking these considerations into account, we might interpret a trend toward enrichment for a small number of ^{13}C-incubated cells as well. It is also probable that a matrix effect leads to dilution of the ^{13}C-signal in methacrylate resin embeddings. However, quantifying the dilution factor is challenging because of variable and unconstrained infiltration in different aggregates that is partly related to material density. This should be considered when combining quantitative measurements, as, e.g., total uptake measurements, with qualitative NanoSIMS measurements of aggregates of different density. The background content of N and S in methacrylate resin is negligible, resulting in stronger signals and low dilution of ^{15}N and ^{34}S enrichments (Fig. 7). Secondary ion yields were comparable to previous applications, such as bacterial samples on gold sputtered polycarbonate filters (Rogge et al. 2017), signifying adequate ionization efficiencies in embedded samples.

The utility of Araldite 502 embeddings for ultra-high vacuum applications, such as NanoSIMS, has been demonstrated previously (Herrmann et al. 2007; Clode et al. 2009; Mueller et al. 2012; Kaiser et al. 2015). Key attributes include very low outgassing characteristics as well as structural stability without ablation. In this study, we did not specifically test its efficacy.

Storage life

In our tests, we started the final resin embedding 2 months after sampling when the agarose blocks were still intact. This time should be sufficient for sample storage during periods between most field collections and lab-based processing. We observed that 50% sterile seawater and storage above the freezing point prevents cell bursting and the presence of ethanol serves as biological preservative. Ethanol is also used as a rRNA preservative for FISH (Shiraishi et al.

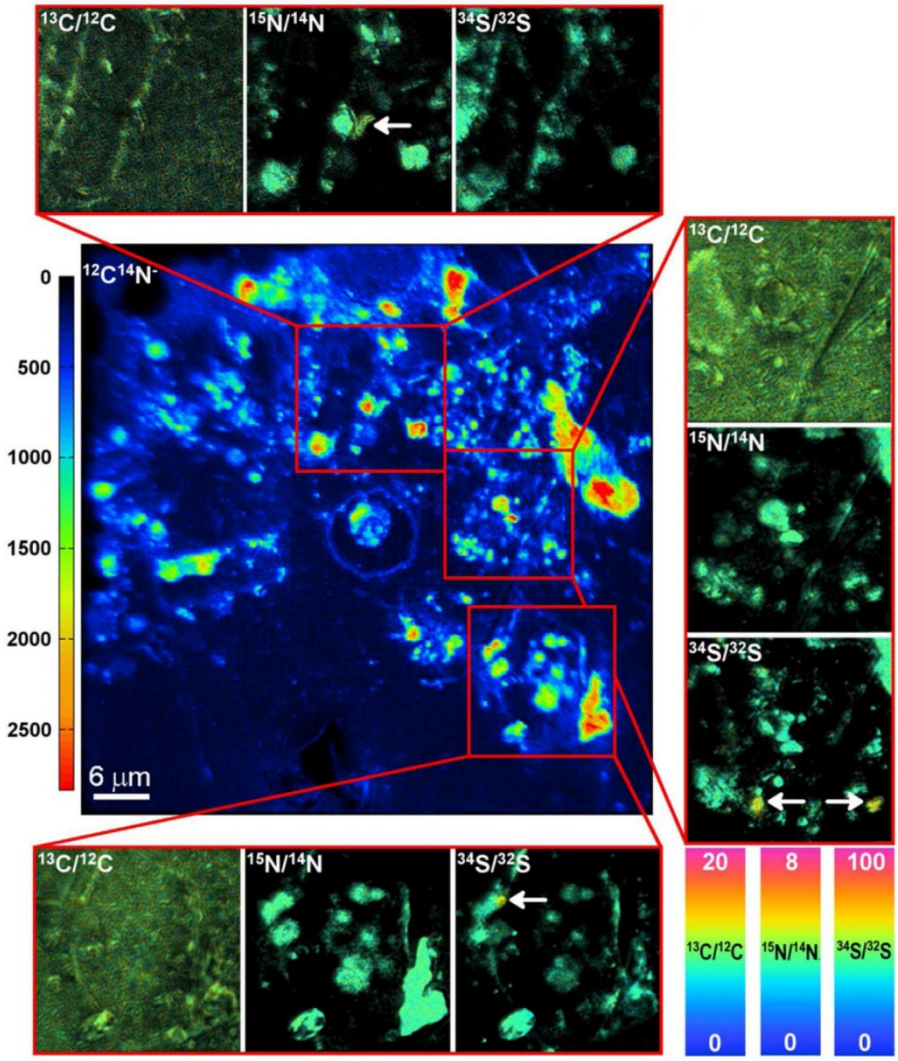

Fig. 7. Secondary ion mass spectrometry measurements on a 2 μm thick methacrylate embedded lab aggregate: The $^{12}C^{14}N^-$ signal as overview image was used to identify biomass and to locate spots for detailed ratio measurements. Significant and visible enrichments of ^{15}N could be detected in one prokaryotic cell in the upper spot while significant and visible enrichments of ^{34}S could be detected in the middle and lower spot. A low background in the N and S signal enables the precise definition of cells. Isotope ratios are presented as HSI-image enabling brightness adjustion of each pixel based on respective ion counts whereas black areas correspond to areas with low ion counts. The scales of isotope ratios are presented in per mill.

2008). We did not perform a time-course study of preservation properties of agarose-embedded and preserved aggregates, as it was secondary to the main issue of optimizing embedding techniques for NanoSIMS analyses. However, given previous findings using ethanol as a preservation solution for both nucleic acids and biofilm samples (Shiraishi et al. 2008), we are confident that biological components were stabilized.

Field test using in situ collected marine snow

To test aggregate handling and pre-embedding in more realistic conditions at sea, we performed aggregate sampling in Fram Strait close to the coast of Svalbard using a marine snow catcher. No difficulty in aggregate handling, leading to material loss due to disaggregation during transfer steps, could be observed. Even though the aggregates were relatively close to the coast and Kongsfjorden, the content of terrigenous material was low, so that slicing of methacrylate

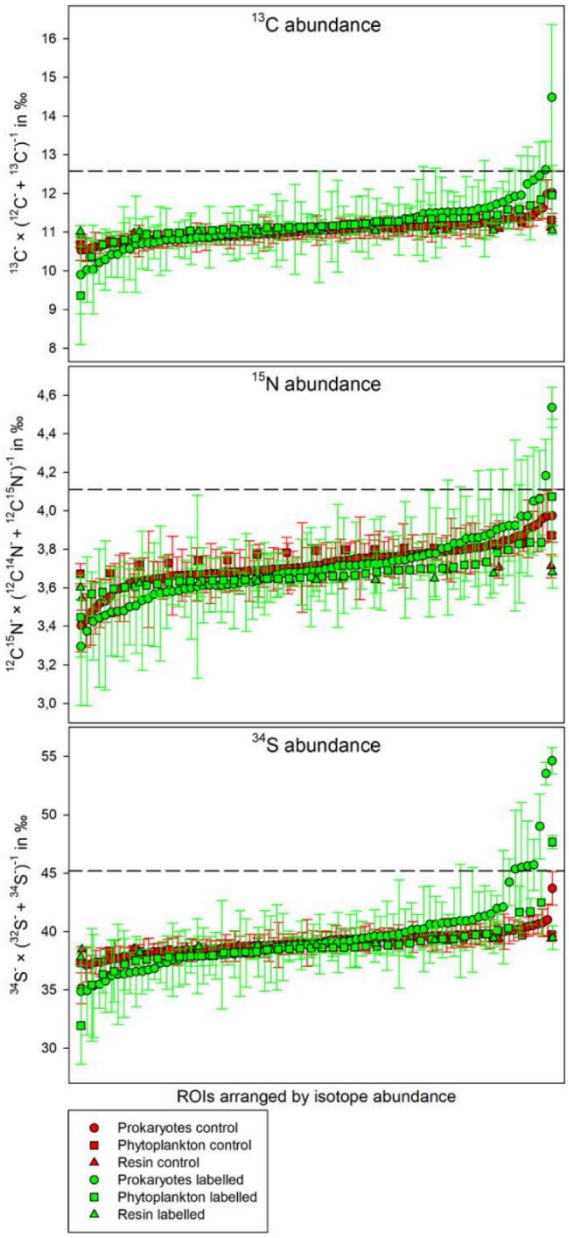

Fig. 8. Isotope abundances in ‰ including Poisson Errors as error bars, of all measured prokaryotic and phytoplankton cells as well as the resin itself corrected by using the resin as internal standard. The dashed line indicates the enrichment threshold (maximum value of the Poisson error of controls). Respective ROIs are shown in Supporting Information Figs. S8–S15.

was successful. As shown in Fig. 9, chlorophyll and nucleic acid signals are distinct and TEP compounds are intensely stained. Also the storage time was adequate for this field

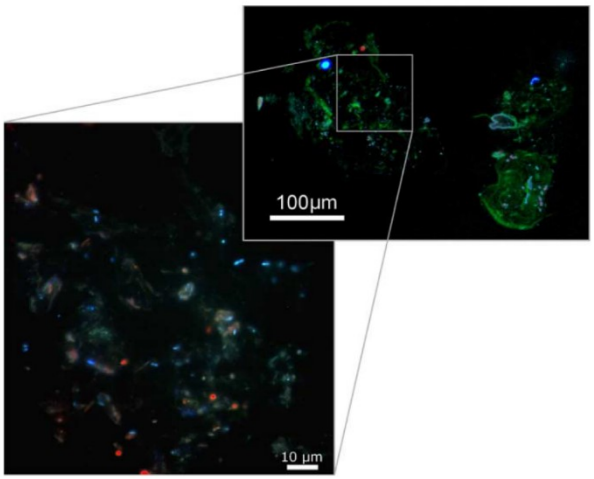

Fig. 9. Overlap micrograph of marine snow sampled off Svalbard, Norway: DAPI stained nucleic acids (blue) and Chl *a* (red) as well as Alcian Blue stained TEP (green) in top image of a slice through the whole aggregate. The bottom image, showing a part of the aggregate in higher magnification, exemplifies nucleic acid staining (blue) and Chl *a* (red).

trip: samples were resin embedded approximately 3 months after sampling and pigment localization and concentration as well as the structure is still undisturbed.

Discussion

The microstructure of marine snow is likely to impact the scale and availability of diverse microbial niches within these particles. In turn, microbially mediated transformations of particulate matter can influence the regeneration of (sometimes limiting) nutrients and carbon-specific remineralization rates. These specific processes within marine snow may affect the efficiency of the biological carbon pump, pelagic-benthic coupling, and physical transport of microbial communities. Understanding the importance of these processes within aggregates is currently limited by a lack of suitable methods. To broaden our knowledge on microscale structures, microbial communities, and uptake rates associated with marine snow, we sought to develop a multipurpose method for the preservation and slicing of marine snow that was compatible with different structural stains and NanoSIMS investigations.

Several approaches for the investigation of marine snow have been developed during recent decades. To date, these have mainly focused on characterizing features on whole aggregates, such as Alcian Blue and Coomassie Blue staining on membrane filters for total exopolymer equivalents (Busch et al. 2017) or fingerprinting and sequencing techniques for aggregate-associated microbial community structure (DeLong et al. 1993; Rath et al. 1998; Fontanez et al. 2015). For such

objectives, capturing particles and aggregates on membrane filters is sufficient. However, such sampling methods lead to loss of 3D structure and material and are not suitable for addressing the microscale structure of individual marine aggregates. The idea of slicing marine snow was developed for TEM investigations using the melamine resin Nanoplast® (Heissenberger et al. 1996b; Leppard et al. 1996). This resin, however, requires high-hardening temperatures of 60°C, which does not ensure intact rRNA for potential taxonomic staining (see below). Moreover, melamine contains high amounts of nitrogen, which leads to dilution of nitrogen enrichments within organisms.

Other embedding matrices for CARDFISH and NanoSIMS analyses of other types of samples include paraffin (e.g., Jaekel et al. 2013 or Musat et al. 2007) and cryogels (e.g., Wilbanks et al. 2014). Those are, however, not useful for detailed single-cell analyses in marine snow due to the impossibility of section preparations thinner than 5 μm. Additionally, paraffin must be removed after sectioning to allow staining and secondary ion mass spectrometry which increases the risk of material loss due to the high fragility of the marine snow sections dramatically. Cryogels, on the other hand, enable uninterrupted staining but the vacuum resistancy is likely to be suboptimal, and shrinking can be expected, limiting the use for biovolume-corrected enrichment calculations.

As described by Kopf et al. (2015), hard plastic resins are often too dense to allow a variety of staining techniques including CARDFISH. Kopf et al. (2015) and McGlynn et al. (2015) used Technovit, a commercially available acrylic resin. In our tests it turned out, that the also broadly used acrylic resin LR-white (Nussbaumer et al. 2006; Gros and Maurin 2008) showed a high-background fluorescence and was thus not useful for fluorescent stains, such as DAPI.

For our study, we chose a well-established embedding medium mixture based on methacrylate. Key benefits of this medium are that it enables the dissipation of heat during the exothermic polymerization and is characterized by negligible nitrogen and sulfur contents which can affect the significance of enrichment measurements. The medium was optimized for the investigation of human and animal tissue (Burkhardt 1966; Velde et al. 1977) which, like most eumetazoan tissues, contains collagen that acts as a stabilizing matrix during embedding. In contrast, the absence of collagen in marine aggregates leads to disaggregation during the dehydration and infiltration steps. In order to circumvent this limitation, our method employs a pre-embedding step to supplement marine snow with an agarose matrix. Agarose has been used previously as an embedding matrix for marine snow pellets concentrated by centrifugation (Biddanda 1986; Carlough 1994) or for small zooplankton fecal pellets (Gowing and Silver 1983). Agar embedding has been intensively used as for methanotrophic consortia from marine sediments (McGlynn et al. 2015) as well as centrifuged pellets of bacteria and algae cells (Slaveykova et al. 2009; Kopf et al. 2015). However, as far as we are aware, our method is the first application of an agarose pre-embedding step for preserving structure of undisturbed marine snow. We used low melting-point agarose (liquid state above gelling range of 24–29°C), which facilitates infiltration into typically porous marine aggregates. Furthermore, carbon and hydrogen, the only constituents of agarose, are an advantage when performing isotopic enrichments with nitrogen and sulfur. Combined with the very low nitrogen and sulfur content in the methacrylate resin, dilutions of those elements are reduced. Carbon uptake measurements, on the other hand, require a higher labeling concentration for precise enrichment identification under the same conditions.

The objective of the present study was to develop a working protocol capable of coupling observations of the physical microstructure of marine snow with single-cell uptake rates of organisms within the aggregates. The aggregates, when treated with agarose-methacrylate embedding method, could be consistently sliced to a thickness of 2 μm and exhibited no background fluorescence from the embedding matrix.

Furthermore, we were able to demonstrate the successful staining of methacrylate embedded slices with Alcian Blue for TEP structure, Coomassie Brilliant Blue for proteins, eosin Y for cytoplasm proteins, and DAPI for nucleic acids. Microbes embedded within TEP exudates around algal cells within individual aggregates could be clearly visualized. In contrast, extracellular proteinaceous compounds were not observed in significant amounts, in the aggregates we studied. Moreover, excess Alcian Blue and Coomassie Brilliant Blue dye could be removed without sample loss, reducing any overestimation of TEP and CSP due to precipitation (Passow and Alldredge 1995; Cisternas-Novoa et al. 2015).

We were able to reconstruct the 3D structure of an aggregate portion with its biological (bacterial, algae, eukaryotic cytoplasm) as well as structural (TEP, CSP) compounds. Moreover, we provided a first step toward alternative porosity and 3D fractal dimension calculations using the software BoneJ and its tools originally constructed for trabeculae bone analyses. We have identified further need for a standardized aggregate boundary definition approach.

Thin methacrylate (2 μm) embedded slices had sufficient structural integrity for NanoSIMS analyses under ultra-high vacuum conditions (10^{-10} mbar) with workable ionization efficiencies. Retention of specimen structural integrity is absolutely critical for the calculation of cell volume-corrected elemental enrichments. This was recently demonstrated with pelagic bacteria (Rogge et al. 2017), and is important for calculating the differential uptake of specific elements by heterogeneously sized environmental microorganisms.

We were able to detect and localize prokaryotic uptake of nitrate and sulfate in our sliced marine aggregate preparations. While a dilution of carbon enrichment signals is likely given the C-rich embedding media, even in incubations with

low glucose concentrations (100 nM), a trend toward enrichments was observed visually. The use of higher labeling concentrations in future studies should provide more pronounced results. Moreover, the resin surrounding the organic matter of the aggregate can be used as internal standard to correct abundance calculations and enables precise interpretations.

As an alternative approach for very dense marine snow or marine particles with incorporated terrigenous material, we performed Araldite 502 embeddings. Resulting specimens could be sectioned to a minimum thickness of 40 μm. The applicability for NanoSIMS has already been proven elsewhere (Herrmann et al. 2007; Mueller et al. 2012; Kaiser et al. 2015). Structural staining, however, was not possible with the greater thicknesses, thereby restricting the use of this resin to investigations of nontransparent compounds, such as frustules, pigments, or terrigenous material, and uptake measurements using NanoSIMS.

Finally, we show that our method is also effective for natural aggregates, and we demonstrate the method using aggregates from polar waters off Svalbard. Even though NanoSIMS analyses were not performed on these samples, the reduction of material loss during processing as well as adequate stainability properties could be exemplified. We used the same resin and slice thickness for these samples as for the lab-generated aggregates, and the natural marine snow particles were characterized by identical or similar vacuum resistance specifications as our laboratory generated aggregates.

Future applications for marine snow would benefit from a combination of single cell uptake measurements with identification methods such as rRNA-based catalyzed reporter deposition in situ hybridization (CARDFISH) and related approaches, as demonstrated by several authors for pelagic bacteria (Musat et al. 2008; Krupke et al. 2013; Rogge et al. 2017). This would enable the investigation of physical and metabolic co-location and community structure analyses in marine snow as shown for microbial consortia from marine sediments (McGlynn et al. 2015). In parallel tests, which were not the main focus of this study, we achieved corresponding signals to both positive and negative controls. However, final hybridization optimization and stringency was never achieved and further development would be required. The protocol applied is provided in the Supporting Information Chapter 1 and a similar approach presented by McGlynn et al. (2015).

The method synthesis developed in the present study meets our objective for investigations on marine snow. The pre-embedding procedure maintains 3D structure of the samples and minimizes sample loss primarily because aggregate sections remain embedded in resin during staining process. We demonstrated the ability to identify structural components such as TEP and alkaline amino acids. The identification of prokaryotes and photoautotrophic organisms was also possible using a combination of successful nucleic acid and eukaryotic cytoplasm staining as wells as Chl *a* autofluorescence of the embedded aggregate slices. Critically, rRNA stays intact during sample preparations with methacrylate resins enabling potential taxonomic staining using CARD-FISH techniques in future applications.

The present protocol provides an opportunity to preserve the structure of marine snow sampled at sea, and investigate microbial activity at the single-cell level within aggregates. We envisage that when our method is applied more broadly to a range of field samples, it will facilitate the development of new insights into aggregate types, sizes and structures, microbial interactions, and aggregate transformation. It will provide input for a new understanding of particle dynamics, as well as for microbial ecology.

We note that in our laboratory-generated aggregates, we also observed the uptake of SO_4, a result which will be of particular interest to follow up in the field, as it points to the potential use of alternative electron acceptors in anoxic microzones within aggregates. The global distribution of aggregate-associated anoxia which increases the global rate of sulfate reduction in the water column was very recently predicted by Bianchi et al. (2018) and our work protocol represents the first tool to investigate those processes in the marine environment. Additionally, slight modifications of the sampling and pre-embedding protocol, such as preaccumulation of aggregates using an elutriation system (Peterson et al. 2005) would enable the investigation of smaller less visible aggregates ($<$ 500 μm). High vacuum tolerance of methacrylate and Araldite resins also allows the use of other modern technologies such as scanning transmission electron microscopy coupled to electron dispersive X-ray analyses, ultimately enabling quantitative element measurements inside organisms, and thus even further possibilities for future applications. A combination of aggregate-related turnover rates with noninvasive optical quantification systems, such as the Underwater Vision Profiler or other systems (Iversen et al. 2010; Picheral et al. 2010; Biard et al. 2016) would ultimately allow us to calculate the contribution of different size classes of aggregates as well as the proportion of involved organisms on regional turnover rates.

We envisage future incorporation into our method of the wide variety of staining protocols already available, enabling further development of application for diverse future investigations.

The cryogel approach presented by Flintrop et al. (2018) focused on structural investigation of marine snow sampled with a Marine Snow Catcher or directly from drifting sediment traps coupled to taxonomic microbial identification using FISH. An overview of major differences and overlaps between plastic resin and the cryogel embedding methods utilized by Flintrop and coworkers is presented in Supporting Information Table S1. In brief, use of a cryogel enables more detailed observations of hydrous compounds due to minimized dehydration, while the resin-embedding process' use

of formaldehyde for chemical fixation, and ethanol or acetone for dehydration, leads to potential loss of diffusible compounds (Grovenor et al. 2006; Kilburn and Clode 2014). If desirable, samples for SIMS analyses of diffusible compounds can be dehydrated using the freeze-approach as described for X-ray microanalyses by Marshall (1980) and more recently for NanoSIMS by Kilburn and Clode (2014). For analyses of nondiffusive compounds, however, acetone dehydration and plastic resin embedding is in fact a widely used method (Herrmann et al. 2007; Clode et al. 2009; Slaveykova et al. 2009; Mueller et al. 2012; Kaiser et al. 2015). Soft and hard plastic embedding resins, particularly methacrylate and Araldite 502, are characterized by ultra-high vacuum-stability, such as minimized shrinking and ablation. Those features, together with the low N and S content, enable cell-volume corrected enrichment calculations with as low as possible isotope dilution effects as reported elsewhere (Rogge et al. 2017). In combination with applicable basic stains (*see* Supporting Information Table S1), detailed elemental uptake investigations of single cells with mechanically undisturbed localization within surrounding organic matrices are possible. Smearing of embedded samples during slicing can go undetected, despite the fact that such smearing significantly reduces their optical resolution and overall effectiveness for analysis. In contrast, any distortion of the sample in a resin can immediately detected because of instantaneous rupture of the slice. Moreover, the alternative embedding matrix Araldite 502, described in this manuscript, enables uptake investigations of marine snow containing very hard compounds as, e.g., terrigenous material. A complementary application of the methods described in this and the manuscript by Flintrop et al. (2018) would enable a wide variety of possible investigations of the microbial ecology and biogeochemical cycling within marine snow as well as effects on the biological carbon pump.

References

Alldredge, A. L., and C. C. Gotschalk. 1988. In situ settling behavior of marine snow. Limnol. Oceanogr. **33**: 339–351. doi:10.4319/lo.1988.33.3.0339

Alldredge, A. L., and M. W. Silver. 1988. Characteristics, dynamics and significance of marine snow. Prog. Oceanogr. **20**: 41–82. doi:10.1016/0079-6611(88)90053-5

Alldredge, A. L., U. Passow, and B. E. Logan. 1993. The abundance and significance of a class of large, transparent organic particles in the ocean. Deep-Sea Res. Part I Oceanogr. Res. Pap. **40**: 1131–1140. doi:10.1016/0967-0637(93)90129-Q

Aylon, Y., and others. 2016. The LATS2 tumor suppressor inhibits SREBP and suppresses hepatic cholesterol accumulation. Genes Dev. **30**: 786–797. doi:10.1101/gad.274167.115

Bako, P., M. Bassiouni, A. Eckhard, I. Gerlinger, C. Frick, H. Löwenheim, and M. Müller. 2015. Methyl methacrylate embedding to study the morphology and immunohistochemistry of adult guinea pig and mouse cochleae. J. Neurosci. Methods **254**: 86–93. doi:10.1016/j.jneumeth.2015.07.017

Becerra, S. C., D. C. Roy, C. J. Sanchez, R. J. Christy, and D. M. Burmeister. 2016. An optimized staining technique for the detection of Gram positive and Gram negative bacteria within tissue. BMC Res. Notes **9**: 216. doi:10.1186/s13104-016-1902-0

Bianchi, D., T. Weber, S. R. Kiko, and C. Deutsch. 2018. Global niche of marine anaerobic metabolisms expanded by particle microenvironments. Nat. Geosci. **65**: 36. doi:10.1038/s41561-018-0081-0

Biard, T., and others. 2016. In situ imaging reveals the biomass of giant protists in the global ocean. Nature **532**: 504–507. doi:10.1038/nature17652

Biddanda, B. A. 1986. Structure and function of marine microbial aggregates. Oceanol. Acta **9**: 209–211.

Burkhardt, R. 1966. Präparative Voraussetzungen zur klinischen histologie des menschlichen Knochenmarkes. Blut **14**: 30–46. doi:10.1007/BF01633163

Busch, K., S. Endres, M. H. Iversen, J. Michels, E.-M. Nöthig, and A. Engel. 2017. Bacterial colonization and vertical distribution of marine gel particles (TEP and CSP) in the Arctic Fram Strait. Front. Mar. Sci. **4**: 1131. doi:10.3389/fmars.2017.00166

Canfield, D. E., F. J. Stewart, B. Thamdrup, L. De Brabandere, T. Dalsgaard, E. F. Delong, N. P. Revsbech, and O. Ulloa. 2010. A cryptic sulfur cycle in oxygen-minimum-zone waters off the Chilean coast. Science **330**: 1375–1378. doi:10.1126/science.1196889

Carlough, L. A. 1994. Origins, structure, and trophic significance of amorphous seston in a blackwater river. Freshw. Biol. **31**: 227–237. doi:10.1111/j.1365-2427.1994.tb00857.x

Carvalho, H. F., and S. R. Taboga. 1996. Fluorescence and confocal laser scanning microscopy imaging of elastic fibers in hematoxylin-eosin stained sections. Histochem. Cell Biol. **106**: 587–592. doi:10.1007/BF02473274

Cisternas-Novoa, C., C. Lee, and A. Engel. 2015. Transparent exopolymer particles (TEP) and Coomassie stainable particles (CSP). Mar. Chem. **175**: 56–71. doi:10.1016/j.marchem.2015.03.009

Clode, P. L., M. R. Kilburn, D. L. Jones, E. A. Stockdale, J. B. Cliff, A. M. Herrmann, and D. V. Murphy. 2009. In situ mapping of nutrient uptake in the rhizosphere using nanoscale secondary ion mass spectrometry. Plant Physiol. **151**: 1751–1757. doi:10.1104/pp.109.141499

Decho, A. W. 1990. Microbial exopolymer secretions in ocean environments: Their role(s) in food webs and marine processes. Oceanogr. Mar. Biol. **28**: 73–153.

DeLong, E. F., D. G. Franks, and A. L. Alldredge. 1993. Phylogenetic diversity of aggregate-attached vs. free-living marine bacterial assemblages. Limnol. Oceanogr. **38**: 924–934. doi:10.4319/lo.1993.38.5.0924

Dörgens, A. L., S. Ahmerkamp, J. Müssig, R. Stocker, M. M. M. Kuypers, A. Khalili, and K. Kindler. 2015. A laboratory model of marine snow. Limnol. Oceanogr.: Methods **13**: 664–671. doi:10.1002/lom3.10056

Doube, M., and others. 2010. BoneJ: Free and extensible bone image analysis in ImageJ. Bone **47**: 1076–1079. doi:10.1016/j.bone.2010.08.023

Fazekas, S., S. Groth, R. G. Webster, and A. Datyner. 1963. Two new staining procedures for quantitative estimation of proteins on electrophoresis strips. Biochim. Biophys. Acta **71**: 377–391. doi:10.1016/0006-3002(63)91092-8

Fazzalari, N. L., and I. H. Parkinson. 1996. Fractal dimension and architecture of trabecular bone. J. Pathol. **178**: 100–105. doi:10.1002/(SICI)1096-9896(199601)178:1<100::AID-PATH429>3.0.CO;2-K

Flintrop, C., A. Rogge, S. Miksch, A. M. Waite, and M. H. Iversen. 2018. Embedding and slicing of intact in situ collected marine snow. Limnol. Oceanogr.: Methods. **16**: 339–355. doi:10.1002/lom3.10251

Fontanez, K. M., J. M. Eppley, T. J. Samo, D. M. Karl, and E. F. DeLong. 2015. Microbial community structure and function on sinking particles in the North Pacific Subtropical Gyre. Front. Microbiol. **6**: 469. doi:10.3389/fmicb.2015.00469

Gormanns, P., S. Reckow, J. C. Poczatek, C. W. Turck, and C. Lechene. 2012. Segmentation of multi-isotope imaging mass spectrometry data for semi-automatic detection of regions of interest. PLoS One **7**: e30576. doi:10.1371/journal.pone.0030576

Gotschalk, C. C., and A. L. Alldredge. 1989. Enhanced primary production and nutrient regeneration within aggregated marine diatoms. Mar. Biol. **103**: 119–129. doi:10.1007/BF00391070

Gowing, M. M., and M. W. Silver. 1983. Origins and microenvironments of bacteria mediating fecal pellet decomposition in the sea. Mar. Biol. **73**: 7–16. doi:10.1007/BF00396280

Gros, O., and L. C. Maurin. 2008. Easy flat embedding of oriented samples in hydrophilic resin (LR White) under controlled atmosphere: Application allowing both nucleic acid hybridizations (CARD-FISH) and ultrastructural observations. Acta Histochem. **110**: 427–431. doi:10.1016/j.acthis.2007.11.001

Grovenor, C. R. M., K. E. Smart, M. R. Kilburn, B. Shore, J. R. Dilworth, B. Martin, C. Hawes, and R. E. M. Rickaby. 2006. Specimen preparation for NanoSIMS analysis of biological materials. Appl. Surf. Sci. **252**: 6917–6924. doi:10.1016/j.apsusc.2006.02.180

Guillard, R. L. L., and J. H. Ryther. 1962. Studies of marine planktonic diatoms. I. Cyclotella nana Hustedt, and Detonula confervacea (cleve) Gran. Can. J. Microbiol. **8**: 229–239. doi:10.1139/m62-029

Heissenberger, A., G. G. Leppard, and G. J. Herndl. 1996a. Relationship between the intracellular integrity and the morphology of the capsular envelope in attached and free-living marine bacteria. Appl. Environ. Microbiol. **62**: 4521–4528.

Heissenberger, A., G. G. Leppard, and G. J. Herndl. 1996b. Ultrastructure of marine snow. II. Microbiological considerations. Mar. Ecol. Prog. Ser. **135**: 299–308. doi:10.3354/meps135299

Herrmann, A. M., P. L. Clode, I. R. Fletcher, N. Nunan, E. A. Stockdale, A. G. O'Donnell, and D. V. Murphy. 2007. A novel method for the study of the biophysical interface in soils using nano-scale secondary ion mass spectrometry. Rapid Commun. Mass Spectrom. **21**: 29–34. doi:10.1002/rcm.2811

Huang, W. M., S. J. Gibson, P. Facer, J. Gu, and J. M. Polak. 1983. Improved section adhesion for immunocytochemistry using high molecular weight polymers of l-lysine as a slide coating. Histochemistry **77**: 275–279. doi:10.1007/BF00506570

Iversen, M. H., N. Nowald, H. Ploug, G. A. Jackson, and G. Fischer. 2010. High resolution profiles of vertical particulate organic matter export off Cape Blanc, Mauritania: Degradation processes and ballasting effects. Deep-Sea Res. Part I Oceanogr. Res. Pap. **57**: 771–784. doi:10.1016/j.dsr.2010.03.007

Jaekel, U., N. Musat, B. Adam, M. Kuypers, O. Grundmann, and F. Musat. 2013. Anaerobic degradation of propane and butane by sulfate-reducing bacteria enriched from marine hydrocarbon cold seeps. ISME J. **7**: 885–895. doi:10.1038/ismej.2012.159

Kaiser, C., M. R. Kilburn, P. L. Clode, L. Fuchslueger, M. Koranda, J. B. Cliff, Z. M. Solaiman, and D. V. Murphy. 2015. Exploring the transfer of recent plant photosynthates to soil microbes: Mycorrhizal pathway vs direct root exudation. New Phytol. **205**: 1537–1551. doi:10.1111/nph.13138

Karner, M., and G. J. Herndl. 1992. Extracellular enzymatic activity and secondary production in free-living and marine-snow-associated bacteria. Mar. Biol. **113**: 341–347. doi:10.1007/BF00347289

Kilburn, M. R., and P. L. Clode. 2014. Elemental and isotopic imaging of biological samples using NanoSIMS. Methods Mol. Biol. **1117**: 733–755. doi:10.1007/978-1-62703-776-1_33

Kimball, S., and P. Mattis, and GIMP Development Team. 1997–2017. GIMP2; [accessed 2018 June 27]. Available from www.gimp.org

Kopf, S. H., S. E. McGlynn, A. Green-Saxena, Y. Guan, D. K. Newman, and V. J. Orphan. 2015. Heavy water and ^{15}N labelling with NanoSIMS analysis reveals growth rate-dependent metabolic heterogeneity in chemostats. Environ. Microbiol. **17**: 2542–2556. doi:10.1111/1462-2920.12752

Kranenburg, C. 1994. The fractal structure of cohesive sediment aggregates. Estuar. Coast. Shelf Sci. **39**: 451–460. doi:10.1016/S0272-7714(06)80002-8

Krupke, A., N. Musat, J. L. Roche, W. Mohr, B. M. Fuchs, R. I. Amann, M. M. M. Kuypers, and R. A. Foster. 2013. In situ identification and N_2 and C fixation rates of uncultivated cyanobacteria populations. Syst. Appl. Microbiol. **36**: 259–271. doi:10.1016/j.syapm.2013.02.002

Leppard, G. G., A. Heissenberger, and G. J. Herndl. 1996. Ultrastructure of marine snow. I. Transmission electron microscopy methodology. Mar. Ecol. Prog. Ser. **135**: 289–298. doi:10.3354/meps135289

Linkert, M., and others. 2010. Metadata matters. J. Cell Biol. **189**: 777–782. doi:10.1083/jcb.201004104

Long, R. A., and F. Azam. 1996. Abundant protein-containing particles in the sea. Aquat. Microb. Ecol. **10**: 213–221. doi:10.3354/ame010213

Lyons, M. M., and F. C. Dobbs. 2012. Differential utilization of carbon substrates by aggregate-associated and water-associated heterotrophic bacterial communities. Hydrobiologia **686**: 181–193. doi:10.1007/s10750-012-1010-7

Maarel, M. J. E. C., W. Sprenger, R. Haanstra, and L. J. Forney. 1999. Detection of methanogenic archaea in seawater particles and the digestive tract of a marine fish species. FEMS Microbiol. Ecol. **173**: 189–194. doi:10.1111/j.1574-6968.1999.tb13501.x

Marshall, A. T. 1980. Freeze-substitution as a preparation technique for biological X-ray microanalysis. Scan. Electron Microsc. 395–408.

Marty, D. G. 1993. Methanogenic bacteria in seawater. Limnol. Oceanogr. **38**: 452–456. doi:10.4319/lo.1993.38.2.0452

McGlynn, S. E., G. L. Chadwick, C. P. Kempes, and V. J. Orphan. 2015. Single cell activity reveals direct electron transfer in methanotrophic consortia. Nature **526**: 531–535. doi:10.1038/nature15512

Moreno-Vivián, C., P. Cabello, M. Martínez-Luque, R. Blasco, and F. Castillo. 1999. Prokaryotic nitrate reduction: Molecular properties and functional distinction among bacterial nitrate reductases. J. Bacteriol. **181**: 6573–6584.

Mueller, C. W., A. Kölbl, C. Hoeschen, F. Hillion, K. Heister, A. M. Herrmann, and I. Kögel-Knabner. 2012. Submicron scale imaging of soil organic matter dynamics using NanoSIMS – from single particles to intact aggregates. Org. Geochem. **42**: 1476–1488. doi:10.1016/j.orggeochem.2011.06.003

Musat, N., O. Giere, A. Gieseke, F. Thiermann, R. Amann, and N. Dubilier. 2007. Molecular and morphological characterization of the association between bacterial endosymbionts and the marine nematode *Astomonema* sp. from the Bahamas. Environ. Microbiol. **9**: 1345–1353. doi:10.1111/j.1462-2920.2006.01232.x

Musat, N., and others. 2008. A single-cell view on the ecophysiology of anaerobic phototrophic bacteria. Proc. Natl. Acad. Sci. USA **105**: 17861–17866. doi:10.1073/pnas.0809329105

Nussbaumer, A. D., C. R. Fisher, and M. Bright. 2006. Horizontal endosymbiont transmission in hydrothermal vent tubeworms. Nature **441**: 345–348. doi:10.1038/nature04793

Paerl, H. W., and J. L. Pinckney. 1996. A mini-review of microbial consortia: Their roles in aquatic production and biogeochemical cycling. Microb. Ecol. **31**: 225–247. doi:10.1007/BF00171569

Passow, U., A. L. Alldredge, and B. E. Logan. 1994. The role of particulate carbohydrate exudates in the flocculation of diatom blooms. Deep-Sea Res. Part I Oceanogr. Res. Pap. **41**: 335–357. doi:10.1016/0967-0637(94)90007-8

Passow, U., and A. L. Alldredge. 1995. A dye-binding assay for the spectrophotometric measurement of transparent exopolymer particles (TEP). Limnol. Oceanogr. **40**: 1326–1335. doi:10.4319/lo.1995.40.7.1326

Passow, U., R. F. Shipe, A. Murray, D. K. Pak, M. A. Brzezinski, and A. L. Alldredge. 2001. The origin of transparent exopolymer particles (TEP) and their role in the sedimentation of particulate matter. Cont. Shelf Res. **21**: 327–346. doi:10.1016/S0278-4343(00)00101-1

Peterson, M. L., S. G. Wakeham, C. Lee, M. A. Askea, and J. C. Miquel. 2005. Novel techniques for collection of sinking particles in the ocean and determining their settling rates. Limnol. Oceanogr.: Methods **3**: 520–532. doi:10.4319/lom.2005.3.520

Phillips, C. J., Z. Smith, T. M. Embley, and J. I. Prosser. 1999. Phylogenetic differences between particle-associated and planktonic ammonia-oxidizing bacteria of the β subdivision of the class *Proteobacteria* in the northwestern Mediterranean Sea. Appl. Environ. Microbiol. **65**: 779–786.

Picheral, M., L. Guidi, L. Stemmann, D. M. Karl, G. Iddaoud, and G. Gorsky. 2010. The underwater vision profiler 5. Limnol. Oceanogr.: Methods **8**: 462–473. doi:10.4319/lom.2010.8.462

Ploug, H., M. H. Iversen, and G. Fischer. 2008. Ballast, sinking velocity, and apparent diffusivity within marine snow and zooplankton fecal pellets: Implications for substrate turnover by attached bacteria. Limnol. Oceanogr. **53**: 1878–1886. doi:10.4319/lo.2008.53.5.1878

Polerecky, L., B. Adam, J. Milucka, N. Musat, T. Vagner, and M. M. M. Kuypers. 2012. Look@NanoSIMS–a tool for the analysis of nanoSIMS data in. Environ. Microbiol. **14**: 1009–1023. doi:10.1111/j.1462-2920.2011.02681.x

Rath, J., K. Y. Wu, G. J. Herndl, and E. F. DeLong. 1998. High phylogenetic diversity in a marine-snow-associated bacterial assemblage. Aquat. Microb. Ecol. **14**: 261–269. doi:10.3354/ame014261

Risović, D. 1998. On correlation of fractal dimension of marine particles with depth. J. Colloid Interface Sci. **197**: 391–394. doi:10.1006/jcis.1997.5277

Rogge, A., A. Vogts, M. Voss, K. Jürgens, G. Jost, and M. Labrenz. 2017. Success of chemolithoautotrophic SUP05 and Sulfurimonas GD17 cells in pelagic Baltic Sea redox zones is facilitated by their lifestyles as K- and r-strategists.

Environ. Microbiol. **19**: 2495–2506. doi:10.1111/1462-2920.13783

Schindelin, J., and others. 2012. Fiji: An open-source platform for biological-image analysis. Nat. Methods **9**: 676–682. doi:10.1038/nmeth.2019

Schindelin, J., C. T. Rueden, M. C. Hiner, and K. W. Eliceiri. 2015. The ImageJ ecosystem. Mol. Reprod. Dev. **82**: 518–529. doi:10.1002/mrd.22489

Schmid, B., J. Schindelin, A. Cardona, M. Longair, and M. Heisenberg. 2010. A high-level 3D visualization API for Java and ImageJ. BMC Bioinf. **11**: 274. doi:10.1186/1471-2105-11-274

Schneider, C. A., W. S. Rasband, and K. W. Eliceiri. 2012. NIH image to ImageJ. Nat. Methods **9**: 671–675. doi:10.1038/nmeth.2089

Shanks, A. L., and J. D. Trent. 1979. Marine snow: Microscale nutrient patches. Limnol. Oceanogr. **24**: 850–854. doi:10.4319/lo.1979.24.5.0850

Shiraishi, F., B. Zippel, T. R. Neu, and G. Arp. 2008. In situ detection of bacteria in calcified biofilms using FISH and CARD-FISH. J. Microbiol. Methods **75**: 103–108. doi:10.1016/j.mimet.2008.05.015

Slaveykova, V. I., C. Guignard, T. Eybe, H.-N. Migeon, and L. Hoffmann. 2009. Dynamic NanoSIMS ion imaging of unicellular freshwater algae exposed to copper. Anal. Bioanal. Chem. **393**: 583–589. doi:10.1007/s00216-008-2486-x

Stoderegger, K. E., and G. J. Herndl. 1999. Production of exopolymer particles by marine bacterioplankton under contrasting turbulence conditions. Mar. Ecol. Prog. Ser. **189**: 9–16. doi:10.3354/meps189009

Swan, B. K., and others. 2011. Potential for chemolithoautotrophy among ubiquitous bacteria lineages in the dark ocean. Science **333**: 1296–1300. doi:10.1126/science.1203690

Turley, C. M., and E. D. Stutt. 2000. Depth-related cell-specific bacterial leucine incorporation rates on particles and its biogeochemical significance in the Northwest Mediterranean. Limnol. Oceanogr. **45**: 419–425. doi:10.4319/lo.2000.45.2.0419

Turner, J. T. 2015. Zooplankton fecal pellets, marine snow, phytodetritus and the ocean's biological pump. Prog. Oceanogr. **130**: 205–248. doi:10.1016/j.pocean.2014.08.005

Velde, J. T., R. Burkhardt, K. Kleiverda, L. Leenheers-Binnendijk, and W. Sommerfeld. 1977. Methyl-methacrylate as an embedding medium in histopathology. Histopathology **1**: 319–330. doi:10.1111/j.1365-2559.1977.tb01671.x

Veta, M., J. P. W. Pluim, P. J. van Diest, and M. A. Viergever. 2014. Breast cancer histopathology image analysis: A review. IEEE Trans. Biomed. Eng. **61**: 1400–1411. doi:10.1109/TBME.2014.2303852

Vojvoda, J., D. Lamy, E. Sintes, J. A. L. Garcia, V. Turk, and G. J. Herndl. 2014. Seasonal variation in marine-snow-associated and ambient-water prokaryotic communities in the northern Adriatic Sea. Aquat. Microb. Ecol. **73**: 211–224. doi:10.3354/ame01718

Waheed, A. A., K. S. Rao, and P. D. Gupta. 2000. Mechanism of dye binding in the protein assay using eosin dyes. Anal. Biochem. **287**: 73–79. doi:10.1006/abio.2000.4793

Waite, A. M., K. A. Safi, J. A. Hall, and S. D. Nodder. 2000. Mass sedimentation of picoplankton embedded in organic aggregates. Limnol. Oceanogr. **45**: 87–97. doi:10.4319/lo.2000.45.1.0087

Waite, A. M., Ö. Gustafsson, O. Lindahl, and P. Tiselius. 2005. Linking ecosystem dynamics and biogeochemistry: Sinking fractionation of organic carbon in a Swedish fjord. Limnol. Oceanogr. **50**: 658–671. doi:10.4319/lo.2005.50.2.0658

Wilbanks, E. G., and others. 2014. Microscale sulfur cycling in the phototrophic pink berry consortia of the Sippewissett Salt Marsh. Environ. Microbiol. **16**: 3398–3415. doi:10.1111/1462-2920.12388

Woebken, D., B. M. Fuchs, M. M. M. Kuypers, and R. I. Amann. 2007. Potential interactions of particle-associated anammox bacteria with bacterial and archaeal partners in the Namibian upwelling system. Appl. Environ. Microbiol. **73**: 4648–4657. doi:10.1128/AEM.02774-06

Zoppini, A., A. Puddu, S. Fazi, M. Rosati, and P. Sist. 2005. Extracellular enzyme activity and dynamics of bacterial community in mucilaginous aggregates of the northern Adriatic Sea. Sci. Total Environ. **353**: 270–286. doi:10.1016/j.scitotenv.2005.09.019

Acknowledgments

We thank Ute Marx for technical support and advice in histology-based questions. The NanoSIMS at the Leibnitz-Institute for Baltic Sea research in Warnemuende (IOW) was funded by the German Federal Ministry of Education and Research (BMBF), grant identifier 03F0626A. Annett Grüttmüller is acknowledged for support during NanoSIMS analyses. We also want to thank Christiane Schott and colleagues from the Department of Geosciences at the University of Bremen for Araldite sample preparations. Ingrid Stimac and Dennis Köhler from the Geochemistry Section at the Alfred-Wegener-Institute (AWI) assisted with nutrient measurements.

Conflict of Interest

None declared.

Submitted 19 April 2018
Revised 13 July 2018
Accepted 24 May 2018

Associate editor: Gordon Taylor

Supplement

Supplementary figures and tables

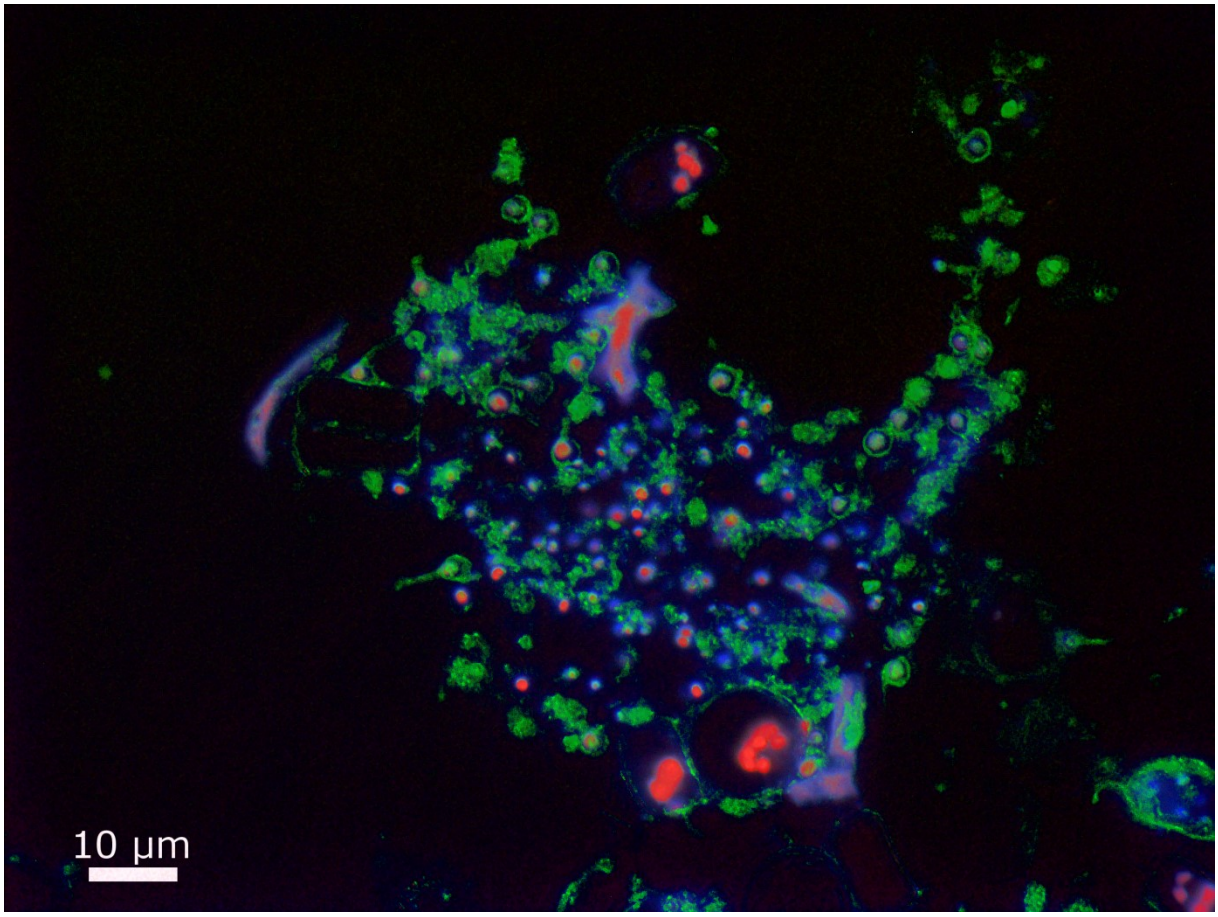

Figure S1: Image overlap of TEP (green), Chlorophyll a autofluorescence (red) and nucleic acids (blue) of methacrylate embedded aggregate sample acquired with a higher magnification using a 63x objective shows TEP exudates around algal cells with embedded prokaryotes.

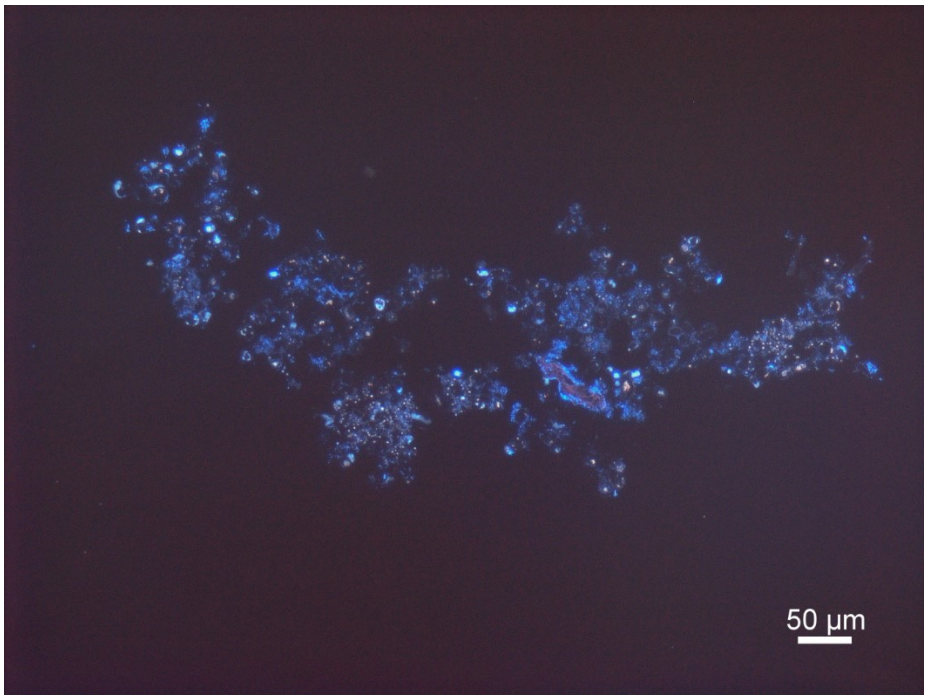

Figure S2: Original micrograph of nucleic acids stained with DAPI of a methacrylate embedded laboratory generated aggregate. Slice thickness: 2 µm.

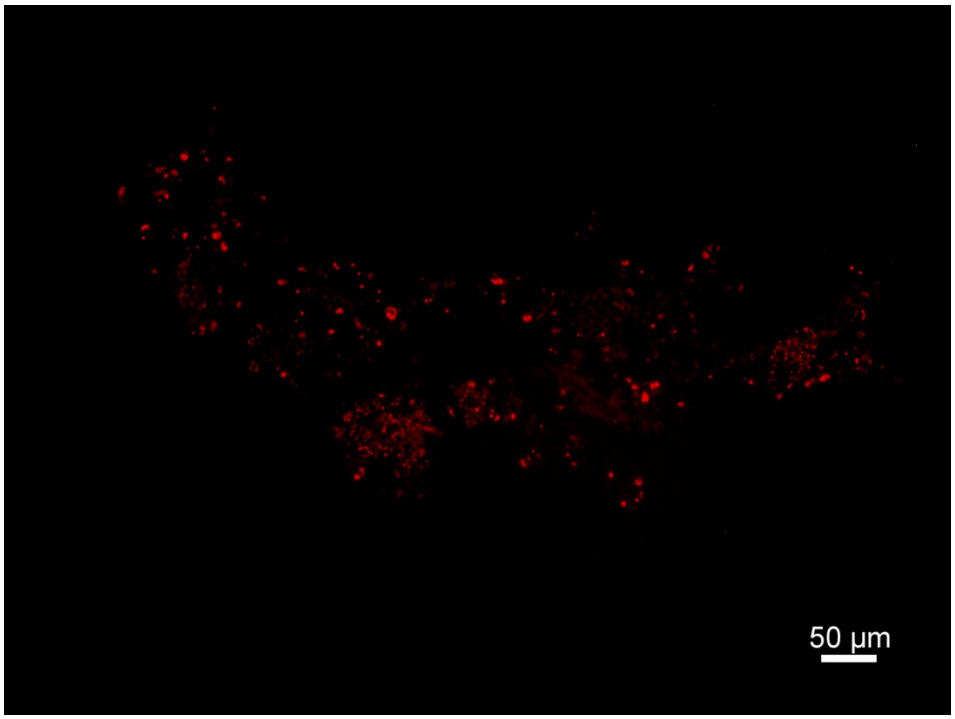

Figure S3: Original micrograph of chlorophyll a autofluorescence of methacrylate embedded laboratory generated aggregate. Slice thickness: 2 µm.

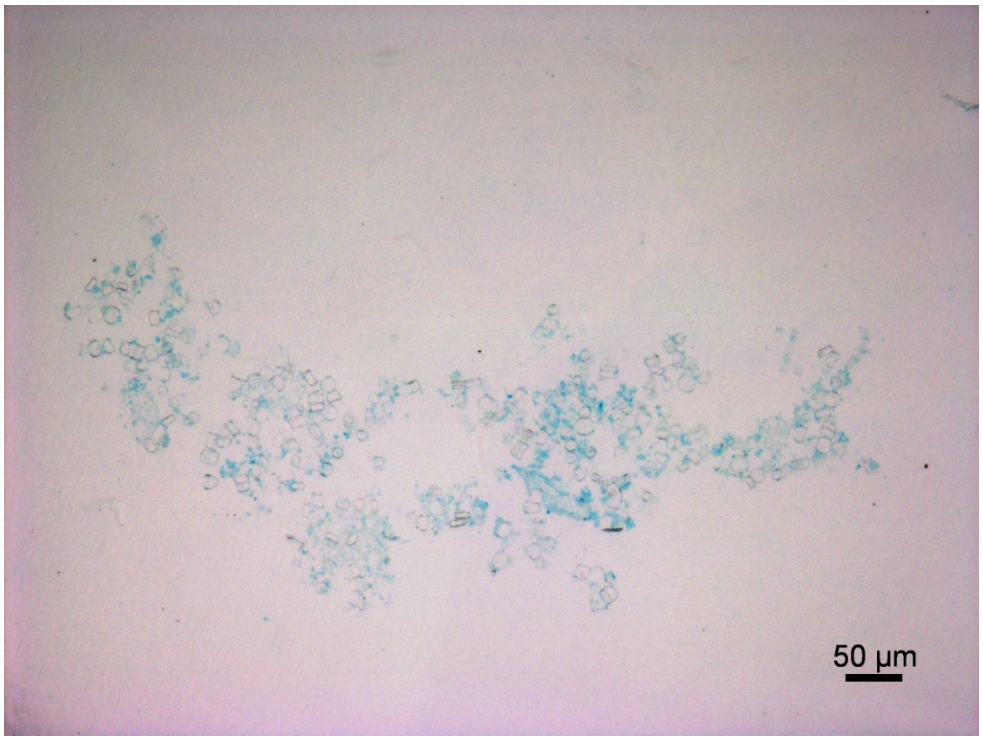

Figure S4: Original micrograph of TEP compounds, stained with Alcian Blue of a methacrylate embedded laboratory generated aggregate. Slice thickness: 2 µm.

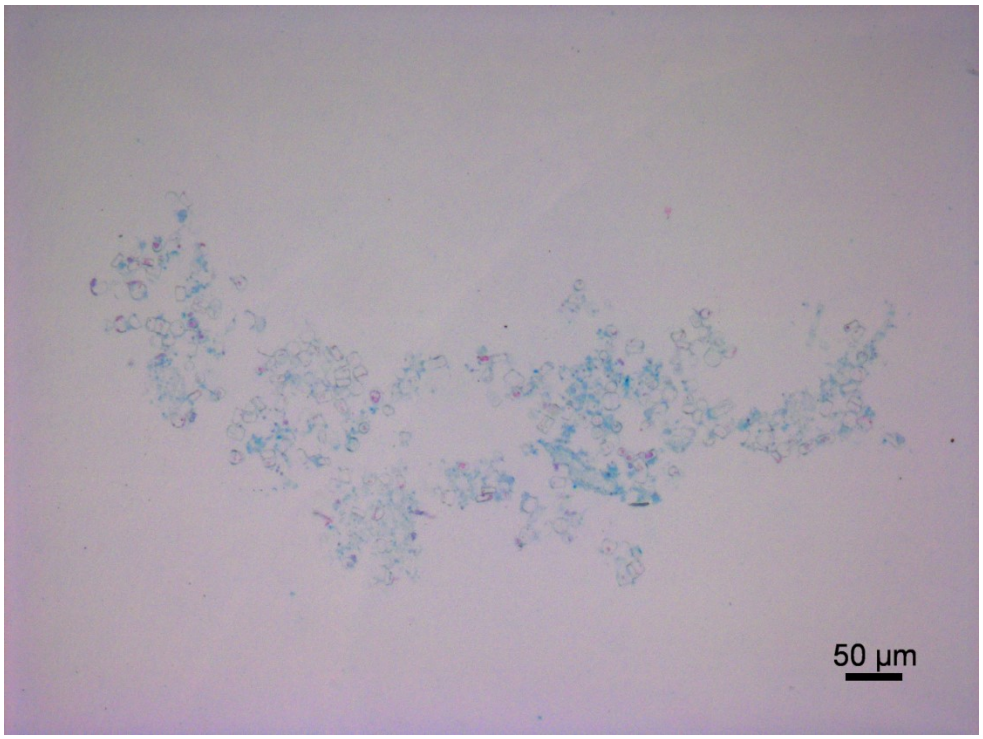

Figure S5: Original micrograph of eukaryotic cytoplasm, stained with eosinY/ phloxine B of a methacrylate embedded laboratory generated aggregate using bright field. Slice thickness: 2 µm.

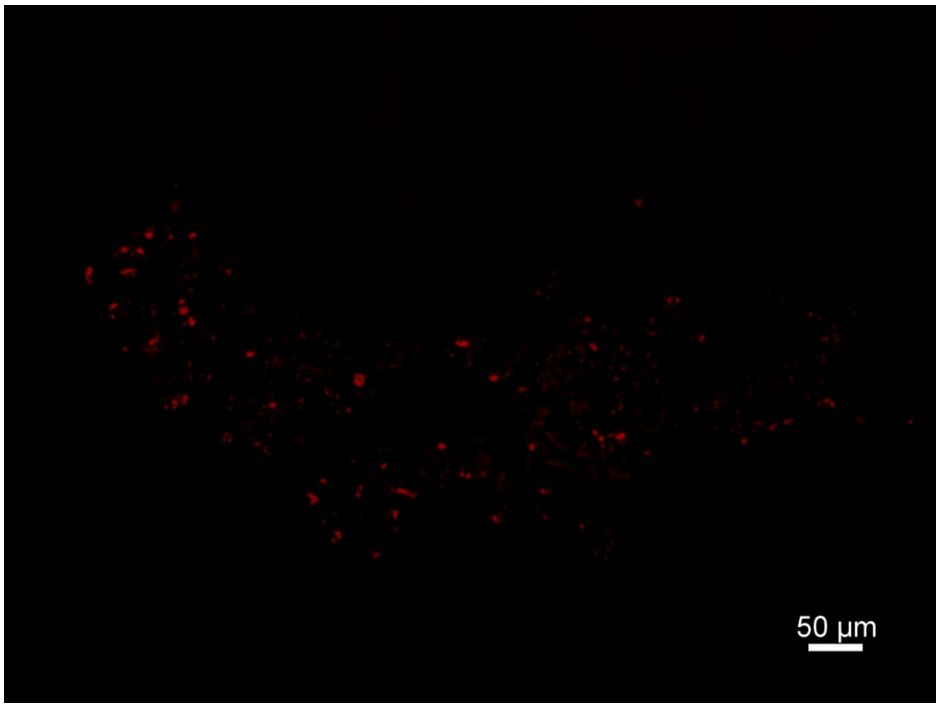

Figure S6: Original micrograph of eukaryotic cytoplasm, stained with eosinY/ phloxine B of a methacrylate embedded laboratory generated aggregate using epifluorescence channel of chlorophyll a. Slice thickness: 2 µm.

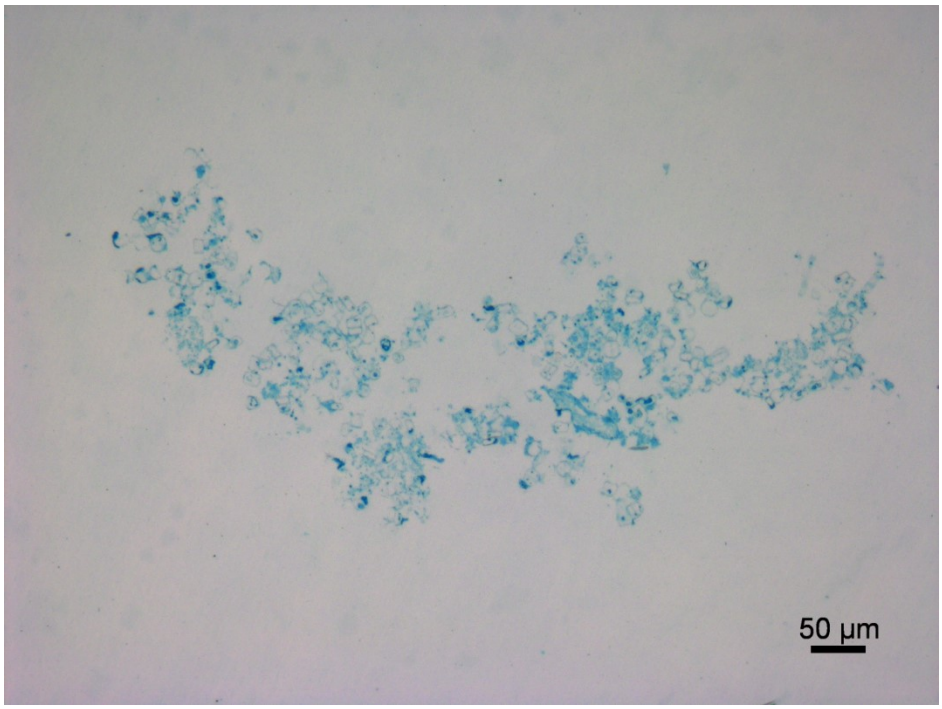

Figure S7: Original micrograph of CSP compounds, stained with Coomassie Brilliant Blue of a methacrylate embedded laboratory generated aggregate. Slice thickness: 2 µm.

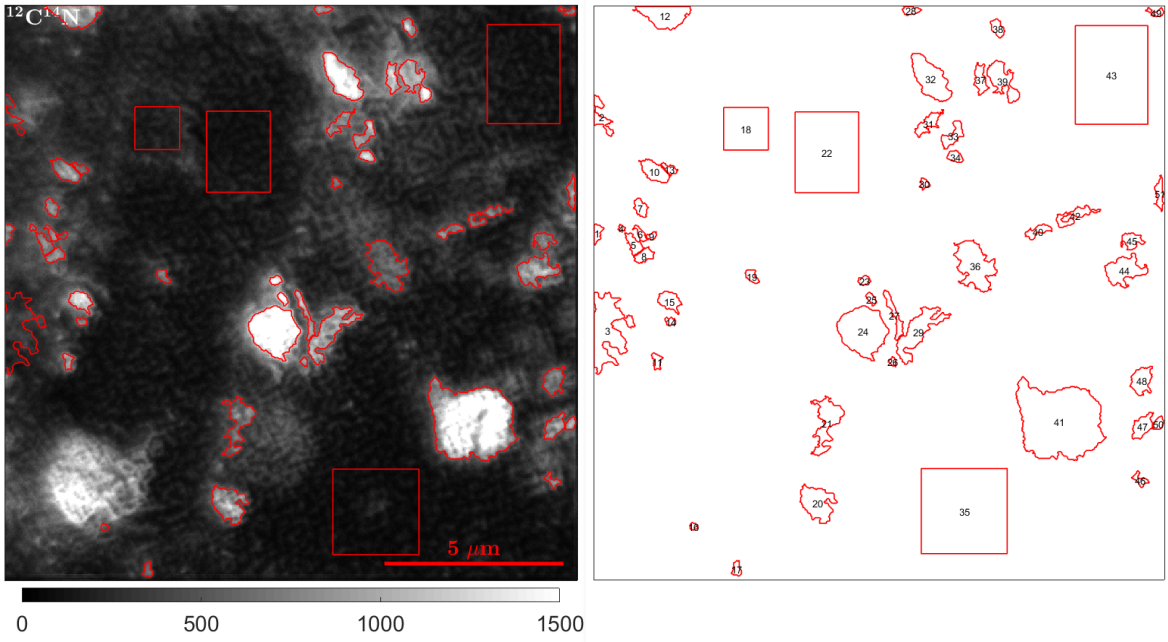

Figure S8: ROI distribution of detail measurement #1 of labelled sample as shown in Figure 8 as well as Figure 7: 1: prokaryotic cell, 2: possibly sulfur particle, 3: possibly sulfur particle, 4: ignored due to insignificant ion counts, 5: prokaryotic cell, 6: prokaryotic cell, 7: prokaryotic cell, 8: prokaryotic cell, 9: prokaryotic cell, 10: prokaryotic cell, 11: prokaryotic cell, 12: prokaryotic cell, 13: prokaryotic cell, 14: prokaryotic cell, 15: prokaryotic cell, 16: ignored due to insignificant ion counts, 17: prokaryotic cell, 18: phytoplankton cytoplasm, 19: prokaryotic cell, 20: prokaryotic cell, 21: prokaryotic cell, 22: phytoplankton cytoplasm, 23: prokaryotic cell, 24: phytoplankton compartment, 25: prokaryotic cell, 26: prokaryotic cell, 27: prokaryotic cell, 28: prokaryotic cell, 29: prokaryotic cell, 30: prokaryotic cell, 31: prokaryotic cell, 32: prokaryotic cell, 33: prokaryotic cell, 34: prokaryotic cell, 35: resin matrix, 36: artefact, 37: phytoplankton compartment, 38: prokaryotic cell, 39: phytoplankton compartment, 40: prokaryotic cell, 41: phytoplankton compartment, 42: prokaryotic cell, 43: resin matrix, 44: phytoplankton compartment, 45: prokaryotic cell, 46: prokaryotic cell, 47: prokaryotic cell, 48: prokaryotic cell, 49: prokaryotic cell, 50: prokaryotic cell, 51: prokaryotic cell.

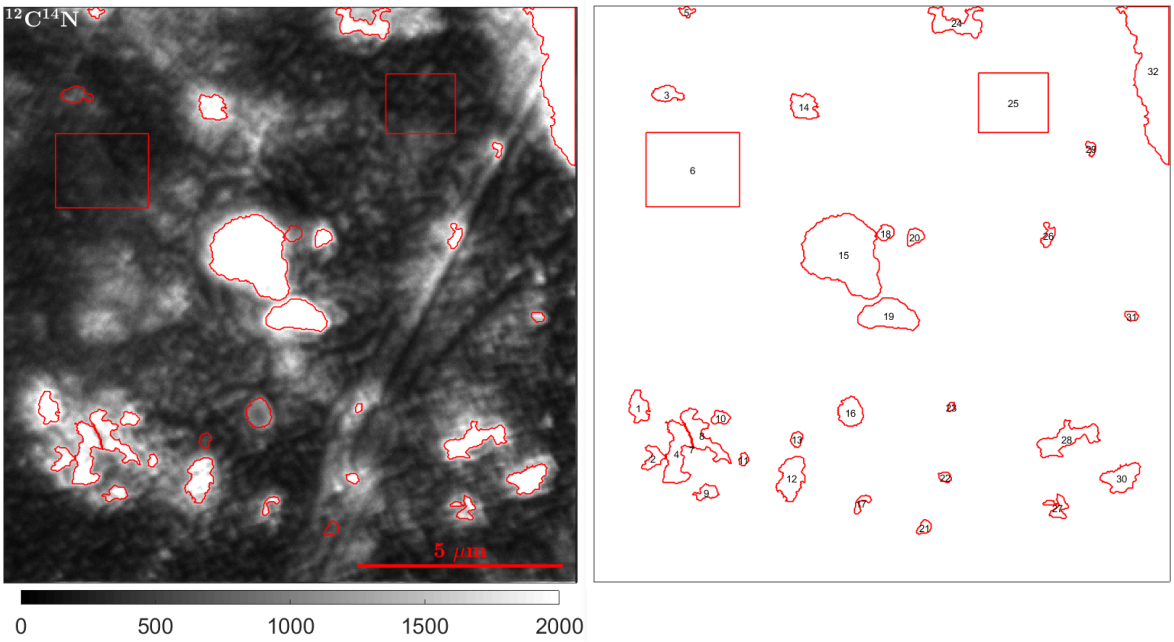

Figure S9: ROI distribution of detail measurement #2 of labelled sample as shown in Figure 8 as well as Figure 7: 1: phytoplankton compartment, 2: phytoplankton compartment, 3: possibly sulfur particle, 4: phytoplankton compartment, 5: prokaryotic cell, 6: resin matrix, 7: ignored due to insignificant ion counts, 8: phytoplankton compartment, 9: prokaryotic cell, 10: prokaryotic cell, 11: prokaryotic cell, 12: prokaryotic cell, 13: possibly sulfur particle, 14: prokaryotic cell, 15: phytoplankton compartment, 16: possibly sulfur particle, 17: prokaryotic cell, 18: possibly sulfur particle, 19: prokaryotic cell, 20: prokaryotic cell, 21: possibly sulfur particle, 22: prokaryotic cell, 23: prokaryotic cell, 24: phytoplankton compartment, 25: resin matrix, 26: prokaryotic cell, 27: prokaryotic cell, 28: prokaryotic cell, 29: prokaryotic cell, 30: prokaryotic cell, 31: prokaryotic cell, 32: phytoplankton compartment.

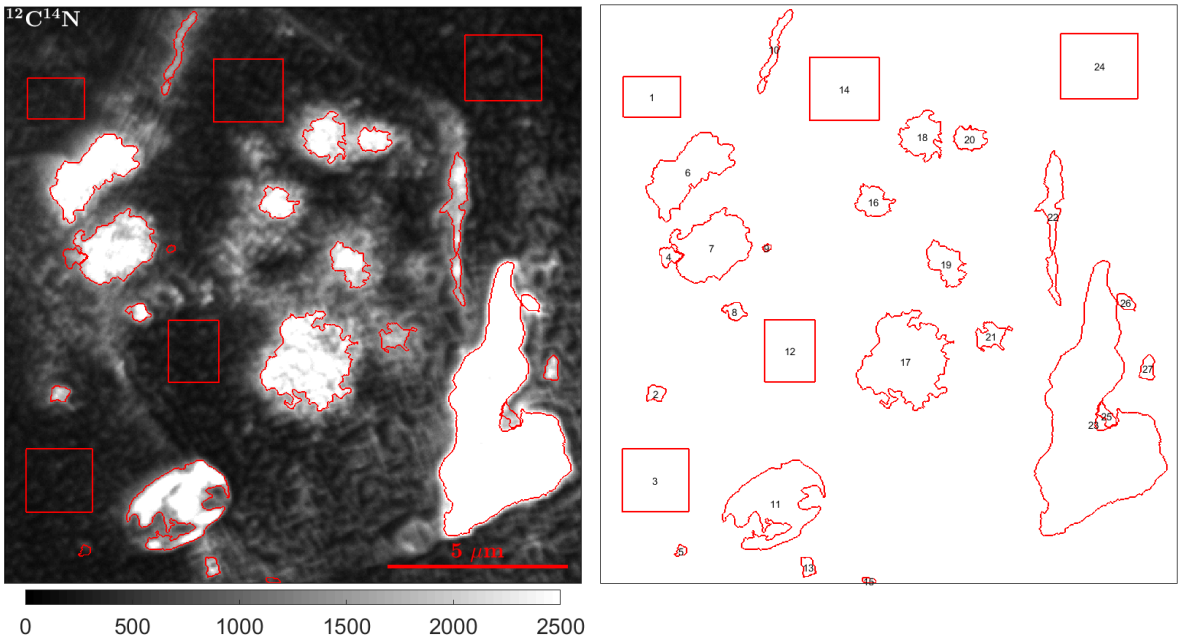

Figure S10: ROI distribution of detail measurement #3 of labelled sample as shown in Figure 8 as well as Figure 7: 1: resin matrix, 2: prokaryotic cell, 3: resin matrix, 4: possibly sulfur particle, 5: possibly sulfur particle, 6: prokaryotic cell, 7: phytoplankton compartment, 8: phytoplankton compartment, 9: possibly sulfur particle, 10: phytoplankton frustule, 11: phytoplankton compartment, 12: phytoplankton cytoplasm, 13: prokaryotic cell, 14: phytoplankton cytoplasm, 15: possibly sulfur particle, 16: phytoplankton compartment, 17: phytoplankton compartment, 18: phytoplankton compartment, 19: phytoplankton compartment, 20: phytoplankton compartment, 21: phytoplankton compartment, 22: phytoplankton frustule, 23: artefact, 24: resin matrix, 25: possibly sulfur particle, 26: prokaryotic cell, 27: prokaryotic cell.

...

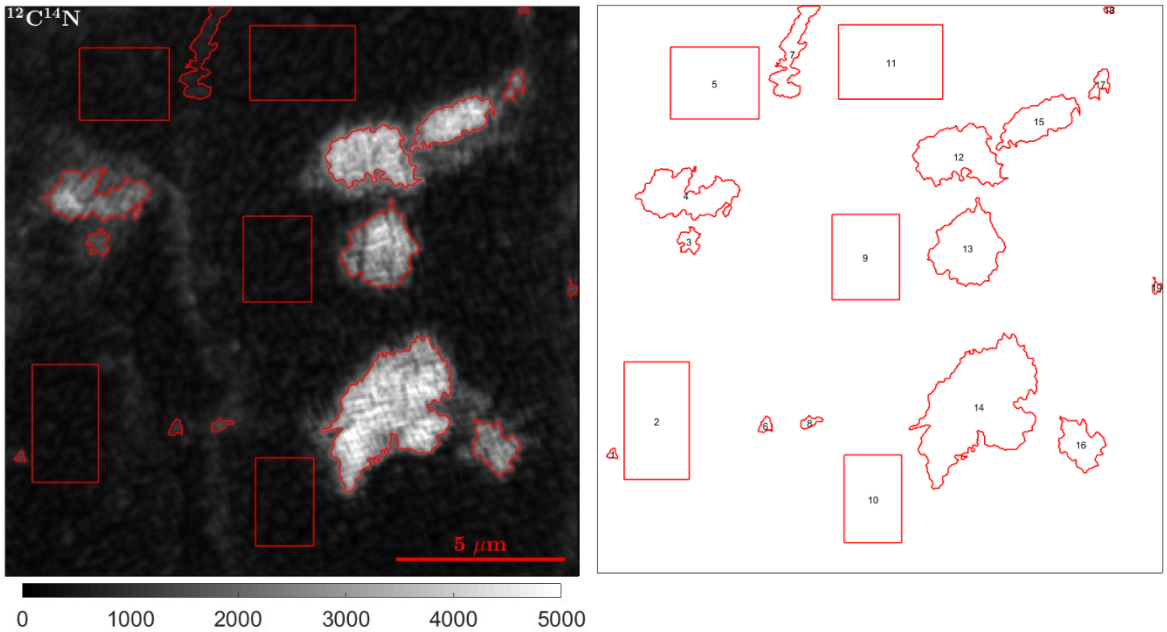

Figure S11 (previous page): ROI distribution of additional detail measurement #1 of labelled sample as shown in Figure 8: ROI distribution of additional detail measurement #1 of labelled sample: 1: phytoplankton compartment, 2: phytoplankton cytoplasm, 3: phytoplankton compartment, 4: phytoplankton compartment, 5: resin matrix, 6: prokaryotic cell, 7: phytoplankton frustule, 8: prokaryotic cell, 9: phytoplankton cytoplasm, 10: phytoplankton cytoplasm, 11: phytoplankton cytoplasm, 12: phytoplankton compartment, 13: phytoplankton compartment, 14: phytoplankton compartment, 15: phytoplankton compartment, 16: phytoplankton compartment, 17: phytoplankton compartment, 18: prokaryotic cell, 19: prokaryotic cell.

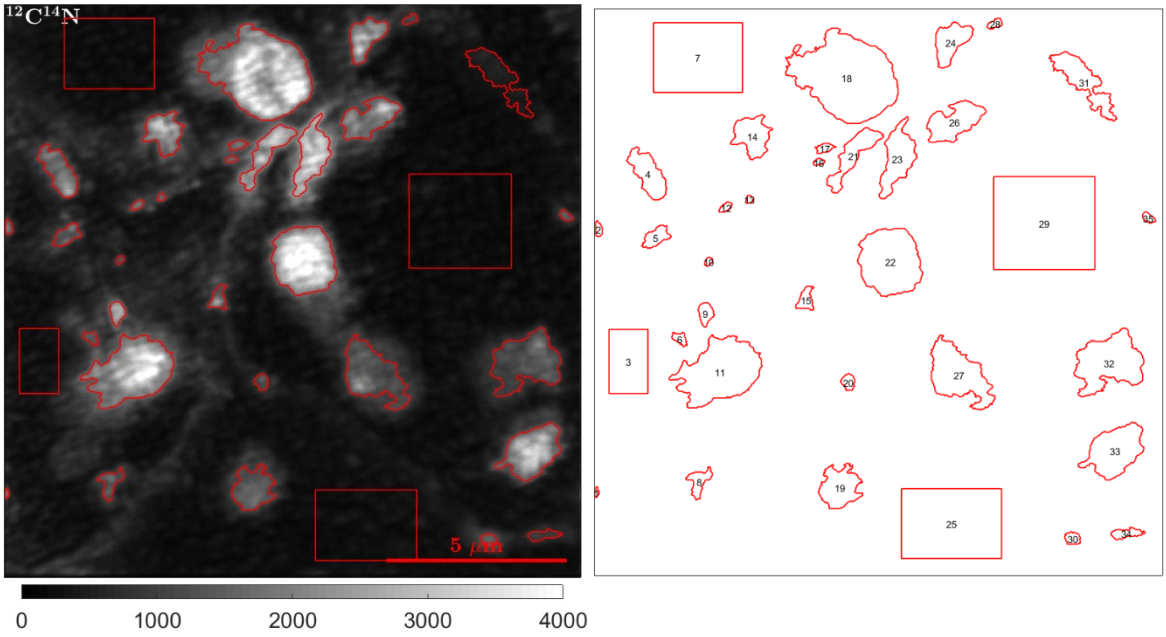

Figure S12: ROI distribution of additional detail measurement #2 of labelled sample as shown in Figure 8: 1: phytoplankton compartment, 2: prokaryotic cell, 3: phytoplankton cytoplasm, 4: prokaryotic cell, 5: prokaryotic cell, 6: phytoplankton compartment, 7: phytoplankton cytoplasm, 8: phytoplankton compartment, 9: phytoplankton compartment, 10: prokaryotic cell, 11: phytoplankton compartment, 12: prokaryotic cell, 13: prokaryotic cell, 14: phytoplankton compartment, 15: prokaryotic cell, 16: prokaryotic cell, 17: prokaryotic cell, 18: phytoplankton compartment, 19: prokaryotic cell, 20: prokaryotic cell, 21: prokaryotic cell, 22: phytoplankton compartment, 23: phytoplankton compartment, 24: prokaryotic cell, 25: resin matrix, 26: phytoplankton compartment, 27: phytoplankton compartment, 28: prokaryotic cell, 29: phytoplankton cytoplasm, 30: prokaryotic cell, 31: phytoplankton frustule, 32: phytoplankton compartment, 33: phytoplankton compartment, 34: phytoplankton frustule, 35: phytoplankton compartment.

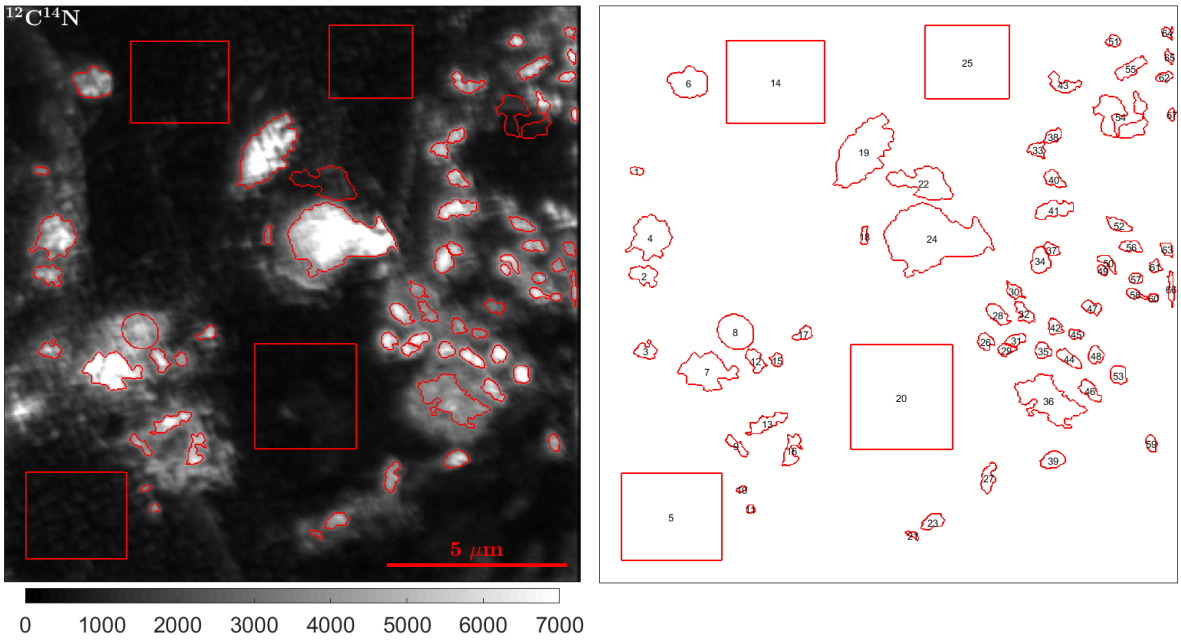

Figure S13: ROI distribution of additional detail measurement #1 of unlabelled control sample as shown in Figure 8: 1: prokaryotic cell, 2: phytoplankton compartment, 3: prokaryotic cell, 4: phytoplankton compartment, 5: resin matrix, 6: phytoplankton compartment, 7: phytoplankton compartment, 8: phytoplankton compartment, 9: artefact, 10: prokaryotic cell, 11: prokaryotic cell, 12: phytoplankton compartment, 13: artefact, 14: resin matrix, 15: artefact, 16: artefact, 17: prokaryotic cell, 18: prokaryotic cell, 19: phytoplankton compartment, 20: resin matrix, 21: prokaryotic cell, 22: possibly sulfur particle, 23: prokaryotic cell, 24: phytoplankton compartment, 25: resin matrix, 26: prokaryotic cell, 27: prokaryotic cell, 28: prokaryotic cell, 29: prokaryotic cell, 30: prokaryotic cell, 31: prokaryotic cell, 32: prokaryotic cell, 33: prokaryotic cell, 34: prokaryotic cell, 35: prokaryotic cell, 36: phytoplankton compartment, 37: prokaryotic cell, 38: prokaryotic cell, 39: prokaryotic cell, 40: prokaryotic cell, 41: prokaryotic cell, 42: prokaryotic cell, 43: prokaryotic cell, 44: prokaryotic cell, 45: prokaryotic cell, 46: prokaryotic cell, 47: prokaryotic cell, 48: prokaryotic cell, 49: prokaryotic cell, 50: prokaryotic cell, 51: prokaryotic cell, 52: prokaryotic cell, 53: prokaryotic cell, 54: possibly sulfur particle, 55: prokaryotic cell, 56: prokaryotic cell, 57: prokaryotic cell, 58: prokaryotic cell, 59: prokaryotic cell, 60: prokaryotic cell, 61: prokaryotic cell, 62: prokaryotic cell, 63: prokaryotic cell, 64: prokaryotic cell, 65: prokaryotic cell, 66: prokaryotic cell, 67: prokaryotic cell.

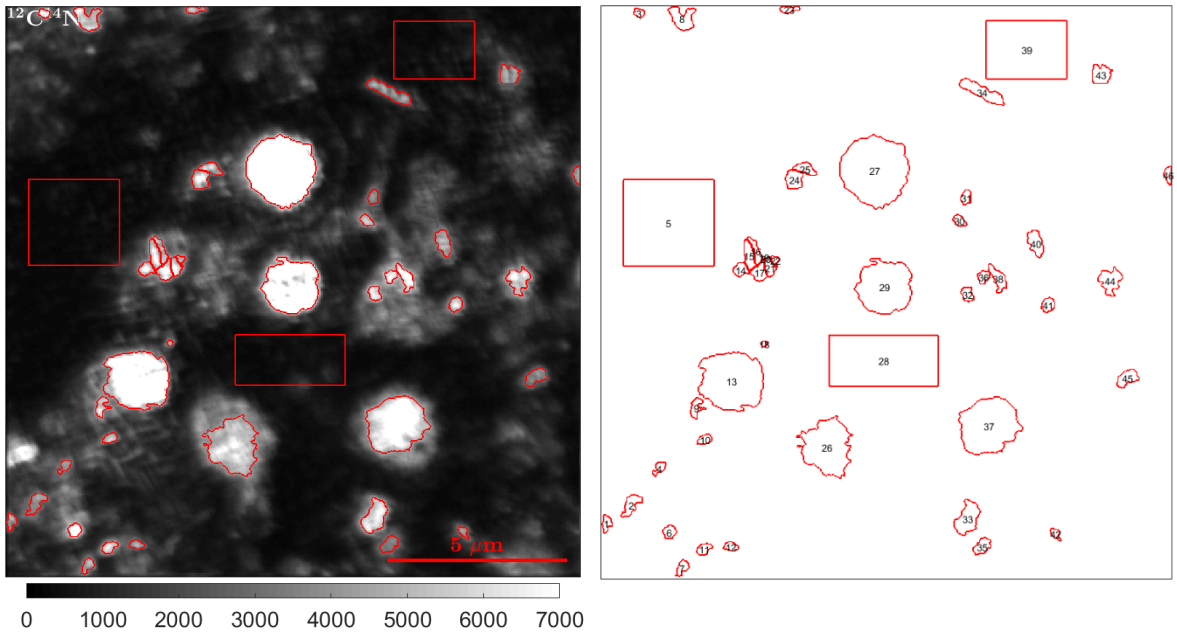

Figure S14: ROI distribution of additional detail measurement #2 of unlabelled control sample as shown in Figure 8: 1: prokaryotic cell, 2: prokaryotic cell, 3: prokaryotic cell, 4: prokaryotic cell, 5: resin matrix, 6: prokaryotic cell, 7: prokaryotic cell, 8: prokaryotic cell, 9: prokaryotic cell, 10: prokaryotic cell, 11: prokaryotic cell, 12: prokaryotic cell, 13: phytoplankton compartment, 14: prokaryotic cell, 15: prokaryotic cell, 16: prokaryotic cell, 17: prokaryotic cell, 18: prokaryotic cell, 19: ignored due to insignificant ion counts, 20: ignored due to insignificant ion counts, 21: prokaryotic cell, 22: prokaryotic cell, 23: prokaryotic cell, 24: prokaryotic cell, 25: prokaryotic cell, 26: phytoplankton compartment, 27: phytoplankton compartment, 28: resin matrix, 29: phytoplankton compartment, 30: prokaryotic cell, 31: prokaryotic cell, 32: prokaryotic cell, 33: prokaryotic cell, 34: prokaryotic cell, 35: prokaryotic cell, 36: prokaryotic cell, 37: phytoplankton compartment, 38: prokaryotic cell, 39: resin matrix, 40: prokaryotic cell, 41: prokaryotic cell, 42: prokaryotic cell, 43: prokaryotic cell, 44: prokaryotic cell, 45: prokaryotic cell, 46: prokaryotic cell.

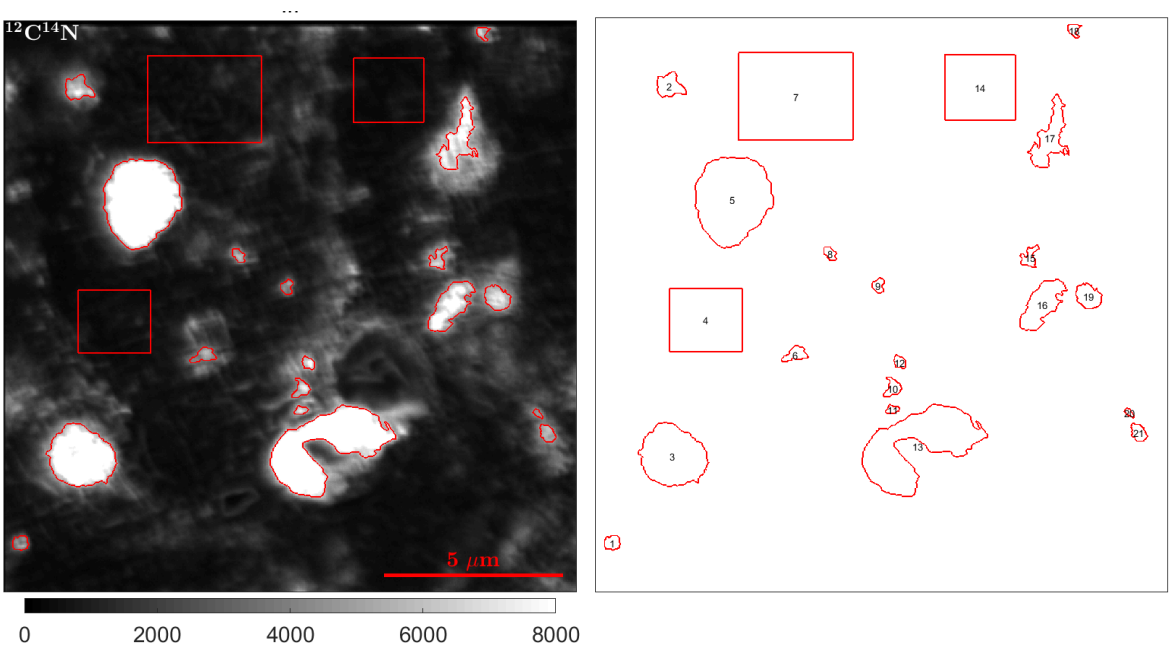

Figure S15: ROI distribution of additional detail measurement #3 of unlabelled control sample as shown in Figure 8: 1: prokaryotic cell, 2: prokaryotic cell, 3: phytoplankton compartment, 4: resin matrix, 5: phytoplankton compartment, 6: prokaryotic cell, 7: resin matrix, 8: prokaryotic cell, 9: prokaryotic cell, 10: prokaryotic cell, 11: prokaryotic cell, 12: prokaryotic cell, 13: phytoplankton compartment, 14: resin matrix, 15: prokaryotic cell, 16: prokaryotic cell, 17: prokaryotic cell, 18: prokaryotic cell, 19: prokaryotic cell, 20: prokaryotic cell, 21: prokaryotic cell.

Figure S16 (next page): Original, uncorrected isotope abundances in ‰, including Poisson Errors as error bars, of all measured prokaryotic and phytoplankton cells as well as the resin itself without correction using the internal standard. The dashed line indicates the enrichment threshold (maximum value of the Poisson error of controls). Respective ROIs are shown in Suppl Figure S8-S15.

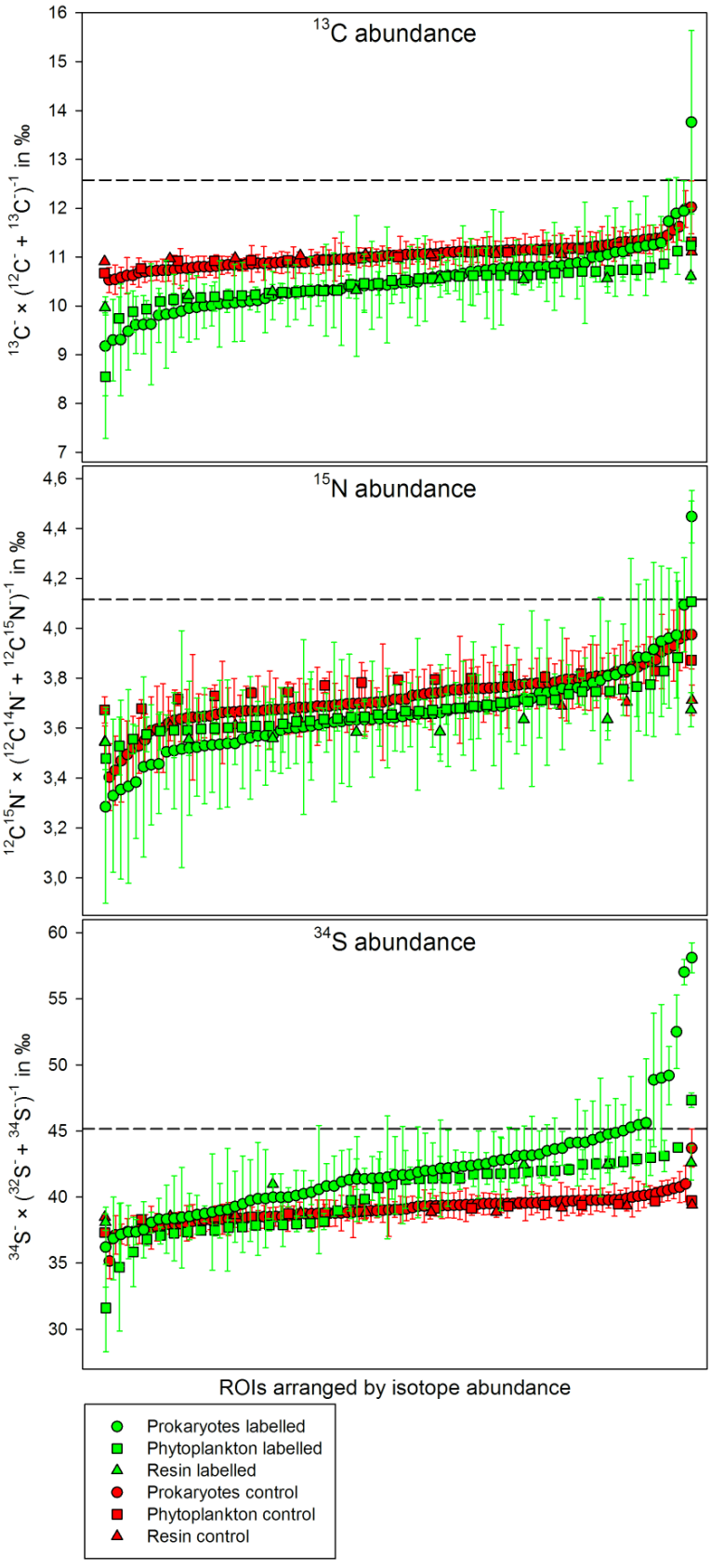
^{13}C abundance
$^{13}C^- \times (^{12}C^- + ^{13}C^-)^{-1}$ in ‰
^{15}N abundance
$^{12}C^{15}N^- \times (^{12}C^{14}N^- + ^{12}C^{15}N^-)^{-1}$ in ‰
^{34}S abundance
$^{34}S^- \times (^{32}S^- + ^{34}S^-)^{-1}$ in ‰
ROIs arranged by isotope abundance
Prokaryotes labelled
Phytoplankton labelled
Resin labelled
Prokaryotes control
Phytoplankton control
Resin control

Protocol and suggestions for CARD-FISH procedure

Catalyzed reporter deposition fluorescence in situ hybridization (CARDFISH; Pernthaler et al. 2002) enables the microscopical identification of specific microbial groups (FISH) with an increased signal (CARD). Our procedure was based on an existing protocol for paraffin embedded specimens on glass slides (Blazejak et al. 2005) with several modifications:

Methacrylate slices were encircled using a hydrophobic immunostaining pen (Daido Sangyo, Japan). Endogenous peroxidase was inactivated by incubating with 0.01 M HCl for 10 min at room temperature followed by a washing step in UW. Enzymatic digestion using Lysozyme as described in the standard protocol (see above) for 1 hour at 37°C followed a washing step in PBST (0.01% Triton X100 in 1 x PBS) and UW for 5 min, respectively. Hybridization buffer (HB) with 55% formamide concentration was prepared according to standard protocols (see above). HB was supplemented with 1% horseradish-peroxidase-labeled probe (final concentration 1pmol/µL) of the control probes for eubacteria EUB338I (Amann et al. 1990), EUB338II and EUB338III (Daims et al. 1999) as well as the nonsense probe as negative control, NonEUB (Wallner et al. 1993).

The samples were incubated with HB-probe mixture for 3 hours at 35°C in a humidity chamber (piece of tissue supplemented with 2 – 3 mL of 55% Formamide and 45% UW in a 50 mL centrifugation tube). HB was washed off twice in washing buffer (WB) for 5 min, followed by a washing step in preheated WB for 30 min up to 1 hour at 37°C depending on background signal intensity. WB was washed off in 1 x PBST for 15 min – 1 hour at 37°C. Immediately after this step CARD was carried out to prevent the specimens running dry. Amplification buffer (AB), containing 0.0015% H_2O_2 and 0.005 – 0.05% fluorescently (carboxyfluorescein) labelled tyramide was added to the slices and incubated for 20 min at 37°C in a humidity chamber (50 mL centrifugation tube including UW soaked tissue) with UW. Afterwards AB was washed off in 1 x PBS twice at room temperature and a third time in PBST for up to 1.5 hours at up to 60°C depending on background signal intensity. After a short washing step in UW slides were air dried and counterstained with DAPI oil (see main text). All washing steps were done under gentle shaking conditions to increase washing, but to prevent slices from peeling off the glass slide.

Positive hybridization could be achieved, as well as negative results using the negative control probe (Figure S17). However, as the overlap with DAPI and Chl *a* autofluorescence (Figure S18) demonstrates, not all cells were hybridized. This may be due to non-optimal temperature or formamide concentrations during hybridization or inhibited penetration of the probes into the resin. Interestingly, the enzymatic digestion seemed not to be necessary, as treatments without digestion resulted in comparable signals. The fact that FISH protocols could successfully be applied for Technovit embedded benthic consortia by McGlynn et al. (2015) points potentially towards inhibited penetration of tyramide conjugate through CARD amplification. The proof for that and optimization requires further investigations.

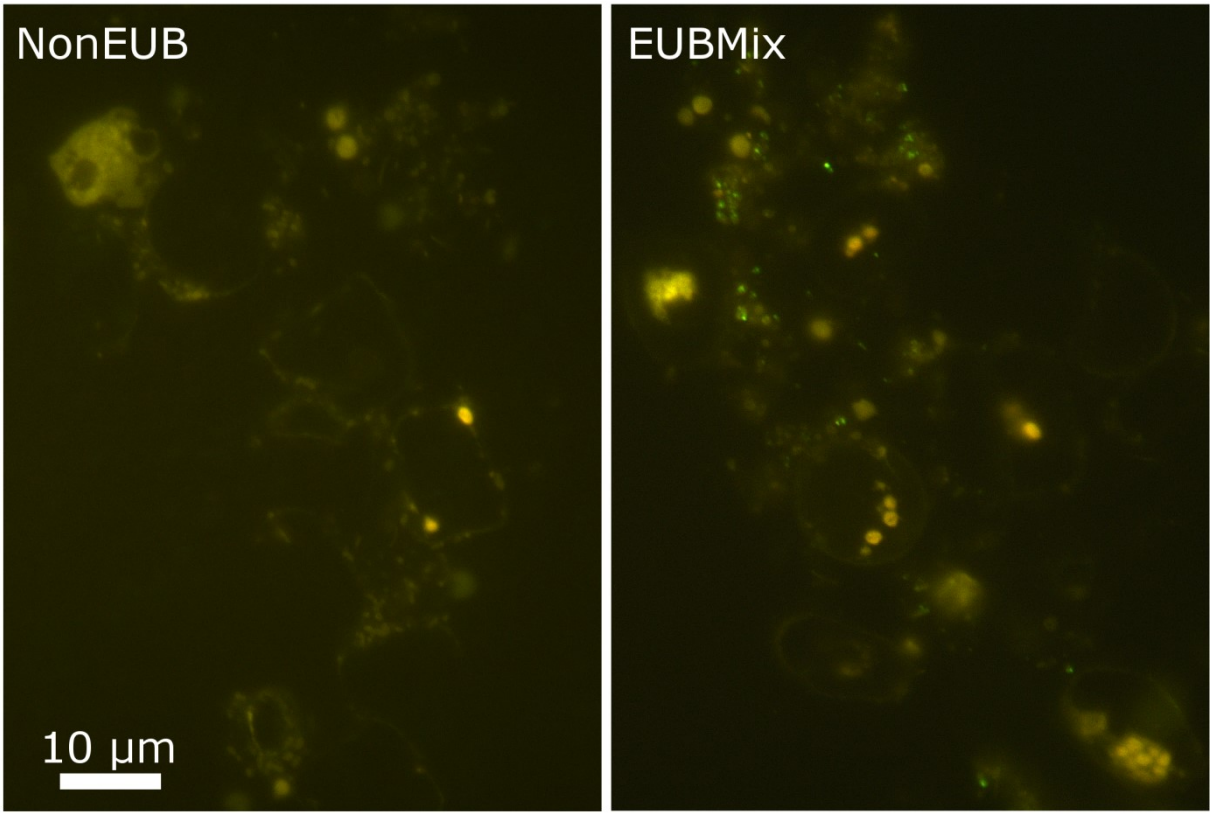

Figure S17: Example for CARDFISH treatment: Fluorescence micrographs show the binding of the mixed EUBI - III (EUBMix) probe in green while the nonsense probe NonEUB shows no hybridization.

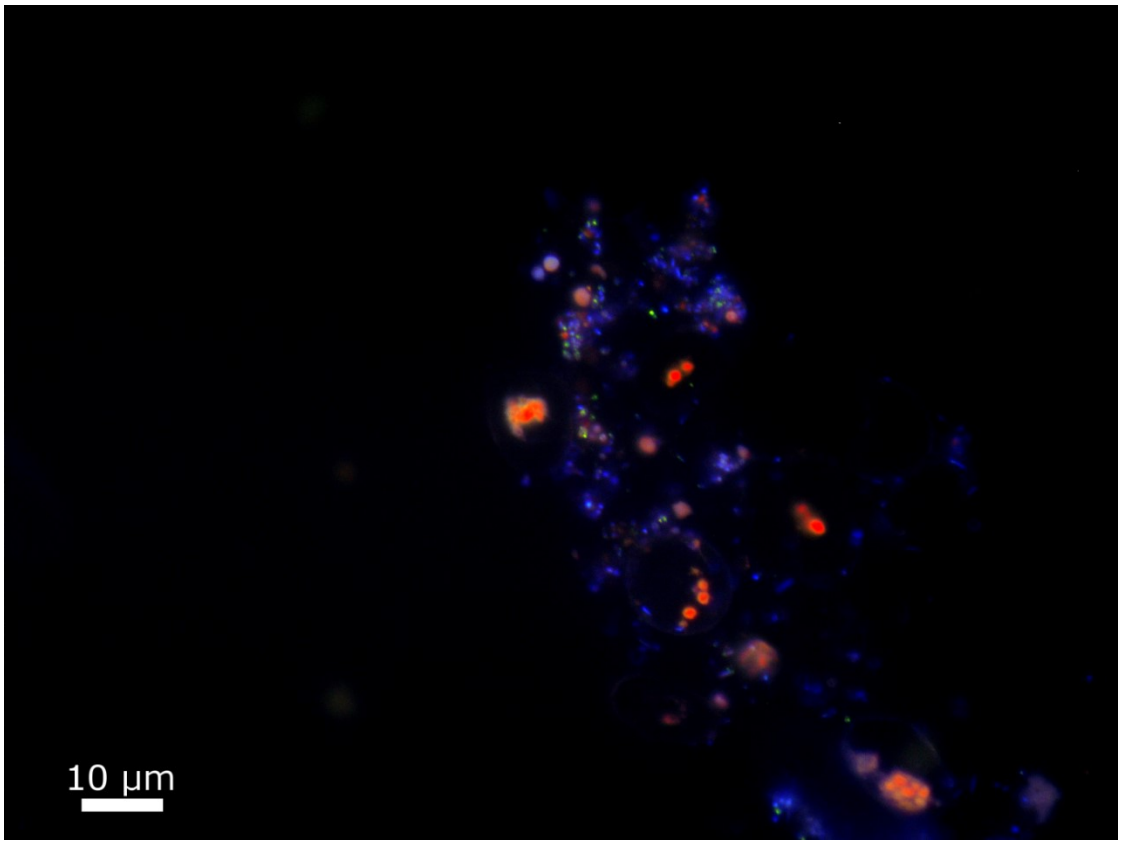

Figure S18: Overlap image of DNA staining using DAPI using DAPI (blue), chlorophyll *a* auto-fluorescence (red) and CARDFISH of the EUBI-III probe (EUBMix; green) demonstrates positive signals but missing stringency.

Further protocol improvements should consider that in our tests Biobond was ineffective as an adhesive during CARDFISH procedure. This is likely due to solvent effects associated with high formamide concentrations in the hybridization buffer. Here, the use of a mixture of 2 – 10% acetone in UW as bedding between the slide and slice showed more promising results. The presence of acetone serves to soften the slice and increases bonding. Furthermore, careful handling during the CARDFISH process, i.e., reduction of shaking and increasing of washing time, notably improved successful binding.

Table S1 (next page): Comparison of embedding techniques between Flintrop et al. (in press), using cryogel (Tissue-Tek® O.C.T.™ Compound; Sakura Fine Tek, Japan) and this study, using hard acrylic and epoxy resins. Here we highlight a number of specific advantages of each method with regard to handling time and convenience, and final analysis. See text and Flintrop et al. (in press) for details.

	Cryogels (Flintrop et al. [2018])	**Hard and soft plastic resins: Methacrylate/ Araldite (Rogge et al.)**
Primary mode of Handling	Cryogel filled drifting sediment traps: passive handling From MSC[a] and lab-made aggregates: active handling	Active for lab-made aggregates and from MSC[a]
Active handling steps until immobilization	Gel traps: no active handling prior to sample mounting MSC[a]: min. 1 transfer from MSC to mold[b]	Gel traps: not tested MSC[a]: min. 2 transfers: pre-warming and pre-embedding[b]
Time required until sample is ready for sectioning[b]	Cryogel filled drifting sediment traps: 0 h (embedded in situ) MSC[a]: <5 min hands-on <1 h hands-off	~1 h hands-on ~74 h hands-off
Storage temperature of embedded samples	Below freezing point	Room temperature
Shelf life of embedded samples	Years to decades[c]	several decades
Slice thickness	5 – 100 µm	1 – 3 µm (methacrylate) 40 – 140 µm (araldite)
Storage temperature of sliced samples	-20°C or 4°C	Room temperature
Shelf life of sliced samples	Years to decades[c]	several decades
Successfully tested FISH protocols	monoFISH, MILFISH, CARDFISH	monoFISH[d]
Usability for NanoSIMS	No existing protocols	Yes: vacuum resistance, low dilution effects of N and S, no shrinking
Limitations when lithogenic compounds are included	Minimum slicing thickness 5µm; >5 µm no detectable rupture[e]	Leads to scratches or rupture with methacrylate / Araldite eliminates structural deformations
Treatment with organic solvents[b]	Polyvinyl alcohol (<11%)	Exchange of water with ethanol or acetone (100%)
Temperature treatment until sample is ready for sectioning	-20°C – room temperature[f]	4 – 50°C[g]
Tested stains	Alcian Blue, Coomassie Brilliant Blue, Concanavalin A, Ruthenium Red, Periodic Acid Schiff-base stain, DAPI, FISH	Alcian Blue, Coomassie Brilliant Blue, eosin Y / phloxine B, DAPI, FISH
Further possibilities	Variety of established staining protocols and cryogels	Variety of established staining protocols and resins

Table S1 (continued): [a] MSC: Marine Snow Catcher; [b] excluding fixation or staining prior to embedding; [c] when stored adequately in air-tight containers to prevent dehydration of cryogel during long-term storage; [d] monoFISH was carried out elsewhere (McGlynn et al. 2015), whereas CARDFISH was tested in this study but requires further development (see Supplementary chapter 1); [e] cannot be ruled out due to pliable nature of cryogel; [f] processing at room temperature, storage at -20°C and slicing at -25 to -30°C; [g] exothermic polymerization temperature does not exceed 50°C on cooling block

References

Amann, R. I., B. J. Binder, R. J. Olson, S. W. Chisholm, R. Devereux, D. A. Stahl. 1990. Combination of 16S rRNA-targeted oligonucleotide probes with flow cytometry for analyzing mixed microbial populations. *Appl Environ Microbiol*. 56: 1919–1925

Blazejak, A., C. Erseus, R. I. Amann, N. Dubilier. 2005. Coexistence of bacterial sulfide oxidizers, sulfate reducers, and spirochetes in a gutless worm (Oligochaeta) from the Peru margin. *Appl. Environ. Microbiol.* 71: 1553–1561, doi: 10.1128/AEM.71.3.1553-1561.2005

Daims, H., A. Brühl, R. Amann, K.-H. Schleifer, M. Wagner. 1999. The Domain-specific Probe EUB338 is Insufficient for the Detection of all Bacteria. *Syst Appl Microbiol.* 22: 434–444, doi: 10.1016/S0723-2020(99)80053-8

Flintrop, C., A. Rogge, S. Miksch, A. M. Waite, M. H. Iversen. 2018. Embedding and slicing of intact in situ collected marine snow. *Limnol. Oceanogr.: Methods,* doi: 10.1002/lom3.10251

McGlynn, S. E., G. L. Chadwick, C. P. Kempes, V. J. Orphan. 2015. Single cell activity reveals direct electron transfer in methanotrophic consortia. *Nature*. 526: 531–535, doi: 10.1038/nature15512

Pernthaler, A., J. Pernthaler, R. I. Amann. 2002. Fluorescence In Situ Hybridization and Catalyzed Reporter Deposition for the Identification of Marine Bacteria. *Appl. Environ. Microbiol*. 68: 3094–3101, doi: 10.1128/AEM.68.6.3094-3101.2002

Wallner, G., R. Amann, W. Beisker. 1993. Optimizing fluorescent in situ hybridization with rRNA-targeted oligonucleotide probes for flow cytometric identification of microorganisms. *Cytometry*. 14: 136–143, doi: 10.1002/cyto.990140205

PAPER III

Rethinking sinking: Imaging the flow fields of natural marine aggregates to measure settling velocity

C. M. Flintrop[1,2†], S. Ahmerkamp[3,2†], N. Moradi[2,5], I. Klawonn[4], Joeran Maerz[7,8], Hans-Peter Grossart[4], M. M. M. Kuypers[3], A. Khalili[3,5], J. Aristegui[6], M. H. Iversen[1,2]

[1] Alfred Wegener Institute for Polar and Marine Research, Bremerhaven, Germany
[2] MARUM and University of Bremen, Bremen, Germany
[3] Max-Planck-Institute for Marine Microbiology, Bremen, Germany
[4] Department of Experimental Limnology, Leibniz-Institute of Freshwater Ecology and Inland Fisheries, Stechlin, Germany
[5] Department of Physics & Earth Sciences, Jacobs University Bremen, Bremen, Germany
[6] Instituto de Oceanografía y Cambio Global (IOCAG), Universidad de Las Palmas de Gran Canaria, Las Palmas, Spain
[7] University of Hamburg, Hamburg, Germany
[8] Max-Planck-Institute for Meterology, Hamburg, Germany

[†] These authors contributed equally to this work

Running head: settling of marine aggregates

Keywords: marine snow, settling velocity, Particle Image Velocimetry (PIV), Stokes' law, drag coefficient

Abstract

The marine biological carbon pump is largely driven by settling particles and aggregates. The velocity with which these particles settle controls the efficiency of the biological carbon pump as it limits the amount of carbon that can be degraded over depth per unit time. Despite its importance, settling velocity of natural marine aggregates is not routinely measured, but often calculated from aggregate size and density using Stokes' law. Yet, comparing calculated and experimentally measured settling velocities has shown that Stokes' law does not accurately predict the size-to-settling relationship of marine snow. To determine the factors controlling the settling of marine aggregates, we analyzed the flow fields around 95 in situ collected aggregates using Particle Image Velocimetry. Additionally, we measured the size, settling velocity, and density of individual aggregates. The flow fields around the aggregates strongly resembled those of impermeable, porous spheres, independent of aggregate type, size, composition, and shape. This suggests that Stokes' law, which is based on the behavior of impermeable spheres, is applicable to settling marine aggregates. It also corroborates previous findings of negligible advective flow through marine aggregates. Hence, mass transfer to and from marine aggregates occurs mainly via diffusion, and it is primarily motile organisms that are able to colonize sinking aggregates.

Introduction

Settling of phytoplankton cells to the deep ocean in the form of marine snow (aggregated phytoplankton and detritus > 500 μm) or as zooplankton fecal pellets causes an average carbon flux of 5 PgC yr^{-1} out of the sea surface (IPCC 2013). The efficiency of this process, known as the biological carbon pump (BCP; Volk and Hoffert, 1985), is strongly regulated by heterotrophic organisms in the water column. Bacteria and (proto)zooplankton commonly respire more than 90% of carbon fixed in the surface ocean back to CO_2 – a process known as remineralization – before it leaves the euphotic zone, and thereby regulate organic matter export to the deep sea (Hedges, 1992). Less than 2% of particulate organic carbon (POC) that is fixed in the surface ocean reaches depths beyond 1000 m, where carbon can be sequestered over periods of 10^3 years (Tréguer et al., 2003).

The amount of biotic remineralization, and thus carbon flux attenuation, is strongly related to aggregate settling velocity, since the settling velocity determines the residence time of aggregate in the upper 1000 m and thereby the time available for degradation (Cavan et al., 2017; Bach et al., 2016; Iversen and Ploug, 2010; Iversen et al., 2010). Natural marine snow has high remineralization rates, and typically 80% of the POC contained within a slow-settling aggregate is remineralized in the first 200 m of the water column (Ploug et al., 1999). Despite the significance of settling velocity for export flux, this parameter is not routinely measured. Direct measurements of aggregate settling velocity are time consuming and require collection of intact in situ formed aggregates (Riley et al., 2012). Several methods are used to measure aggregate settling velocity, e.g., net-jet flow systems (Ploug and Jørgensen, 1999; Ploug et al., 2008; Iversen and Ploug, 2010), settling columns (Silver et al., 1984; Gorsky et al., 1984; Hansen et al., 1996), or roller tanks (Ploug et al., 2010; Engel and Schartau, 1999). However, direct measurements of settling velocity for in situ formed aggregates are rare.

Collecting aggregates in situ imposes certain restrictions, such as limited sampling depths as well as severely limiting the throughput. Instead, in situ camera systems like the Video Plankton Recorder (VPR; Ashjian et al., 2001; Davis et al., 1996) or the Underwater Velocity Profiler (UVP; Stemmann et al., 2004; Picheral et al., 2010) have become the gold

standard for high-throughput vertical profiling of particle abundance, volume, and size-spectra. Although optical systems do not measure settling velocity, they have increasingly been used to calculate carbon flux by comparing to sediment trap fluxes and assuming that aggregate size scales as a power function to both settling velocity and mass (Guidi et al., 2015, 2008; Iversen et al., 2010).

To indirectly determine flux using in situ camera profiles, aggregate settling velocity is calculated according to Stokes' law (Jackson and Checkley, 2011). Following Stokes' law (Stokes, 1851), settling velocity is a function of the squared particle radius and the excess density of marine aggregates. However, it has been observed that settling velocities calculated using Stokes' law tend to underestimate the settling velocity of smaller aggregates while overestimating the velocity of larger aggregates (e.g., Stemmann et al., 2004). Several properties of marine snow, including its highly variable morphology, surface roughness and permeability, have been considered to explain the non-compliance with Stokes' law (Laurenceau-Cornec et al., 2015; Li and Logan, 2001; Alldredge and Gotschalk, 1988; Baba and Komar, 1981; Matsumoto and Suganuma, 1977; Williams, 1966).

It has been suggested that deviation from Stokes' law due to the heterogeneity of the aggregates in the ocean makes it difficult to determine a global relationship between size and settling (e.g., Iversen and Ploug, 2010; McDonnell and Buesseler, 2010). However, we hypothesize that general relationships can be identified when testing Stokes' settling for different types of aggregates. We used Particle Image Velocimetry (PIV) to visualize the flow field around in situ collected aggregates. At the same time, we used impermeable agar spheres as a control, since Stokes' law predict their settling well. For both the agar spheres and the in situ collected aggregates we compared measured settling velocities to Stokes' prediction and related the settling to aggregates' hydrodynamic flow field (from the equatorial boundary layer thickness) and other selected descriptors of aggregate structure and composition.

Material and Methods

Aggregate collection

The study was carried out in July and August 2017 on board the B/O Sarmiento de Gamboa in the North-West African Eastern Boundary Upwelling System (fig. 1). Aggregates were collected non-destructively with a Marine Snow Catcher (MSC; Riley et al., 2010) at depths between 20-150 m, and left to settle for 5-10 h. Hereafter, single aggregates were picked from the base of the MSC with a wide mouth bore pipette and gently transferred to a vertical flow system to record the size, settling velocity and flow field around each aggregate. The flow system was modified from (Ploug and Jørgensen, 1999) to maximize laminarity of the water flow (see supplementary information S1 for flow chamber specifications). The water in the vertical flow system was collected from the same MSC deployment as the aggregates, GF/F-filtered and kept at a constant temperature of 18.2°C (±0.2°C).

In addition to collecting natural, in situ formed particles, we created agar spheres made up of 1% agar (wt/wt) mixed with 1% yeast (wt/wt) dissolved in seawater. They were used as model aggregates for impermeable, perfect spheres where solute and gas exchange between the interior and the ambient water only occurs via diffusion. Yeast was added for the sole purpose of increasing the visibility of the agar spheres. Spheres were formed by dripping the agar solution into a layer of paraffin oil and letting the spheres settle out into an underlying layer of filtered seawater (Cronenberg, 1994; Ploug et al., 2002). Before use, agar spheres were immersed in the same water as used for the experiments for at least 10 minutes to allow salt to diffuse between the ambient and pore water until equilibrium was reached.

Particle Image Velocimetry (PIV)

For Particle Image Velocimetry, the water reservoir of the vertical flow system was seeded with polyamide particles with a mean diameter of 5 µm and a density of 1.1 g/cm^3 (ILA 5150 GmbH) to track the velocity and direction of water flow around the aggregates. The center section of the flow chamber was illuminated with a green LED Pulsing System (LPS2, ILA 5150 GmbH) attached to an LED head with optics to create a vertical, 500 µm-wide light

sheet illuminating the flow chamber (fig. S1). The LPS was pulsed at frequencies ranging from 20 Hz at low flow velocities up to 30 Hz for fast-settling aggregates. The upward flow in the vertical flow system was adjusted until aggregates remained suspended at a distance of approximately 3-5 aggregate diameters above the net to eliminate any interaction between surfaces. A series of at least 150 images was recorded with a camera (µEye CP, IDS Imaging Development Systems GmbH), with an attached macro zoom telecentric lens (computar, TEC-V7X, 47.65 - 106.26 mm). The camera was triggered by the LPS, i.e., the frame rate was automatically adjusted according to the LED pulse frequency.

Particle image velocimetry analysis was performed using the software PivView (PivTech GmbH). The PIV pictures were divided into interrogation windows with an area of 32 pixels each and a 50% overlap. It was qualitatively ensured that each interrogation window contained at least five individual PIV beads. Cross-correlation of each interrogation window between two consecutive images was performed using a discrete fast Fourier transform following the Wiener–Khinchin theorem. To maximize spatial resolution, multi-grid refinement analysis was performed (Raffel et al., 2018). The result was a 2-dimensional velocity matrix with a size of 16 px × 16 px at a resolution of 7 µm/px. The procedure was repeated for at least 80 consecutive images using a batch script. Further processing was performed in Matlab 2015b (Mathworks).

Although marine aggregates were mostly stable within the imposed flow conditions, slight movements in the range of a few pixels were observed. To avoid any blurring while averaging, the movement of the aggregate was corrected using a detection algorithm to re-center the aggregate. For this, PIV seeding was filtered from the raw images using a 2-dimensional median filter with a pixel size of 6 px × 6 px. Subsequently, the image was binarized and the edges of the aggregate were traced. The aggregate was cropped and a cross correlation analysis with the subsequent images was performed to determine the aggregate movement.

Based on the position of the center of gravity, a velocity matrix stack composed of the 80 instantaneous velocity measurements was created with the centered aggregate. Finally, the velocity matrix stack was averaged and the position of the aggregate was masked. Aggregates that exceeded a movement of 20 pixels in horizontal or vertical

direction within 2-3 seconds of every possible image sequence were excluded from further analysis.

Terminal settling velocity and fluid boundary layer thickness were determined from the averaged magnitude of the flow field. For that, a horizontal cross section was extracted along the equator of the aggregate. The undisturbed maximum velocity along the cross section is equal to the terminal settling velocity of the aggregate. We then defined the fluid boundary layer as the distance between the aggregate surface and the point where the velocity increases to 90% of the terminal velocity.

Aggregate properties

We measured properties relating to the settling, porosity and shape of marine aggregates to relate them to each other and to numerically describe aggregate settling behavior. Selected properties including settling velocity, size, shape factors, solid hydrated density and fluid boundary layer thickness were measured directly, while porosity, excess density and drag coefficient were derived as described in the following.

Particle size was measured in three different ways: i) equivalent circular diameter (ECD) of aggregates was calculated from the two-dimensional projected area of aggregates as determined by the edge detection algorithm described above, ii) equivalent spherical diameter (ESD) was calculated from the length of three perpendicular axes of an aggregate extracted from two frames representing all three axes, and iii) the x-axis diameter was extracted from images of the PIV recording as the diameter of the particle that is perpendicular to the falling direction. Because the x-axis diameter has a direct impact on the aggregate flow field and is a common input parameter many hydrodynamic equations, e.g., the drag coefficient (White 1974), we used the x-axis diameter as the length measure for the aggregates throughout this manuscript (see fig. S2 for a comparison of all sizing methods).

For comparison to previous settling velocity measurements, settling velocity of aggregates was also directly determined in the flow chamber by dividing the flow rate by the cross-sectional area of the flow chamber. For this, settling velocity was recorded for aggregates suspended one diameter above the net as recommended by Ploug et al. (2010) according to Ploug and Jørgensen (1999). However, PIV results indicated that the flow field

around the aggregates were affected by the proximity to the surface. Therefore, PIV measurements were recorded with the aggregates suspended 3-5 diameters above the net in order to ensure an undisturbed flow field. Unless stated otherwise, the settling velocities presented throughout the manuscript are based on the PIV recordings. After recordings in the vertical flow system, aggregates were transferred to Utermöhl chambers (Utermöhl, 1931) and imaged using brightfield, epifluorescence, and phase-contrast microscopy at 100x-400x magnification for high-resolution imaging of aggregate composition, type, and structure. To maximize image resolution, images taken at different depths of field were stacked with Zerene Stacker (Zerene Systems LLC).

To compare the flow field around aggregates of different sizes, the non-dimensional Reynolds number was calculated using

$$Re = wd\frac{\rho_w}{\eta} \quad 1$$

where w is the measured settling velocity (cm s^{-1}), d is the x-axis diameter (cm), ρ_w is the water density (g cm^{-3}), and η is the dynamic viscosity of seawater (g cm^{-1} s^{-1}). Theoretical settling velocity was calculated using Stokes' law

$$w = \frac{d^2 g(\rho_s - \rho_w)}{18\eta} \quad 2$$

where g is gravitational acceleration (981 cm s^{-1}). Excess density ($\Delta\rho$, g cm^{-3}) was calculated using the Stokes' drag equation (1851)

$$\Delta\rho = \frac{C_D\,\rho_w\,w^2}{\frac{4}{3}gd} = (1-\varphi)\rho_s + \rho_w\varphi - \rho_w \quad 3$$

where C_D is the dimensionless drag force. The drag force (C_D) was calculated using the drag equation for $1 < Re \leq 2 \times 10^5$ (White, 1974)

$$C_D = \left(\frac{24}{Re}\right) + \left(\frac{6}{1 + Re^{0.5}}\right) + 0.4 \quad 4$$

Additionally, we independently derived the drag coefficient from the fluid boundary layer thickness using empirical relationships. We used a cubic polynomial function given by

$$C_D = a + b\delta_s + c{\delta_s}^2 + d{\delta_s}^3 \quad 5$$

with a = 8.793, b = -15.046, c = 22.320, and d = -2.636 to mathematically relate the drag coefficient to the fluid boundary layer for 0.02 ≤ Re ≤ 20, where δ_s is the equatorial fluid boundary layer (δ) normalized by the x-axis diameter (d) (see supplementary section S4 for a detailed description).

Aggregate porosity (φ) was calculated by re-arranging Eq. 3 as follows

$$\varphi = \frac{\Delta\rho + \rho_w - \rho_s}{\rho_w - \rho_s} \quad 6$$

where $\Delta\rho$ is the excess density (g cm^{-3}) derived from Stokes' drag equation, and ρ_s is the measured solid hydrated density (g cm^{-3}) for the different aggregate types. The solid hydrated density (ρ_s) of aggregates was determined in a seven-layer density gradient made with dilutions from Ludox TM colloidal silica (Sigma-Aldrich), sucrose and distilled water (following Gärdes et al. [2011] and Iversen and Robert [2015] who modified the method from Schwinghamer et al. [1991], and Feinberg and Dam [1998]). The dilutions ranged in density from 1.155 to 1.428 g cm^{-3}. Starting with the densest solution, 2 ml of each dilution were gently transferred to 15 ml centrifuge tubes (Corning) and topped with 2 ml of GF/F-filtered seawater. Single aggregates were gently added to the topmost layer of the density gradient using a wide-mouth bore pipette and left to settle into the gradient at 4°C overnight. The following day, 1 ml was sampled from the layer the aggregate had settled into, which is representative of the density of the solid components of the aggregate. Samples were kept at 4°C in sealed 1ml-tubes until the end of the cruise, and measured with a density meter (DMA 38, Anton Paar) back in the home laboratory.

We characterized the fractal microstructure of the aggregates by determining their 1-, 2- and 3-dimensional fractal numbers DF1, DF2 and DF3, respectively. Following Kilps et al. (1994), the 1- and 2-dimensional fractal numbers (DF1 and DF2), were calculated from the slopes of log-log relationships of perimeter and area respectively, against the x-axis diameter. The 3-dimensioal fractal dimension was calculated based on the correlation between solid material and diameter, following Logan and Wilkinson (1990):

$$(1 - \varphi) = ad^{DF3-3} \quad 7$$

where a and DF3 are the fitting parameters.

To test the effects of aggregate shape on settling velocities, we used images from the

PIV recording to extract the parameters for morphological roughness, textural roughness, and form. Most shape descriptors, including aspect ratio, area:perimeter, circularity, sphericity, and form factor, Feret diameter, Paris factor, and solidity, were calculated according to Liu et al. (2015), and Heilbronner and Barrett (2013). The Corey shape factor (Corey, 1949; McNown and Malaika, 1950) representing particle flatness was also used.

Results

Particle type, size and settling velocity

In total, we collected 141 particles, which we separated into five separate categories (fig. 1, fig. 4). It is important to stress that very few particles were comprised of a single constituent and we therefore categorized the aggregates based on their dominant component.

Marine snow made up 40% of analyzed aggregates and was distinguished from other types of aggregates by their heterogeneous composition and structure (compare fig. 1). Marine snow was formed from diatom chains, acantharia, radiolaria, mucilaginous particles from discarded feeding webs, fresh and degraded fecal pellets, copepod carapaces, and other unidentified phyto- and zoo-detritus. Because of their large compositional variability, we further subdivided marine snow into *compact* and *loose* marine snow. They were present in equal amounts, with each representing 20% of all aggregates.

30% of the analyzed aggregates were catagorized as appendicularian fecal pellets at various stages of degradation (from here on simply referred to as “fecal pellets”). The categorization of fecal pellets was made based on particle size, homogeneous distribution of matter, uniform coloring, and the oval shape. 22% were categorized as mucus aggregates, as they were solely, or largely, comprised of a translucent, mucilaginous substance ostensively originating from discarded zooplankton feeding webs. The remaining 8% of analyzed particles could not be assigned to any of the above categories and were classified as “other”. They include a dead copepodite, very loose, gel-like mucus, and other unidentified organic structures (fig. 1b).

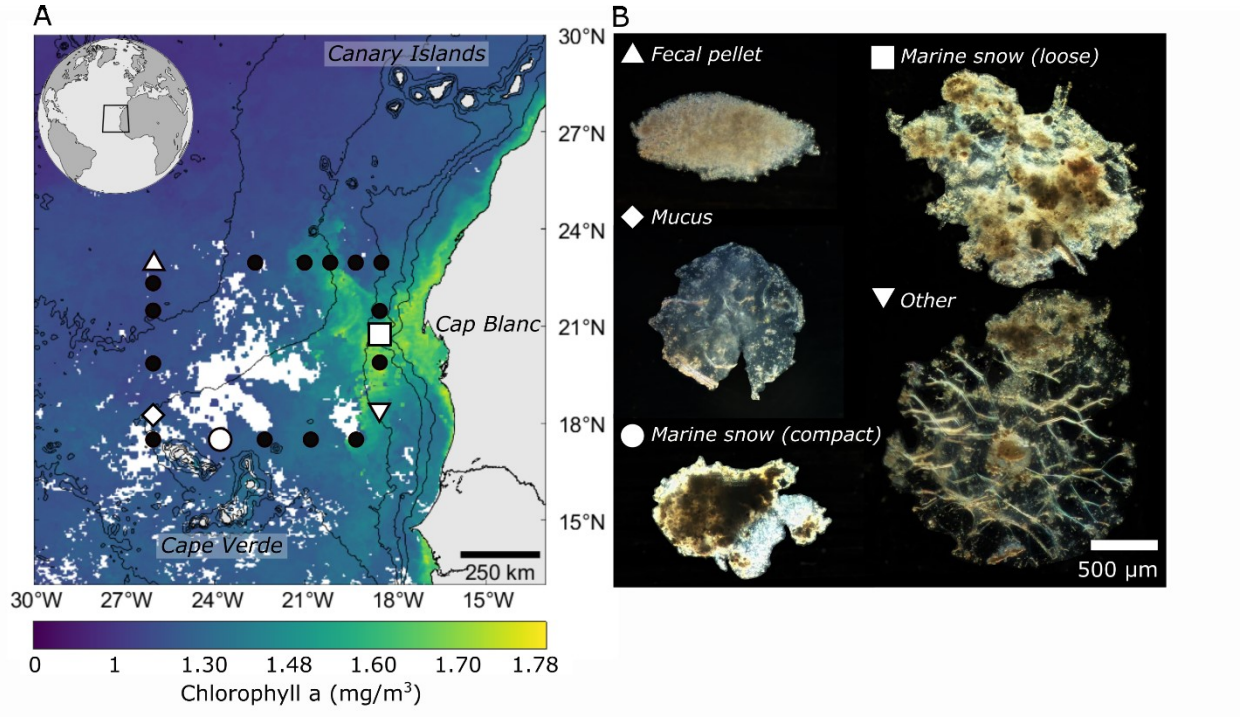

Figure 1. a) Chlorophyll a concentration during the sampling period and sampling stations (black dots) with white symbols corresponding to representative stations at which the identified aggregate types (b) were collected.

Aggregate x-axis diameter (from now on simply referred to as aggregate diameter) ranged from 0.38 to 3.56 mm with a mean size of 1.15 mm (±0.65 SD). Fecal pellets and compact marine snow were the smallest collected aggregates (mean size 0.82±0.26 mm and 0.81±0.29 mm, respectively), while loose marine snow had the largest mean size (1.92±0.74 mm).

The settling velocity when measured using consecutive images from the PIV recording of aggregates suspended 3-5 diameter above the flow chamber net ranged from 70 to 720 meters per day (average settling velocity 195±115 m/d). The elevated position within the flow chamber resulted in 1.4 times higher settling velocities than the settling velocities of aggregates suspended one diameter above the net of the flow chamber (fig. S3a). This indicates that the settling velocity is not fully balanced by the imposed flow when the aggregate is too close to the flow chamber net. The increase factor was size-dependent, with larger aggregates showing bigger differences than smaller aggregates (fig. S3b). The settling velocities presented in the following are for aggregates suspended more than 3

diameters above the net, i.e., on average 1.4 times higher than those measured using the suspension height proposed by Ploug et al. (2010). In some cases, the aggregates were too heavy to balance their settling velocity. In these cases, the flow velocity and flow field was measured 1 diameter above the net and subsequently the settling velocity was corrected using the following equation:

$$w_{PIV} = 23 + 1.4\, w_{1\ diameter} \quad (8)$$

Fecal pellets settled with the lowest average velocities (149±42 m/d) while mucus aggregates had the highest average settling velocities (255±149 m/d). There was no positive trend observed when looking at settling velocity as a function of size for all types of aggregates combined. However, some trends emerged when aggregates were separated into different types: Mucus aggregates showed the highest size-specific settling velocities, while there was no positive correlation between size and settling of pooled marine snow (fig. 2).

Settling velocity was significantly positively correlated to aggregate size for fecal pellets (FP) ($p<0.05$, $R^2=0.12$), compact marine snow (CMS) ($p<0.05$, $R^2=0.29$), and mucus (M) ($p<0.001$, $R^2=0.73$), but there was no significant correlation for loose marine snow (LMS) ($p=0.97$, $R^2=-0.06$; one-way ANOVA with Tukey multiple comparisons). There was a statistically significant difference in the size-specific settling velocity of loose marine snow compared to all other aggregate types (LMS:CMS=$p<0.001$; LMS:M=$p<0.01$; LMS:FP=$p<0.05$). CMS and FP also differed in their size-specific settling ($p=0.055$), while there was no difference between FP:CM ($p=0.3$) and FP:CMS ($p=0.3$) respectively (pairwise t-test, p-value adj. method: Benjamini-Hochberg).

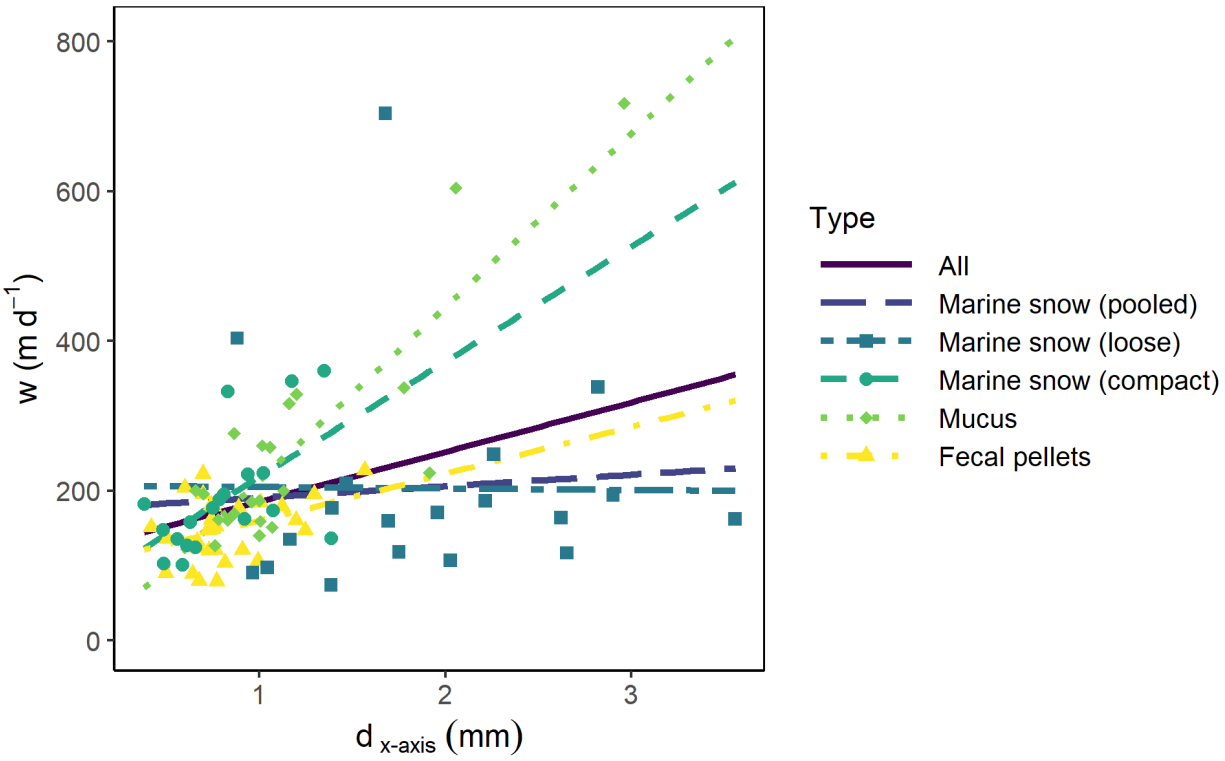

Figure 2. Size-to-settling relationship of categorized in-situ collected aggregates with regression lines for each type as well as the regression over all samples (purple line).

Flow fields around settling marine snow

Particle image velocimetry was performed with 108 particles (aggregates and agar spheres) to visualize flow fields around settling marine aggregates. Marine aggregates were kept in balance 3-5 diameters above the net (unless other stated). In order to compare the flow fields of different settling velocities and aggregate sizes, we calculated the Reynolds number. Reynolds numbers ranged from 0.48 to 22 with an average of 2.7 (±3.3 standard deviation).

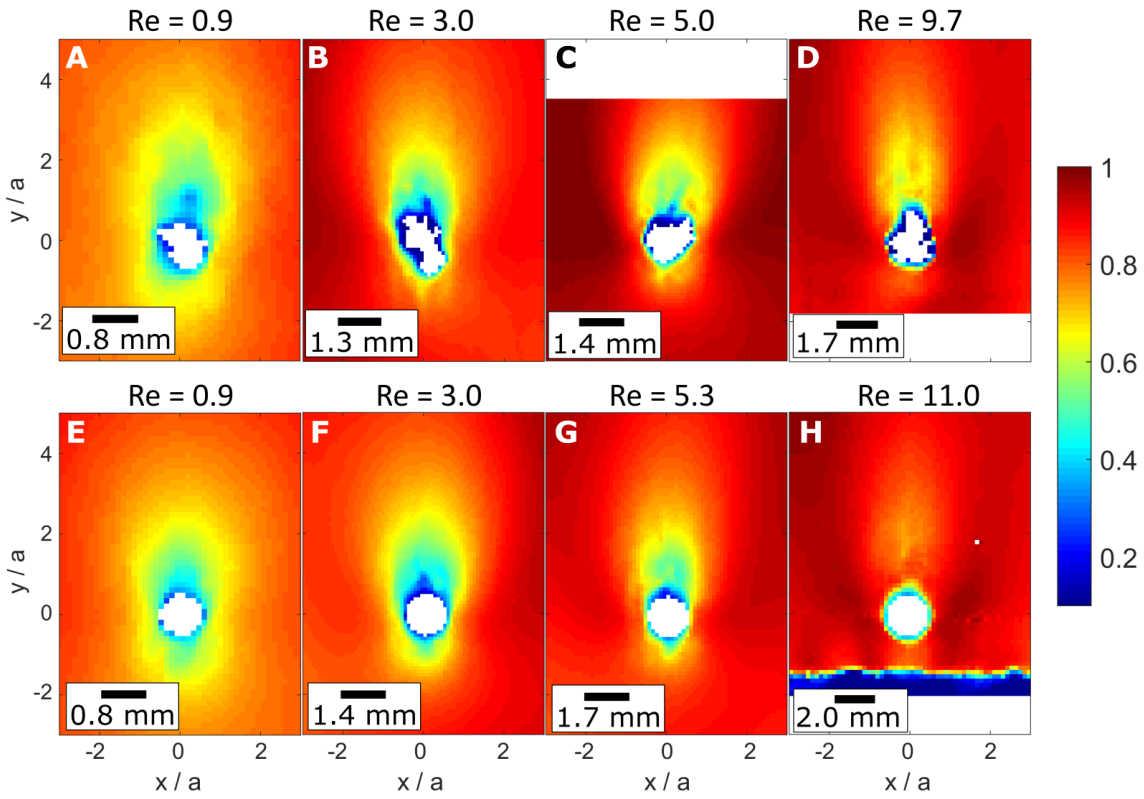

Figure 3. Velocity magnitude inferred from the PIV results for various Reynolds numbers. Panel A-D are showing marine aggregates, while panels E-H are showing agar spheres; please note that the vertical pairs are selected based on corresponding Reynolds numbers.

This Reynolds number regime represented an intermediate range above creeping flow conditions ($Re << 1$) and far below turbulent regime ($Re > 2300$). For Reynolds number $Re \sim 1$ the flow field was mostly symmetric, i.e., fluid boundary layer thickness in front of the aggregate equaled the lee side fluid boundary layer thickness, with only small variations (fig. 3). With increasing Reynolds number, the flow field became increasingly asymmetric. Qualitatively, the flow fields of agar spheres and and marine aggregates of various shapes matched very well (fig. 4).

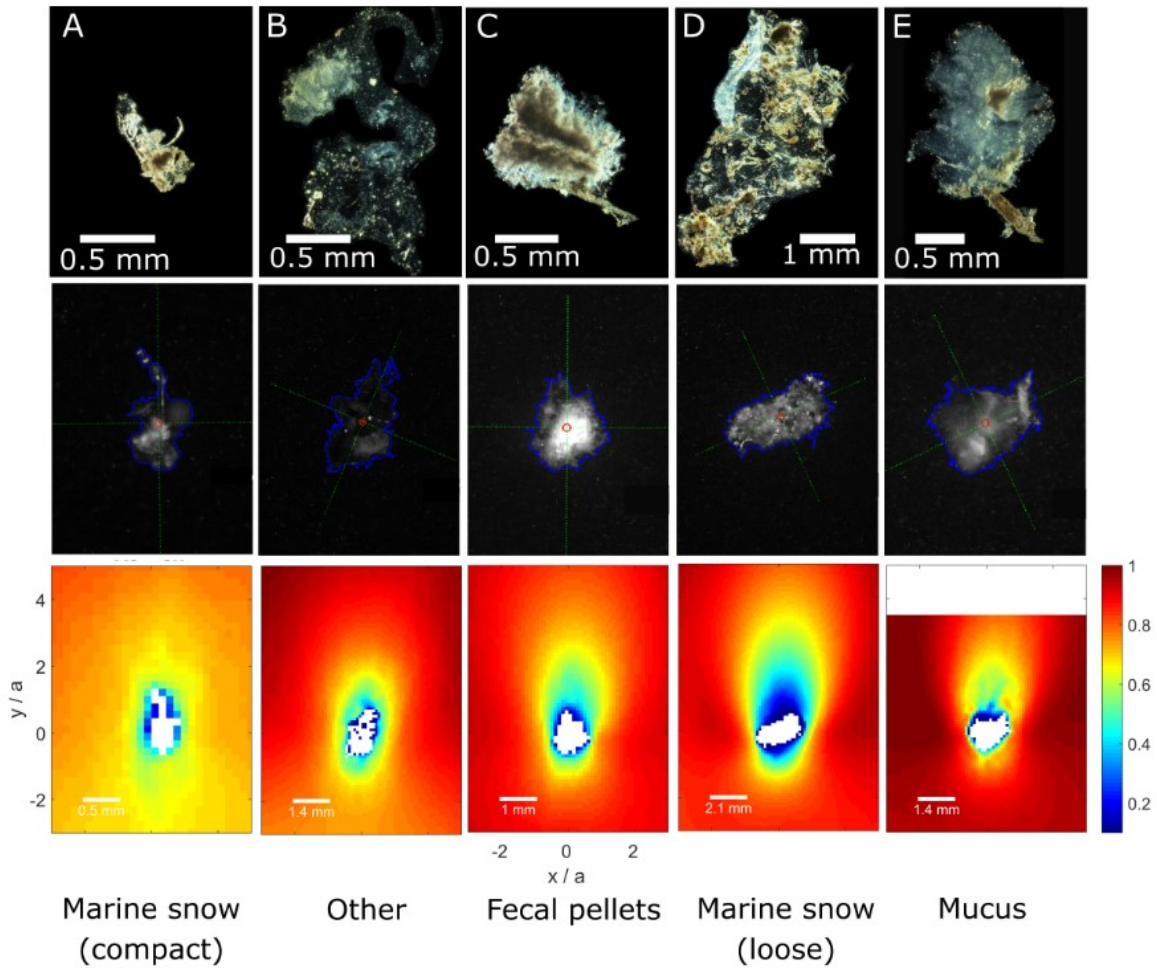

Figure 4. a-e) Examples of each aggregate type (top row), with aggregate masking applied to images extracted from the PIV recording (middle row), and the resulting flow fields (bottom row).

Scaling of boundary layer thickness and drag coefficient with Reynolds number

To quantify the variations in the flow field for different *Re* regimes, we estimated the fluid boundary layer thickness. The fluid boundary layer ranged from 0.73 to 3.41 mm, and was between 0.6 and 3.6 times the size of the diameter (fig. 5a).

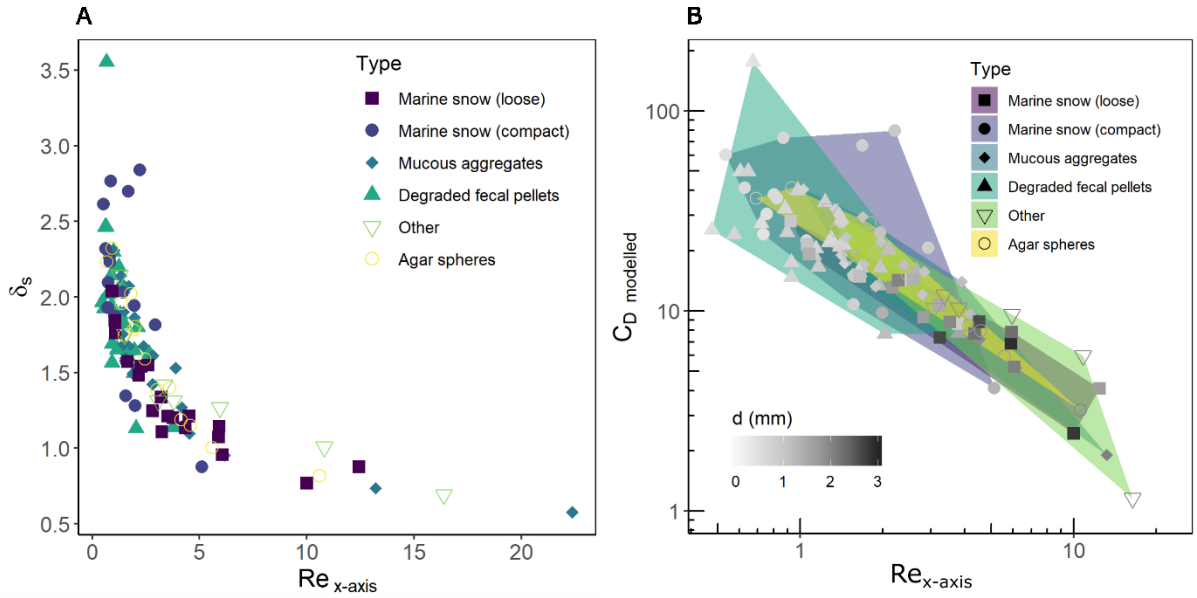

Figure 5. a) Relationship between the scaled equatorial boundary layer thickness and Reynolds number for the different aggregate types and agar spheres. b) based on the scaled boundary layer thickness the drag coefficient was estimated following Eq. 5.

Irrespective of the aggregate type, the boundary layer scaled with the Reynolds number following a power law ($\delta_s = 2.0 \times Re^{-0.33}$). While the agar aggregates represented very spherical shapes, the in situ collected aggregates had very irregular shapes and rough surfaces (fig. 1b). Yet, there was no significant difference between the power law coefficients for agar spheres and any of the aggregate types ($\delta_s = 2.0 \times Re^{-0.33}$) for all aggregates R2 = 0.66; ($\delta_s = 2.2 \times Re^{-0.37}$) for agar spheres, R2=0.91), but as indicated by the increased R2 values, the fitting deviation, i.e., residuals, increased for irregularly shaped aggregates.

To investigate the extent to which the deviation between theory and our measurements affects settling velocity prediction, the drag coefficient was estimated based on the measured boundary layer thickness (Eq. 5 and section S4). In general, the drag coefficients for aggregates and agar spheres scaled with the Reynolds number as expected from Stokes' law (Figure 3b, best fit $C_D = 32/Re^{0.8}$). Residuals between estimated drag coefficients and predicted drag coefficients were calculated: $((C_D - C_{D_{Stokes}})/C_{D_{Stokes}})$. Residuals were largest for small Reynolds numbers ($Re < 1.5$), i.e., large boundary layer thickness, where the drag coefficient is underestimated by Stokes' law (up to 5-fold, on

average 2-fold). This deviation translates into an overestimation of the settling velocity by 40% - 120% when calculated by Stokes' law. For larger Reynolds numbers ($Re > 1.5$), the residuals strongly decreased in magnitude (up to 2 fold, in average 1.5 fold), translating into settling velocity overestimation of 20% - 40% when calculated with Stokes' law. By following the White extension for the drag coefficient, the residuals further decreased by an average of 30% across the whole Reynolds range and the trend towards overestimation of settling velocity for large aggregates was diminished.

The magnitude of the residuals could not be explained by any of the measured individual aggregate properties. Still, the residuals strongly varied between the different aggregate types, showing that Stokes Law was better at predicting the settling velocity of some aggregate types, especially in the low Reynolds ($Re < 1.5$) number range. The average error in predicting settling velocity based on the White drag coefficient uncertainty was estimated to be 10% for fecal pellets and 14% for loose marine snow followed by 18% for compact marine snow. Mucous and other aggregates deviated by 26% and 34%, respectively.

Porosity, fractality, shape, and excess density

Microscope imaging of the sampled aggregates revealed heterogeneous compositions and variabilities in the aggregate microstructures between the different aggregate types. To investigate the effect of individual aggregate properties on settling velocity and microbial colonization, we measured solid hydrated density, diameter, fractality, various shape factors, and estimated porosity as well as excess density based on the PIV results and Eq. 5 (table 1).

Table 1. Overview of measured parameters for the different aggregates types. "All aggregates" denote the sum of in situ collected particles (excluding agar spheres).

Type	n (#)	d (mm)	w (m/d)	Re	ϕ	Δρ (g/cm^3)	C_D	δ_S	DF1	DF2	DF3
All aggregates	95	1.2 ±0.7	201 ±125	2.9 ±3.4	0.93 ±0.07	0.016 ±0.018	21.9 ±21.8	1.7 ±0.5	1.2	1.7	2.1
Marine snow (pooled)	38	1.4 ±0.8	196 ±116	2.9 ±2.6	0.89 ±0.11	0.016 ±0.016	21.6 ±19.6	1.6 ±0.6	1.2	1.8	2.1
Marine snow (loose)	19	1.9 ±0.7	203 ±147	4.1 ±3.0	0.81 ±0.10	0.006 ±0.005	11.2 ±6.4	1.3 ±0.3	1.1	2.0	2.0
Marine snow (compact)	19	0.8 ±0.3	190 ±78	1.8 ±1.2	0.87 ±0.09	0.024 ±0.016	32.0 ±22.9	2.0 ±0.6	1.2	1.3	2.6
Fecal pellets	28	0.8 ±0.3	149 ±42	1.3 ±0.7	0.93 ±0.08	0.021 ±0.025	28.6 ±30.6	1.9 ±0.5	1.2	1.4	2.0
Mucus	21	1.2 ±0.6	255 ±150	3.9 ±5.0	0.94 ±0.04	0.013 ±0.009	17.0 ±10.2	1.6 ±0.5	1.1	1.6	1.6
Other	8	1.9 ±0.4	264 ±205	5.8 ±5.3	0.98 ±0.98	0.003 ±0.001	12.6 ±9.5	1.4 ±0.4	0.9	1.1	NA
Agar spheres	14	1.3 ±0.4	203 ±104	3.2 ±2.6	0.96 ±0.01	0.004 ±0.001	18.1 ±11.4	1.6 ±0.5	1.3	2.0	NA

The excess density of the aggregate depends on solid hydrated density and water density, related by the porosity (Eq. 3). While solid hydrated density could be measured directly, we estimated the excess density using Eq. 5, where the PIV-estimated drag coefficient ($C_{D_{modelled}}$) was used to avoid circular reasoning. We found the excess density to range over two orders of magnitude from 0.39 mg cm^{-3} to 99 mg cm^{-3}. The measured solid hydrated density based on the different aggregate types varied between 1155 mg cm^{-3} to 1323 mg cm^{-3} only explaining a minor fraction of the variability of excess densities (fig. S4).

Porosity ranged from 0.7 to 0.997 indicating the large water fraction in the interstitials of the aggregate. Despite the large range of porosities, only compact marine snow aggregate had a significantly decreased average porosity compared to the other groups (Anova, $p<0.05$). The role of porosity becames more pronounced when looking at the solid fraction of the aggregate ($1 - \varphi$) (fig. 6). The volume made up by solid material ranged from 0.3% to 0.003% encompassing two orders of magnitude and thereby explaining most

of the observed variability of the excess densities. The amount of the solid fraction was related to the diameter of the aggregate by a power law function ($(1-\varphi) = 0.3384 \times d^{-1.46}$). This implies that larger aggregates had an increased porosity, and therefore a reduced excess density. This behavior is expected if taking fractal theories as a basis.

The 1-dimensional fractal number (DF1) (inferred from log-log relationship between perimeter and diameter) indicates the roughness of the outer structure relative to a smooth sphere. Values around unity are indicating a smooth surface, while larger numbers indicate uneven surface with structures that may reach into the boundary layer surrounding the aggregates. Agar spheres and fecal pellets showed smooth outer structures and values of DF1 were 1.2 and 1.4, respectively. Mucus aggregates, compact marine snow and loose marine snow exhibited intermediate roughness with values of DF1 between 2 and 2.4. "Other" particle types had the largest DF1 with a value of 3.3.

The 2- dimensional fractal number (DF2) (inferred from the log-log relationship between diameter and area) relates the area of the aggregate to the area of a sphere with the same diameter. Values of DF2 varied between 0.35 and 1.4 with means between 0.67 and 0.95. DF2 values of loose aggregates were on average significantly smaller than the other groups with a mean around 0.6. Similar to the diameter, DF2 values were correlated to the fraction of solids in the aggregate.

The 3-dimensional fractal number (DF3) was inferred from the correlation between the solid fraction $(1-\varphi)$ and the diameter of the aggregate (Eq. 7). Values for DF3 ranged between 1.6 and 2.6, being highest for the compact marine snow and lowest for mucus aggregates.

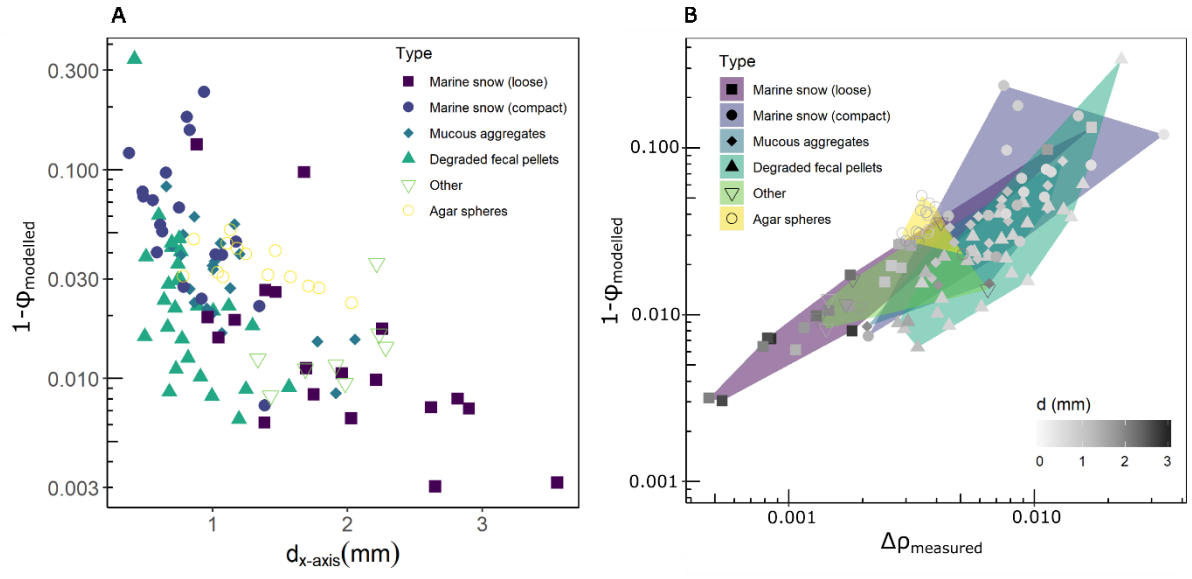

Figure 6. a) Relationship between aggregate solid fraction and aggregate size for the different aggregate types and agar spheres. b) Relationship between aggregate solid fraction, aggregate excess density, and aggregate size for the different aggregate types and agar spheres.

Discussion

We used four independent measurements, (i) aggregate size, (ii) settling velocity, (iii) fluid boundary layer to estimate the drag coefficient, and (iv) solid hydrated density, to characterize the settling behavior of marine aggregates. We collected particles with a wide range of primary-particle composition, sizes and settling velocities that reflect the diversity and heterogeneity of in situ formed aggregates and match previously reported values of size and settling velocity for natural marine aggregates (Alldredge and Gotschalk, 1988; Nowald et al., 2009).

Marine snow settling velocity is a major determinant of the efficiency of the biological carbon pump. Currently there are large deviations between measured and predicted size-specific settling. To gain a better understanding of settling of marine aggregates, we performed particle image velocimetry with 95 in situ sampled aggregates. Visualization of the flow field around the aggregates showed that the fluid boundary layer thickness, drag coefficient, and general flow field did not noticeably differ from that of

impermeable spheres with similar Reynolds numbers, suggesting that in situ formed aggregates behave according to Stokes' law.

In line with previous comparisons of size-to-settling relationships for marine aggregates, we also observed that Stokes' law underestimates the settling velocities of small aggregates and overestimates the settling velocity of larger aggregates (Stemmann et al., 2004). This deviation seems to be due to the fractality of marine aggregates making their porosity increase with increasing size following a power-function (Jagt et al., 2018; Iversen and Robert, 2015; Iversen and Ploug, 2010; Alldredge and Gotschalk, 1988). The increased porosity for large aggregates caused the excess density of our aggregates to decrease noticeably with increasing diameter. This resulted in lower settling velocities for large aggregates than predicted by Stokes' law. The drag coefficient, estimated from the boundary layer thickness, scaled with the Reynolds number.

As expected from the Reynolds number regime (Re = 0.5-24), the Stokes' drag (C_D=24/Re) was not sufficient to predict settling velocity. The White relationship (Eq. 4, White 1974) as well as our best fit $C_D = 32 \times Re^{-0.8}$ yielded a significant improvement. By applying the drag as well as the porosity relationships, the controlling variables can be reduced to diameter, solid hydrated density, gravitational acceleration, water viscosity and density. Knowing these parameters, the settling velocity of marine aggregates can be calculated in a straightforward manner by combining equations 2, 3, and 8 as presented in fig. 7.

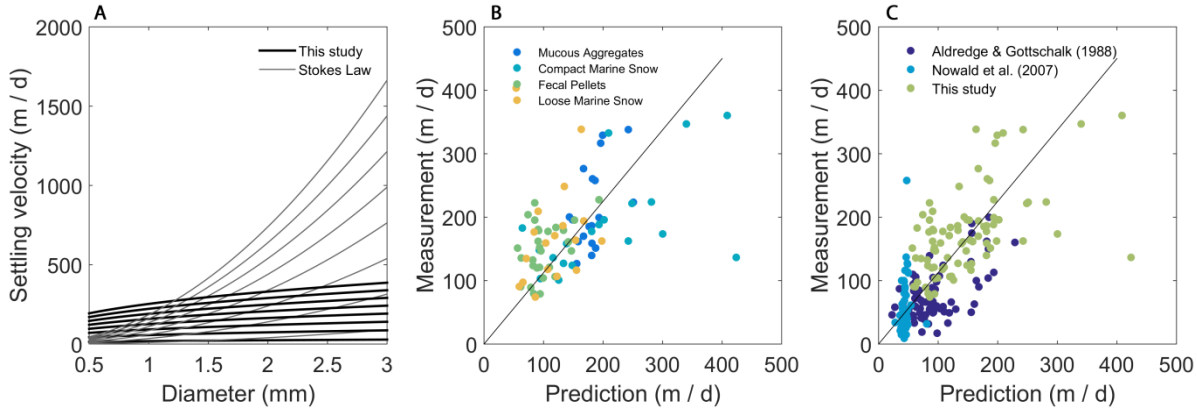

Figure 7. a) Modelled settling velocity for aggregate diameters between 0.5 and 3 mm and solid hydrated densities ranging from 1.05 to 1.4 g/cm^{-3}. b) and c) comparison of model results with the here presented data and previous studies, respectively.

Even though the model predicts the magnitude and trends well, larger uncertainties can be observed which are mainly induced by the solid hydrated density which, despite the comparatively low content of solids in marine aggregates, contributes significantly to the settling behavior of marine snow. Solids can affect marine aggregate settling in two major ways: the density of solid components affects marine snow by increasing the mass, i.e., excess density. At the same time, the shape and properties of solids affect how tightly they can be packed within an aggregate (the compactness) and directly affect the porosity of the aggregate. The solid hydrated density is likely to be determined by the phytoplankton community, i.e., domination by diatoms or coccolitophorids (Iversen and Ploug, 2010; Laurenceau-Cornec et al., 2015; Engel et al., 2009) and ballasting by dust particles (Jagt et al., 2018). However, it remains a task for future studies to investigate the regulatory mechanisms for solid hydrated density.

Furthermore, we did not find any indication that irregularities in aggregate shape influenced the drag coefficient, even when comparing between aggregate types and to agar spheres (fig. 5b). This supports previous studies which found that shape, permeability, and surface roughness are poor predictors to settling velocity (Williams 1966; Matsumoto and Suganuma, 1977; Baba and Komar, 1981; Alldredge and Gotschalk, 1988; Li and Logan, 2001). Overall, we did not find any difference in physical properties, including settling behavior, between the in situ formed aggregates and the impermeable agar spheres.

This not only shows that Stokes' law is a good predictor for settling once the solid hydrated density is known, but also that in situ aggregates are impermeable despite their high porosities. This has been explained be the presence of high concentrations of transparent exopolymer particles (TEP) that may limit advection rather than diffusion within aggregates (Ploug et al., 2008). TEP is also the most likely reason that large aggregates, albeit being highly porous, are not permeable, as they occupy the vast majority of the pore space, and constitute a much larger amount of the “non-water” fraction than solid components (Engel et al., 2002; Passow, 2002). This suggests that in situ aggregates are purely diffusive systems where any mass transport to or from the aggregates has to occur across the diffusive boundary layer.

That aggregates are purely diffusive also implies that organisms have to be motile in order to colonize a settling aggregate. It has not been conclusively shown if bacterial colonization is a purely active process requiring chemotaxis and motility, or if aggregates indiscriminately scavenge bacteria out of the water column as they settle. Despite the high porosities measured and the fractal nature of marine aggregates, there was no indication advective flow through the aggregates during our PIV experiments. This indicates that bacterial colonization would occur from the outside or while forming and due to a fluid flow through the aggregate. Several studies have used the approach of comparing free-living versus attached bacterial assemblages on aggregates and at different depths in the water column to address this question. Case studies from a panoceanic cruise (Mestre et al., 2018), the Fram Strait (Fadeev et al., in prep.), the Scoresby Sund fjord system (Hufnagel et al., unpublished data) and from the Northeast African Upwelling System (Bachmann et al., 2018; Thiele et al., 2014) have all shown that particle-attached bacterial assemblages resemble free-living assemblages in the surface more closely than those at any other water depth, including the depth at which the particle was collected. This strongly suggests that most bacteria already colonize marine aggregates in the ocean surface before they start settling out, or that they colonize smaller particles that then aggregate and form the marine snow particle.

On a microscale, the fluid boundary layer around a settling particle presents a physical barrier to bacteria, which they have to actively cross. As shown in this study, the fluid boundary layer thickness scales mainly with settling velocity, i.e., size-normalized fluid boundary layer becomes thinner with increasing settling velocity, meaning that the distance bacteria would have to cross also becomes shorter. However, the shear stress also increases as a result of stronger velocity gradients. This presumably makes it more difficult for bacteria to cross the fluid boundary layer. On the other hand, shear stress has been shown to lead to bacterial rheotaxis (Marcos et al., 2012) and trap bacteria (Rusconi et al., 2014). The trade-off between boundary layer thickness, shear stress, and rheotaxis begs the question if there is an optimum in the fluid boundary layer thickness-to-settling velocity relationship where bacteria can attach to a settling aggregate.

In this study, we found the boundary layer thickness to range between 0.73 and 3.41 mm. Assuming a body length of 0.4 to 2 μm, this means that bacteria would have to swim 400 to 8000 body lengths to cross the boundary layer, all while the particle continues to settle. Assuming a chemotactic velocity towards a higher solute concentration of 10 μm/sec (Stocker and Seymour, 2012) and ignoring continued settling and possible hindrance by shear stress, it would take the bacteria 1-5 minutes to cross the boundary layer. However, while the surface roughness of marine aggregates does not seem to influence the flow field or the settling velocity, it could be responsible for scavenging of bacteria as the aggregate sinks through the water column. In our recordings, we did observe PIV beads getting stuck to the aggregate, especially when the aggregates had irregular shapes with parts of the aggregate surface intruding into the boundary layer. This suggests that the outer shape and microstructures along the surface of marine aggregates can have important implications for mass transfer and for microbial colonization of settling aggregates.

In summary, the resemblance of flow fields around natural marine aggregates to those of agar spheres, supports previous findings that microstructures do not decisively affect settling velocity and that aggregates settle in accordance with Stokes' law. This also indicates that marine aggregates are diffusive systems with negligible advective flow, which consequently suggests that chemotactic behavior is required for bacteria to sense and attach to settling aggregates. Still, some of the PIV beads were observed sticking to the outside of the aggregates, suggesting that the intrusion of microstructures on the aggregate surface into the fluid boundary layer leads to passive scavenging of particles and microorganisms. This microstructure-related scavenging is likely a major mechanism by which ballast and microorganisms are entrained in marine aggregates as they settle through the water column.

Acknowledgments

The authors thank the captain and crew of the B/O Sarmiento de Gamboa for enabling this study and Cora Hörstmann for her contribution to developing the modified flow chamber set-up. This study was supported by the Helmholtz Association and the Alfred Wegener Institute for Polar and Marine Research, the DFG-Research Center/Cluster of Excellence "The Ocean in the Earth System", and the Max Planck Institute for Marine Microbiology. This publication is supported by the HGF Young Investigator Group SeaPump "Seasonal and regional food web interactions with the biological pump": VH-NG-1000.

Conflict of interest

The authors declare no conflict of interest.

References

Alldredge, A. L. and Gotschalk, C. 1988. In situ settling behavior of marine snow, *Limnology and Oceanography*, vol. 33, no. 3, pp. 339–351. DOI: 10.4319/lo.1988.33.3.0339.

Ashjian, C. J., Davis, C. S., Gallager, S. M. and Alatalo, P. 2001. Distribution of plankton, particles, and hydrographic features across Georges Bank described using the Video Plankton Recorder, *Deep Sea Research Part II: Topical Studies in Oceanography*, Coupled biological and physical studies of plankton populations on Georges Bank and related North Atlantic regions, vol. 48, no. 1, pp. 245–282. DOI: 10.1016/S0967-0645(00)00121-1.

Baba, J. and Komar, P. D. 1981. Settling velocities of irregular grains at low Reynolds numbers, *Journal of Sedimentary Research*, vol. 51, no. 1, pp. 121–128. DOI: 10.1306/212F7C25-2B24-11D7-8648000102C1865D.

Bach, L. T., Boxhammer, T., Larsen, A., Hildebrandt, N., Schulz, K. G. and Riebesell, U. 2016. Influence of plankton community structure on the sinking velocity of marine aggregates, *Global Biogeochemical Cycles*, vol. 30, no. 8, p. 2016GB005372. DOI: 10.1002/2016GB005372.

Bachmann, J., Heimbach, T., Hassenrück, C., Kopprio, G. A., Iversen, M. H., Grossart, H. P. and Gärdes, A. 2018. Environmental Drivers of Free-Living vs. Particle-Attached Bacterial Community Composition in the Mauritania Upwelling System, *Frontiers in Microbiology*, vol. 9. DOI: 10.3389/fmicb.2018.02836.

Cavan, E. L., Trimmer, M., Shelley, F. and Sanders, R. 2017. Remineralization of particulate organic carbon in an ocean oxygen minimum zone, *Nature Communications*, vol. 8, p. 14847. DOI: 10.1038/ncomms14847.

Corey, A. T. 1949. Influence of Shape on Fall Velocity of Sand Grains, Colorado A&M College.

Cronenberg, C. C. H. 1994. Biological engineering on a microscale: Biofilms investigated with needle-type glucose sensors., University of Amsterdam.

Davis, C. S., Gallager, S. M., Marra, M. and Kenneth Stewart, W. 1996. Rapid visualization of plankton abundance and taxonomic composition using the Video Plankton Recorder, *Deep Sea Research Part II: Topical Studies in Oceanography*, vol. 43, no. 7, pp. 1947–1970. DOI: 10.1016/S0967-0645(96)00051-3.

Engel, A., Meyerhöfer, M. and von Bröckel, K. 2002. Chemical and Biological Composition of Suspended Particles and Aggregates in the Baltic Sea in Summer (1999), *Estuarine, Coastal and Shelf Science*, vol. 55, no. 5, pp. 729–741. DOI: 10.1006/ecss.2001.0927.

Engel, A. and Schartau, M. 1999. Influence of transparent expolymer particles (TEP) on sinking velocity of Nitzschia closterum aggregates, *Marine Ecology Progress Series*, no. 182, pp. 69–76. DOI: 10.3354/meps182069

Engel, A., Szlosek, J., Abramson, L., Liu, Z. and Lee, C. 2009. Investigating the effect of ballasting by CaCO3 in Emiliania huxleyi: I. Formation, settling velocities and physical properties of aggregates, *Deep Sea Research Part II: Topical Studies in Oceanography*, MedFlux:Investigations of Particle Flux in the Twilight Zone, vol. 56, no. 18, pp. 1396–1407. DOI: 10.1016/j.dsr2.2008.11.027.

Fadeev, E., Salter, I., Schourup-Kristensen, V., Nöthig, E.-M., Metfies, K., Engel, A., Piontek, J., Boetius, A. and Bienhold, C. 2018. Microbial Communities in the East and West Fram Strait During Sea Ice Melting Season, *Frontiers in Marine Science*, vol. 5. DOI: 10.3389/fmars.2018.00429.

Feinberg, L. and Dam, H. 1998. Effects of diet on dimensions, density and sinking rates of fecal pellets of the copepod Acartia tonsa, *Marine Ecology Progress Series*, vol. 175, pp. 87–96. DOI: 10.3354/meps175087.

Gärdes, A., Iversen, M. H., Grossart, H.-P., Passow, U. and Ullrich, M. S. 2011. Diatom-associated bacteria are required for aggregation of Thalassiosira weissflogii, *The ISME Journal*, vol. 5, no. 3, pp. 436–445. DOI: 10.1038/ismej.2010.145.

Gorsky, G., Fisher, N. S. and Fowler, S. W. 1984. Biogenic debris from the pelagic tunicate, Oikopleura dioica, and its role in the vertical transport of a transuranium element, *Estuarine, Coastal and Shelf Science*, vol. 18, no. 1, pp. 13–23. DOI: 10.1016/0272-7714(84)90003-9.

Guidi, L., Jackson, G. A., Stemmann, L., Miquel, J. C., Picheral, M. and Gorsky, G. 2008. Relationship between particle size distribution and flux in the mesopelagic zone, *Deep Sea Research Part I: Oceanographic Research Papers*, vol. 55, no. 10, pp. 1364–1374. DOI: 10.1016/j.dsr.2008.05.014.

Guidi, L., Legendre, L., Reygondeau, G., Uitz, J., Stemmann, L. and Henson, S. A. 2015. A new look at ocean carbon remineralization for estimating deepwater sequestration, *Global Biogeochemical Cycles*, vol. 29, no. 7, pp. 1044–1059. DOI: 10.1002/2014GB005063.

Hedges, J. I. 1992. Global biogeochemical cycles: progress and problems, *Marine Chemistry*, vol. 39, no. 1, pp. 67–93. DOI: 10.1016/0304-4203(92)90096-S.

Heilbronner, R. and Barrett, S. 2013. *Image Analysis in Earth Sciences: Microstructures and Textures of Earth Materials*, Springer Science & Business Media.

Iversen, M. H., Nowald, N., Ploug, H., Jackson, G. A. and Fischer, G. 2010. High resolution profiles of vertical particulate organic matter export off Cape Blanc, Mauritania: Degradation processes and ballasting effects, *Deep-Sea Research Part I-Oceanographic Research Papers*, vol. 57, no. 6, pp. 771–784. DOI: 10.1016/j.dsr.2010.03.007.

Iversen, M. H. and Ploug, H. 2010. Ballast minerals and the sinking carbon flux in the ocean: carbon-specific respiration rates and sinking velocity of marine snow aggregates, *Biogeosciences*, vol. 7, no. 9, pp. 2613–2624. DOI: 10.5194/bg-7-2613-2010.

Iversen, M. H. and Robert, M. L. 2015. Ballasting effects of smectite on aggregate formation and export from a natural plankton community, *Marine Chemistry*, Particles in aquatic environments: from invisible exopolymers to sinking aggregates, vol. 175, pp. 18–27. DOI: 10.1016/j.marchem.2015.04.009.

Jackson, G. A. and Checkley, D. M. 2011. Particle size distributions in the upper 100m water column and their implications for animal feeding in the plankton, *Deep Sea Research Part I: Oceanographic Research Papers*, vol. 58, no. 3, pp. 283–297. DOI: 10.1016/j.dsr.2010.12.008.

Jagt, H. van der, Friese, C., Stuut, J.-B. W., Fischer, G. and Iversen, M. H. 2018. The ballasting effect of Saharan dust deposition on aggregate dynamics and carbon export: Aggregation, settling, and scavenging potential of marine snow, *Limnology and Oceanography*, vol. 63, no. 3, pp. 1386–1394. DOI: 10.1002/lno.10779.

Jls, H., T, K. and Al, A. 1996. Marine snow derived from abandoned larvacean houses: sinking rates, particle content and mechanisms of aggregate formation, *Marine Ecology Progress Series*, vol. 141, pp. 205–215. DOI: 10.3354/meps141205.

Kilps, J. R., Logan, B. E. and Alldredge, A. L. 1994. Fractal dimensions of marine snow determined from image analysis of in situ photographs, *Deep Sea Research Part I: Oceanographic Research Papers*, vol. 41, no. 8, pp. 1159–1169. DOI: 10.1016/0967-0637(94)90038-8.

Laurenceau-Cornec, E., Trull, T., Davies, D., De La Rocha, C. and Blain, S. 2015. Phytoplankton morphology controls on marine snow sinking velocity, *Marine Ecology Progress Series*, vol. 520, pp. 35–56. DOI: 10.3354/meps11116.

Li, X.-Y. and Logan, B. E. 2001. Permeability of Fractal Aggregates, *Water Research*, vol. 35, no. 14, pp. 3373–3380. DOI: 10.1016/S0043-1354(01)00061-6.

Liu, E. J., Cashman, K. V. and Rust, A. C. 2015. Optimising shape analysis to quantify volcanic ash morphology, *GeoResJ*, vol. 8, pp. 14–30. DOI: 10.1016/j.grj.2015.09.001.

Marcos, Fu, H. C., Powers, T. R. and Stocker, R. 2012. Bacterial rheotaxis, *Proceedings of the National Academy of Sciences*, vol. 109, no. 13, pp. 4780–4785. DOI: 10.1073/pnas.1120955109.

Matsumoto, K. and Suganuma, A. 1977. Settling velocity of a permeable model floc, *Chemical Engineering Science*, vol. 32, no. 4, pp. 445–447. DOI: 10.1016/0009-2509(77)85009-4.

McDonnell, A. M. P. and Buesseler, K. O. 2010. Variability in the average sinking velocity of marine particles, *Limnology and Oceanography*, vol. 55, no. 5, pp. 2085–2096. DOI: 10.4319/lo.2010.55.5.2085.

McNown, J. S. and Malaika, J. 1950. Effects of particle shape on settling velocity at low Reynolds numbers, *Eos, Transactions American Geophysical Union*, vol. 31, no. 1, pp. 74–82. DOI: 10.1029/TR031i001p00074.

Mestre, M., Ruiz-González, C., Logares, R., Duarte, C. M., Gasol, J. M. and Sala, M. M. 2018. Sinking particles promote vertical connectivity in the ocean microbiome, *Proceedings of the National Academy of Sciences of the United States of America*, vol. 115, no. 29, pp. E6799–E6807. DOI: 10.1073/pnas.1802470115.

Nowald, N., Fischer, G., Ratmeyer, V., Iversen, M., Reuter, C. and Wefer, G. 2009. In-situ sinking speed measurements of marine snow aggregates acquired with a settling chamber mounted to the Cherokee ROV, *OCEANS 2009-EUROPE*, pp. 1–6. DOI: 10.1109/OCEANSE.2009.5278186.

Passow, U. 2002. Production of transparent exopolymer particles (TEP) by phyto- and bacterioplankton, *Marine ecology-progress series*, vol. 236, pp. 1–12.

Picheral, M., Guidi, L., Stemmann, L., Karl, D. M., Iddaoud, G. and Gorsky, G. 2010. The Underwater Vision Profiler 5: An advanced instrument for high spatial resolution studies of particle size spectra and zooplankton, *Limnology and Oceanography: Methods*, vol. 8, no. 9, pp. 462–473. DOI: 10.4319/lom.2010.8.462.

Ploug, H. 1999. A net-jet flow system for mass transfer and microsensor studies of sinking aggregates, *Marine Ecology - Progress Series*, vol. 176, pp. 279–290.

Ploug, H., Grossart, H. P., Azam, F. and Jørgensen, B. B. 1999. Photosynthesis, respiration, and carbon turnover in sinking marine snow from surface waters of Southern California Bight: Implications for the carbon cycle in the ocean., *Marine ecology-progress series*, vol. 179, pp. 1–11.

Ploug, H., Hietanen, S. and Kuparinen, J. 2002. Diffusion and advection within and around sinking, porous diatom aggregates, *Limnology and Oceanography*, vol. 47, no. 4, pp. 1129–1136. DOI: 10.4319/lo.2002.47.4.1129.

Ploug, H., Iversen, M. H. and Fischer, G. 2008. Ballast, sinking velocity, and apparent diffusivity within marine snow and zooplankton fecal pellets: Implications for substrate turnover by attached bacteria, *Limnology and Oceanography*, vol. 53, no. 5, pp. 1878–1886. DOI: 10.4319/lo.2008.53.5.1878.

Ploug, H. and Jørgensen, B. B. 1999. A net-jet flow system for mass transfer and microsensor studies of sinking aggregates, *Marine Ecology Progress Series*, vol. 176, pp. 279–290. DOI: 10.3354/meps176279.

Ploug, H., Terbrüggen, A., Kaufmann, A., Wolf-Gladrow, D. and Passow, U. 2010. A novel method to measure particle sinking velocity in vitro, and its comparison to three other in vitro methods, *Limnology and Oceanography: Methods:* vol. 8, pp. 386–393.

Raffel, M., Willert, C. E., Scarano, F., Kähler, C., Wereley, S. T. and Kompenhans, J. 2018. *Particle Image Velocimetry: A Practical Guide*, 3rd edn, Springer International Publishing. Available at https://www.springer.com/de/book/9783319688510.

Riley, J. S., Sanders, R., Marsay, C., Le Moigne, F. a. C., Achterberg, E. P. and Poulton, A. J. 2012. The relative contribution of fast and slow sinking particles to ocean carbon export, *Global Biogeochemical Cycles*, vol. 26, no. 1, p. GB1026. DOI: 10.1029/2011GB004085.

Rusconi, R., Guasto, J. S. and Stocker, R. 2014. Bacterial transport suppressed by fluid shear, *Nature Physics*, vol. 10, no. 3, pp. 212–217. DOI: 10.1038/nphys2883.

Schwinghamer, P., Anderson, D. M. and Kulis, D. M. 1991. Separation and concentration of living dinoflagellate resting cysts from marine sediments via density-gradient centrifugation, *Limnology and Oceanography*, vol. 36, no. 3, pp. 588–592. DOI: 10.4319/lo.1991.36.3.0588.

Silver, M. W., Gowing, M. M., Brownlee, D. C. and Corliss, J. O. 1984. Ciliated protozoa associated with oceanic sinking detritus, *Nature*, vol. 309, no. 5965, pp. 246–248. DOI: 10.1038/309246a0.

Stemmann, L., Jackson, G. A. and Ianson, D. 2004. A vertical model of particle size distributions and fluxes in the midwater column that includes biological and physical processes—Part I: model formulation, *Deep Sea Research Part I: Oceanographic Research Papers*, vol. 51, no. 7, pp. 865–884. DOI: 10.1016/j.dsr.2004.03.001.

Stocker, R. and Seymour, J. R. 2012. Ecology and physics of bacterial chemotaxis in the ocean, *Microbiology and molecular biology reviews: MMBR*, vol. 76, no. 4, pp. 792–812. DOI: 10.1128/MMBR.00029-12.

Stokes, G. G. 1851. On the Effect of the Internal Friction of Fluids on the Motion of Pendulums, *Transactions of the Cambridge Philosophical Society*, vol. 9, p. 8.

Thiele, S., Fuchs, B. M., Amann, R. and Iversen, M. H. 2014. Colonization in the photic zone and subsequent changes during sinking determines bacterial community composition in marine snow, *Applied and Environmental Microbiology*, p. AEM.02570-14. DOI: 10.1128/AEM.02570-14.

Tréguer, P., Légendre, L., Rivkin, R. T., Ragnueneau, O. and Dittert, N. 2003. Water column biogeochemstry below the euphotic zone, in Michael J. R. Fasham (ed), *Ocean Biogeochemistry: The Role of the Ocean Carbon Cycle in Global Change*, Springer-Verlag Berlin Heidelberg New York.

Utermöhl, von H. 1931. Neue Wege in der quantitativen Erfassung des Planktons. (Mit besonderer Berücksichtigung des Ultraplanktons)., *Verh. Int. Verein. Theor. Angew. Limnol., 5, 567–595.*

Volk, T. and Hoffert, M. I. 1985. Ocean Carbon Pumps: Analysis of Relative Strengths and Efficiencies in Ocean-Driven Atmospheric CO_2 Changes, in Sundquist, E. T. and Broecker, W. S. (eds), *The Carbon Cycle and Atmospheric CO_2: Natural Variations Archean to Present*, American Geophysical Union, pp. 99–110. Available at http://onlinelibrary.wiley.com/doi/10.1029/GM032p0099/summary.

White, F. M. 1974. *Viscous fluid flow*, McGraw-Hill.

Williams, W. E. 1966. Boundary effects in Stokes flow, *Journal of Fluid Mechanics*, vol. 24, no. 2, pp. 285–291. DOI: 10.1017/S0022112066000648.

Supplement

S1. Flow chamber modifications

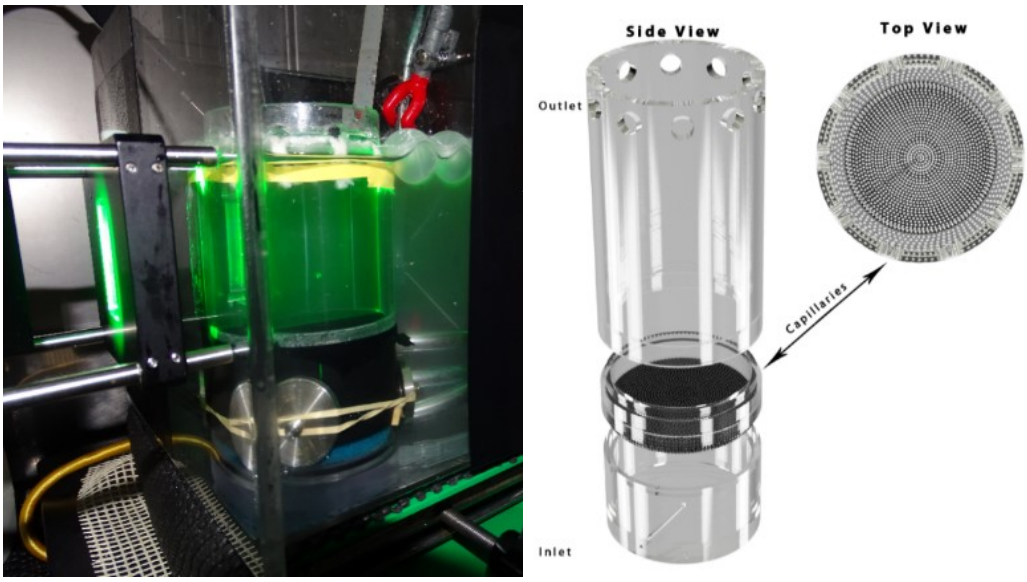

Figure S1. a) Flow chamber set-up on board B/O Sarmiento de Gamboa. The aggregate is freely suspended in the chamber and illuminated by a light sheet (green). a) Modified net-jet flow chamber with an optimized inlet to allow for an undisturbed laminar flow.

S2. Comparison of sizing methods and settling velocities

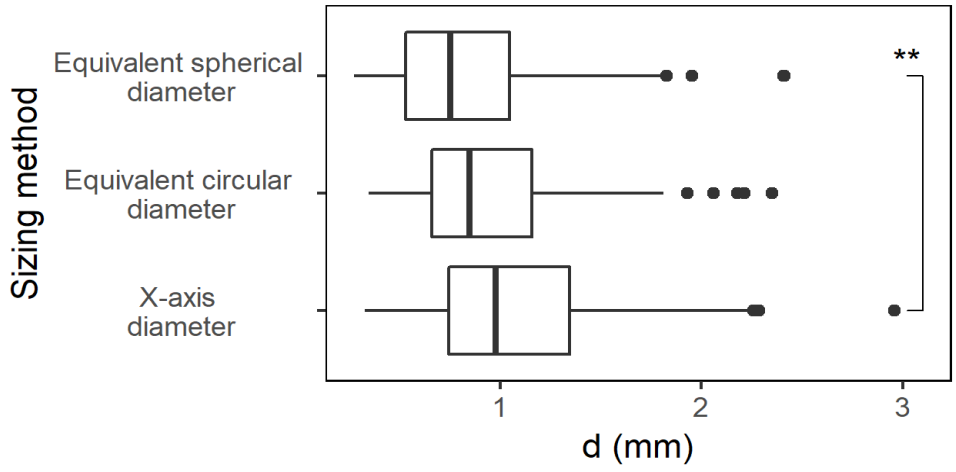

Figure S2. Differences in aggregate diameter based on the sizing method. Asterisks (*) denote a significant difference in SHD (pairwise t-test, p value adjustment method: Benjamini-Hochberg method).

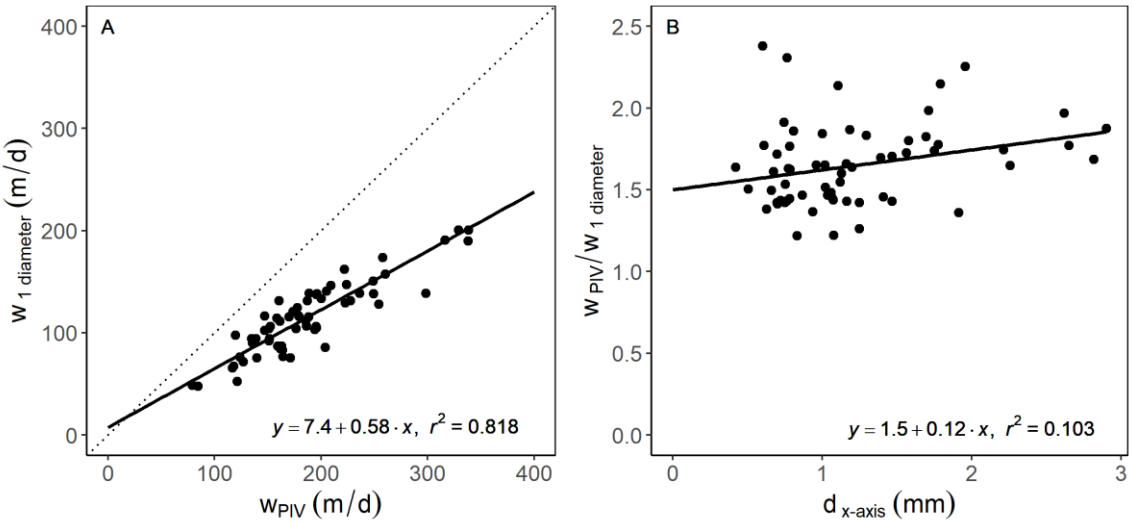

Figure S3. Size dependence of increase factor of settling velocity between PIV measured settling velocity and flow velocity-measured settling velocity (n=87).

S3. Comparison of solid hydrated densities

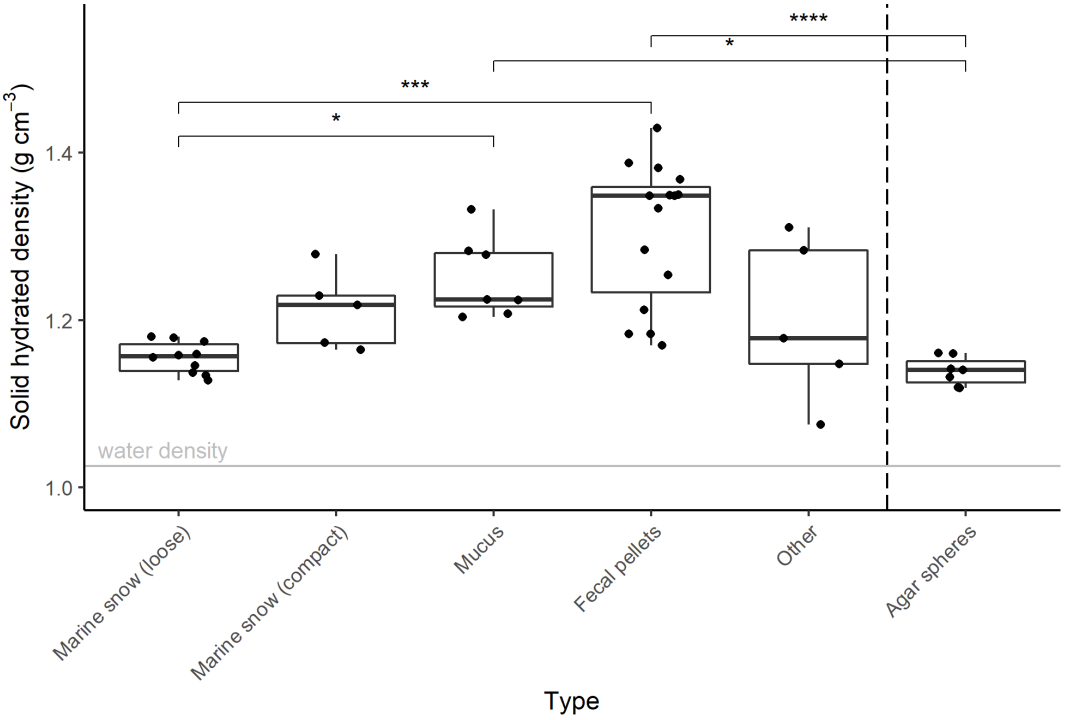

Figure S4. Comparison of solid hydrated density between different aggregate types. Asterisks (*) denote a significant difference in SHD (pairwise t-test, p value adjustment method: Benjamini-Hochberg method).

S4. Derivation of the drag coefficient from the fluid boundary layer thickness

In order to obtain a mathematical relation for the drag coefficient as a function of fluid boundary layer we considered stagnant spherically-shaped impermeable aggregate of radius R subjected to a constant upward velocity U_∞ at the far field. The Lattice Boltzmann method was employed to numerically solve the incompressible Navier-Stokes equations and to obtain the full velocity field around the aggregate (see Moradi et al. [2018] and references therein for model validation). The drag coefficient was calculated according to

$$C_D = \frac{2F}{\rho U_\infty^2 A} \tag{9}$$

in which F is the upward component of the total force acting on the aggregate by the fluid along the z direction, ρ is the fluid density and $A = \pi R^2$ is the reference area. The upward force and the fluid boundary layer (BL) were calculated using the Newton's second law of motion and the determination of the distance from the aggregate center at witch fluid velocity reached 90% of U_∞, respectively. In fig. 1 we have plotted the drag coefficient and its corresponding normalized boundary layer calculated at different far-field velocities.

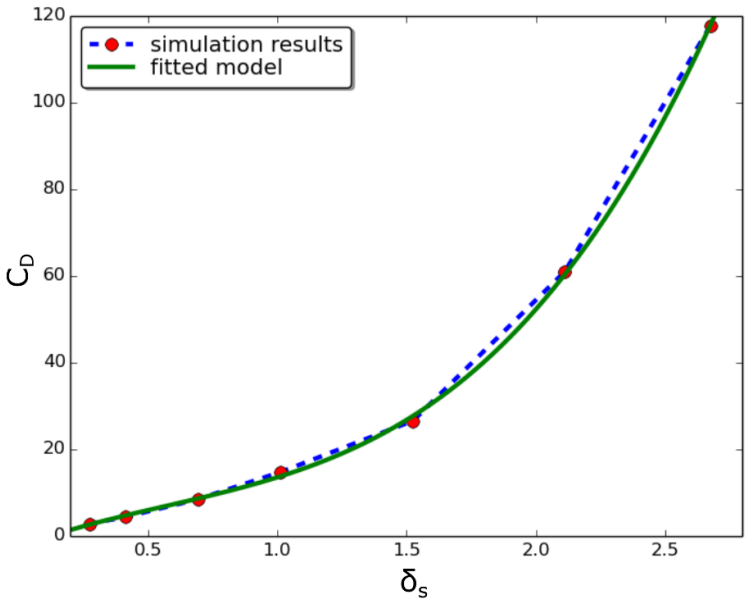

Figure S5. Drag coefficient plotted against the fluid boundary layer with simulation results vs the fitted model.

As shown, a cubic polynomial function given by

$$C_D = a + b\delta_s + c{\delta_s}^2 + d{\delta_s}^3 \quad (10)$$

with the fitting parameters a = 8.793, b = -15.046, c = 22.320 and d = -2.636 can mathematically relate the drag coefficient of sinking spherical aggregates and the fluid boundary layer for the considered range of Reynolds numbers ($0.02 \leq Re \leq 20$) where Re is defined based on aggregate diameter. In the above equation δ_s denotes the fluid boundary layer (δ) normalized by the x-axis diameter (d).

PAPER IV

Plastic microfibers reduce the efficiency of the biological carbon pump by decreasing the settling velocity of marine snow

Cordelia Roberts[1,2,3,†], Clara M. Flintrop[2,3,†], Alexander Khachikyan[4], Jana Milucka[4], Colin B. Munn[1], and Morten H. Iversen[2,3,*]

[1]School of Biological and Marine Sciences, University of Plymouth, Drake Circus, Plymouth, Devon PL4 8AA, United Kingdom
[2]Alfred Wegener Institute for Polar and Marine Research, Am Handelshafen 12, 27570 Bremerhaven, Germany
[3]MARUM and University of Bremen, Leobener Straße, 28359 Bremen, Germany
[4]Max-Planck-Institute for Marine Microbiology, Celsiusstr. 1, 28359 Bremen, Germany

[†]These authors have contributed equally

*Corresponding author email: morten.iversen@awi.de

Running head: Microplastics decrease vertical carbon flux in the ocean

Keywords: marine snow; sinking velocity; microplastics; microfibers; carbon export; biological carbon pump

Graphical abstract

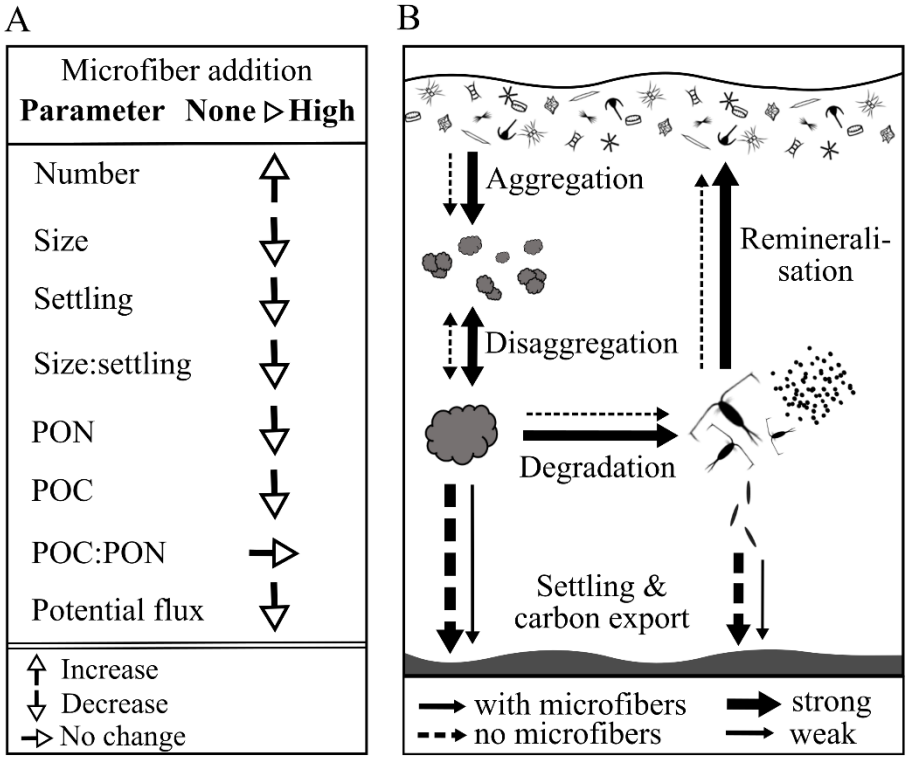

Abstract

Microplastics influence the transport of organic matter from the ocean surface to the deep sea by altering the settling behavior of marine aggregates. We formed diatom aggregates with differing concentrations of microfibers and observed that microfiber addition stimulated aggregate formation, but decreased structural cohesion and caused them to break apart more readily, resulting in a smaller average size. Microfiber addition also reduced the settling velocity of diatom aggregates in laboratory simulations of particle export using roller tanks. Slower sinking extends aggregate retention time in the upper ocean, thereby increasing the time available for organic matter remineralization in the upper water column. Our laboratory experiments suggest that microfiber concentrations typical of those occurring in the ocean decrease potential export flux by 30-60%. If confirmed in situ, this means that present day microfiber concentrations in surface waters may substantially reduce the efficiency of the biological carbon pump relative to the pre-plastic era.

Introduction

High production and usage of plastics in combination with poor waste management has resulted in enormous amounts of plastic litter in the oceans[1, 2]. Increasing amounts of plastic debris in the marine environment are affecting marine processes and ecosystem functioning [3, 4]. Plastic particles with sizes between 0.1 µm and 5 mm, referred to as microplastics [2], are of particular concern because of their pervasiveness in marine food webs [5, 6]. Microplastics originate from materials used in manufacturing, cosmetics, and washing machine effluent in the form of microfibers ("primary" microplastics) as well as from fragmentation of macroplastic debris ("secondary" microplastics) [1,7]. Of these, synthetic microfibers from washing machine effluent constitute the single largest source of marine primary microplastics [8, 9].

Microfibers have been observed to accumulate in deep sea sediments at concentrations up to four orders of magnitude higher than in surface waters [10]. This is at odds with the fact that most microfibers are positively buoyant [11,12] and it has therefore been hypothesized that microfibers reach the deep sea after incorporation into settling material such as marine snow [10,13]. Marine snow, i.e., aggregates larger than 0.5 mm, form through the aggregation of smaller particles, typically diatoms and other planktonic organisms, polymeric substances, cell debris and fecal pellets from protists and zooplankton[14, 15]. It is the settling of marine snow that drives the biological carbon pump (BCP) by exporting carbon fixed by phytoplankton from the surface to the deep ocean[16]. The efficiency of the BCP is determined by the turnover and settling velocity of marine snow[17-19].

Microplastics have been shown to be efficiently incorporated into aggregates, subsequently leading to the downward transport of microplastics in the water column [12,20]. At the same time, incorporation of microplastics into marine aggregates make them more buoyant and cause the aggregates to sink more slowly than they would without microplastic [12,21]. Most studies to date have focused on the transport of microfibers, but not on the impact from microplastic on particulate organic carbon (POC) export. To improve predictions of the efficiency of the BCP in a world with ever-increasing amounts of plastic [22], studies are needed to assess the impact of microfibers on the settling velocity of marine snow. In this

study, the ubiquitous diatom *Skeletonema marinoi* was incubated with four different concentrations of synthetic microfibers common in clothing fabrics to assess their influence on aggregation dynamics and settling velocity.

Results

Aggregate formation and structure

We incubated the diatom *Skeletonema marinoi* in roller tanks with four different microfiber concentrations: no microfibers and low, medium, and high concentrations of microfibers. The low and high concentrations were representative of microfiber concentrations observed in the English Channel and the Atlantic Ocean, respectively[37,38]. The aggregate sizes and settling velocities were determined from video recordings following the method by Ploug et al. [23] as described in Materials and Methods. During the first 48 h of roller tank incubation, aggregate formation followed a similar pattern in all treatments, with 7-10 comparably sized aggregates formed (fig. 1). Aggregation dynamics started to diverge between 48 h and 118 h: At zero, low, and medium microfiber concentrations, both the number and size of aggregates increased. At high microfiber concentration, average aggregate size also increased but the number of aggregates remained low. From 118h, there was a continued increase in larger aggregates accompanied by a decrease of smaller size classes in the control treatment with no added microfibers. This effect was not as pronounced in the treatments with added microfibers, especially at medium and high concentrations.

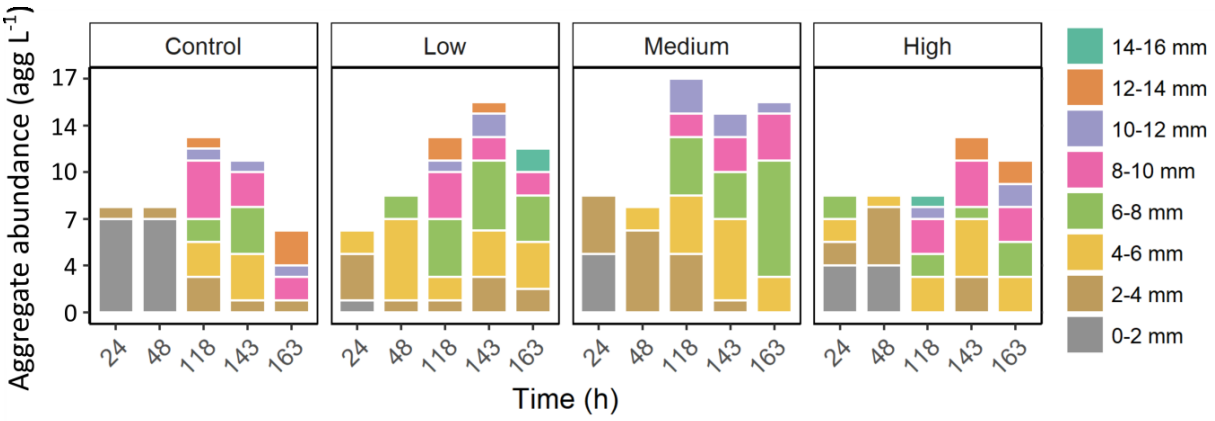

Figure 1. Aggregate abundances in the different size-bins throughout the study. Each panel show the distribution of aggregates sizes for the four different treatments: i) without addition of microfibers (Control) and for low, medium, and high amounts of microfibers added to the diatom (*S. marinoi*) incubations.

Aggregate settling velocity

We determine the size-specific sinking velocities of the formed aggregates in the different treatments at five time points during the incubations; 24 h, 48 h, 118 h, 143 h, and 163 h. Over the course of the experiment, some aggregates were observed to be positively buoyant, i.e., they were rising rather than sinking. These aggregates were only observed in the treatments to which microfibers were added, and overall the number of positively buoyant aggregates decreased over time (fig. 2): After 24 h of roller tank incubation, 22% of the aggregates in the microfiber treatments were rising with a mean velocity of 6.0 (±2.8) m d^{-1}. This decreased to only 10% of the aggregates at 48 h (10.9 (±5.2) m d^{-1}) and at 118 h none of the aggregates were rising. After 143 h, 10% of the aggregates in the microfiber treatments were rising with a mean velocity of 3.8 (±1.85) m d^{-1} (fig. 2).

A clear positive relationship between aggregate size and settling velocity was only established after 48 h (fig. 2). The size-to-settling relationship followed a power function for all treatments and the size-specific settling velocity was generally lower for the microfiber treatments compared to the control treatment without added microfibers (fig. 2). After 143 h we also observed that the size-specific sinking velocities decreased with increasing microfiber concentrations (fig. 2).

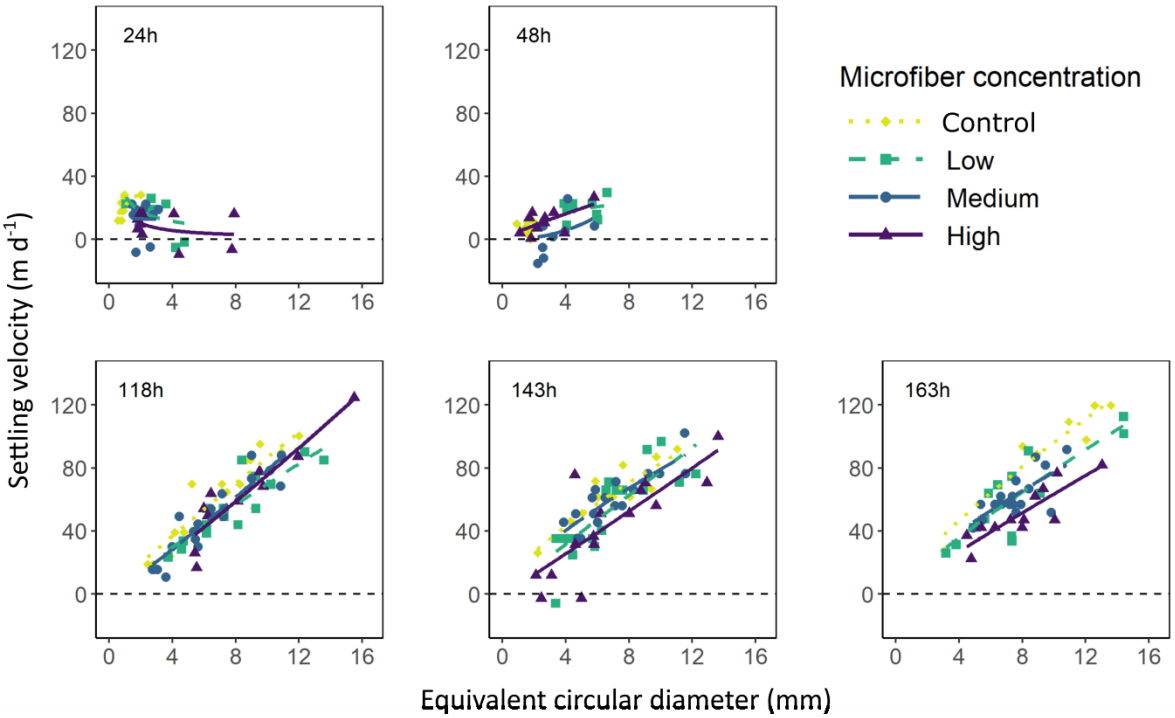

Figure 2. Aggregate settling velocities plotted against their equivalent circular diameter throughout the study. The microfiber was added in four concentrations: no addition of microfiber (None) and as low, medium and high concentration of microfibers. We only plotted the regression lines if their slope was significantly different from zero (Table S2).

Potential export flux

Total aggregated volume did not significantly differ between treatments ($\chi^2 = 5.8205$, df = 3, p = 0.1207) (fig. 3A). POC and PON (particulate organic nitrogen) content of individual aggregates decreased with increasing microfiber concentration, with a change in POC from 303 to 93 µgC per aggregate, and in PON from 40 to 12 µgN per aggregate (fig. 3B). Combined, the decrease in carbon content and decrease in size-specific settling velocity in the microfiber treatments resulted in a reduction in potential carbon flux compared to the control (fig. 3C). This reduction was up to 60% in the treatment with high microfiber concentrations (Table S1).

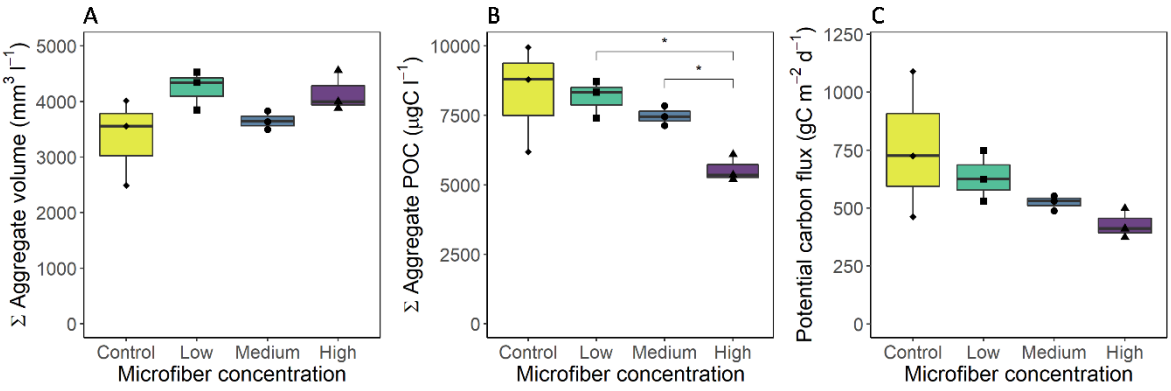

Figure 3. Total aggregate volume (A), total aggregated POC (B) and Potential POC flux (C) for aggregates averaged from days 5, 6, 7 from all treatments.

Discussion

In this study, we investigated the effect of microfibers on the formation and settling velocity of marine snow to assess how plastic pollution in the oceans might impact the efficiency of the biological pump. It has previously been suggested that marine aggregates are vehicles for vertical transport of buoyant microplastic to the seafloor[10, 12, 21]. Incorporation of microfibers into aggregates had a notable impact on their properties. The aggregates formed in microfiber treatments were more abundant, but smaller, and with lower settling velocities than aggregates in the control treatment, both of which have the potential to decrease the magnitude of export flux.

In general, a smaller aggregate will sink more slowly than a large aggregate of similar composition, but this was not the only reason for the observed lower sinking velocities. Size-specific sinking velocities also decreased as a function of increasing microfiber concentration. This indicates that the decrease in settling velocities observed in the microfiber treatments was due to increased buoyancy of the aggregates. In fact, during the first phase of the study we observed positively buoyant aggregates. However, over time the sinking velocities of the microfiber-rich aggregates did increase, which is typical for aging aggregates due to an increase in density over time [18].

The reduced settling velocity of aggregates in the treatments with added microfibers combined with lower carbon content led to a reduction of the estimated potential carbon flux compared to the treatment without microfibers. This reduction was

in the range of 30 to 60 % for microfiber concentrations typical of those found in the English Channel and Atlantic Ocean, respectively. We hypothesize that the reduction in carbon flux is likely even higher in situ, as reduced settling velocities would prolong the residence times of microfiber-containing aggregates in the ocean surface. Prolonged residence times would extend the time available for microbial remineralization in the upper water column, as well as increase the probability of encounters with aggregate-feeding zooplankton such as copepods[24-26,] salps[27], polychaetes [28], and protozoans [29, 30]. Together, this would result in higher microbial degradation and turnover of microfiber-containing aggregates in the upper water column where respiratory CO_2 production will be readily exchanged with the atmosphere. Hence, incorporation of buoyant microplastics into aggregates may substantially reduce the efficiency of the biological carbon pump in a high plastic world.

There has been an increase of plastic in solid waste from 1% in 1960 to 10% in 2005[31]. Geyer et al.[22] reported that in the year 2015, 6.3 million metric tons of plastic ended as up as waste products, with 79% accumulated in landfills or the natural environment. For 2010 alone, it is estimated that 4 to 12 million metric tons of plastic waste entered the oceans[31]. It is clear that all major ocean basins are already heavily contaminated by microplastics[32, 33,] and plastic debris is currently found throughout the marine environment[2]. This implies that the functioning of the biological carbon pump could already be compromised by microplastic pollution. Consequently leading to ocean services not working at peak efficiency in their efforts of mitigating the ever increasing atmospheric CO_2 levels via carbon sequestrations in the deep ocean and sediments.

Material and Methods

Microfiber composition and phytoplankton cultures

We used microfibers less than 3 mm in size in different concentration to form marine snow together with a constant concentration of diatoms. We determined the microfiber composition using a confocal Raman microscope (NTEGRA Spectra; NT-MDT, Eindhoven, The Netherlands). Spectra were acquired using an excitation line of 532-nm from the solid-

state laser and an Olympus 100x objective (NA = 0.9). Data were recorded using the software Nova_Px 3.1.0.0. (NT-MDT, Eindhoven, The Netherlands). The Raman spectra showed that the microfibers were primarily composed of dyed cotton and polyamide (fig. S1). This was identified from comparisons to known Raman spectra of dyed cotton and polyamide (Lepot et al. 2008). Still, some peaks within the spectra were unmatched (fig. S1), suggesting that the microfiber contained additional materials.

Cultures of *Skeletonema marinoi* (Sarno & Zingone)[35] were grown in GF/F-filtered Arctic seawater with salinity 32 enriched with f/2 medium[36] and silicate at a 1:1 molar ratio of silicate to nitrate. Cultures were grown at 15°C under a 14:10 h light:dark cycle at 150 µmol photons m^{-2} s^{-1} until they reached the stationary growth phase at 5.85 x 10^7 cells mL^{-1}.

Aggregate formation and settling velocity

Aggregates were formed by incubating *S. marinoi* cultures at a concentration of 5.4 x 10^4 cells mL^{-1} in four 1.15 L roller tanks and rotating them at 3 rpm at 15°C under low light conditions (~30 µmol photons m^{-2} s^{-1}). The microfiber concentrations added to each of the four roller tanks were representative of current oceanic concentrations:

i) low concentrations ("low") of 240 (±0.2) microfibers L^{-1}. This amount is close to concentrations found in the western English Channel (~ 270 microplastics L^{-1})[37],

ii) medium concentrations ("medium") of 680 (±0.9) microfibers L^{-1};

iii) high concentrations ("high") of 840 (±1.1) microfibers L^{-1}. This is in the range of concentrations found in the Atlantic Ocean (1150 microplastics L^{-1})[38],

iv) no fibers ("zero/control") were added to the fourth roller tank, which acted as a control without microfibers.

At five time points over a period of 163 hours (24h, 48h, 118h, 143h and 163h), recordings of the rotating tanks were made with a DSLR camera equipped with a 50 mm lens. This enabled detection of aggregates larger than 0.5 mm for measuring aggregate formation, size distribution, abundance, and size-specific settling velocities for each treatment. Aggregate size was measured using the projected area of each aggregate and calculating the equivalent circular diameter (ECD).

The video recordings were used to determine size-specific sinking velocities of the formed aggregates based on the method developed by Ploug et al [23]. This method is based on the observation that aggregates follow circular trajectories around a center (x_n) from which the settling velocity can be predicted knowing the distance between the aggregate orbit center to the center of the roller tank (x_b). A circle radius (R_n) was calculated for the center position of each aggregate using the equation

$$R_n = \sqrt{(\boldsymbol{x_n} - \boldsymbol{x_b})^2 + (\boldsymbol{y_n} - \boldsymbol{y_b})^2} \quad 1$$

where $\boldsymbol{x_n}$ and $\boldsymbol{y_n}$ are the particle positions, n= 1, 2, ..., N, and $(\boldsymbol{x_b}, \boldsymbol{y_b})$ is the putative centre of the aggregate orbit. Using the radii and the orbit center position an idealized circle was plotted. The circle was manipulated to find the best fit of the actual aggregate orbit, R_n, to the center position for each aggregate. The value produced for x_b was used to calculate the aggregate settling velocity using the equation

$$x_b = \frac{\boldsymbol{W_s}}{\boldsymbol{\omega}} = w_s \times \frac{T}{2\pi} \quad 2$$

where w_s is the settling velocity of the aggregate (cm s^{-1}), $\omega = 2\pi/T$ is the rotation rate (s^{-1}) and T is the rotation period of the roller tank.

Potential export flux

At the end of the experiment, one aggregate of known volume from each of the four treatments was filtered onto 25 µm pre-weighed GF/F filters. Filters were dried at 40 °C for 48h and re-weighed on a Mettler Toledo (UMX2) balance with a sensitivity of ±0.1 µg to determine their volume-specific dry weight (DW). After fuming with hydrochloric acid, filters were measured with an EA mass spectrometer (EA-IRMS, ANCA-SL 20-20, Sercon Ltd. Crewe, UK) with a precision of ±0.7 µgC to determine the PON and POC content of aggregates. The potential export flux was estimated for each treatment as an average of the final three time points (118h, 143h and 163h) of the experimental period. This was done for each treatment by using the POC-to-volume ratio to determine the POC content per aggregate and multiplying with the measured settling velocity to get potential POC flux

from each aggregate. The potential POC flux was summed for all aggregates in each treatment to get total potential export flux using the equation

$$\int Flux = \int_{\mathbf{0}}^{\infty} \frac{POC_i}{V_w} \boldsymbol{w_i} \quad 3$$

where POC_i is the size-specific POC content (gC) of each aggregate, i= 1, 2, …, I, V_w is the water volume (0.00115 m^3 for the roller tanks used), and w_i is the settling velocity (m day^{-1}) of each aggregate, i= 1, 2, …, I.

Acknowledgments

We thank Christiane Lorentzen for POC and PON analyses. We thank Michael Cunliffe and Hannah Marchant for discussions during the writing of the manuscript. CR and CM are funded by the University of Plymouth, CR, CMF, and MHI are funded by the Alfred Wegener Institute Helmholtz Centre for Polar and Marine Research and the DFG-Research Centre/Cluster of Excellence "The Ocean in the Earth System", AK and JM are funded by the Max Planck Institute for Marine Microbiology. This study was funded by the HGF Young Investigator Group SeaPump "Seasonal and regional food web interactions with the biological pump": VH-NG-1000.

References

1. Thompson, R.C., Olsen, Y., Mitchell, R.P., Davis, A., Rowland, S.J., John, A.W.G., McGonigle, D., Russell, A.E. (2004). Lost at Sea: Where Is All the Plastic? *Science*. 304(5672):838. doi: 10.1126/science.1094559

2. Barnes, D.K.A., Galgani, F., Thompson, R.C., Barlaz, M. (2009). Accumulation and fragmentation of plastic debris in global environments. *Philosophical Transactions of the Royal Society of London B: Biological Sciences*. 363(1526):1985-98. doi:10.1098/rstb.2008.0205

3. Gregory, M.R. (1996). Plastic 'scrubbers' in hand cleansers: a further (and minor) source for marine pollution identified. *Marine Pollution Bulletin*. 32: 867-871. https://doi.org/10.1016/S0025-326X(96)00047-1

4. Andrady, A.L. and Neal, M.A. (2009). Applications and Societal Benefits of Plastics. *Philosophical Transactions of the Royal Society B: Biological Sciences*. 364: 1977-1984. https://doi.org/10.1098/rstb.2008.0304

5. Carbery, M., O'Connor, W. and Palanisami, T. (2018). Trophic transfer of microplastics and mixed contaminants in the marine food web and implications for human health. *Environment International*. **115**: 400–409. https://doi.org/10.1016/j.envint.2018.03.007.

6. Setälä, O., Lehtiniemi, M., Coppock, R. and Cole, M. Chapter 11 - Microplastics in Marine Food Webs. *Microplastic Contamination in Aquatic Environments*, Ed.: Zeng, E.Y. pp339–63. Elsevier, 2018. https://doi.org/10.1016/B978-0-12-813747-5.00011-4.

7. Ryan, P.G., Moore, C.J., van Franeker, J.A., Moloney, C.L. (2009). Monitoring the abundance of plastic debris in the marine environment. *Philosophical Transactions of the Royal Society B: Biological Sciences*. **364**: 1999-2012. https://doi.org/10.1098/rstb.2008.0207

8. Browne, M.A., Crump, P., Niven, S.J., Tueten, E., Tonkin, A., Galloway, T., Thompson, R.C. (2011). Accumulation of Microplastic on Shorelines Worldwide: Sources and Sinks. *Environmental Science and Technology*. **45**: 9175-9179. https://doi.org/10.1021/es201811s

9. Pirc, U., Vidmar, M., Mozer, A., Kržan, A. (2016). Emissions of microplastic fibers from microfiber fleece during domestic washing. *Environmental Science and Pollution Research*. **23**(21): 22206-22211. doi: 10.1007/s11356-016-7703-0)

10. Woodall, L.C., Sanchez-Vidal, A., Canals, M., Paterson, G.L.J., Coppock, R., Sleight, V., Calafat, A., Rogers, A.D., Narayanaswamy, B.E., Thompson, R.C. (2014). The deep sea is a major sink for microplastic debris. *Royal Society Open Science*. **1**: 140317. https://doi.org/10.1098/rsos.140317

11. Kaiser, D., Kowalski, N. and Waniek, J.J. (2017). Effects of Biofouling on the sinking behaviour of microplastics. *Environmental Research Letters* **12**(12): 124003. https://doi.org/10.1088/1748-9326/aa8e8b.

12. Porter, A., Lyons, B.P., Galloway, T.S., Lewis, C.N. (2018). The role of marine snows in microplastic fate and bioavailability. *Environmental Science and Technology*. **52**(12): 7111-7119. https://doi.org/10.1021/acs.est.8b01000

13. Van Cauwenberghe, L., Vanreusel, A., Mees, J., Janssen, C.R. (2013). Microplastic pollution in deep-sea sediments. *Environmental Pollution*. **182**: 495-499. https://doi.org/10.1016/j.envpol.2013.08.013

14. Alldredge, A.L., and Silver, M.W. (1988). Characteristics, dynamics, significance of marine snow. *Progress in Oceanography*. **20**(1): 41-82. https://doi.org/10.1016/0079-6611(88)90053-5

15. Alldredge, A.L. and Gotschalk, C.C., 1989. Direct observations of the mass flocculation of diatom blooms: characteristics, settling velocities and formation of diatom aggregates. *Deep Sea Research Part A. Oceanographic Research Papers*. **36**(2):159-171.https://doi.org/10.1016/0198-0149(89)90131-3

16. Volk, T., and Hoffert, M.I. Ocean Carbon Pumps: Analysis of Relative Strengths and Efficiencies in Ocean-Driven Atmospheric CO_2 Changes. In *The Carbon Cycle and Atmospheric CO_2: Natural Variations Archean to Present*. Ed.: Sundquist, E.T. and Broecker, W.S. pp99–110. American Geophysical Union. 1985. https://doi.org/10.1029/GM032p0099

17. Ploug, H., Grossart, H-P., Azam, F., Jørgsen, B.B. (1999). Photosynthesis, respiration and carbon turnover in sinking marine snow from surface waters of Southern California Bight: implications for the carbon cycle in the ocean. *Marine Ecology Progress Series*. **179**: 1-11. doi:10.3354/meps179001

18. Ploug, H., Iversen, M.H. and Fischer, G. (2008). Ballast, sinking velocity, and apparent diffusivity within marine snow and zooplankton fecal pellets: Implications for substrate turnover by attached bacteria.*Limnology and Oceanography*.**53**(5): 1878-1886. https://doi.org/10.4319/lo.2008.53.5.1878

19. Iversen, M.H and Ploug, H., (2010). Ballast minerals and the sinking carbon flux in the ocean: carbon-specific respiration rates and sinking velocity of marine snow aggregates. *Biogeosciences*. **7**: 2613-2624. doi:10.5194/bgd-7-3335-2010

20. Michels, J., Stippkugel, A., Lenz, M., Wirtz, K., Engel, A. (2018). Rapid aggregation of biofilm-covered microplastics with marine biogenic particles. *Proceedings of the Royal Society B*: *Biological Sciences*. **285**(1885): 20181203. https://doi.org/10.1098/rspb.2018.1203.

21. Long, M., Moriceau, B., Gallinari, M., Lambert, C., Huvet, A., Raffray, J., Soudant, P. (2015). Interactions between microplastics and phytoplankton aggregates: Impact on their respective fates. *Marine Chemistry*. **175**: 39-46. https://doi.org/10.1016/j.marchem.2015.04.003

22. Geyer, R., Jambeck, J. R., Law, K. L. (2017). Production, use, and fate of all plastics ever made. *Science Advances* **3**(7): e1700782. doi:10.1126/sciadv.1700782

23. Ploug, H. Terbrüggen, A., Kaufmann, A., Wolf-Gladrow, D., Passow, U. (2010). A novel method to measure particle sinking velocity in vitro, and its comparison to three other in vitro methods. *Limnology and Oceangraphy: Methods*. **8**: 386-393. https://doi.org/10.4319/lom.2010.8.386

24. Lombard, F., Guidi, L. and Kiørboe, T. (2013). Effect of Type and Concentration of Ballasting Particles on Sinking Rate of Marine Snow Produced by the Appendicularian *Oikopleura dioica*. *PLoS ONE*. **8**: 9. https://doi.org/10.1371/journal.pone.0075676.

25. Poulsen, L.K. and Kiørboe. T. (2005). Coprophagy and Coprorhexy in the Copepods *Acartia tonsa* and *Temora longicornis*: Clearance Rates and Feeding Behaviour. *Marine Ecology Progress Series*. **299:** 217–27. https://doi.org/10.3354/meps299217

26. Iversen, M.H. and Poulsen, L.K. (2007). Coprohexy, coprophagy, and coprochaly in the copepods *Calanus helgolandicus, Pseudocalanus elongatus and Oithona similis. Marine Ecology Progress Series*. **350**: 79-89. https://doi.org.10.3354/meps07095

27. Iversen, M.H., Pakhomov, E.A., Hunt, B.P., van der Jagt, H., Wolf-Gladrow, D. and Klaas, C. (2017). Sinkers or floaters? Contribution from salp pellets to the export flux during a large bloom event in the Southern Ocean. *Deep Sea Research Part II: Topical Studies in Oceanography*. **138**: 116 -125. https://doi.org/10.1016/j.dsr2.2016.12.004.

28. Christiansen, S., Hoving, H.J., Schütte, F., Hauss, H., Karstensen, J., Körtzinger, A., Schröder, S.M., Stemmann, L., Christiansen, B., Picheral, M., Brandt, P. (2018). Particulate matter flux interception in oceanic mesoscale eddies by the polychaete *Poeobius sp.Limnology and Oceanography*. **63**(5): 2093-2109. https://doi.org/10.1002/lno.10926

29. Poulsen, L.K., and Iversen, M.H. (2008). Degradation of Copepod Fecal Pellets: Key Role of Protozooplankton". *Marine Ecology Progress Series*. **367**: 1–13. https://doi.org/10.3354/meps07611.

30. Poulsen, L.K., Moldrup, M., Berge, T., Hansen, P.J. (2011). Feeding on copepod fecal pellets: a new trophic role of dinoflagellates as detritivores. *Marine Ecology Progress Series*. **441**:65–78. https://doi.org/10.3354/meps09357.

31. Jambeck, J. R., Geyer, R., Wilcox, C., Siegler, T. R., Perryman, M., Andrady, A., Narayan, R., Law, K. L. (2015) Plastic waste inputs from land into the ocean. *Science* **347**:768–771. DOI: 10.1126/science.1260352

32. Gago, J., Carretero, O., Filgueiras, A. V., Vinas, L. (2018). Synthetic microfibres in the marine environment: A review on their occurrence in seawater and sediments. *Marine Pollution Bulletin*. **127**: 365-376. https://doi.org/10.1016/j.marpolbul.2017.11.070

33. Peeken, I., Primpke, S., Beyer, B., Gütermann, J., Katlein, C., Krumpen, T., Bergmann, M., Hehemann, L., Gerdts, G. (2018). Arctic sea ice is an important temporal sink and means of transport for microplastic. Nature Communications. **9**:1505. doi: 10.1038/s41467-018-03825-5

34. Lepot, L., De Wael, K., Gason, F., Gilbert, B. (2008). Application of Raman spectroscopy to forensic fibre cases. *Science and Justice*. **48**(3): 109-117. doi: 10.1016/j.scijus.2007.09.013.

35. Sarno, D., Kooistra, W.H., Medlin, L.K., Percopo, I., Zingone, A. (2005). Diversity in the genus *Skeletonema* (bacillariophyceae). ii. an assessment of the taxonomy of *S. costatum*-like species with the description of four new species 1. *Journal of phycology*. **41**(1):151-176. https://doi.org/10.1111/j.1529-8817.2005.04067.x

36. Guillard, R.R.L. (1975). Culture of phytoplankton for feeding marine invertebrates, in: *Culture of marine invertebrate animals*. Ed.: Smith, W.L., and Chanley, M.H. pp 29-60. Plenum Press, New York, London. https://doi.org/10.1007/978-1-4615-8714-9_3

37. Cole, M., Webb, H., Lindeque, P.K., Fileman, E.S., Halsband, C., Galloway, T.S. (2014). Isolations of microplastics in biota-rich seawater samples and marine organisms. *Scientific Reports*.**4**: 4528. https://doi.org/10.1038/srep04528

38. La Daana, K.K., Officer, R., Lyashevska, O., Thompson, R.C., O'Connor, I. (2017). Microplastic abundance, distribution and composition along a latitudinal gradient in the Atlantic Ocean. M*arine Pollution Bulletin*. **115**(1-2): 307-314. https://doi.org/10.1016/j.marpolbul.2016.12.025

Supplement

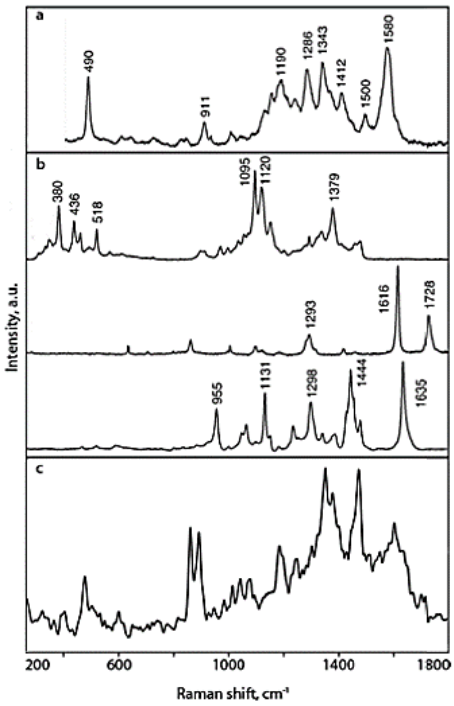

Figure S1. Raman spectra of rope sample used in experiments a, dyed cotton fiber; b (from top to bottom) undyed cotton, PET and polyamide; c, the rope sample.

Table S1. POC and PON content of aggregate, calculated flux of carbon calculated from each roller tank each corresponding to number of microfibers per liter at the end of the experiment (t_{fin}).

Treatment	Microfiber conc. (L^{-1})	POC ($\mu gC\ agg^{-1}$)	PON ($\mu gN\ agg^{-1}$)	Aggregates at t_{fin} (n)	Estimated flux ($gC\ m^{-2}\ d^{-1}$)	% decrease in flux compared to control
Control	0	302.84	39.69	7	1089.57	-
Low	240 (±0.2)	254.44	35.01	14	747.74	31
Medium	680 (±0.9)	222.57	27.30	18	531.58	51
High	840 (±1.1)	93.43	11.72	13	411.57	62

DISCUSSION

The methods developed in **Paper I** and **Paper II** to thin-section and stain structurally preserved marine aggregates visualized the ubiquity of microbial colonizers throughout the entire aggregate matrix. This is further confirmation of aggregates being microbial hotspots in the water column (Azam and Long, 2001; Azam, 1998) or, put another way, "cities of bacteria", where bacterial cell numbers can be 1-4 orders of magnitude higher than in the surrounding seascape, which in comparison is relatively sparsely populated (Thiele et al., 2014; Simon et al., 2002).

Despite the attractions of city life, there are stark differences in the bacterial assemblage in settling aggregates compared to the ambient water column (Bachmann et al., 2018; Mestre et al., 2018; Thiele et al., 2014; Fadeev et al., in prep.) once aggregates have settled out of the euphotic zone. This indicates that there is limited colonization of aggregates at depth, and suggests that changes in bacterial assemblages arise from successional dynamics rather than new colonization. **Paper I** and **Paper II** further show the high variability in structure and composition between aggregates, and, most importantly, within aggregates as well.

The microstructures within single aggregates give rise to a wide range of microniches that can enable successional divergence and affect how the particulate organic matter in marine aggregates is remineralized. **Paper III** shows high similarities between the flow fields of in situ collected aggregates and agar spheres, meaning that aggregate settling behavior is comparable to that of impermeable spheres and that aggregates are largely impermeable.

Without large channels that permit advective flow, diffusion kinetics control mass transfer, both within individual aggregates but also between aggregates and the ambient water column. Additionally, the diffusion kinetics create strong gradients of gases (e.g., O_2) but also solutes that can act as attractants for nearby colonizers, e.g., bacteria and grazing zooplankton. This supports previous studies that found marine

aggregates to be dominated by diffusion with little to no advection (Ploug and Passow, 2007; Ploug et al., 2002).

1. Bacterial motility and aggregate colonization

Before considering the processes by which bacteria colonize settling aggregates, it is important to remind oneself that marine aggregates do not start out as sterile particles that only get colonized during settling. All the constituents that make up the marine snow matrix, i.e., phytoplankton cells, fecal pellets, larvacean houses, and many more (see Introduction), are already inoculated with their own bacterial communities (Sapp et al., 2007) that inhabit their respective "phycospheres" (Seymour et al., 2007; Bell and Mitchell, 1972). This is supported by the ubiquity of bacterial cells throughout the aggregate matrix as visualized in **Paper I** and **Paper II** and is a likely contributor to the diversity of microniches inside marine aggregates.

Motility and aggregate formation

Colonization of single phytoplankton cells in the ocean surface is very different from colonizing a settling aggregate: Motility, and attachment of bacteria to suspended (e.g., phytoplankton) cell surfaces in the upper ocean is mediated via the excretion of EPS (Liu et al., 2016; Amin et al., 2012). EPS production has been correlated to enhanced biofilm formation (Amin et al., 2012; Rinta-Kanto et al., 2012) but their role in the formation of marine aggregates compared to, e.g., TEP (the anionic subclass of EPS) remains poorly understood. As a thought experiment, one could imagine that bacteria, after colliding with a phytoplankton cell in the ocean's euphotic zone, secrete EPS to move around in the phycosphere (Liu et al. 2016, Amin et al. 2012). Some classes of EPS, such as TEP, are sticky and glue particles together, which leads to the formation of larger particles with stronger chemical signatures (and stronger chemical gradients because clogging of pore space with EPS and TEP leads to impermeability). This will attract more colonizers, which then in a self-reinforcing process will produce more EPS, thus making the particles stickier, and eventually lead to the formation of marine snow.

EPS secretion may not only enhance aggregate formation, but also have a potentially long-lasting impact on aggregate structural properties: Imaging of aggregate thin-sectioning in **Paper I** showed channels in the Ruthenium Red-stained matrix with elevated bacterial cells concentrations, which could be a marine equivalent to certain soil bacteria that build EPS microchannels to direct bacterial motility and signaling (Berleman et al., 2016). Hence, detailed imaging of structurally preserved aggregates (**Paper I**) may provide information about the swarming behavior and gliding motility of bacteria inside aggregates, which can in turn help to better understand the microbial ecology and micro-niches within settling aggregates.

Motility and settling aggregates

Active attachment to settling aggregates requires chemotaxis that is rapid enough to enable crossing the fluid boundary layer and attaching to the aggregate before it has settled past (**Paper III**). Intuitively, one would assume that slow-settling particles are easier to colonize. However, there are many factors that play a role in microbial attachment and they are not easy to disentangle. For example, there is an inverse relationship between settling velocity and the thickness of the fluid boundary layer (**Paper III**). The thin fluid boundary layer coupled with strong chemical gradients associated with the diffusive boundary layer could mean that it is easier for bacteria to detect a fast-settling aggregate and cross the boundary to colonize it. In addition, the formation of stable vortices at the back of very fast settling aggregates (Re > ~5-15; fig. 1) can lead to a "back-flushing" of bacteria that are entrained in these vortices, and will be directed onto the aggregate surface. While we did not directly observe vortex formation in the PIV recordings, 6% of aggregates analyzed with PIV (n= 95) had Re > 10, indicating that there is a relevant fraction of marine aggregates that settle fast enough for colonization to happen via vortex formation at the back (**Paper III**).

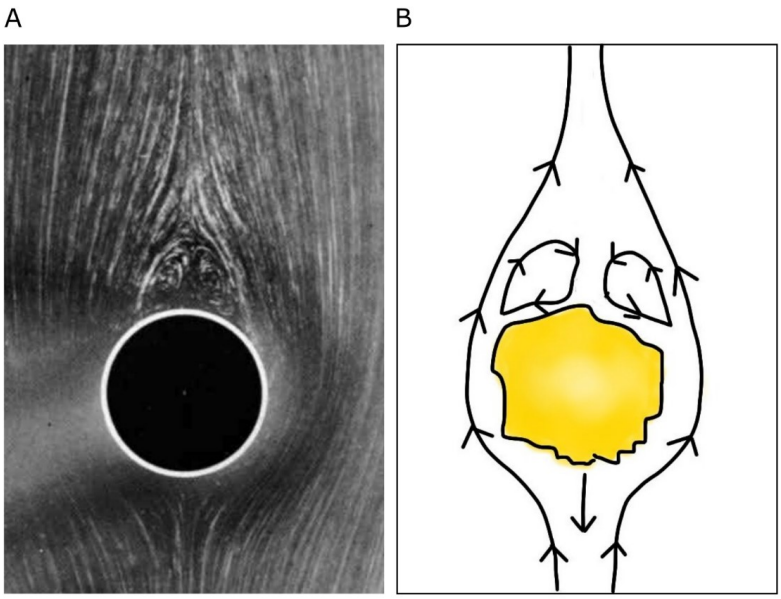

Figure 1. a) Flow around a cylinder at *Re=13*, with stable vortex formation at the back. Modified from (Dyke, 1982); b) schematic representation of a settling aggregate with similar *Re* with emphasis on the flow direction in the vortex cells that leads to the flushing of bacteria onto the aggregate surface. Image credit: Morten Iversen.

Motility and microstructures

Although aggregate flow fields obtained from particle image velocimetry indicate that marine aggregates behave like impermeable spheres and deflect flow around them as they sink (**Paper III**), model studies have shown that microstructures on the aggregate surface can lead to passive scavenging of smaller particles in a thin layer at the outer surface that is much smaller than the aggregate radius, but larger than the size of the primary particles (Stolzenbach, 1993). In fact, interflow across the aggregate surface can increase the collision efficiency with small particles (such as bacteria) by an order of magnitude for porosities that are typical in marine aggregates (Stolzenbach and Elimelech, 1994). Surface microstructures were visible in aggregate thin-sections, and likely contributed to the difficulty of defining the aggregate boundary (**Paper II**). Protruding structures were also seen in microscopic images of in situ collected aggregates (**Paper III**), as well as in the masked flow fields of aggregates analyzed with

PIV, where structures can be seen to extrude from the aggregate and into the fluid boundary, which has the potential to greatly enhance passive scavenging of bacteria (**Paper III**). Stolzenbach (1993) also showed that scavenging is independent of the porosity in the interior of the aggregate and will persist even with increasing compactness of aggregates caused by microbial degradation. This supports our suggestion that surface microstructures might intrude into the fluid boundary layer and scavenge minerals and non-motile bacteria as the aggregate sinks (**Paper III).**

Motility and settling aggregates- a case study

In an unpublished study, we separately incubated fluorescently stained chemotactic, motile *Marinobacter adherence*, and a non-motile *M. adherence* mutant (courtesy of Matthias Ullrich) with in situ collected marine snow in rotating exetainers to examine whether they showed differences in colonization efficiency over time. The study did not reveal statistically significant differences in aggregate colonization between the chemotactic, motile *M. adhaerens* and its non-motile mutant. Still, some trends may be teased out of the data and I cautiously suggest that the chemotactic, motile *M. adhaerens* strain showed somewhat higher colonization than the non-motile mutant, or that there was at least higher variability in aggregate colonization by the chemotactic *M. adhaerens* strain, which could even be indicative of detachment (fig. 2a, putative trends indicated by arrows). Furthermore, chemotactic *M. adhaerens* seemed to more efficiently colonize smaller aggregates compared to larger ones (fig. 2b), while there was no difference for the mutant strain. Because the mutant non-motile *M. adhaerens* still had its flagellar hook (just visible in fig. 2d below the letter) it is also possible that they were passively scavenged by surface microstructures of the aggregates as outlined above, meaning that the difference in colonization would have been even more pronounced with a non-motile mutant that did not have any appendages.

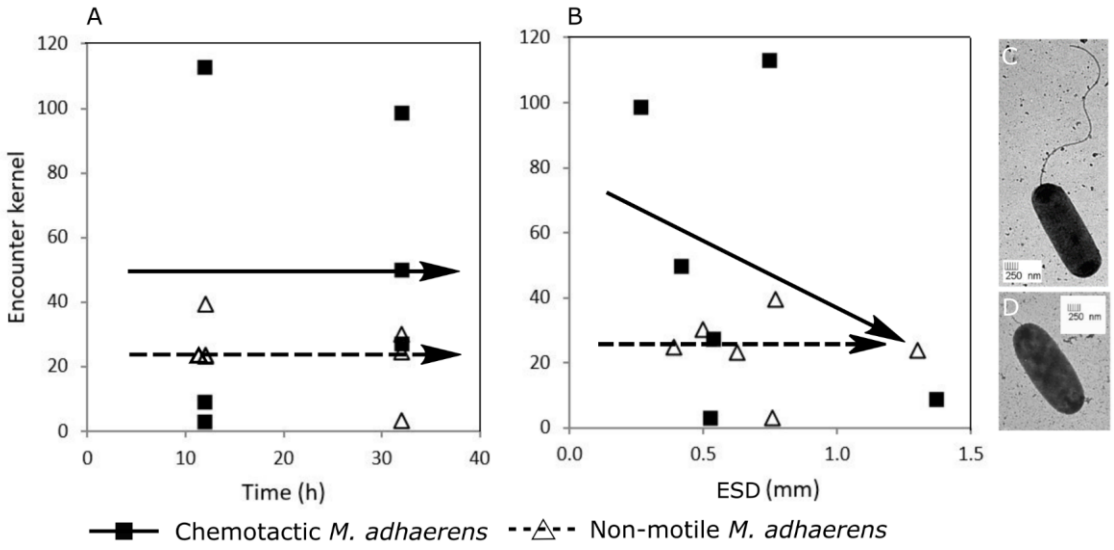

Figure 2. Differences in colonization efficiency a) over time, and b) in relation to aggregate size between c) the chemotactic *M. adhaerens* wild type and d) the non-motile mutant *M. adhaerens* ΔfliC. The encounter kernel is the factor of attached to non-attached cells, taking into account the settling velocity and surface area of the aggregates. The arrows in panel a) and b) show the mean of all values, except for chemotactic *M. adhaerens* in panel b), which is the linear regression to the data ($Encounter\ kernel = -39 \times ESD + 76$, R^2 = 0.12). Images of *M. adhaerens* are modified from (Sonnenschein et al., 2011).

Motility and hydrodynamic trapping

The observed differences in colonization efficiency of the chemotactic *M. adhaerens* with changing aggregate size may be partially explained by the effect of hydrodynamic trapping on the colonization of sinking aggregates (Desai et al., 2019). Hydrodynamic trapping describe hydrodynamic interactions between a settling aggregate and a motile bacterium that result in the bacterial cell becoming temporarily trapped in the near-surface flow field of the aggregate (Desai et al., 2019). The "critical trapping radius" as Desai et al. (2019) called it in their model paper, is dependent on aggregate size and excess density, and hydrodynamics-mediated trapping of bacteria based on the marine snow measurements in **Paper III** was calculated to occur at excess densities of

10^{-4} to 10^{-3} g/cm^3 and an ESD between 0.4 mm and 1.3 mm. This covers a broad range of aggregates collected in **Paper III,** suggesting that hydrodynamic trapping could be a frequent occurrence in situ.

The model by Desai et al. (2019) did not allow contact between the bacteria and the aggregate surface which led to tangential movement of bacteria along the surface of the aggregate and the possibility to rotate away and escape from the aggregate. Although detachment from surfaces has been observed in aggregate colonizers (Kiørboe et al., 2003), the presence of microstructure on the aggregate surface (**Paper I**, **Paper II**, **Paper III**), as described above, would more likely lead to more permanent bacterial scavenging by settling aggregates.

2. Microbial metabolism in aggregate microniches

Marine aggregates are hotspots of bacterial activity that are structurally and compositionally diverse and support highly variable microniches (**Paper I** and **Paper II**). Niche-partitioning can occur at the single-aggregate level as well as the sub-aggregate level. Duret et al. (2019) found two different metabolic strategies (*K*- and *r*-strategists) on suspended versus settling aggregates, respectively, which they related to difference in organic matter lability between the two aggregate types. This creates a close link to microniches inside aggregates. For example, fig. 3d of **Paper I** shows a copepod appendage which is densely colonized by bacteria (stained in blue). Since copepod carapaces are made from chitin (Kirchner, 1995), it may be assumed that the colonizing bacteria were chitin degraders. Targeted staining of taxonomic groups known to degrade specific compounds (e.g., chitin) using FISH-hybridization techniques (**Paper I**) can be used to further characterize such microniches within aggregates. In OMZs, the probability of anoxic microniches forming are higher because of the low ambient concentration. Ploug and Bergkvist (2015) found that the center of marine aggregates may already become anoxic at ambient O_2 concentrations below 100 µM. OMZs are only scarcely populated by zooplankton (Wishner et al., 2013), and

microbial remineralization is likely the most important turnover process of organic aggregates within OMZs (Cavan et al., 2017). It is therefore important to better understand the oxygen distribution within aggregates settling through OMZs to determine their importance for nutrient cycling such as denitrification and sulfate reduction in aggregates (e.g., Klawonn et al., 2015; Ploug et al., 1997; Paerl and Prufert, 1987). Aggregate embedding and thin-sectioning can improve the characterization of anoxic microniches and show where in the aggregate nitrogen cycling occurs. In combination with nanoSIMS and FISH it can be possible to determine rates and identify functional groups that drive these processes (**Paper I** and **Paper II).**

3. Retention time and colonization of slow-settling, porous aggregates

Plastic microfiber incorporation into marine snow acts as an anti-ballasting agent (**Paper IV**) that decreases the settling of marine aggregates and reduces the magnitude of C flux. This is opposite to the ballasting effects observed from incorporation of lithogenic materials which increase settling velocity and export of marine aggregates (Jagt et al., 2018; Iversen and Robert, 2015; Iversen et al., 2010; Rocha et al., 2008; Hamm, 2002).

While incorporation of microplastic into aggregates may only have a small effect in regions with high mineral ballasting, microplastics may prevent organic aggregates from settling in regions with little ballast from either lithogenic material and/or biominerals (**Paper IV**). For example, in regions with high abundances of *Phaeocystis* spp. and high concentrations of microplastics, such as the Arctic Ocean (Bergmann et al., 2017), it is likely that microplastic incorporation can retain organic aggregates in the upper water column where they are recycled.

It is important to emphasize that a decrease in aggregate settling velocity and volumetric carbon content already had the potential to reduce carbon export flux by up to 60%, and that aggregates do not have to become positively buoyant through incorporation of microfibers for microplastics to have an effect on marine carbon

cycling (**Paper IV**). Nevertheless, it is interesting to consider what ratios of microfibre content:solid matter content would stop aggregates from settling altogether. Azetsu-Scott and Passow (2004) used a model to examine the ratio of TEP content: solid matter content and its effect on aggregate buoyancy. Based on fig. 3 and Eq. 8 in Azetsu-Scott and Passow (2004), TEP in the model is replaced with plastic microfibers with an assumed density of 0.9 g/cm3 (Porter et al. 2018). By simulating microfiber incorporation into aggregates similar to those collected in **Paper III,** the buoyancy effect from microfibers can be evaluated for different ratios of microfiber content to (non-plastic-)solid matter content in: i) loose marine snow (ρ_s = 1.154 g cm^{-3}), ii) compact marine snow (ρ_s= 1.213 g cm^{-3}), iii) mucus aggregates (ρ_s = 1.257 g cm^{-3}) and iv) degraded fecal pellets (ρ_s = 1.302 g cm^{-3}) (fig. 3). The water density was averaged from values measured in **Paper III** (ρ_w = 1.025 g cm^{-3}).

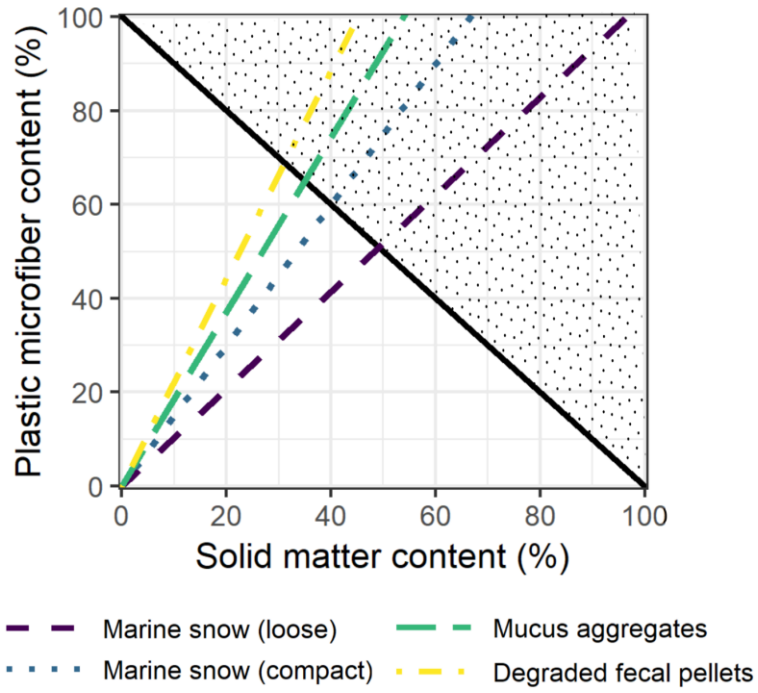

Figure 3 (previous page). Ratios of plastic microfiber content to (non-plastic-)solid matter content at which different types of aggregates would be rising (any plastic microfiber:solid matter ratio to the left of the respective regression line), settling (any plastic microfiber:solid matter ratio to the right of the respective regression line), or be neutrally buoyant (any plastic microfiber:solid matter ratio on the respective regression line). The solid line indicates the threshold where aggregates are made up completely of plastic and solids, with no interstitial water. The hatched area covers a scenario where the sum of solid matter content and plastic microfiber content is above 1. This scenario is impossible and was hatched for clarity.

For example, a mucus aggregate with 10% microfiber content and 20% solid matter content contains 70% porewater and is negatively buoyant. At constant solid matter content, it would become neutrally buoyant only if the plastic microfiber content rose to ~30%, thereby decreasing porewater content to 50%. The most interesting aspect, however, are the responses of different aggregate types to changing ratios of microplastic content to solid matter content: As loose marine snow had the lowest solid matter density of all aggregates collected in **Paper III**, a 1:1 ratio of plastic microfiber content to solid matter content would be enough to cause neutral buoyancy; compact marine snow requires a 3:2 ratio, mucus aggregates a 2:1 ratio, and degraded fecal pellets a slightly higher than 2:1 ratio. This is a conservative approach as samples were collected off the coast of Mauretania and were probably heavily dust-ballasted (Iversen et al., 2010). Secondly, this back-of-the-envelope-calculation does not take into account TEP content at all. The reduction of pore space filled with interstitial water by clogging with TEP was estimated to be between 10% and 30% (**Paper I** and **Paper II**), which suggests that the slopes for the respective aggregate types in fig. 3 will be even lower and that less plastic is needed to cause aggregates to be neutrally or positively buoyant.

In pycnoclines, the entrainment of porewater leads to the retention of aggregates at density interfaces where salinity increases (or decreases) with increasing depth (Prairie et al., 2013; Kindler et al., 2010). Without advective flow (**Paper III**) due to pore-clogging by TEP (**Paper I** and **Paper II**), this process is purely diffusion-limited

and becomes a function of aggregate size, excess density, and the strength of the density gradient. Climate change scenarios predict an increase in stratification in the ocean surface, i.e., an increase in the strength of density gradients. Water density can either decrease in the ocean surface relative to deeper water layers, for example due to meltwater discharge, or show a relative increase, for example due to evaporation. This can further exacerbate changes in export efficiency due to a change in phytoplankton community. For example, increasingly steep density gradients with depth due to meltwater discharge in the Arctic Ocean coupled to an increase in non-ballasted *Phaeocystis* spp. can increase remineralization in the surface ocean and limit particle export to depth.

Similarly, reduced settling velocities of microfiber-containing aggregates allow more time for degradation and remineralization of marine aggregates by bacteria and zooplankton in the upper water column. Natural marine snow has high remineralization rates, with 80% of the POC contained in a slow-settling aggregate being remineralized in the first 200 m of the water column via microbial degradation alone (Ploug et al., 1999). In addition to the reduced size-specific settling velocity, we also observed a reduction in average aggregate size **(Paper IV)**, which increases the surface:volume ratio of the microfiber-containing aggregates compared to those without microfibers. This can support colonization by microorganisms and potentially increase the turnover rate of the organic matter within aggregates (Cavan et al., 2017). All in all, increased residence time in the euphotic zone due to reduced settling velocities coupled with biofilm formation and increased bacterial activity will likely result in higher bacterial remineralization rates of marine snow with incorporated microplastics, as well as increased grazing by copepods and other zooplankton. From **Paper IV** and **Paper SI** we can expect some aggregates to settle more slowly in the future ocean compared to the present ocean. Decreased settling may cause higher turnover of aggregates in the surface ocean through increased microbial colonization, remineralization and zooplankton grazing, resulting in a decrease in carbon export and a less efficient biological carbon pump in the future ocean.

OUTLOOK

Following up on the findings and methods used in **Papers I-IV**, I am outlining four lines of research, and specific projects therein, that can further add to our ever-evolving understanding of the processes underlying the marine biological carbon pump:

Direct visualization of microbial attachment

Imaging the spatial distribution of selected taxonomic groups across aggregate thin-sections, especially in combination with specific substrates (**Paper I** and **Paper II**), is a powerful tool to detect and study microniches inside marine snow, and potentially infer life strategies of microbial and protozoan colonizers from their co-localization with each other and with substrates in the aggregate matrix.

Yet, thin-sectioning does not directly reveal the process of microbial attachment, and at what stage(s) of aggregation and aggregate settling the attachment happens. Because of dynamic aggregation and disaggregation processes, especially in the euphotic and upper mesopelagic zone, the localization of colonizers at the center of aggregates does not mean that they were there originally. While several studies on colonization of stagnant particles have been performed (see Introduction), the effect of hydrodynamic forcing on bacterial colonization (Desai et al., 2019) caused by aggregate flow fields (as visualized in **Paper III**) can only be studied on settling aggregates, and require a flow through system such as the modified flow chamber presented in **Paper III**.

To directly study bacterial attachment and aggregate colonization, a way of labelling and tracking bacteria incubated with marine snow is needed. Fluorescent labelling of bacteria with a live stain, as described earlier, or genetically-encoded fluorescent tags can be a way to visually track the attachment of bacteria to settling particles. Instead of using a closed system in which aggregates are rotating around a very small orbit, the modified flow chamber-system (**Paper III**) can be used.

Seeding of the water with fluorescently labelled bacteria instead of (or possibly in addition to) PIV seeding particles, could potentially directly visualize the interactions of motile and non-motile bacteria with the settling aggregate. This could be especially interesting with differently labelled motile and non-motile bacteria, for example the wild type chemotactic *M. adhaerens* together with motile non-chemotactic, and non-motile mutants of *M. adhaerens* (Stahl, 2015). Analogous to Smriga et al. (2016) this would enable video microscopy to track the trajectories of bacteria around the suspended aggregate. Furthermore, direct visualization and tracking of fluorescently-tagged bacteria can also reveal the extent of passive scavenging of non-motile bacteria by aggregate microstructures.

Direct visualization of metabolic heterogeneity

Spatially resolved single-cell uptake measurements of microbial colonizers using NanoSIMS on aggregate thin-sections (**Paper II**) are a powerful tool to detect microniches and characterize the flow of organic matter between living organisms inside aggregates at nanometer-scale resolution. However, isotope labelling poses certain limitations to studying in situ collected aggregates as opposed to laboratory-formed aggregates of enriched phytoplankton. Furthermore, difficulties of combining FISH with hard-resin embedding techniques presented in **Paper II** do not enable concurrent taxonomic characterization.

A complementary method that is potentially suited to study in situ collected aggregates is matrix-assisted laser desorption ionization mass spectrometry imaging (MALDI-MSI). MALDI-MSI enables analysis of biomolecules produced by organisms in marine snow, and can visualize niche partitioning and metabolic heterogeneity within single marine aggregates. Metabolic profiling of entire aggregates using mass spectrometry has revealed a comprehensive suite of metabolites present in marine snow that changes with depth (Johnson et al., 2018). The metaFISH pipeline developed by Geier et al. (2019) combines fluorescence in situ hybridization of colonizers (FISH) with

analysis of the spatial distribution of selected metabolic products (MALDI-MSI) and can be applied to aggregate thin-sections using methods developed in **Paper I** (pending modification of the embedding medium for MALDI-MSI).

For example, the presence of certain bacterial membrane lipids called hopanoids is strongly associated with microaerophilic environments (Blumenberg et al., 2013; Kharbush et al., 2013; Sáenz et al., 2011). There is evidence that an isomer of the common hopanoid bacteriohopanetetrol is linked to a producer that is more abundant in low-oxygen environments (Kharbusch et al., 2013). This way, hopanoids can act as biomarkers to identify microniches of anaerobic metabolism inside aggregates (Kharbusch et al., 2013). This method could also be used in combination with thin-sectioning to identify micro-scale distributions of hopanoid composition to visualize the low oxygen regions inside marine snow.

Direct visualization of aggregate pore space to model mass exchange and transport processes in marine aggregates

Without large channels that permit advective flow, diffusion kinetics control mass transfer within aggregates, and between aggregates and the ambient water column. Because the average apparent diffusivities of gases within aggregates is very close to the free diffusion coefficient in seawater (Ploug and Passow, 2007), it is the distances between the solid primary particles within aggregates (visualized in **Paper I** and **Paper II**), and the concentration gradients between the solid particles and the pore space, that will determine the direction and the rate of flux.

Although advective flow through aggregates is too negligible to influence aggregate settling (**Paper III**), multiscale microstructures can cause local advective flow within diffusion-limited aggregates. Yet, the effect of microscale advection on oxygen distribution, mass transport and reaction rates is not known (Chu et al., 2005; Chu and Lee, 2004). Respiratory carbon turnover rates are typically inferred from O_2 bulk measurements (e.g., Boyd et al., 2015) or at a single-aggregate level using O_2

microsensors (Ploug, 1999), but little is known about chemical reaction rates and exchange processes that occur at the sub-aggregate level, which can best be resolved by imaging pore-space connectivity.

We successfully reconstructed entire aggregates from consecutive thin-sections (**Paper I**), but the high precision needed for 3D-alignment to accurately resolve pore connectivity could not be obtained with this method. Furthermore, the minimum slicing thickness of 5-10 µm likely exceeded the minimum pore size, leading to omission of pore and a potential underestimation of porosity.

Instead, methods are needed that image solid components (and consequently, aggregate pore space) of marine snow at high resolution without the need to section the aggregate. One such method is synchrotron radiation micro-computed tomography (SRµCT). SRµCT can allow us to reconstruct the aggregate pore space at a spatial resolution high enough to generate a mesh for a transport model.

In combination with methods from **Paper I**, **Paper III**, and flow field modelling, SRµCT can be a comprehensive approach to investigate mass transport and microbial colonization at the single aggregate-level with the following workflow: (i) PIV to determine surrounding flow field and pressure distribution (**Paper III**), (ii) fix aggregates with formaldehyde solution for fluorescence in situ hybridization of bacterial colonizers (**Paper I**), (iii) embed aggregate in a resin suitable for matrix staining and FISH (based on methods developed in **Paper II**), (iv) scan with SRµCT, (v) use the output for transport-reaction modelling, e.g., with OpenFOAM (Weller et al., 1998). This multidisciplinary approach establishes a framework for comprehensive transport-reaction modelling and the results can give us insights into the mass exchange within single marine aggregates and the interaction of transport processes with microbial reactions.

Direct coupling of multiple stressor experiments with aggregation dynamics and carbon export

Several studies using multiple stressors have found changes in the growth and cellular stoichiometry of single phytoplankton species in response to projected future CO_2, temperature and light conditions in the ocean surface (Hoppe, Flintrop and Rost, 2018 [see **Paper SI** in Additional Publications]; Wolf et al., 2018; Trimborn et al., 2017). There is a reported shift in phytoplankton community composition from diatom-dominated silica-ballasted systems towards small flagellates, e.g., *Phaeocystis* sp. (Nöthig et al., 2015; Lasternas and Agustí, 2010) and eukaryotic picoplankton (Li et al., 2009) e.g., *Micromonas pusilla*, all leading to less ballasted aggregates.

A change in primary particle composition can heavily impact aggregation dynamics, physical aggregate properties, and aggregate settling velocity (**Paper IV**) of diatoms, and a shift to non-ballasted picoplankton- or flagellate-based systems can have a pervasive impact on C cycling and export flux in these regions. However, these aspects have so far not been coupled to studies exploring the effect of multiple stressors on phytoplankton communities.

To assess the potential for future biological CO_2 sequestration in regions with shifts in phytoplankton community composition from silica-ballasted, diatom-dominated systems towards systems where non-ballasted picoplankton (**Paper SI**) and/or small flagellates like *Phaeocystis* spp. dominate, multiple stressor experiments (**Paper SI)** are necessary to characterize individual responses of phytoplankton functional groups to changes in environmental conditions in the field as well as in the laboratory. Followed by analyses of taxon-specific (dis)aggregation dynamics and settling velocity measurement according to the experimental set-up in **Paper IV,** this can directly relate changes in phytoplankton community composition to C export and burial.

CONCLUDING REMARKS

With this thesis, I have attempted to draw a comprehensive picture of the dynamic environment in which aggregates and their colonizers exist, and of the processes underlying the formation, settling, and degradation of marine snow. The physical forces acting on objects the size of bacteria and aggregates are difficult to comprehend for us who live in a world dominated by inertia. Still, I hope to have made a convincing appeal for the importance of not only studying the biochemical, but also the biophysical world surrounding settling marine aggregates to better understand the processes that control carbon export in the ocean. The research in this thesis has resulted in the development of methods to image the composition, microstructure and settling behavior of natural marine aggregates at a single- and even sub-aggregate level. These methods can, and should, be developed further for a comprehensive characterization of aggregate colonization, and subsequent degradation. Synthesizing the results of this thesis has given rise to several interesting ideas and hypotheses that may be investigated further as presented in the Outlook. This thesis may only be a small contribution, but by joining efforts we every day edge closer to a more thorough understanding of the processes supporting life on our planet, and how we have to change to be able to inhabit it in the more distant future.

REFERENCES

Amin, S. A., Parker, M. S. and Armbrust, E. V. 2012. Interactions between Diatoms and Bacteria, *Microbiology and Molecular Biology Reviews*, vol. 76, no. 3, pp. 667–684. DOI: 10.1128/MMBR.00007-12.

Azam, F. 1998. Microbial Control of Oceanic Carbon Flux: The Plot Thickens, *Science*, vol. 280, no. 5364, pp. 694–696. DOI: 10.1126/science.280.5364.694.

Azam, F. and Long, R. A. 2001. Sea snow microcosms, *Nature*, vol. 414, no. 6863, p. 495. DOI: 10.1038/35107174.

Azetsu-Scott, K. and Passow, U. 2004. Ascending marine particles: Significance of transparent exopolymer particles (TEP) in the upper ocean, *Limnology and Oceanography*, vol. 49, no. 3, pp. 741–748. DOI: 10.4319/lo.2004.49.3.0741.

Bachmann, J., Heimbach, T., Hassenrück, C., Kopprio, G. A., Iversen, M. H., Grossart, H. P. and Gärdes, A. 2018. Environmental Drivers of Free-Living vs. Particle-Attached Bacterial Community Composition in the Mauritania Upwelling System, *Frontiers in Microbiology*, vol. 9. DOI: 10.3389/fmicb.2018.02836.

Bell, W. and Mitchell, R. 1972. Chemotactic and growth responses of marine bacteria to algal extracellular products, *The Biological Bulletin*, vol. 143, no. 2, pp. 265–277. DOI: 10.2307/1540052.

Bergmann, M., Wirzberger, V., Krumpen, T., Lorenz, C., Primpke, S., Tekman, M. B. and Gerdts, G. 2017. High Quantities of Microplastic in Arctic Deep-Sea Sediments from the HAUSGARTEN Observatory, *Environmental Science & Technology*, vol. 51, no. 19, pp. 11000–11010. DOI: 10.1021/acs.est.7b03331.

Berleman, J. E., Zemla, M., Remis, J. P., Liu, H., Davis, A. E., Worth, A. N., West, Z., Zhang, A., Park, H., Bosneaga, E., van Leer, B., Tsai, W., Zusman, D. R. and Auer, M. 2016. Exopolysaccharide microchannels direct bacterial motility and organize multicellular behavior, *The ISME Journal*, vol. 10, no. 11, pp. 2620–2632. DOI: 10.1038/ismej.2016.60.

Blumenberg, M., Berndmeyer, C., Moros, M., Muschalla, M., Schmale, O. and Thiel, V. 2013. Bacteriohopanepolyols record stratification, nitrogen fixation and other biogeochemical perturbations in Holocene sediments of the central Baltic Sea, *Biogeosciences*, vol. 10, no. 4, pp. 2725–2735. DOI: https://doi.org/10.5194/bg-10-2725-2013.

Boyd, P. W., McDonnell, A., Valdez, J., LeFevre, D. and Gall, M. P. 2015. RESPIRE: An in situ particle interceptor to conduct particle remineralization and microbial dynamics studies in the oceans' Twilight Zone, *Limnology and Oceanography: Methods*, vol. 13, no. 9, pp. 494–508. DOI: 10.1002/lom3.10043.

Cavan, E. L., Trimmer, M., Shelley, F. and Sanders, R. 2017. Remineralization of particulate organic carbon in an ocean oxygen minimum zone, *Nature Communications*, vol. 8, p. 14847. DOI: 10.1038/ncomms14847.

Chu, C. P. and Lee, D. J. 2004. Multiscale structures of biological flocs, *Chemical Engineering Science*, Complex Systems and Multi-scale Methodology, vol. 59, no. 8, pp. 1875–1883. DOI: 10.1016/j.ces.2004.01.040.

Chu, C. P., Lee, D. J. and Tay, J. H. 2005. Floc model and intrafloc flow, *Chemical Engineering Science*, vol. 60, no. 2, pp. 565–575. DOI: 10.1016/j.ces.2004.07.132.

Desai, N., Shaik, V. A. and Ardekani, A. M. 2019. Hydrodynamic Interaction Enhances Colonization of Sinking Nutrient Sources by Motile Microorganisms, *Frontiers in Microbiology*, vol. 10. DOI: 10.3389/fmicb.2019.00289.

Duret, M. T., Lampitt, R. S. and Lam, P. 2019. Prokaryotic niche partitioning between suspended and sinking marine particles, *Environmental Microbiology Reports*, vol. 11, no. 3, pp. 386–400. DOI: 10.1111/1758-2229.12692.

Dyke, M. V. 1982. Album of Fluid Motion, The Parabolic Press.

Geier, B. K., Sogin, E., Michellod, D., Janda, M., Kompauer, M., Spengler, B., Dubilier, N. and Liebeke, M. 2019. Spatial metabolomics of in situ, host-microbe interactions, *bioRxiv*, p. 555045. DOI: 10.1101/555045.

Hamm, C. E. 2002. Interactive aggregation and sedimentation of diatoms and clay-sized lithogenic material, *Limnology and Oceanography*, vol. 47, no. 6, pp. 1790–1795. DOI: 10.4319/lo.2002.47.6.1790.

Hoppe, C. J. M., Flintrop, C. M. and Rost, B. 2018. The Arctic picoeukaryote Micromonas pusilla benefits synergistically from warming and ocean acidification, *Biogeosciences*, vol. 15, no. 14, pp. 4353–4365. DOI: https://doi.org/10.5194/bg-15-4353-2018.

Iversen, M. H., Nowald, N., Ploug, H., Jackson, G. A. and Fischer, G. 2010. High resolution profiles of vertical particulate organic matter export off Cape Blanc, Mauritania: Degradation processes and ballasting effects, *Deep-Sea Research Part I-Oceanographic Research Papers*, vol. 57, no. 6, pp. 771–784. DOI: 10.1016/j.dsr.2010.03.007.

Iversen, M. H. and Robert, M. L. 2015. Ballasting effects of smectite on aggregate formation and export from a natural plankton community, *Marine Chemistry*, Particles in aquatic environments: from invisible exopolymers to sinking aggregates, vol. 175, pp. 18–27. DOI: 10.1016/j.marchem.2015.04.009.

Jagt, H. van der, Friese, C., Stuut, J.-B. W., Fischer, G. and Iversen, M. H. 2018. The ballasting effect of Saharan dust deposition on aggregate dynamics and carbon export: Aggregation, settling, and scavenging potential of marine snow, *Limnology and Oceanography*, vol. 63, no. 3, pp. 1386–1394. DOI: 10.1002/lno.10779.

Johnson, W. M., Longnecker, K., Soule, M. C. K., Arnold, W. A., Bhatia, M. P., Hallam, S. J., Mooy, B. A. S. V. and Kujawinski, E. B. 2018. Metabolite composition of sinking particles reflects a changing microbial community and differential metabolite degradation, *bioRxiv*, p. 459461. DOI: 10.1101/459461.

Kharbush, J. J., Ugalde, J. A., Hogle, S. L., Allen, E. E. and Aluwihare, L. I. 2013. Composite Bacterial Hopanoids and Their Microbial Producers across Oxygen Gradients in the Water Column of the California Current, *Applied and Environmental Microbiology*, vol. 79, no. 23, pp. 7491–7501. DOI: 10.1128/AEM.02367-13.

Kindler, K., Khalili, A. and Stocker, R. 2010. Diffusion-limited retention of porous particles at density interfaces, *Proceedings of the National Academy of Sciences of the United States of America*, vol. 107, no. 51, pp. 22163–22168. DOI: 10.1073/pnas.1012319108.

Kiørboe, T., Tang, K. W., Grossart, H. P. and Ploug, H. 2003. Dynamics of microbial communities on marine snow aggregates : Colonization, growth, detachment, and grazing mortality of attached bacteria, *Applied and Environmental Microbiology*, vol. 69, no. 6, pp. 3036–3047.

Kirchner, M. 1995. Microbial colonization of copepod body surfaces and chitin degradation in the sea, *Helgoländer Meeresuntersuchungen*, vol. 49, no. 1, pp. 201–212. DOI: 10.1007/BF02368350.

Klawonn, I., Bonaglia, S., Brüchert, V. and Ploug, H. 2015. Aerobic and anaerobic nitrogen transformation processes in N2-fixing cyanobacterial aggregates, *The ISME journal*, vol. 9, no. 6, pp. 1456–1466. DOI: 10.1038/ismej.2014.232.

Lasternas, S. and Agustí, S. 2010. Phytoplankton community structure during the record Arctic ice-melting of summer 2007, *Polar Biology*, vol. 33, no. 12, pp. 1709–1717. DOI: 10.1007/s00300-010-0877-x.

Li, W. K. W., McLaughlin, F. A., Lovejoy, C. and Carmack, E. C. 2009. Smallest Algae Thrive As the Arctic Ocean Freshens, *Science*, vol. 326, no. 5952, pp. 539–539. DOI: 10.1126/science.1179798.

Liu, A., Mi, Z.-H., Zheng, X.-Y., Yu, Y., Su, H.-N., Chen, X.-L., Xie, B.-B., Zhou, B.-C., Zhang, Y.-Z. and Qin, Q.-L. 2016. Exopolysaccharides Play a Role in the Swarming of the Benthic Bacterium Pseudoalteromonas sp. SM9913, *Frontiers in Microbiology*, vol. 7. DOI: 10.3389/fmicb.2016.00473.

Mestre, M., Ruiz-González, C., Logares, R., Duarte, C. M., Gasol, J. M. and Sala, M. M. 2018. Sinking particles promote vertical connectivity in the ocean microbiome, *Proceedings of the National Academy of Sciences of the United States of America*, vol. 115, no. 29, pp. E6799–E6807. DOI: 10.1073/pnas.1802470115.

Nöthig, E.-M., Bracher, A., Engel, A., Metfies, K., Niehoff, B., Peeken, I., Bauerfeind, E., Cherkasheva, A., Gäbler-Schwarz, S., Hardge, K., Kilias, E., Kraft, A., Kidane, Y. M., Lalande, C., Piontek, J., Thomisch, K. and Wurst, M. 2015. Summertime plankton ecology in Fram Strait—a compilation of long- and short-term observations, *Polar Research*, vol. 34, no. 1, p. 23349. DOI: 10.3402/polar.v34.23349.

Paerl, H. W. and Prufert, L. E. 1987. Oxygen-Poor Microzones as Potential Sites of Microbial N2 Fixation in Nitrogen-Depleted Aerobic Marine Waters, *Applied and Environmental Microbiology*, vol. 53, no. 5, pp. 1078–1087.

Ploug, H. 1999. A net-jet flow system for mass transfer and microsensor studies of sinking aggregates, *Marine Ecology - Progress Series*, vol. 176, pp. 279–290.

Ploug, H. and Bergkvist, J. 2015. Oxygen diffusion limitation and ammonium production within sinking diatom aggregates under hypoxic and anoxic conditions, *Marine Chemistry*, vol. 176, pp. 142–149. DOI: 10.1016/j.marchem.2015.08.012.

Ploug, H., Grossart, H. P., Azam, F. and Jørgensen, B. B. 1999. Photosynthesis, respiration, and carbon turnover in sinking marine snow from surface waters of Southern California Bight: Implications for the carbon cycle in the ocean., *Marine ecology-progress series*, vol. 179, pp. 1–11.

Ploug, H., Hietanen, S. and Kuparinen, J. 2002. Diffusion and advection within and around sinking, porous diatom aggregates, *Limnology and Oceanography*, vol. 47, no. 4, pp. 1129–1136. DOI: 10.4319/lo.2002.47.4.1129.

Ploug, H., Kühl, M., Buchholz-Cleven, B. and Jørgensen, B. 1997. Anoxic aggregates - an ephemeral phenomenon in the pelagic environment?, *Aquatic Microbial Ecology*, vol. 13, no. 3, pp. 285–294. DOI: 10.3354/ame013285.

Ploug, H. and Passow, U. 2007. Direct measurement of diffusivity within diatom aggregates containing transparent exopolymer particles, *Limnology and Oceanography*, vol. 52, no. 1, pp. 1–6. DOI: 10.4319/lo.2007.52.1.0001.

Prairie, J. C., Ziervogel, K., Arnosti, C., Camassa, R., Falcon, C., Khatri, S., McLaughlin, R. M., White, B. L. and Yu, S. 2013. Delayed settling of marine snow at sharp density transitions driven by fluid entrainment and diffusion-limited retention, *Marine Ecology Progress Series*, vol. 487, pp. 185–200. DOI: 10.3354/meps10387.

Rinta-Kanto, J. M., Sun, S., Sharma, S., Kiene, R. P. and Moran, M. A. 2012. Bacterial community transcription patterns during a marine phytoplankton bloom, *Environmental Microbiology*, vol. 14, no. 1, pp. 228–239. DOI: 10.1111/j.1462-2920.2011.02602.x.

Rocha, C. L. D. L., Nowald, N. and Passow, U. 2008. Interactions between diatom aggregates, minerals, particulate organic carbon, and dissolved organic matter: Further implications for the ballast hypothesis, *Global Biogeochemical Cycles*, vol. 22, no. 4. DOI: 10.1029/2007GB003156.

Sáenz, J. P., Wakeham, S. G., Eglinton, T. I. and Summons, R. E. 2011. New constraints on the provenance of hopanoids in the marine geologic record: Bacteriohopanepolyols in marine suboxic and anoxic environments, *Organic Geochemistry*, vol. 42, no. 11, pp. 1351–1362. DOI: 10.1016/j.orggeochem.2011.08.016.

Sapp, M., Schwaderer, A. S., Wiltshire, K. H., Hoppe, H.-G., Gerdts, G. and Wichels, A. 2007. Species-Specific Bacterial Communities in the Phycosphere of Microalgae?, *Microbial Ecology*, vol. 53, no. 4, pp. 683–699.

Seymour, J. R., Marcos, null and Stocker, R. 2007. Chemotactic response of marine micro-organisms to micro-scale nutrient layers, *Journal of Visualized Experiments: JoVE*, no. 4, p. 203. DOI: 10.3791/203.

Simon, M., Grossart, H. P., Schweitzer, B. and Ploug, H. 2002. Microbial Ecology of Organic Aggregates in Aquatic Ecosystems., *Aquatic microbial ecology*, vol. 28, no. 2, pp. 175–211.

Smriga, S., Fernandez, V. I., Mitchell, J. G. and Stocker, R. 2016. Chemotaxis toward phytoplankton drives organic matter partitioning among marine bacteria, *Proceedings of the National Academy of Sciences of the United States of America*, vol. 113, no. 6, pp. 1576–1581. DOI: 10.1073/pnas.1512307113.

Sonnenschein, E. C., Gärdes, A., Seebah, S., Torres-Monroy, I., Grossart, H.-P. and Ullrich, M. S. 2011. Development of a genetic system for Marinobacter adhaerens HP15 involved in marine aggregate formation by interacting with diatom cells, *Journal of Microbiological Methods*, vol. 87, no. 2, pp. 176–183. DOI: 10.1016/j.mimet.2011.08.008.

Stahl, A. 2015. Interaction of the Marine Bacterium Marinobacter adhaerens HP15 with the Diatom Thalassiosira weissflogii Analyzed by Proteomics Approaches, Bremen, Jacobs University.

Stolzenbach, K. D. 1993. Scavenging of small particles by fast-sinking porous aggregates, *Deep Sea Research Part I: Oceanographic Research Papers*, vol. 40, no. 2, pp. 359–369. DOI: 10.1016/0967-0637(93)90008-Q.

Stolzenbach, K. D. and Elimelech, M. 1994. The effect of particle density on collisions between sinking particles: implications for particle aggregation in the ocean, *Deep Sea Research Part I: Oceanographic Research Papers*, vol. 41, no. 3, pp. 469–483. DOI: 10.1016/0967-0637(94)90091-4.

Thiele, S., Fuchs, B. M., Amann, R. and Iversen, M. H. 2014. Colonization in the photic zone and subsequent changes during sinking determines bacterial community composition in marine snow, *Applied and Environmental Microbiology*, p. AEM.02570-14. DOI: 10.1128/AEM.02570-14.

Trimborn, S., Brenneis, T., Hoppe, C. J. M., Laglera, L. M., Norman, L., Santos-Echeandía, J., Völkner, C., Wolf-Gladrow, D. and Hassler, C. S. 2017. Iron sources alter the response of Southern Ocean phytoplankton to ocean acidification, *Marine Ecology Progress Series*, vol. 578, pp. 35–50. DOI: 10.3354/meps12250.

Weller, H. G., Tabor, G., Jasak, H. and Fureby, C. 1998. A tensorial approach to computational continuum mechanics using object-oriented techniques, *Computers in Physics*, vol. 12, no. 6, pp. 620–631. DOI: 10.1063/1.168744.

Wishner, K. F., Outram, D. M., Seibel, B. A., Daly, K. L. and Williams, R. L. 2013. Zooplankton in the eastern tropical north Pacific: Boundary effects of oxygen minimum zone expansion, *Deep Sea Research Part I: Oceanographic Research Papers*, vol. 79, pp. 122–140. DOI: 10.1016/j.dsr.2013.05.012.

Wolf, K. K. E., Hoppe, C. J. M. and Rost, B. 2018. Resilience by diversity: Large intraspecific differences in climate change responses of an Arctic diatom, *Limnology and Oceanography*, vol. 63, no. 1, pp. 397–411. DOI: 10.1002/lno.10639.

ADDITIONAL PUBLICATIONS

Paper SI

Clara J.M. Hoppe, Clara M. Flintrop, Björn Rost, 2018. *The Arctic picoeukaryote* Micromonas pusilla *benefits synergistically from warming and ocean acidification.* Biogeosciences, 15 (14), pp. 4353-4365. doi: 10.5194/bg-15-4353-2018

Abstract

In the Arctic Ocean, climate change effects such as warming and ocean acidification (OA) are manifesting faster than in other regions. Yet, we are lacking a mechanistic understanding of the interactive effects of these drivers on Arctic primary producers. In the current study, one of the most abundant species of the Arctic Ocean, the prasinophyte *Micromonas pusilla*, was exposed to a range of different pCO_2 levels at two temperatures representing realistic current and future scenarios for nutrient-replete conditions. We observed that warming and OA synergistically increased growth rates at intermediate to high pCO_2 levels. Furthermore, elevated temperatures shifted the pCO_2 optimum of biomass production to higher levels. Based on changes in cellular composition and photophysiology, we hypothesize that the observed synergies can be explained by beneficial effects of warming on carbon fixation in combination with facilitated carbon acquisition under OA. Our findings help to understand the higher abundances of picoeukaryotes such as *M. pusilla* under OA, as has been observed in many mesocosm studies.

Conclusions

Our results confirm beneficial effects of warming and OA on growth and biomass production of *M. pusilla* under nutrient-replete conditions. *M. pusilla* is characterized by an exceptionally high cellular C: N ratio compared to other Arctic phytoplankton. Higher growth rates and abundances of *M. pusilla* not only affect the food web due to its small size and concurrent grazer preferences but also in terms of food quality, and may strengthen the microbial food web. Together with a weakening of the classical

diatom-fuelled food web, this could have severe implications for the flow of energy and nutrients through future marine Arctic ecosystems.

Contribution to manuscript

CJM and BR designed the study. CH and CMF did phytoplankton culturing, biogeochemical analyses and measuring of photosynthetic activity, automated cell counting and analyses, and processed the data. CH wrote the manuscript with input from BR and CMF. It is important to note that the contribution of CMF during the time of the PhD consisted of providing input to the manuscript, and that the experimental work took place during the MSc studies of CMF.

AUTHOR CONTRIBUTIONS

Paper I

Clara M. Flintrop, Andreas Rogge, Sebastian Miksch, Stefan Thiele, Anya M. Waite, Morten H. Iversen. 2018. Embedding and slicing of intact in situ collected marine snow. *Limnol. Oceanogr. Methods 16: 339-355.* DOI:10.1002/lom3.10251

Specific contribution to manuscript

The study was designed by CMF, AR, AMW and MHI. Samples for the study were collected by CMF and MHI. Development and optimization of the embedding and slicing method was done by CMF. Staining and FISH-protocols were developed by CMF, SM and ST. Data processing and analysis were done by CMF. CMF wrote and revised the manuscript with input from AR, AM and MHI.

Paper II

Andreas Rogge, Clara M. Flintrop, Morten H. Iversen, Ian Salter, Allison A. Fong, Anja Vogts, Anya M. Waite. 2018. Hard and soft plastic resin embedding for single-cell element uptake investigations of marine-snow-associated microorganisms using nano-scale secondary ion mass spectrometry. *Limnol. Oceanogr. Methods 16: 484-503.* DOI:10.1002/lom3.10261

Specific contribution to manuscript

The study was designed by AR, CMF, IS, AAF and AMW. Samples for the study were collected and produced in roller tank incubations by AR. Development and optimization of the embedding and slicing method was done by AR. Staining protocols were developed by AR. NanoSIMS measurements were carried out by AR and AV. Data processing and analysis were done by AR. AR wrote and revised the manuscript with input from CF, MHI, IS, AAF, AV and AMW.

Paper III

Clara M. Flintrop†, Soeren Ahmerkamp†, Isabell Klawonn, Nasrollah Moradi, Marcel M.M. Kuypers, Hans-Peter Grossart, Arzhang Khalili, Javier Aristegui, Morten H. Iversen. Manuscript in preparation. Rethinking sinking: Imaging the flow fields of natural marine aggregates to measure settling velocity.

(†these authors contributed equally to this work)

Specific contribution to manuscript

The study was designed by CMF, SA and MHI. The method for recording freely suspended aggregates with particle image velocimetry was developed by CMF and SA with contribution from MHI, AK, HPG and MMMK. Sample collection was carried out by CMF and IK. On-board aggregate recordings and measurements were carried out by CMF with input from IK and JA. Processing and data analysis were done by CMF and SA with contribution from NM and AK. The manuscript was written by CMF and SA with input from MHI and NM.

Paper IV

Cordelia Roberts†, Clara M. Flintrop†, Alexander Khachikyan, Jana Milucka, Colin C. Munn, Morten H. Iversen. Manuscript in preparation. Microplastics reduce the efficiency of the biological carbon pump by decreasing the settling velocity of marine snow.

(†these authors contributed equally to this work)

Specific contribution to manuscript

The study was designed by CR, CMF and MHI. Roller tank incubations and recordings were done by CR with guidance from CMF and MHI. Image processing from the recordings was carried out by CMF and CR. Sample preparation for biogeochemical analysis was done by CR. Raman spectroscopy was carried out by AK and JM. Data processing and analysis was done by CMF and CR. The manuscript was written by CMF and CR with input from MHI, AK, JM and CCM.

ACRONYMS

ANOVA	Analysis of variance
AS	Agar spheres
BCP	Biological carbon pump
BF	Bright field
CARD-FISH	Catalyzed reporter deposition fluorescence in situ hybridization
CLSM	Confocal laser scanning microscopy
CMS	Compact marine snow
CSP	Coomassie-stainable particles
Chl a	Chlorophyll a
DAPI	4',6-diamidino-2-phenylindole
DIC	Dissolved inorganic carbon
DOC	Dissolved organic carbon
DW	Dry weight
ECD	Equivalent circular diameter
EPS	Extracellular polymeric substances
ESD	Equivalent spherical diameter
FISH	Fluorescence in situ hybridization
FP	Fecal pellets
HSI	Hue, saturation, and intensity
ISC	In situ camera
LED	Light emitting diode
LMS	Loose marine snow
M	Mucus
MALDI-MSI	Matrix-assisted laser desorption ionization mass spectrometry imaging
MS	Marine snow
MSC	Marine snow catcher
MiL-FISH	Multi-labeled fluorescence in situ hybridization
NanoSIMS	Nano-scale secondary ion mass spectrometry
O	Other
OM	Organic matter
OMZ	Oxygen minimum zone
PIP	Particle injection pump

PIV	Particle image velocimetry
POC	Particulate organic carbon
PON	Particulate organic nitrogen
ROI	Region of interest
SD	Standard deviation
SIMS	Secondary Ion Mass Spectrometry
SRμCT	synchrotron radiation micro-computed tomography
TEP	Transparent exopolymer particles
UPW	Ultra-pure water
UVP	Underwater velocity profiler
UVP	Underwater vision profiler
VPR	Video plankton recorder
mono-FISH	Mono-labeled fluorescence in situ hybridization
rRNA	Ribosomal ribonucleic acid
sNSW	Sterile-filtered North Sea water

SYMBOLS

$\mathbf{C_D}$	Drag coefficient
d	Aggregate diameter
g	Gravitational acceleration
Re	Reynolds number
w	Settling velocity
$\boldsymbol{\delta}$	Fluid boundary layer
$\boldsymbol{\delta_s}$	Scaled fluid boundary layer
$\boldsymbol{\Delta\rho}$	Excess density
$\boldsymbol{\eta}$	Dynamic viscosity of seawater
$\boldsymbol{\rho_s}$	Solid hydrated density
$\boldsymbol{\rho_w}$	Density of sea water
φ	Porosity
$\boldsymbol{\omega}$	Rotation rate

Versicherung an Eides Statt / *Affirmation in lieu of an oath*

gem. § 5 Abs. 5 der Promotionsordnung vom 18.06.2018 /
according to § 5 (5) of the Doctoral Degree Rules and Regulations of 18 June, 2018

Ich / I, _____
(Vorname / First *Name*, Name / *Name*, Anschrift / *Address*, ggf. Matr.-Nr. / *student ID no., if applicable)*

versichere an Eides Statt durch meine Unterschrift, dass ich die vorliegende Dissertation selbständig und ohne fremde Hilfe angefertigt und alle Stellen, die ich wörtlich dem Sinne nach aus Veröffentlichungen entnommen habe, als solche kenntlich gemacht habe, mich auch keiner anderen als der angegebenen Literatur oder sonstiger Hilfsmittel bedient habe und die zu Prüfungszwecken beigelegte elektronische Version (PDF) der Dissertation mit der abgegebenen gedruckten Version identisch ist. / *With my signature I affirm in lieu of an oath that I prepared the submitted dissertation independently and without illicit assistance from third parties, that I appropriately referenced any text or content from other sources, that I used only literature and resources listed in the dissertation, and that the electronic (PDF) and printed versions of the dissertation are identical.*

Ich versichere an Eides Statt, dass ich die vorgenannten Angaben nach bestem Wissen und Gewissen gemacht habe und dass die Angaben der Wahrheit entsprechen und ich nichts verschwiegen habe*. / I affirm in lieu of an oath that the information provided herein to the best of my knowledge is true and complete.*

Die Strafbarkeit einer falschen eidesstattlichen Versicherung ist mir bekannt, namentlich die Strafandrohung gemäß § 156 StGB bis zu drei Jahren Freiheitsstrafe oder Geldstrafe bei vorsätzlicher Begehung der Tat bzw. gemäß § 161 Abs. 1 StGB bis zu einem Jahr Freiheitsstrafe oder Geldstrafe bei fahrlässiger Begehung. / *I am aware that a false affidavit is a criminal offence which is punishable by law in accordance with § 156 of the German Criminal Code (StGB) with up to three years imprisonment or a fine in case of intention, or in accordance with § 161 (1) of the German Criminal Code with up to one year imprisonment or a fine in case of negligence.*

_____ _____
Ort / *Place*, Datum / *Date* Unterschrift / *Signature*